

DISSERTATION

THE DEVELOPMENT AND APPLICATIONS OF LIGHT-GATED COBALT CATALYSIS

Submitted by

Kyle E. Ruhl

Department of Chemistry

In partial fulfillment of the requirements

For the Degree of Doctor of Philosophy

Colorado State University

Fort Collins, Colorado

Spring 2017

Doctoral Committee:

Advisor: Tomislav Rovis

Andrew McNally

James R. Neilson

Matthew J. Kipper

Copyright by Kyle E. Ruhl 2017

All Rights Reserved

## ABSTRACT

### THE DEVELOPMENT AND APPLICATIONS OF LIGHT-GATED COBALT CATALYSIS

Transition metals are an important natural resource and an essential component of many industrial processes and applications. Examples of these include air-quality control, electronics manufacture, agriculture, pharmaceuticals, and petro-chemistry. Within the field of synthetic chemistry, transition metal catalysts minimize waste, decrease expense, and enable rapid construction of small molecules. Over the past decade, transition-metal-based polypyridyl complexes have been the cornerstone of photo-redox catalysis which facilitate electron transfer and allow synthetic chemists to functionalize inert functionalities using visible-light energy.

The first chapter of this work introduces rhodium- and cobalt-catalyzed [2+2+2] cycloadditions as well as photo-redox catalysis. The following chapter covers our group's progress toward the merger of photo-redox and cobalt catalysis as well as the multi-disciplinary approach we have used to understand mechanism.

The third chapter explores light-gated catalysis and its importance for spatially and temporally resolved methods.

Finally, the fourth chapter focuses on the applications of light-gated cobalt catalysis. We have found a light-gated cobalt catalyst to temporally control the [2+2+2] cycloaddition, and when combined with photolithography, enable a spatially resolved method for arene formation.

## ACKNOWLEDGMENTS

The most important thing I have learned in graduate school is that failure is not always bad—failing is an essential part of succeeding.

First, I thank my wife, Laura, who supported me through every emotional up and down I experienced in graduate school. Her intelligence, motivation, steadfast faith and unwavering compassion has inspired me from the moment I met her.

Secondly, for this opportunity I thank my advisor, Prof. Tomislav Rovic. Joining Tom's group and his guidance over the past five years has not only developed me as a scientist, but also as an individual. I owe a huge debt of gratitude to the members of the Rovic group, both past and present, for fostering a group culture that works hard and does impactful research but maintains a strong sense of camaraderie.

Without the support of family and the values they instilled in me I would have never made it this far. Thank you all for seeing the bigger picture when I could not.



## TABLE OF CONTENTS

ABSTRACT.....	ii
ACKNOWLEDGMENTS.....	iii
CHAPTER ONE: Introduction to Transition-Metal Catalysis.....	1
1.1 --- Metal-Catalyzed [2+2+2] Cycloaddition Reactions.....	1
1.2 --- Cobalt Catalyzed [2+2+2] Cycloadditions.....	6
1.3 --- Photo-Redox Catalysis.....	9
REFERENCES.....	13
CHAPTER TWO: Merging Photo-Redox and Cobalt Catalysis.....	16
2.1 --- Background.....	16
2.2 --- Results and Discussion.....	20
2.2.1 -- Reaction Screening and Development.....	20
2.2.2 -- Substrate Scope and Limitations.....	26
2.2.3 -- Investigation of Light's Role.....	30
2.2.4 -- Mechanistic Insight (Electrochemistry).....	31
2.2.5 -- Mechanistic Insight (Investigation of Light, Dark and Heat).....	44
2.2.6 -- Proposed Catalytic Cycle.....	46
2.3 --- Photo-active Cobalt Species.....	49
2.3.1 -- Reaction Development.....	49
2.3.2 -- Proposed Mechanism.....	52
2.4 --- Pyridine Formation.....	55
2.5 --- Summary.....	58

REFERENCES.....	60
CHAPTER THREE: Introduction to Light-Gated Catalysis.....	62
3.1 --- Light-Gated Catalysis.....	62
3.2 --- Temporally Controlled Catalysis.....	66
3.3 --- Spatially Controlled Catalysis.....	71
REFERENCES.....	78
CHAPTER FOUR: Applications of Light-Gated Cobalt Catalysis.....	81
<i>PART A: Light-Controlled [2+2+2] Cycloaddition Polymerization</i>	
4.1 --- Background.....	81
4.2 --- Results and Discussion.....	83
4.2.1 -- Monomer Development.....	83
4.2.2 -- Monomer Consumption Experiments.....	87
4.2.3 -- Polymer Optimization.....	88
4.2.4 -- Polymer Growth Experiments.....	90
4.3 --- Summary.....	93
<i>PART B: Spatially Controlled Arene Formation</i>	
4.4 --- Background.....	94
4.5 --- Results and Discussion.....	97
4.6 --- Summary.....	114
REFERENCES.....	116
APPENDIX ONE: Merging Photo-Redox and Cobalt Catalysis: Experimental.....	119
APPENDIX TWO: Applications of Light-Gated Cobalt Catalysis: Experimental.....	173

## CHAPTER ONE

### Introduction to Transition-Metal Catalysis

#### 1.1 --- Metal-Catalyzed [2+2+2] Cycloaddition Reactions

Reactions which incorporate three or more starting materials into one product represent a convergent synthetic approach.<sup>[1]</sup> By joining several fragments at once, multi-component transformations minimize waste, maximize atom economy, and rapidly form complex structures.<sup>[2]</sup> One archetypal example of a multi-component reaction is the [2+2+2] alkyne cycloaddition which cyclizes three  $\pi$ -components to generate three new  $\sigma$  bonds and a new aromatic compound. The [2+2+2] cycloaddition to form arenes has been known for nearly 150 years, but the first report used temperatures in excess of 400 °C.<sup>[3]</sup> Reppe made an important discovery nearly seventy years ago which made the [2+2+2] cycloaddition a viable method for benzene formation. He found that a nickel catalyst trimerizes gaseous acetylene at much lower temperatures to give benzene (120-150 °C) (**Figure 1.1**).<sup>[4]</sup> Since Reppe's seminal report, the [2+2+2] cycloaddition has grown into a valuable transformation with innumerable synthetic applications.



**Figure 1.1:** Low Temperature Nickel-Catalyzed [2+2+2]

Despite the synthetic power of the [2+2+2] cycloaddition, poor chemo- and regioselectivity is a recurrent issue which limits the reactions efficiency and utility (**Figure 1.2**). In fact, a proper [2+2+2] cycloaddition which catalytically incorporates three distinct, non-tethered  $\pi$ -components selectively remains unreported. Nevertheless, chemists have developed myriad

techniques to sidestep this problem and reach a favorable product distribution. These approaches include stoichiometric metal salts<sup>[5]</sup>, reagent tethering strategies<sup>[6]</sup> and exploiting alkyne surrogates.<sup>[7]</sup>

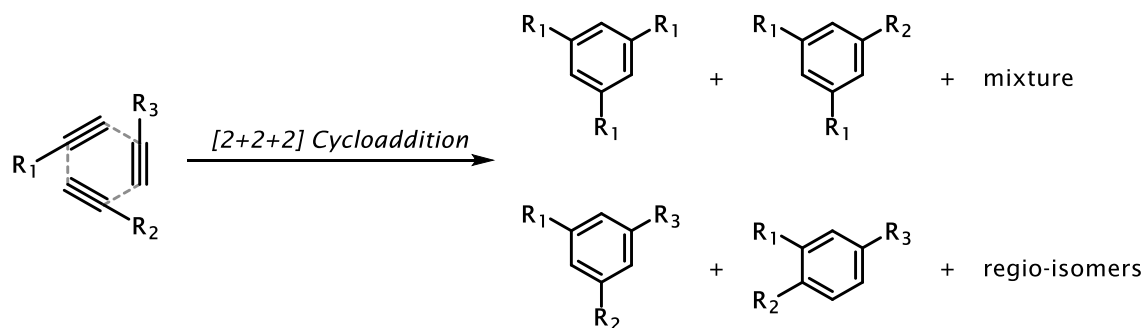


**Figure 1.2:** [2+2+2] Cycloaddition and Chemo- and Regio-selectivity

In addition, applications of the [2+2+2] cycloaddition extend well beyond benzene formation. Many metal-catalyzed methods are also efficacious for the synthesis of heterocycles via nitrogen-containing  $\pi$ -components (**Figure 1.3**). Motifs such as pyridines<sup>[8]</sup>, pyridones<sup>[9]</sup>, pyridinylidenes<sup>[10]</sup> and dihydropyridines<sup>[11]</sup> have all been reported.

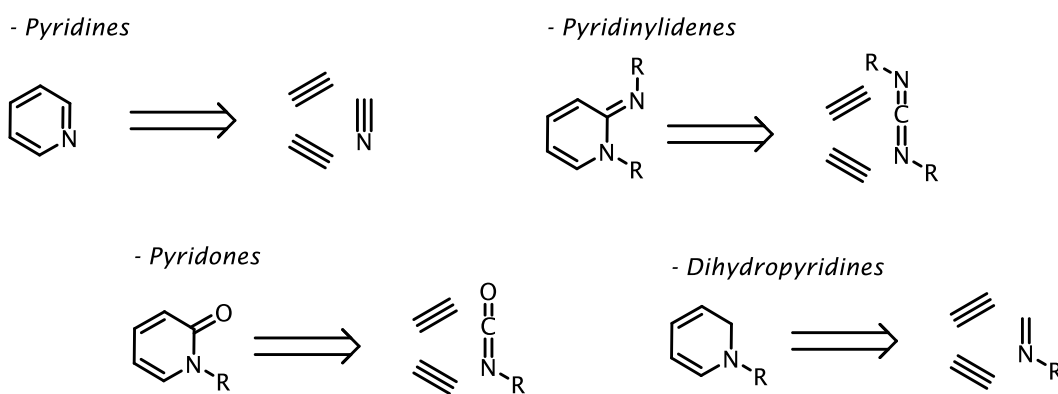


**Figure 1.3:** Nitrogen Heterocycle Formation via [2+2+2] Cycloaddition

The Rovis group has a long, rich history in the field of rhodium-catalyzed cycloadditions that form nitrogen heterocycles. The work in our group stems from Dr. Robert Yu's discovery in 2006; he found that a rhodium(I)phosphine catalyst efficiently couples alkenyl isocyanate **1** with diphenyl acetylene (**2**) via a [2+2+2] cycloaddition to afford the indolizidinone product **3** (**Figure**

**1.4).**<sup>[12]</sup> Unexpectedly, the vinylogous lactam product (**3**) was isolated as the major product, and the predicted lactam product (**4**) was isolated with lower yields. Further studies revealed that bis-aryl alkynes (ie **2**) predominantly formed the vinylogous lactam product (**3**) whereas aliphatic alkynes (ie **5**) favored the lactam product (**6**).

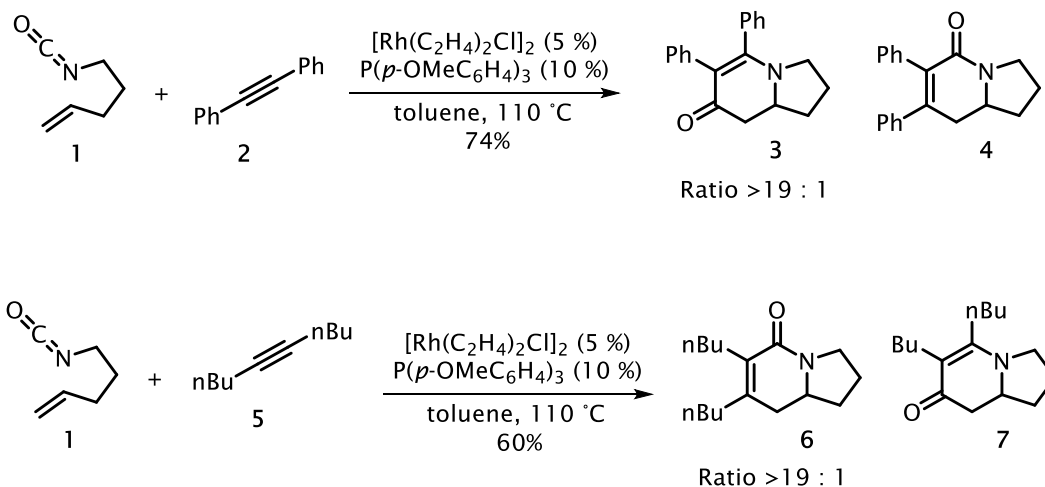


**Figure 1.4:** Rhodium-Catalyzed [2+2+2] Cycloadditions from the Rovis Group

Yu went on to expand the reaction's utility and found that chiral phosphoramidite ligands induce high levels of enantioselectivity (**Figure 1.5**).<sup>[13]</sup> Cyclizing aliphatic alkyne **8** with the alkenyl isocyanate **1** gives the enantioenriched indolizidione product **9** in 60% yield and 95% ee. The power of this method is illustrated with the enantioselective synthesis of (+)-Lasubine II (**10**), a quinolizine-based compound, which is accomplished in only three steps from **1**.

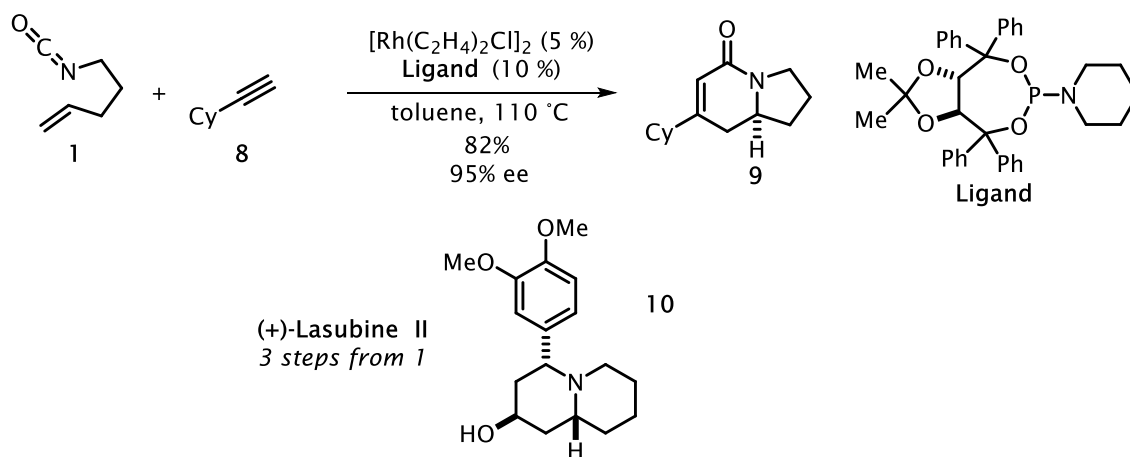


**Figure 1.5:** Chiral Phosphoramidite Ligand Imparts High Enantioselectivity

Moreover, this methodology is valuable for the synthesis of many alkaloid natural products<sup>[14]</sup> and even larger eight-membered rings have been reported by our group.<sup>[15]</sup> However, high selectivity for the lactam or vinylogous lactam product remained an unpredictable aspect of the transformation. To rationalize and address the observed product distribution, the group investigated the reaction mechanism.<sup>[16]</sup> Selectivity for the vinylogous lactam product is rationalized by the mechanism illustrated in **Figure 1.6**. Coordination of the alkyne and isocyanate forms rhodium(I) intermediate **I**.<sup>[17]</sup> Oxidative cyclization<sup>[18]</sup> results in C-N bond formation to give the acyl rhodium species **II**. Since alkene insertion at intermediate **II** would require formation of a bicyclic coordination complex, a CO migration is preferred at intermediate **III** which affords intermediate **IV**. Finally, migratory insertion of the tethered alkene and a subsequent reductive elimination from intermediate **V** furnishes the vinylogous lactam product and regenerates the catalyst (**I**).

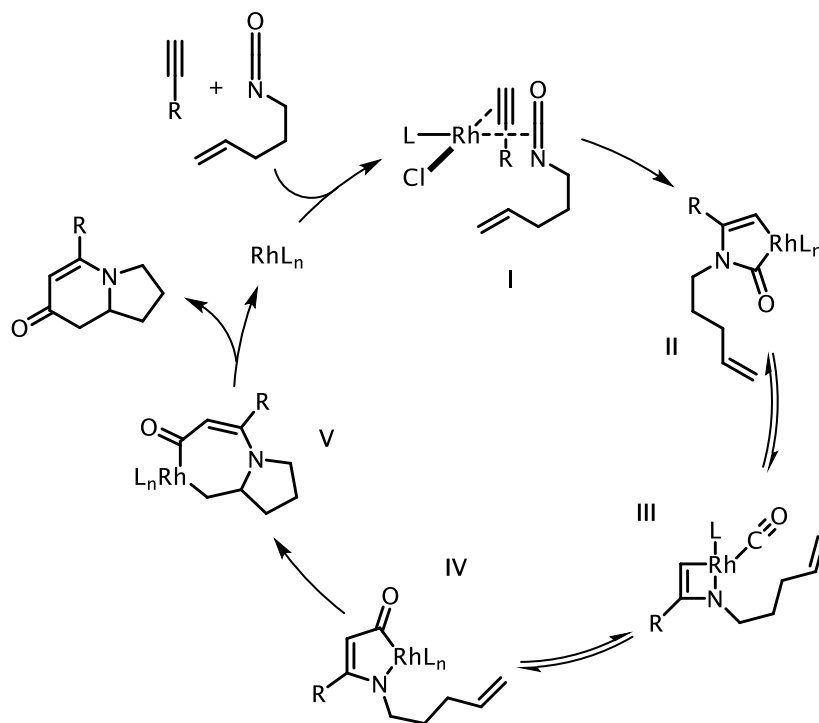


**Figure 1.6:** Proposed Mechanism of the Rhodium-Catalyzed [2+2+2] Cycloaddition

With a better understanding of the mechanism, we believed catalyst design would provide an opportunity to favorably obtain one regioisomer in high yield. Another former Rovis group member, Dr. Derek Dalton, found that the highly fluorinated electron deficient chiral phosphoramidite ligand CKPhos (**11**) imparts excellent selectivity for **10** with high yield and enantiomeric excess (**Figure 1.7**).<sup>[19]</sup> Additionally, X-ray analysis and calculations suggest that CKPhos (**11**) influences high selectivity because of an advantageous stacking interaction between the metal center and the electron deficient arenes.<sup>[20]</sup>

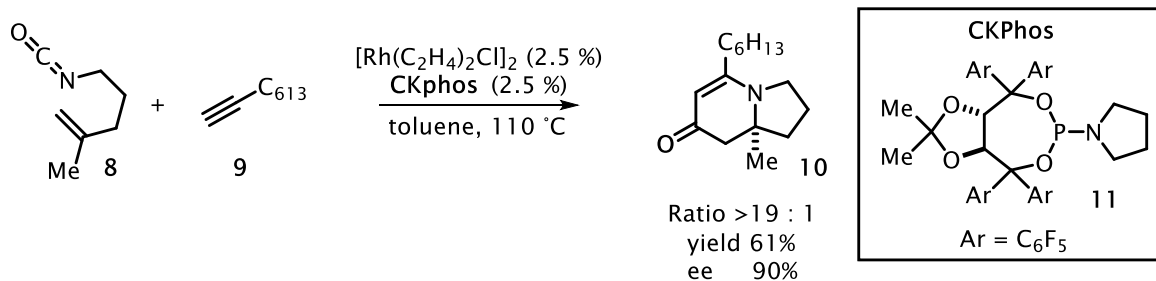


**Figure 1.7:** Highly Fluorinated Ligand Imparts Selectivity

Rhodium-based catalysts have brought great progress, but has also inspired other metal-based methodologies. As a result of the success we had with rhodium-catalyzed [2+2+2] cycloadditions, we believed cobalt could also be an effective catalysts for these types of transformations. Since rhodium resides in the same periodic group, cobalt has been explored for complementary techniques as well as original.

## 1.2 --- Cobalt Catalyzed [2+2+2] Cycloadditions

Over the past seventy years many metal catalysts have been found to catalyze a variety of [2+2+2] cycloadditions. Our group has focused exclusively on rhodium-based methods but other metals make competent catalysts and include Ir, Pd, Fe, Co, Ni, Ru, Ti, etc. The expense and limited amounts of precious metals (e.g. Ir, Pd, Ru, Rh) have recently directed efforts toward cheaper and more abundant metals.

The first report demonstrating cobalt's capacity to catalyze the [2+2+2] cycloaddition came from Vollhart in 1975, where he showed that carbonyl-containing pre-catalyst **15** constructs annulated benzenes of various ring sizes in fair to high yields (**Figure 1.8**).<sup>[21]</sup> In addition to high product yields, the reaction also tolerates a wide variety of alkyne substitution patterns. Alkyl, aryl, and vinyl substituents all participate, as well as electron withdrawing and donating groups such as esters, acids, amides, ethers, and amines.



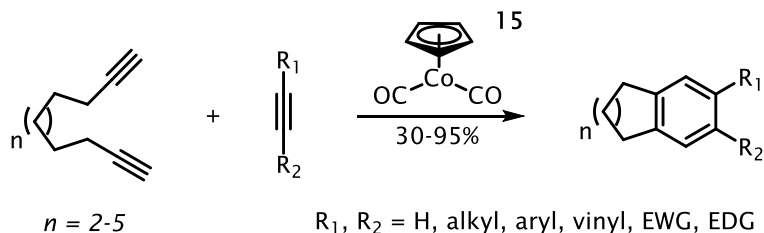


**Figure 1.8:** Cobalt-Catalyzed [2+2+2] Alkyne Cycloaddition

Cobalt catalyzed [2+2+2] cycloadditions which form stereogenic carbon centers are also well documented with isolable cobalt(I) pre-catalysts (e.g. **15**) (**Figure 1.9**).<sup>[22]</sup> Incorporating a tethered alkene with two alkyne equivalents (**16**) forms a diene motif (**17**) and thus a chiral carbon. Unfortunately, the diene functional group is an exceptional ligand for cobalt and therefore the reaction requires a full equivalent of **15**.

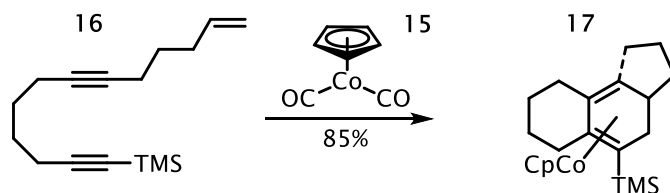


**Figure 1.9:** Stoichiometric Cobalt [2+2+2] Gives a Stereogenic Carbon

Catalytic enantioselective cobalt-catalyzed [2+2+2] cycloaddition have been realized to form nitrogen heterocycles. Heller first reported chiral tartaric acid<sup>[23]</sup> and menthyl-based<sup>[24]</sup> cyclopentadienyl cobalt pre-catalysts in the mid-2000s. He also reported an indenyl-based chiral<sup>[25]</sup> complex (**20**) (**Figure 1.10**), which efficiently cyclizes naphthyl-diyne **18** with benzonitrile (**19**) to furnish axially chiral, enantioenriched 2-aryl pyridines in high yields.

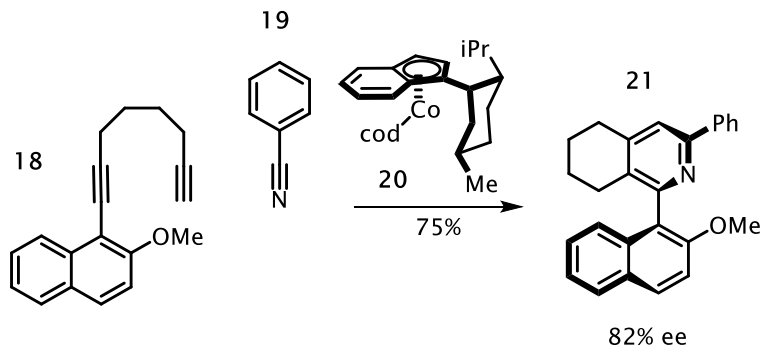


**Figure 1.10:** Chiral Indenyl Cobalt Complex

In addition to chiral cyclopentadiene-based ligands, enantioselective transformations have been accomplished using enantiopure phosphine-based complexes (e.g. **23**) (**Figure 1.11**). Complex **23** has an added advantage of being bench stable compared to the isolable but air sensitive chiral cobalt(I) pre-catalysts. Hapke and co-workers demonstrate the chiral cobalt(II) complex, easily reduced by zinc metal, forms **24** smoothly from **22** in good yields with high ee.

[26]

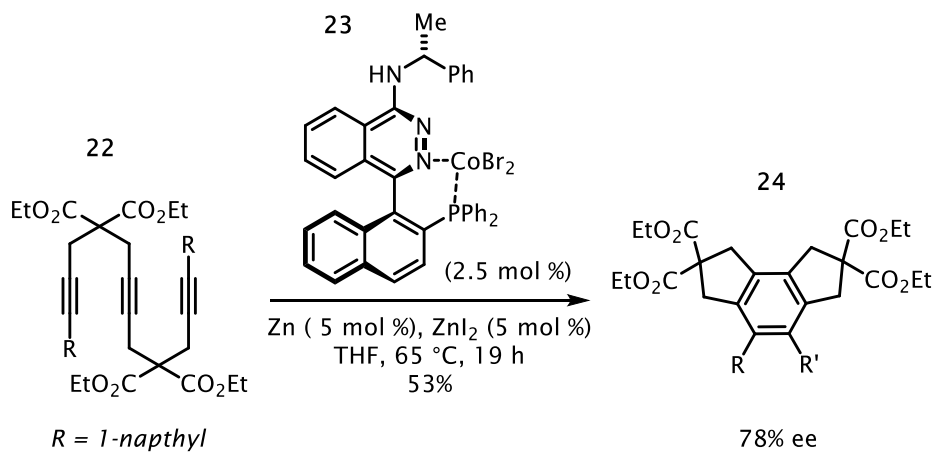


**Figure 1.11:** Enantioselectivity with Phosphine-Based Ligands

Cobalt-catalyzed [2+2+2] cycloadditions competently form a variety of benzene and pyridine<sup>[27]</sup> compounds. Although we have not covered them here, methods for pyridone<sup>[28]</sup> and

pyridazine<sup>[29]</sup> formation have also been reported with cobalt pre-catalysts. While cobalt-catalyzed methodologies currently do not replace all existing examples using precious metals, cobalt catalysis remains a large area of research and holds great potential for future applications.

### 1.3 --- Photo-Redox Catalysis

Over the past ten years, photo-redox catalysis has garnered significant attention for synthetic applications. Photo-catalysis utilizes metal poly-pyridyl complexes,<sup>[30]</sup> which function either as oxidants or reductants upon absorbing visible light radiation. With this ability to facilitate electron transfer events, photo-catalysts are widely applicable for many radical transformations,<sup>[31]</sup> and more recently, have been combined with transition metal catalysts (e.g. metallophoto-redox). Publications from the Molander, MacMillan, and Doyle groups demonstrate new radical-based transmetallation<sup>[32, 33]</sup> and electron transfer-induced reductive eliminations<sup>[34]</sup> all facilitated by visible light. Essentially, photo-catalysis circumvents a thermodynamically unfavorable process observed in an Earth-abundant transition-metal catalyst (**Figure 1.12**).

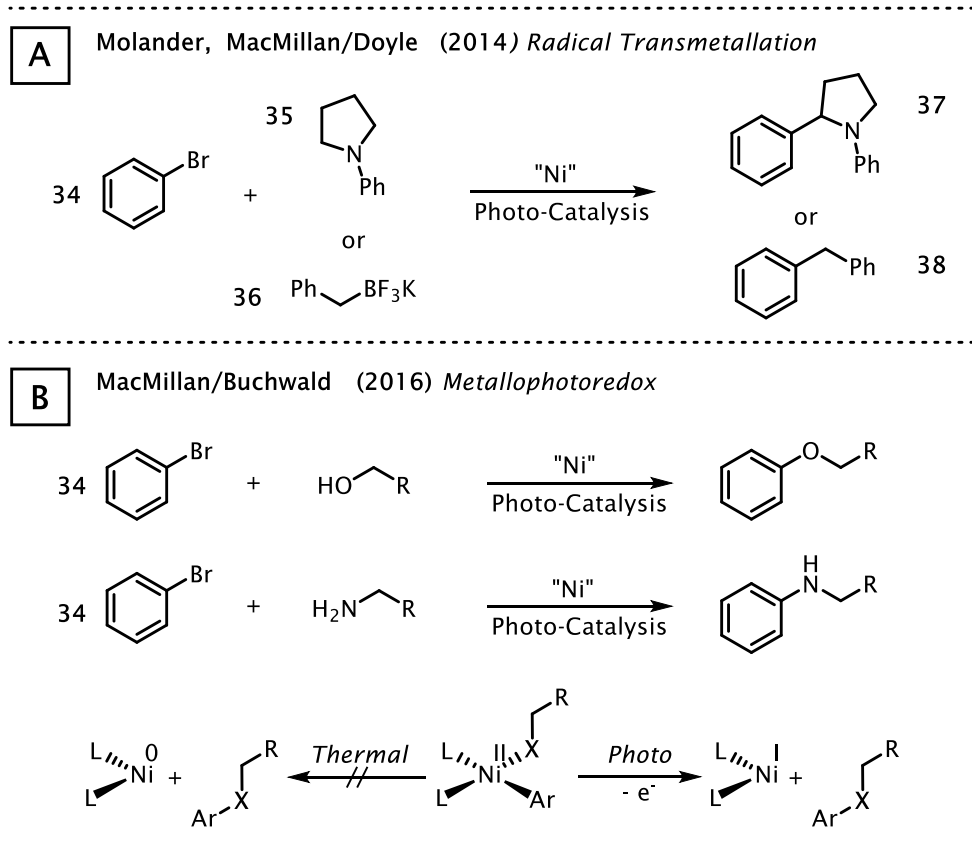


**Figure 1.12:** Nickel/Photo-Catalysis Reported by Molander, MacMillan and Doyle

**Figure 1.13** illustrates the electron transfer mechanism commonly observed with many photo-redox catalysts. For example,  $\text{Ru}(\text{bpy})_3\text{Cl}_2$  absorbs visible light and undergoes a metal-to-ligand charge transfer (MLCT) to give a charge separated  $\text{Ru}^{\text{II}*}$  excited state. Under normal conditions, the short-lived triplet state ( $\text{Ru}^{\text{II}*}$ ) relaxes to the ground state ( $\text{Ru}^{\text{II}}$ ) by emission of a photon (fluorescence) at 620 nm. The fate of this excited state changes when a fluorescence quencher is present in solution. Interaction of the excited state with a reductive quencher induces electron transfer to the excited state [ $E_{1/2} = +0.77$  V vs. SCE] to deliver a highly reducing  $\text{Ru}^{\text{I}}$  species [ $E_{1/2} = -1.33$  V vs. SCE]. Conversely, an oxidative quencher will abstract an electron from the excited state [ $E_{1/2} = -0.81$  V vs. SCE] giving a strongly oxidizing  $\text{Ru}^{\text{III}}$  complex [ $E_{1/2} = 1.29$  V

vs. SCE]. Regardless of the redox pathway, the ground state  $\text{Ru}^{\text{II}}$  is ultimately regenerated to close the catalytic cycle.

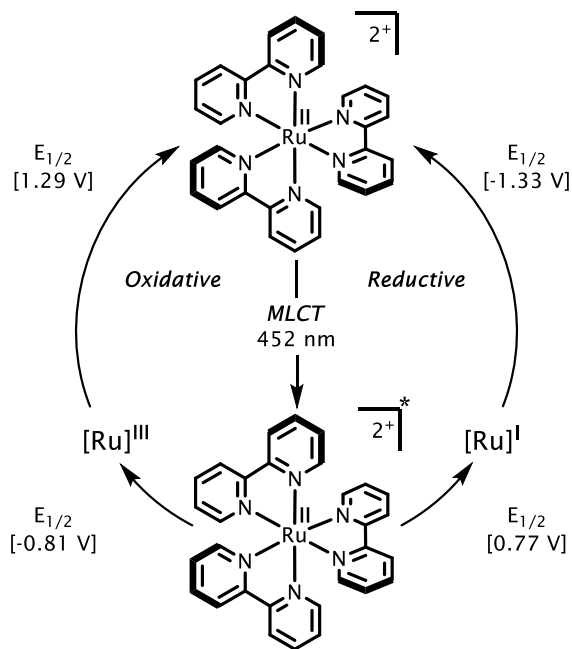


**Figure 1.13:** Catalytic Cycle of a Common Photo-Redox Catalyst— $\text{Ru}(\text{bpy})_3\text{Cl}_2$

Over the past half century, the proliferation of rhodium and related precious-metal catalysts have drastically advanced synthetic organic chemistry. Unfortunately, the low abundance of these metals in the Earth's crust increases cost and raises sustainability concerns.<sup>[35]</sup> Since the earliest reports of rhodium catalysis in the Rovis group, several students have sought to replace and/or complement existing methods with a more abundant metal comparable to rhodium. Thus, cobalt was seen as an attractive alternative. In addition to decreased expense, cobalt's accessible oxidation states include -1, 0, +1, +2, and +3. By contrast, rhodium is limited to the +1, +2, and +3 oxidation states with a large majority of reactivity catalyzed via a  $\text{Rh}^{\text{I}}/\text{Rh}^{\text{III}}$  cycle. After gaining experience on rhodium(I)- and rhodium(III)-based projects, we pursued new methods in cobalt

catalysis. The following chapter details our initial interest in contemporary cobalt-catalyzed methods and the development of a light-controlled [2+2+2] cycloaddition.

## REFERENCES

- [1] Gore, R. P.; Rajput, A. P. *Drug Invention Today* **2013**, *5*, 148-152.
- [2] Trost, B. M. *Science* **1991**, *254*, 1471-1477.
- [3] Berthelot, M. C. R. *Hebd. Seances Acad. Sci.* **1866**, *62*, 905.
- [4] Reppe, V. W.; Schweckendiek, W. J. *Liebigs Ann.* **1948**, *560*, 104-116.
- [5] a) Takahashi, T.; Yamazaki, A.; Liu, Y.; Nakajima, K.; Kitora, M. *J. Am. Chem. Soc.* **1998**, *120*, 1672-1680. b) Suzuki, D.; Urabe, H.; Sato, F. *J. Am. Chem. Soc.* **2001**, *123*, 7925-7926. c) Vollhardt, P. C. *Angew. Chem. Int. Ed.* **1984**, *23*, 539-556.
- [6] a) Yamamoto, Y.; Ishii, J.-I.; Nishiyama, H.; Itoh, K. *J. Am. Chem. Soc.* **2004**, *126*, 3712-3713. b) Martin, T. J.; Rovis, T. *Angew. Chem. Int. Ed.* **2013**, *52*, 5368-5371.
- [7] Hara, H.; Hirano, M.; Tanaka, K. *Org. Lett.* **2008**, *10*, 2537-2540.
- [8] a) Chopade, P. R.; Louie, J. *Adv. Syn. Catal.* **2006**, *348*, 2307-2327. b) Heller, B.; Hapke, M. *Chem. Soc. Rev.* **2007**, *36*, 1085-1094. c) Varela, J. A.; Saa, C. *Synlett* **2008**, 2571-2578.
- [9] Tanaka, K.; Wada, A.; Noguchi, K. *Org. Lett.* **2005**, *7*, 4737-4739.
- [10] a) Hoberg, H.; Burkhart, G. *Synthesis* **1979**, 525-526. b) Young, D. D.; Teske, J. A.; Deiters, A. *Synthesis* **2009**, 3785-3790.
- [11] Ogoshi, S.; Ikeda, H.; Kurosawa, H. *Pure Appl. Chem.* **2008**, *80*, 1115-1125.
- [12] Yu, R. T.; Rovis, T. *J. Am. Chem. Soc.* **2006**, *128*, 2782-2783.
- [13] Yu, R. T.; Rovis, T. *J. Am. Chem. Soc.* **2006**, *128*, 12370-12371.
- [14] a) Perreault, S.; Rovis, T. *Chem. Soc. Rev.* **2009**, *38*, 3149-3159. b) Yu, R. T.; Lee, E. E.; Malik, G.; Rovis, T. *Angew. Chem. Int. Ed.* **2009**, *48*, 2379-2382.
- [15] Yu, R. T.; Friedman, R. K.; Rovis, T. *J. Am. Chem. Soc.* **2009**, *131*, 13250-13251.

- [16] Dalton, D. M.; Oberg, K. M.; Yu, R. T.; Lee, E. E.; Perreault, S.; Oinen, M. E.; Pease, M. L.; Malik, G.; Rovis, T.. *J. Am. Chem. Soc.* **2009**, *131*, 15717-15728.
- [17] Isolation and X-Ray analysis of a rhodium(I) phosphoramidite complex indicated a square planar complex, likely due to the ligands strong trans-effect.
- [18] Steric competition and concentration studies indicate that the alkyne and isocyanate preferentially undergo oxidative cyclization first, rather than initial reaction between isocyanate and alkene.
- [19] Dalton, D. M.; Rovis, T. *Org. Lett.* **2013**, *15*, 2346-2349.
- [20] Dalton, D. M.; Rappe, A. K.; Rovis, T.. *Chem. Sci.* **2013**, *4*, 2062-2070.
- [21] Aalbersberg, W. G. L.; Barkovich, A. J.; Funk, R. L.; Hillard, R. L.; Vollhardt, K. P. C. *J. Am. Chem. Soc.* **1975**, *87*, 5600.
- [22] Wakatsuki, Y.; Kuramitsu, T.; Yamazaki, H. *Tetrahedron. Lett.* **1974**, 4549. For diene formation with cobalt(II) pre-catalyst, see: Hilt, G.; Hess, W.; Harms, K. *Synthesis* **2008**, *1*, 75-78.
- [23] Gutnov, A.; Heller, B.; Drexler, H.-J.; Spannenberg, A.; Oehme, G. *Organometallics* **2003**, *22*, 1550-1553.
- [24] Gutnov, A.; Drexler, H.-J.; Spannenberg, A.; Oehme, G.; Heller, B. *Organometallics* **2004**, *23*, 1002-1009.
- [25] Gutnov, A.; Heller, B.; Fischer, C.; Drexler, H.-J.; Spannenberg, A.; Sundermann, B.; Sundermann, C. *Angew. Chem. Int. Ed.* **2004**, *43*, 3795-3797. For additional examples of chiral cobalt transformations, see: Jungk, P.; Taufer, T.; Thiel, I.; Hapke, M. *Synthesis* **2016**, *48*, 2026-2035.
- [26] Jungk, P.; Fischer, F.; Hapke, M. *ACS Catal.* **2016**, *6*, 3025-3029.
- [27] Varela, J. A.; Saa, C. *Chem. Rev.* **2003**, *103*, 3787-3801.



- [28] Bonaga, L. V. R.; Zhang, H.-C.; Gauthier, D. A.; Reddy, I.; Maryanoff, B. E. *Org. Lett.* **2003**, *5*, 4537-4540.
- [29] Cai, C.; Audet, M.; Synder, J. K. *Heterocycles* **2014**, *88*, 179-186. For more examples see: Tanaka, K. *Transition-Mediated Aromatic Ring Construction* **2013**, 3-35.
- [30] Many organic photo-redox catalysts have also been reported in recent years.
- [31] Prier, C. K.; Rankic, D. A.; MacMillan, D. W. C. *Chem. Rev.* **2013**, *113*, 5322-5363.
- [32] Tellis, J. C.; Primer, D. N.; Molander, G. A. *Science*, **2014**, *345*, 433-436.
- [33] Zuo, Z.; Ahneman, D. T.; Chu, L.; Terrett, J. A.; Doyle, A. G.; MacMillan, D. W. C. *Science*. **2014**, *345*, 437-440.
- [34] a) Terrett, J. A.; Cuthbertson, J. D.; Shurtleff, V. W.; MacMillan, D. W. C. *Nature*. **2015**, *524*, 330-334. b) Corcoran, E. B.; Pirnot, M. T.; Lin, S.; Dreher, S. D.; DiRocco, D. A.; Davies, I. W.; Buchwald, S. L.; MacMillan, D. W. C. *Science*. **2016**, *353*, 279-283.
- [35] Dunn, Peter. J.; Hii, K. K.; Krische, Michael. J.; Williams, Michael. T. *Sustainable Catalysis: Challenges and Practices for the Pharmaceutical and Fine Chemical Industries*, Wiley: Hoboken, NJ. **2013**.

## CHAPTER TWO

### Merging Photo-Redox and Cobalt Catalysis

#### 2.1 --- Background

The Rovis group's work on rhodium-catalyzed methods generated significant interest in cobalt catalyzed methods. To extend reactivity beyond the rhodium-based methods we performed a search of the literature to examine known cobalt pre-catalysts. Reports from Vollhardt, Brookhardt, and Petit indicate that a variety of isolable phosphine-ligated cobalt(0/I) and cobalt(I)cyclopentadienyl complexes (**Figure 2.1, A**) are competent catalysts in [2+2+2] cycloadditions<sup>[1]</sup>, hydroacylations<sup>[2]</sup>, and C-H activations<sup>[3]</sup> (**Figure 2.1, B**). Unfortunately, many of these pre-catalysts are air sensitive and rapidly decompose even under anaerobic conditions. This instability presents a barrier to the wide adoption of this methodology.

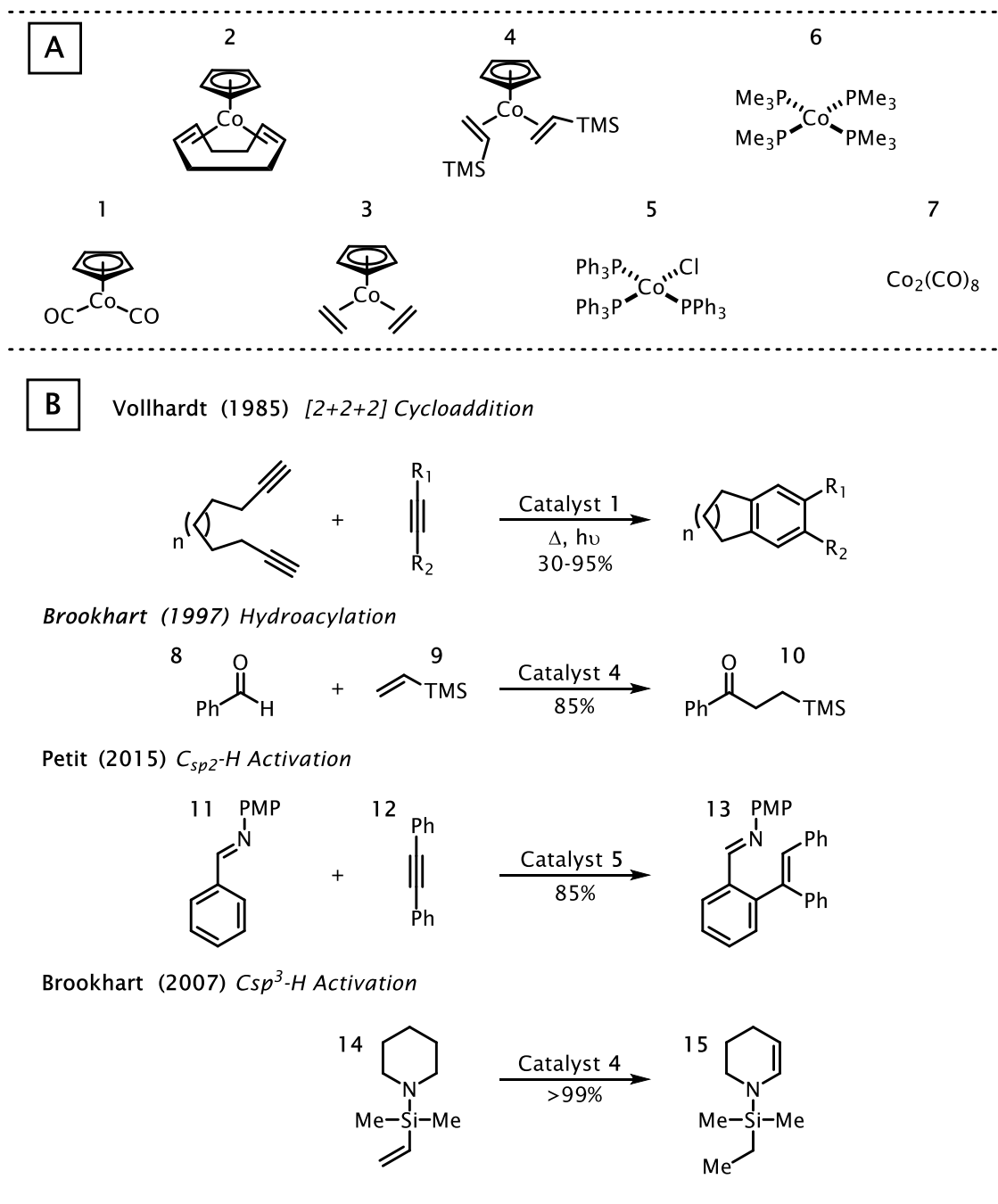


**Figure 2.1:** Low-Valent Cobalt Pre-catalyst and Reactivity

As an alternative to isolable pre-catalysts, low-valent cobalt species can also be generated *in situ* via reduction with heterogeneous metals or Grignard reagents from bench stable cobalt(II) precursors (**Figure 2.2**). This reductive approach allows chemists to manipulate reagents under ambient conditions and negates the need for isolating, storing, and handling unstable complexes.

Similarly, *in situ* reduction enables a variety of reactivity, including cobalt catalyzed [2+2+2] cycloadditions,<sup>[4]</sup> hydroacylation reactions,<sup>[5]</sup> and C-H bond activations<sup>[6]</sup>; however, this technique has drawbacks. For example, heterogeneous reducing agents are not pragmatic in large scale applications and the strongly basic/nucleophilic nature of Grignard reagents is incompatible with electrophilic or protic compounds. Although it does not necessarily prohibit its use, active species are often difficult to characterize, assign, or study because instability or rapid electron transfer events generate NMR-incompatible, paramagnetic species.

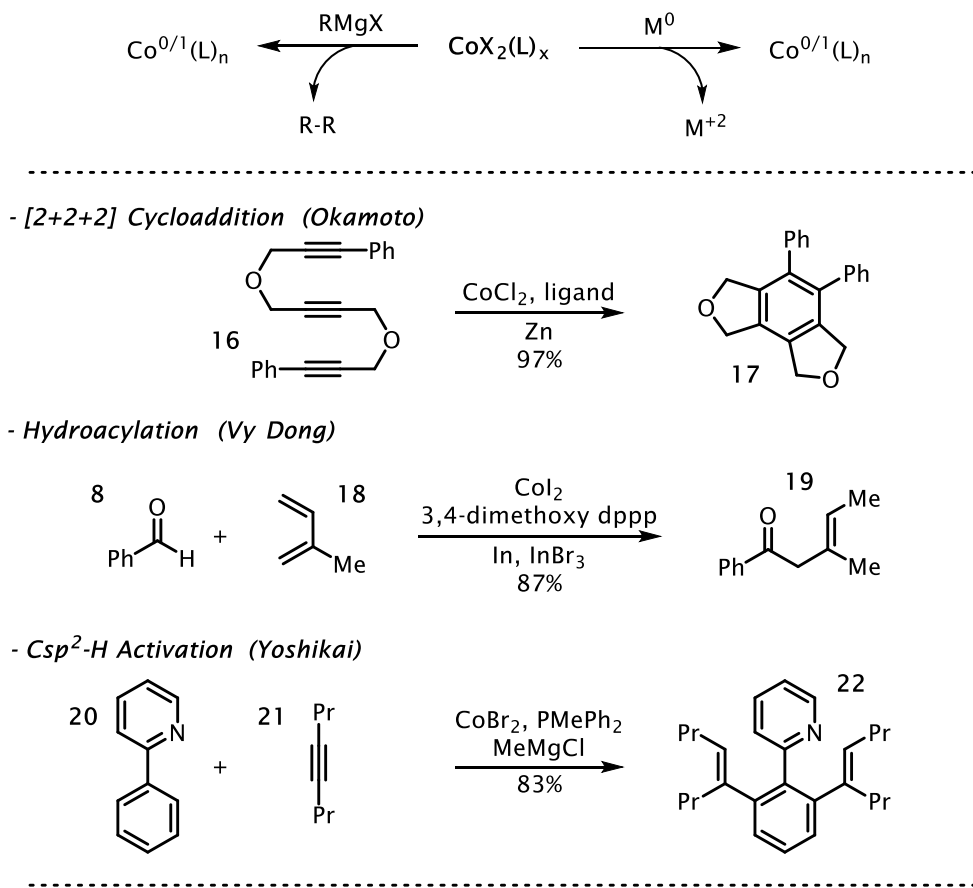


**Figure 2.2:** Reduction of Cobalt(II) Precursors and Reactivity

Low valent cobalt is notorious for its low barriers to electron transfer, therefore we believed a photo-redox catalyst could reduce cobalt to catalytically active species with benign sacrificial organic reductants. We also felt that the unprecedented combination of cobalt and photo-redox catalysts would offer unique and untapped reactivity. However, since metals that are often used as reductants for cobalt (i.e.: zinc and manganese) are moderately strong reductants, we initially questioned whether a photo-catalyst and sacrificial reductant would be sufficient to deliver an active species.

As shown in **Figure 2.3**, we envisioned that photoexcitation of  $\text{Ru}(\text{bpy})_3\text{Cl}_2$  would give  $\text{Ru}(\text{II})^*$  in the presence of a tertiary amine. Reductive quenching would then deliver the highly

reducing Ru(I) ( $E_{1/2}[\text{Ru}^{\text{II}}/\text{Ru}^{\text{I}}] = -1.33 \text{ V}$ ). The strong reductant Ru(I) should reduce the cobalt(II) pre-catalyst to active low-valent species **I**. We assumed intercepting low-valent cobalt with two equivalents of alkyne would result in an oxidative cyclization to give a cobaltacyclopentadiene intermediate **II**. Finally, insertion of a third equivalent of alkyne followed by reductive elimination from **III** would provide an arene product and ultimately regenerate the active cobalt catalyst.

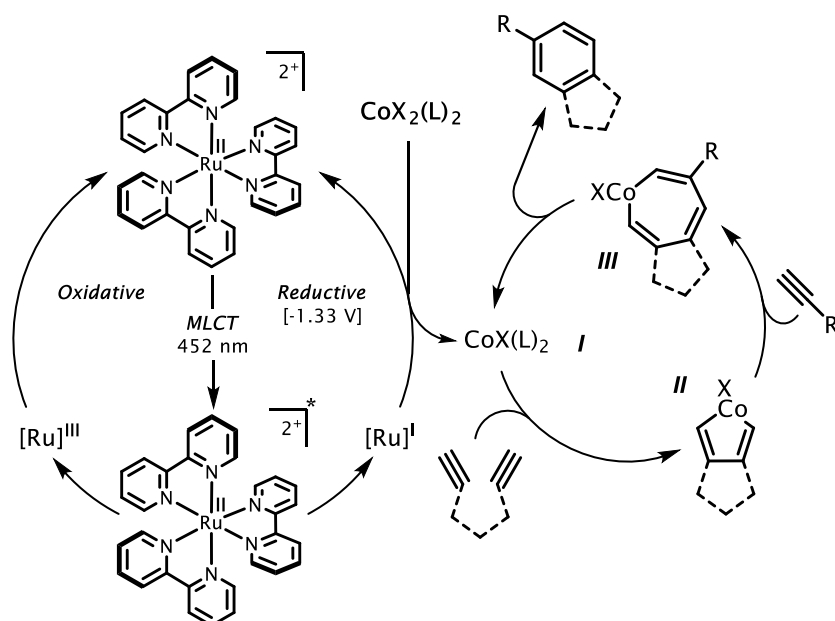


**Figure 2.3:** Proposed Reduction of a Cobalt Pre-Catalyst

## 2.2 --- Results and Discussion

### 2.2.1 -- Reaction Screening and Development

To explore the proposed idea, we began by investigating combinations of sacrificial organic reductants and photo-redox catalysts. Initially, the reaction of interest was a cobalt-catalyzed [2+2+2] cycloaddition between diyne **23** and phenylacetylene **24** to give **25**. This system served as a metric to determine which conditions are suitable to reduce bench stable cobalt(II) pre-catalysts. Using the high throughput experimentation platform at Colorado State University, the

initial experiment included six cobalt pre-catalysts, four photo-redox catalysts, two sacrificial organic reductants, and two solvents (**Figure 2.4**). Irradiating the wells was done with an LED array (472 nm) and a false bottom plate we specifically constructed for photo-redox catalysis.

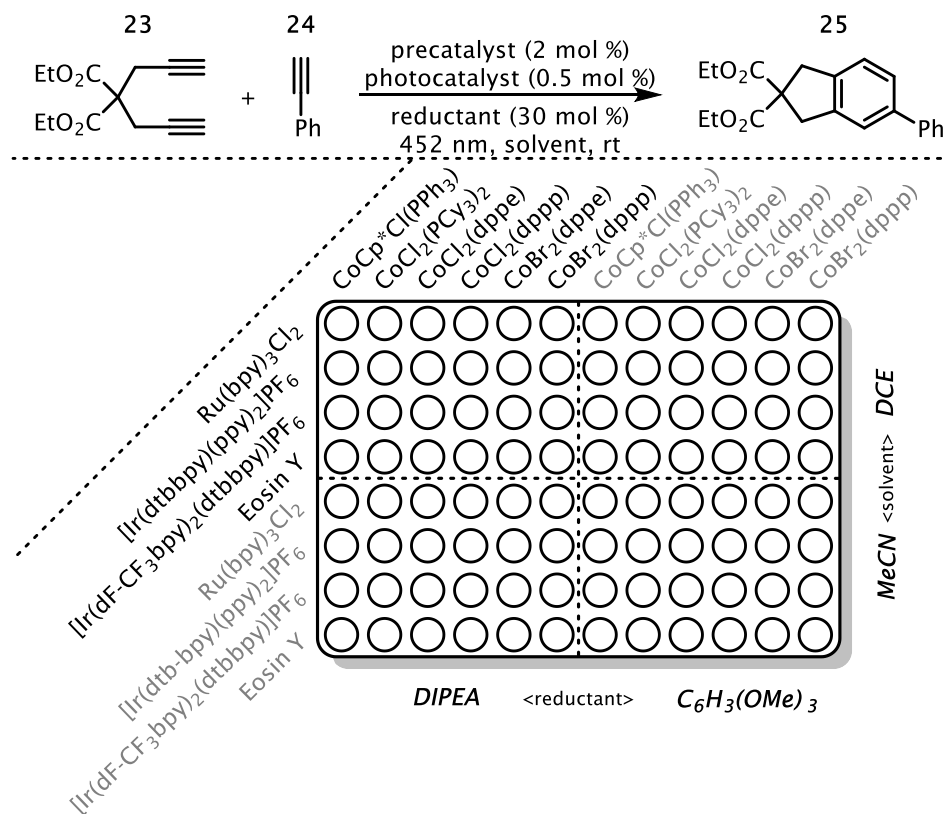


**Figure 2.4:** High Throughput Experiment With a Cobalt-Catalyzed [2+2+2] Cycloaddition

Analysis of this experiment via liquid chromatography with an internal standard indicated that several combinations of pre-catalysts and photo-catalysts provide reactivity (**Figure 2.5**). Although bidentate ligands such as diphenylphosphinoethane (dppe) and diphenylphosphinopropane (dppp) provide low reactivity, the large electron-rich alkyl phosphine-containing pre-catalyst  $\text{CoCl}_2 \cdot (\text{PCy}_3)_2$  delivers **25** in yields up to 92%. Two photo-catalysts  $\{[\text{Ir}(\text{ppy})_2(\text{dtbbpy})]\text{PF}_6$  and  $[\text{Ir}(\text{dF-CF}_3\text{ppy})_2(\text{dtbbpy})]\text{PF}_6\}$  function equally well in both solvents, DCE and MeCN. The common photo-catalyst quencher, diisopropylamine (DIPEA), appears

superior. Yet, under certain circumstances, the electron-rich aromatic reductant, trimethoxybenzene ( $C_6H_3(OMe)_3$ ), is marginally better. Upon scale-up, however, this did not remain consistent.

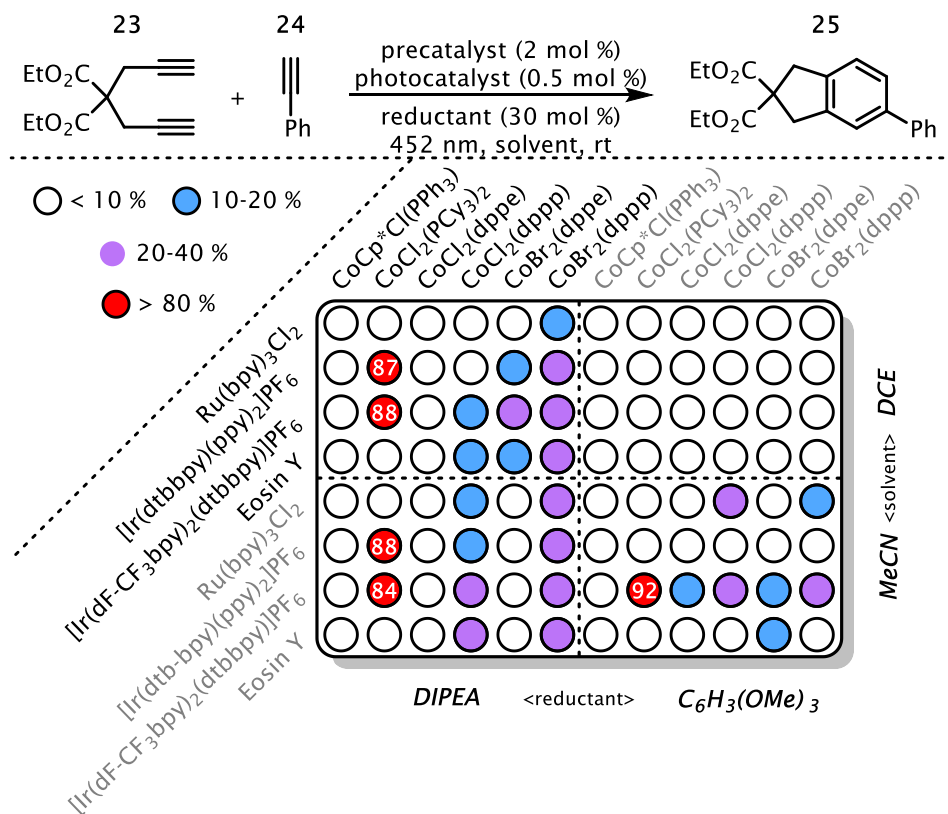


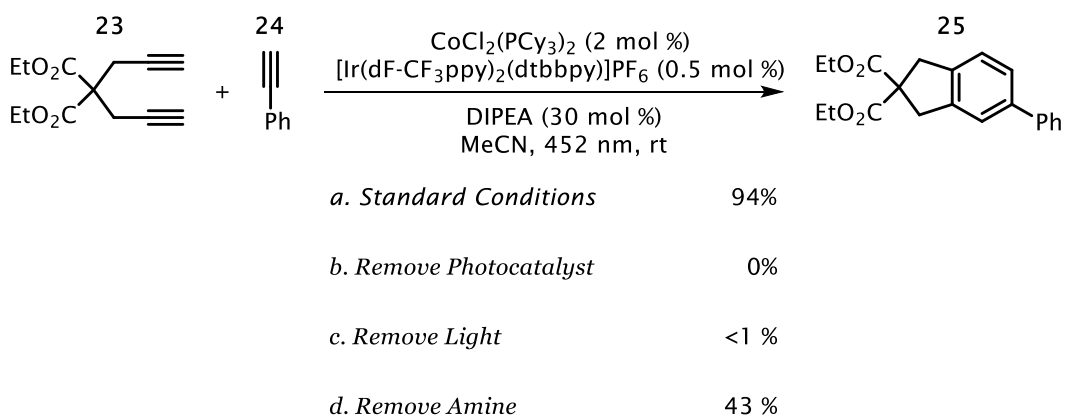
**Figure 2.5:** Analysis of High Throughput Experiment

To determine which reaction components are essential for reactivity, we conducted a battery of control experiments (**Table 2.1**). Removal of the photo-catalyst shuts down reactivity entirely (**Table 2.1, b**). Additionally, irradiation of the reaction for three hours without a photo-catalyst gives no product, suggesting that the photo-catalyst is absolutely required. Excluding light from the reaction (**Table 2.1, c**) also hinders catalysis, implying excitation of the photo-catalyst to the excited state is necessary for catalysis. Lastly, omission of the sacrificial organic reductant (DIPEA) delivers product, but in diminished yield (**Table 2.1, d**). It is conceivable that without a

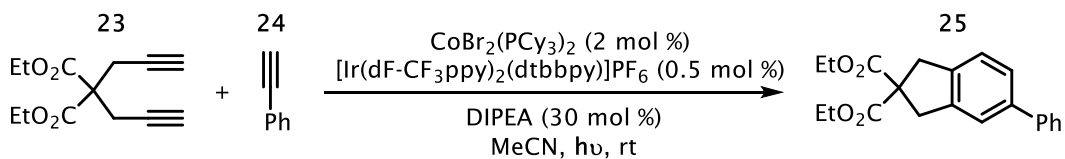


sacrificial reductant present, the photo-catalyst is reductively quenched by unbound tricyclohexylphosine (PCy<sub>3</sub>) [ $E_{1/2} = 0.87$  V vs. SCE]. This alternative reductive quenching event would explain the decrease in yield, assuming that an effective decrease in ligand loading by oxidation would decrease the amount of ligand available to the active cobalt species.

**Table 2.1:** Examination of Reagent Importance



During reaction development, the LEDs used were mainly narrow band blue LEDs in the 450 nm to 470 nm range with various wattage levels. To be certain the reaction proceeds under different wavelengths, we also included a short screen of light sources (**Table 2.2**). Both violet (410 nm) and blue (450 nm) 35 Watt Kessel LEDs performed well, delivering high yields with short reaction times (**Table 2.2**, entry 1 and 2). A common household 14-Watt compact fluorescent light bulb (CFL) also provides high yield in one hour (**Table 2.2**, entry 3)—indicating that powerful light sources are not required. Strict control of ambient light and substitution with red LEDs (590 nm) provides trace product. Considering that the UV-Vis absorption of the photocatalyst used has a  $\lambda_{\text{max}}$  of 380 nm, it is no surprise catalysis is limited when using low energy light.

**Table 2.2:** Various Light Sources are Competent for Reactivity

Entry	Light Source	Time (hr)	Yield (%)
1	410 nm Kessel (35 W)	1	92
2	452 nm Kessel (35 W)	1	96
3	14 W CFL	1	98
4	590 nm LED	24	1%

After screening several photo-catalysts, we investigated various phosphine ligands (**Figure 2.6**). Acyclic alkyl phosphines **27** and **28** also deliver product in 60% and 32% yields respectively. However, tri-tertbutyl phosphine **29** gives no conversion, likely due to its sterically demanding cone angle, which may prevent coordination and stabilization of the catalyst. The electron-rich and aromatic tri-paramethoxyphenyl phosphine **30** is also competent in the reaction, but similarly substituted ligands **31** and **32** provide little or no reactivity. Notably, aromatic phosphines (**34-36**) give no activity, but bidentate and electron-rich alkyl phosphines (**33** and **37**) provide product in moderate yields.

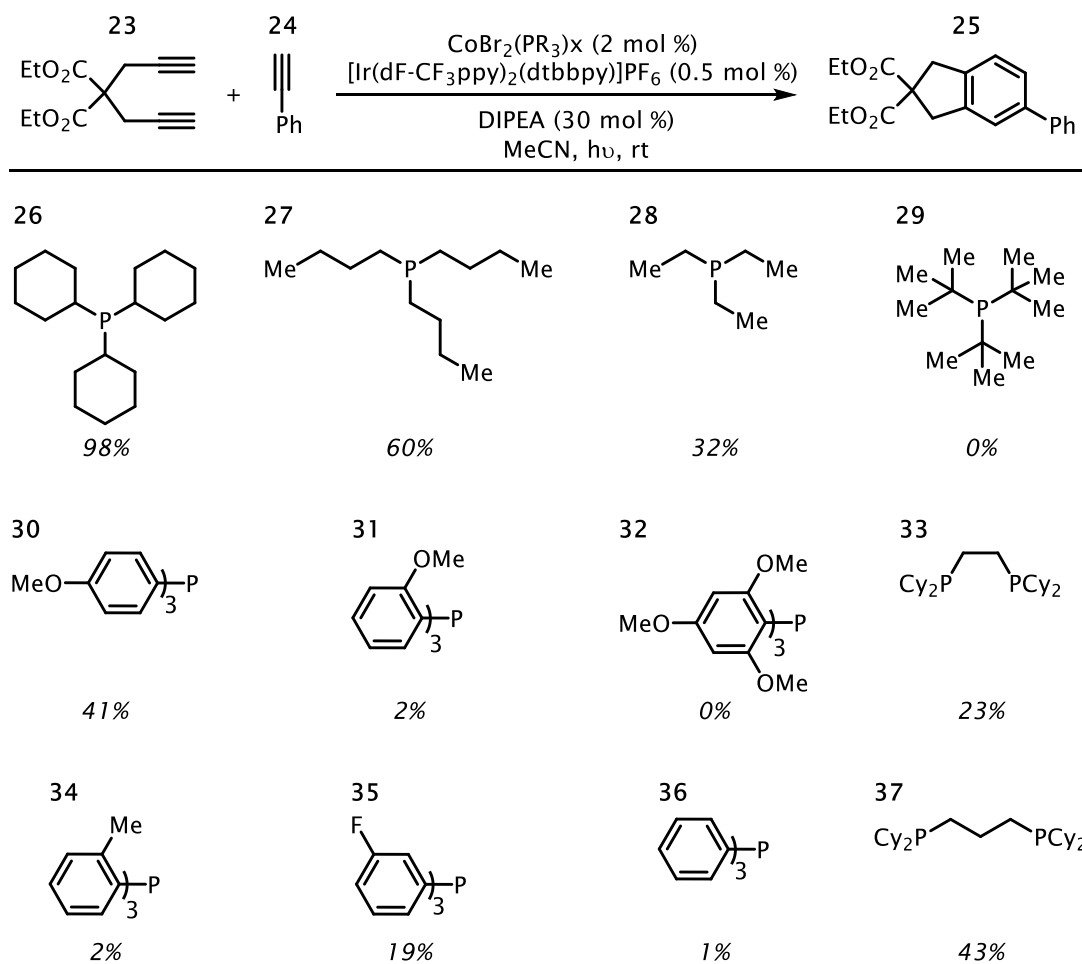


**Figure 2.6:** Additional Ligand Screen

Lastly, little difference in reactivity is observed between complexes containing bromide (**39**) or chloride (**40**) counterions (**Figure 2.7**). Although the iodide containing pre-catalyst  $\text{CoI}_2 \cdot (\text{PCy}_3)_2$  (**38**) gives low levels of reactivity (34%), acetate complex **41** gives yields closer to the chloride-containing pre-catalyst (68%).

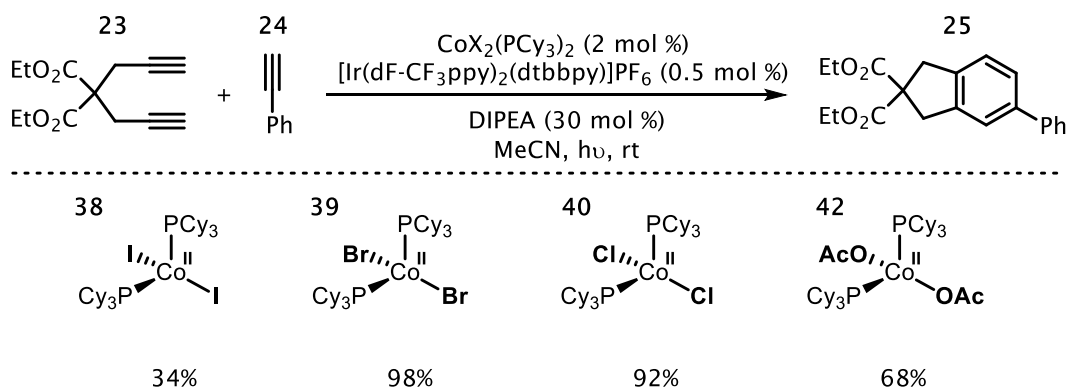


**Figure 2.7:** Impact of the Pre-Catalyst Counterion

### 2.2.2 -- Substrate Scope and Limitations

With optimized conditions in hand, we then explored reaction scope. As shown in **Figure 2.8**, it is clear the reaction tolerates a wide variety of substituted diynes. These diynes include various diesters, beta-keto esters and beta diketones (**42-44**, **46-48**). Electron-rich and electron-deficient aryl alkynes are also tolerated (**50**, **51**). Cyclopropyl-substituted phenyl acetylene performs well as the corresponding product is isolated in 67% yield (**45**). It is particularly interesting that the electron rich para-dimethylamino moiety (**50**) ( $E_{1/2} = 0.85$  V vs SCE) is not detrimental to the reaction given the opportunity for  $p\text{NMe}_2$  oxidation.

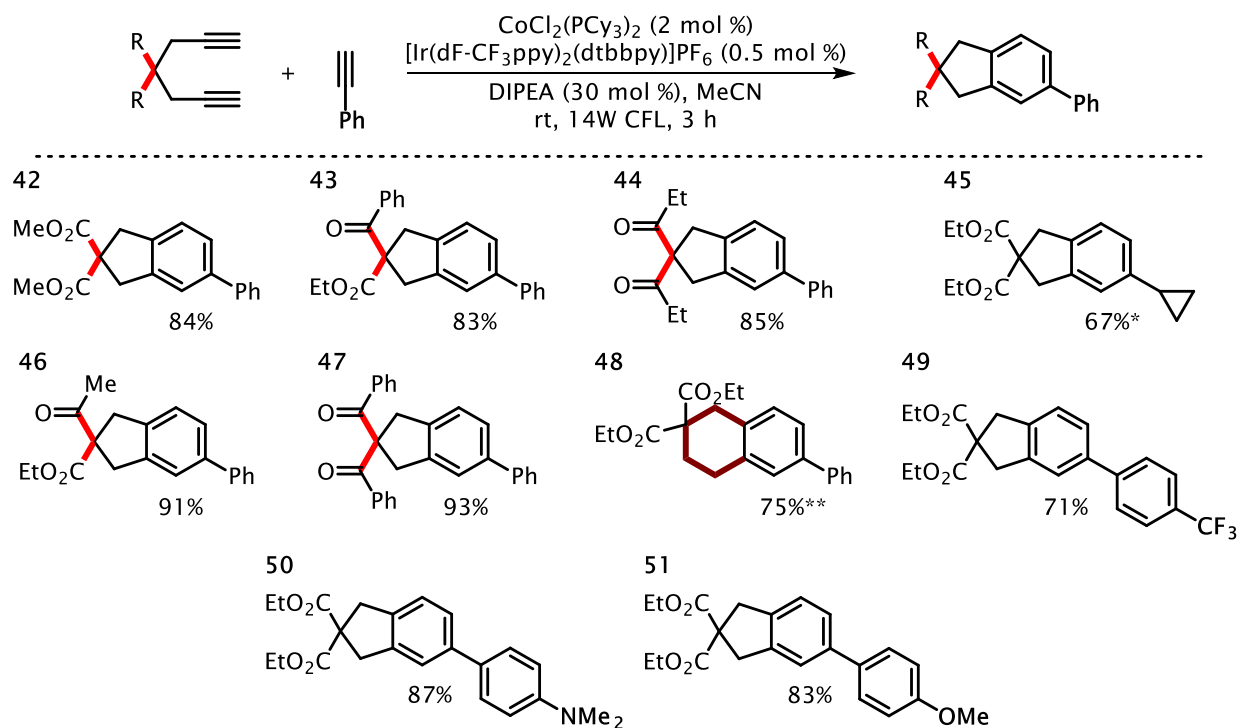


**Figure 2.8:** Modifications to Diyne and Aryl Alkyne Substitution

Aliphatic alkynes also participate, but generally require extended reaction times to deliver good yields (**Figure 2.9**). Substrates bearing nitrogenous or oxygenated functional groups, often problematic for metal catalysis, also provide product in excellent yield (**55, 56**). Di-substituted alkynes participate, but require longer reaction times in addition to slightly elevated temperatures to reach acceptable yields (**57-60**).

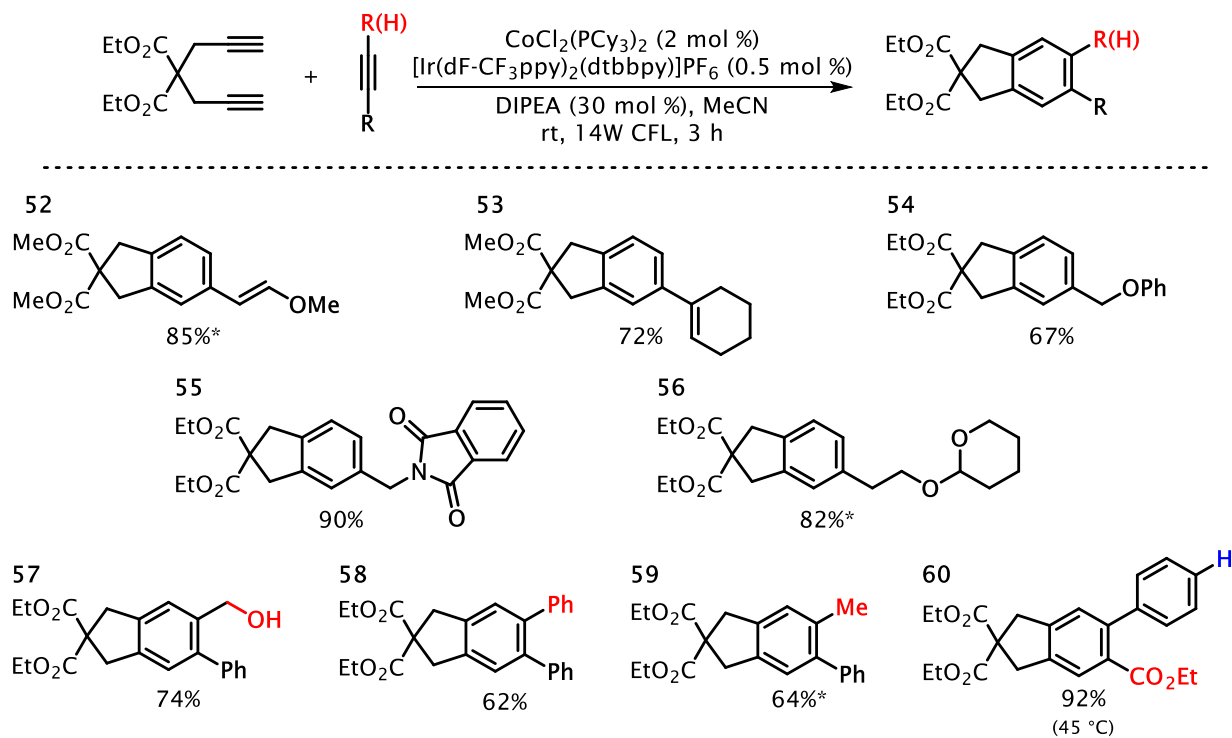


**Figure 2.9:** Aliphatic and Di-Substituted Alkynes

Finally, we found that the Thorpe-Ingold effect is not a necessity as compounds **61** and **62** furnish their corresponding arenes in 68% and 60% yields respectively (**Figure 2.10**). Higher levels of conversion for compound **62** are observed when dichloromethane is used as the solvent, as opposed to acetonitrile. This could be because acetonitrile may be involved in the reaction pathway, resulting in a depressed yield. Substrates **63** and **64** demonstrate a surprising tolerance to secondary amides and amino esters, which are often problematic in many metal catalyzed reactions.

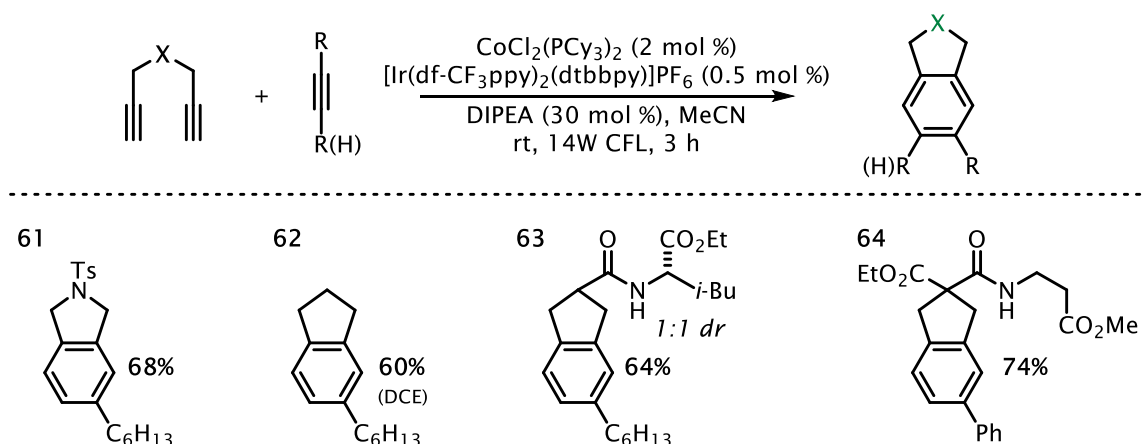


**Figure 2.10:** Substrates Without a Thorpe-Ingold Effect and With Coordinating Groups

Despite a wide variety of compounds undergoing the [2+2+2] cycloaddition, several substrates do not provide product (**Figure 2.11**). All attempts to couple alkenyl isocyanate **65** and diazo **68** to aryl or aliphatic alkynes proved fruitless. Additionally, the expected alkyne trimerization byproducts are not observed, suggesting that compounds **65** and **68** decompose the cobalt catalyst. Attempts to couple **66** and **67** with two equivalents of alkyne show slight consumption of starting material. Unfortunately, the desired products were not observed. Sterically demanding alkynes such as the tert-butyl alkyne **69** do not participate and the C-Br bond in compound **70** may be susceptible to oxidative addition by low-valent cobalt.

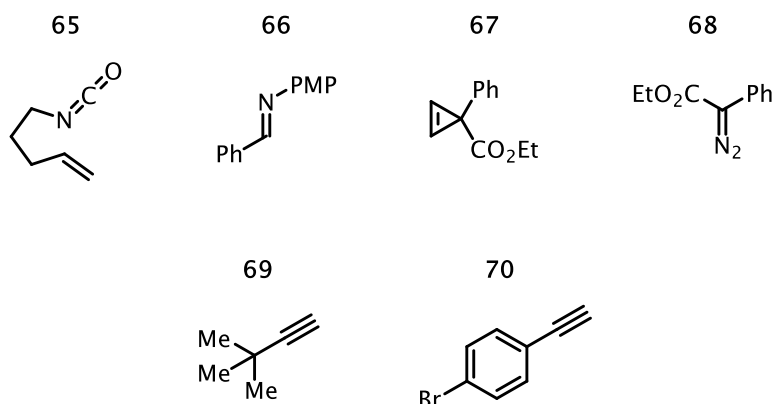


**Figure 2.11:** Substrates Which Do Not Participate

### 2.2.3 -- Investigating the Role of Light Radiation

After discerning that both light and photo-catalyst are necessary for reactivity we then questioned to what extent light is involved in the catalytic cycle. In essence, we wondered if catalysis is merely initiated or if the entire catalytic cycle relies on light irradiation. Despite a Yoon group publication cautioning about this type of experiment,<sup>[7]</sup> we followed the reaction progress while alternating periods of irradiation and darkness to gauge light's involvement in the catalytic cycle. Using liquid chromatography and an internal standard we gathered data on several reactions using three different cobalt pre-catalysts. Interestingly, the pre-catalyst  $\text{CoCl}_2\cdot(\text{dppp})$  delivers an active catalyst, but shows no response to light irradiation indicating no control beyond initiation (**Figure 2.12, a**).  $\text{CoCl}_2\cdot(\text{PEt})_2$  delivers product in higher yield, but with slightly different rates between "light on" and "light off" conditions (**Figure 2.12, b**). Although catalysis continues in periods of darkness, it is clear that periods of irradiation increase reactivity. It is difficult to conclude, but is conceivable that rates are influenced by initial reduction levels of the cobalt pre-catalyst.

Remarkably, the reaction profile of  $\text{CoCl}_2\cdot(\text{PCy}_3)_2$  contains large differences between "light on" and "light off" states (**Figure 2.12, c**). Initial irradiation for two minutes gives a yield of 28%, but removal of light arrests catalysis completely. A second irradiation period restarts catalysis and reaction progress can be further controlled by alternating between light "on" and "off" states. Ultimately the reaction reaches high yields in less than ten minutes of total irradiation, and allows control throughout the entire duration of the reaction. This observation will further be addressed in the following mechanism section (1.2.6).



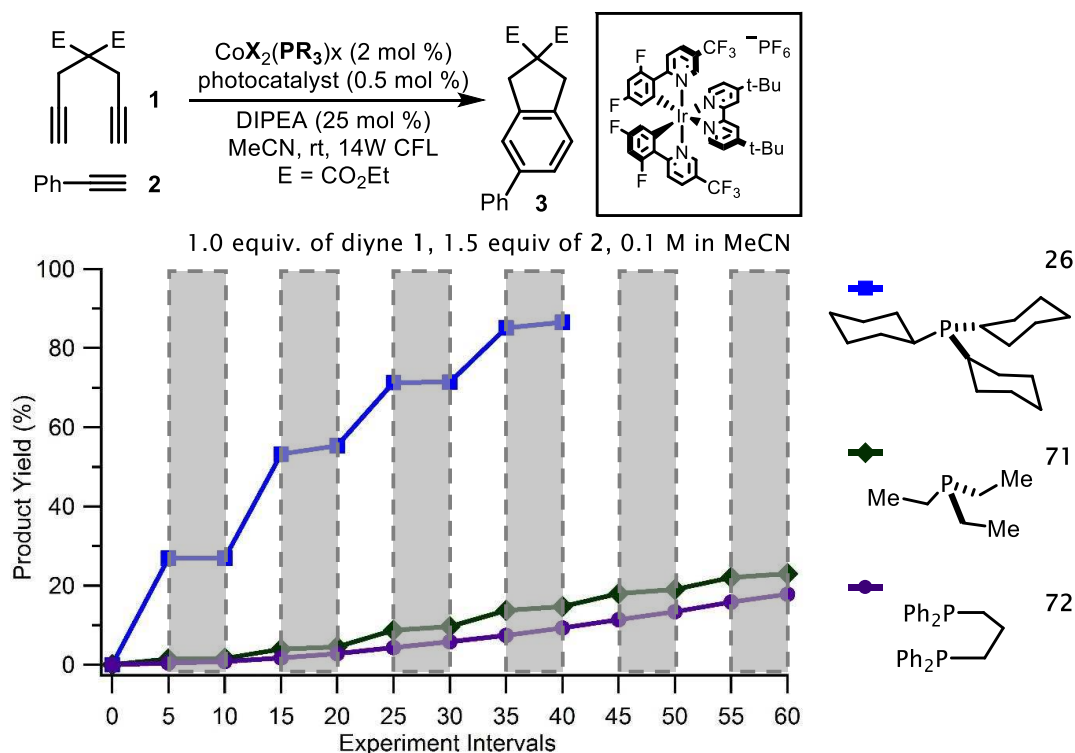


**Figure 2.12:** Comparing Pre-Catalysts in Light and Dark Periods

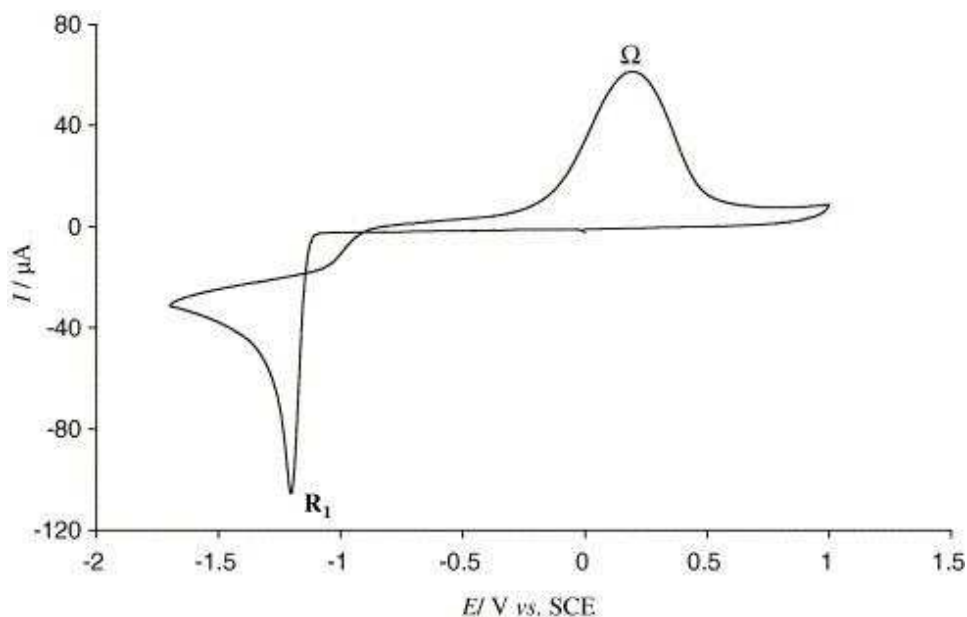
Thus far, we found that a photo-redox catalyst, coupled with a sacrificial organic reductant and light, is capable of reducing a cobalt(II) pre-catalyst to an active [2+2+2] cycloaddition catalyst. We also discovered that the presence light radiation is responsible for large differences in reaction rates and is directly influenced by the ligand. The reaction tolerates a variety of diene substrates and substituted alkynes and, in general, reaction times are short even at room temperature. At this point we believed mechanism studies and CV experiments would potentially reveal an origin for the unique reactivity observed.

#### 2.2.4 -- Mechanistic Investigation (Electrochemistry)

Control studies and additional light studies strongly suggest that photo-catalytic reduction of the cobalt pre-catalyst is required for catalysis. Although the photo- and electrochemical properties of iridium-based photo-catalysts are well studied, electrochemical potentials of

phosphine-based cobalt(II) complexes are not well documented. To obtain this data, we used various voltammetry techniques to measure half-wave potentials and investigate low-valent cobalt stability after reduction of the cobalt(II) pre-catalysts.

Although few in number, electrochemical studies of cobaltous halide salts have been reported in the literature. Périchon and coworkers have reported that cobalt(I) is not adequately stabilized in the absence of additives such as acetonitrile<sup>[8]</sup>, pyridine, or metal salts (ie: ZnBr<sub>2</sub>).<sup>[9]</sup> Relative to the reduction event **R**<sub>1</sub> in **Figure 2.13**, CV experiments show that no anodic current (**O**<sub>1</sub>) is observed during the oxidative sweep. Instead, at more oxidizing potentials, a broad anodic current is measured and **Ω** is indicative of material being oxidized from the electrode surface.

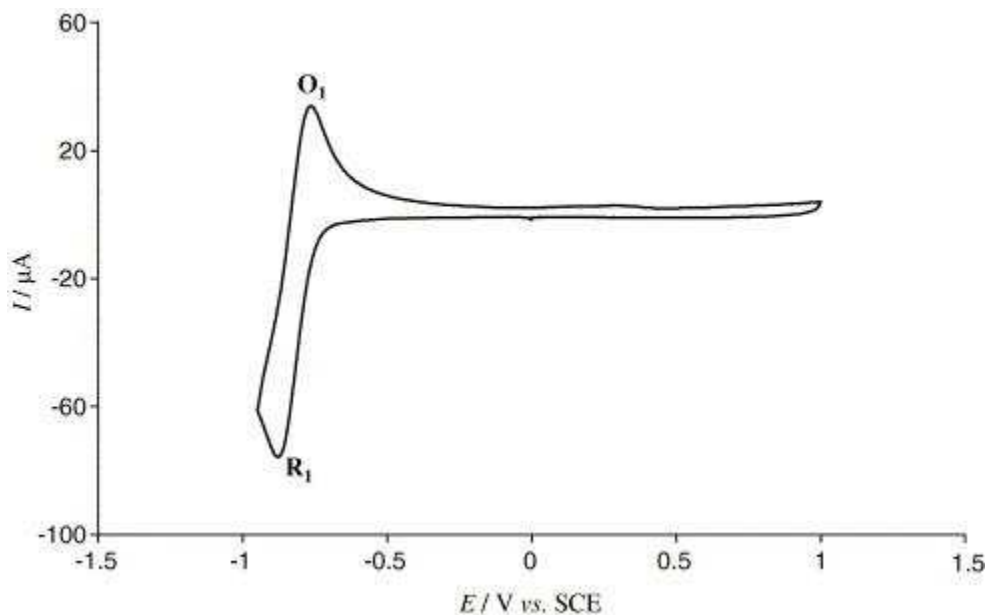


(3mM Co(BF<sub>4</sub>)<sub>2</sub> in DMF, 3-mm glassy carbon, 100 mV/s, 0.1 M TBAPF<sub>4</sub>)

**Figure 2.13:** Cobalt(I) Rapidly Decomposes Without Additive <sup>[8]</sup>

However, addition of acetonitrile (or other additives) sufficiently stabilizes cobalt(I). In acetonitrile, the half-wave for Co<sup>II/I</sup> (**R**<sub>1</sub>/**O**<sub>1</sub>) is now reversible even at slow scan rates (V/s < 200

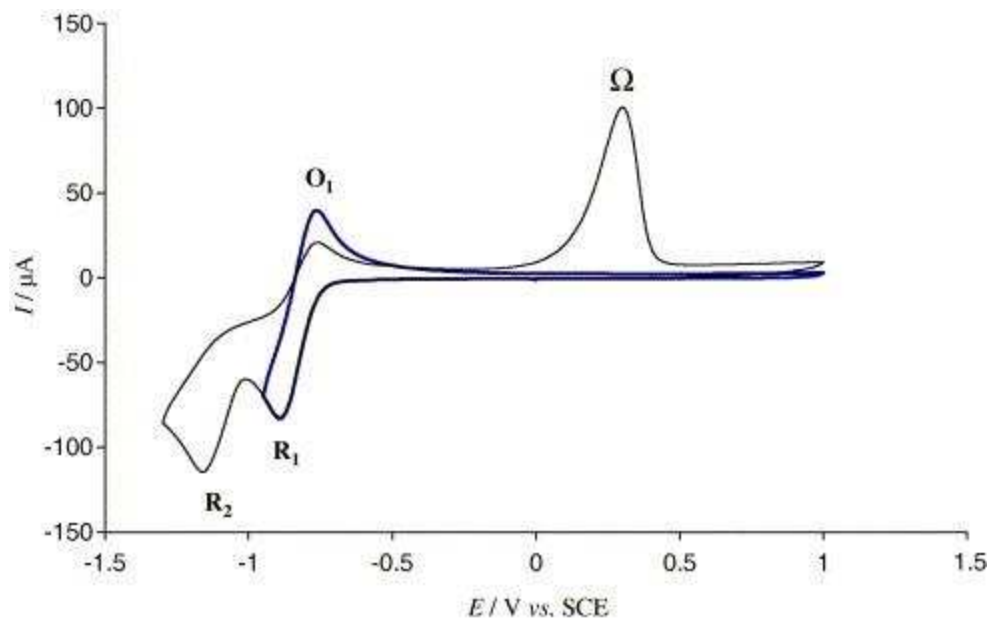
mV/s). Since cobalt(I) persists and is re-oxidized during the anodic sweep, the broad oxidation ( $\Omega$ ) is no longer observed (**Figure 2.14**).



(3mM  $\text{Co}(\text{BF}_4)_2$  in MeCN, 3-mm glassy carbon, 100 mV/s, 0.1 M TBAPF<sub>4</sub>)

**Figure 2.14:** An Additive Stabilizes Cobalt(I) <sup>[8]</sup>

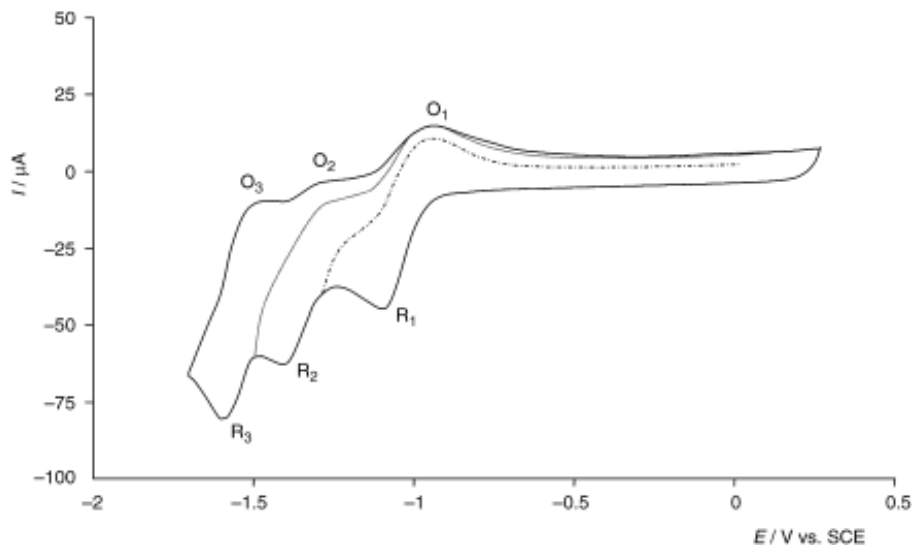
Périchon further confirms that the plating event  $\Omega$ , first observed in the absence of an additive, likely results from an unstabilized cobalt(0). To test this hypothesis, larger negative potentials were applied to force cobalt(I) reduction and therefore, cobalt(0) formation. This alternative generation of cobalt(0) again leads to signs of electrode fouling ( $\Omega$ ) (**Figure 2.15**). This could also be explained by lack of an additive to stabilize cobalt(I), which can lead to disproportionation wherein two equivalents of cobalt(I) generate one equivalent of cobalt(II) and one equivalent of cobalt(0), is the dominant reaction pathway. Whether cobalt(0) is formed by disproportionation or direct reduction. Thus, cobalt(0) is certainly responsible for electrode fouling and the broad anodic current  $\Omega$  observed by CV.



(5mM  $\text{Co}(\text{BF}_4)_2$  in DMF, 3-mm glassy carbon, 100 mV/s, 0.1 M TBAPF<sub>4</sub>)

**Figure 2.15:** Electrogeneration of Cobalt(0) and Electrode Fouling <sup>[8]</sup>

In a separate report, Périchon also finds the highest stability for cobalt is obtained using bipyridine ligands. This is reflected in the voltammogram of  $\text{CoBr}_2 \cdot (\text{bpy})$  which shows three quasi-reversible reduction waves at a glassy carbon electrode (**Figure 2.16**).<sup>[9]</sup> The redox couples **R<sub>1</sub>/O<sub>1</sub>** and **R<sub>2</sub>/O<sub>2</sub>** correspond to  $E_{1/2}[\text{Co}^{\text{II}}/\text{Co}^{\text{I}}]$  and  $E_{1/2}[\text{Co}^{\text{I}}/\text{Co}^0]$  respectively, while the redox couple **R<sub>3</sub>/O<sub>3</sub>** is a ligand reduction  $E_{1/2}[\text{Co}^0/(\text{Co}^0)^{\bullet-}]$ . It is worth noting that the observed currents are similar in magnitude and the voltammogram is absent of any features reminiscent of electrode fouling.

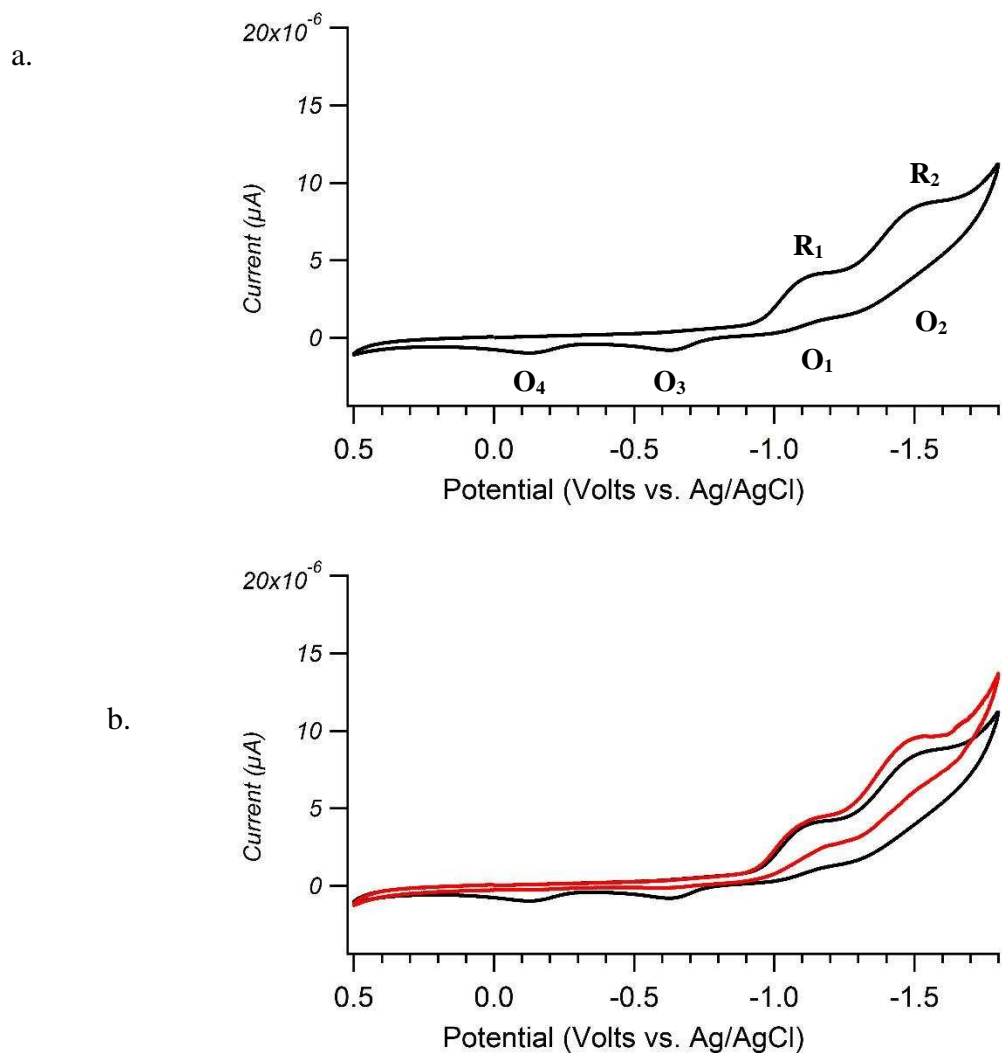


(5mM CoBr<sub>2</sub>(bpy) in MeCN, 2-mm glassy carbon, 200 mV/s, 0.1 M TBAPF<sub>4</sub>)

**Figure 2.16:** Cyclic voltammogram of CoBr<sub>2</sub>•(bpy) at a glassy carbon electrode<sup>[9]</sup>

We began our electrochemical studies using cyclic voltammetry and a 5 mM CoBr<sub>2</sub>•(PCy<sub>3</sub>)<sub>2</sub> solution in acetonitrile using a 1mm-disc glassy carbon electrode (**Figure 2.17, a**). The first cathodic sweep reveals two reduction waves (**R<sub>1</sub>**, **R<sub>2</sub>**) which we tentatively assigned as  $E_{1/2}[\text{Co}^{\text{II}}/\text{Co}^{\text{I}}]$  and  $E_{1/2}[\text{Co}^{\text{I}}/\text{Co}^0]$ . After the switching potential, a subsequent anodic sweep indicates the previous two reductions are quasi-reversible resulting in four oxidation half waves (**O<sub>1</sub>-O<sub>4</sub>**). Although the Co<sup>I</sup>/Co<sup>0</sup> couple (**O<sub>2</sub>**) passes marginally more anodic current than the analogous Co<sup>II</sup>/Co<sup>I</sup> (**O<sub>1</sub>**), both generate less current than expected. Continuing to higher potentials eventually shows that two additional oxidation events (**O<sub>3</sub>**, **O<sub>4</sub>**) are coupled to the previously observed Co<sup>II</sup>/Co<sup>I</sup> and Co<sup>I</sup>/Co<sup>0</sup> reductions, **R<sub>1</sub>** and **R<sub>2</sub>**. An additional stirred cyclic voltammogram shown in **Figure 2.17, b** further suggests the oxidations **O<sub>3</sub>** and **O<sub>4</sub>** result from the cathodic events. This is likely due to an EC mechanism where a chemical event follows reduction causing a large voltage separation in half-waves (ie: ligand loss, ligand association, solvent coordination, etc.). Stirred experiments are useful indicators of chemical changes since the electrode surface and

diffusion layer are constantly being refreshed following electron transfer. With this data we concluded that the cobalt pre-catalyst undergoes reduction, but does not display Nernstian or well behaved redox character.



(5 mM in MeCN, 1-mm glassy carbon electrode, 200 mV/sec, leak-less Ag/AgCl reference)

**Figure 2.17:** a) Cyclic voltammogram of  $\text{CoBr}_2 \cdot (\text{PCy}_3)_2$  b) A stirred CV illustrates potential chemical events occurring after electrochemical reductions.

Although cyclic voltammetry experiments were informative, the quasi-reversible nature of the pre-catalyst redox events led us to conduct square wave voltammetry to accurately measure  $E_{1/2}$  potentials (**Figure 2.18**). Unlike the linear sweeps conducted during cyclic voltammetry,

square wave voltammetry (SWV) uses a step-wise sequence of alternating pulse and sampling segments while incrementally increasing voltage. Fundamentally, measuring current at constant voltages minimizes the charging current caused by changing potential with a constant resistance ( $V=I \cdot R$ ). Consequently, faradaic current from the analyte is observed exclusively. From the SWV experiments we can assign the following half wave potentials:  $E_{1/2}[\text{Co}^{\text{II}}/\text{Co}^{\text{I}}] = -1.09 \text{ V vs. Ag}^+/\text{AgCl}$  and  $E_{1/2}[\text{Co}^{\text{I}}/\text{Co}^0] = -1.39 \text{ V vs Ag}^+/\text{AgCl}$ . Comparison of the reduced state photocatalyst potential ( $E_{1/2}[\text{Ir}^{\text{III}}/\text{Ir}^{\text{II}}] = -1.37 \text{ V vs SCE}$ ) to the first pre-catalyst reduction  $E_{1/2}[\text{Co}^{\text{II}}/\text{Co}^{\text{I}}]$  indicates an over potential of approximately 250 mV. Thermodynamically speaking, pre-catalyst reduction is favored. Additionally, SWV experiments illustrate the pre-catalyst's non-Nernstian behavior in a visually distinct way. Examination of the peak currents ( $I_{\text{pc}}$ ) in both reductions (**R**<sub>1</sub> and **R**<sub>2</sub>) reveals that they are not equivalent to the corresponding anodic currents ( $I_{\text{pa}}$ ) for **O**<sub>1</sub> and **O**<sub>2</sub>. When  $I_{\text{pc}} \neq I_{\text{pa}}$  it strongly suggests that decomposition or chemical changes follow reduction.

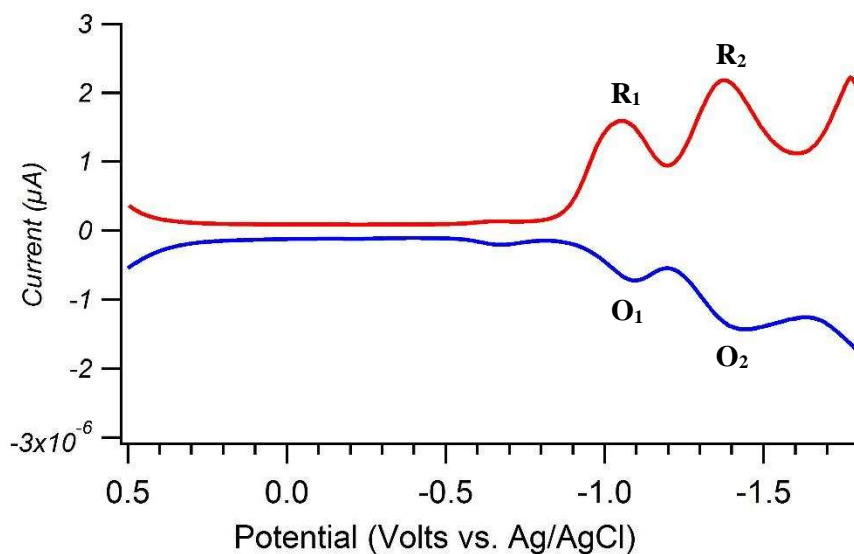
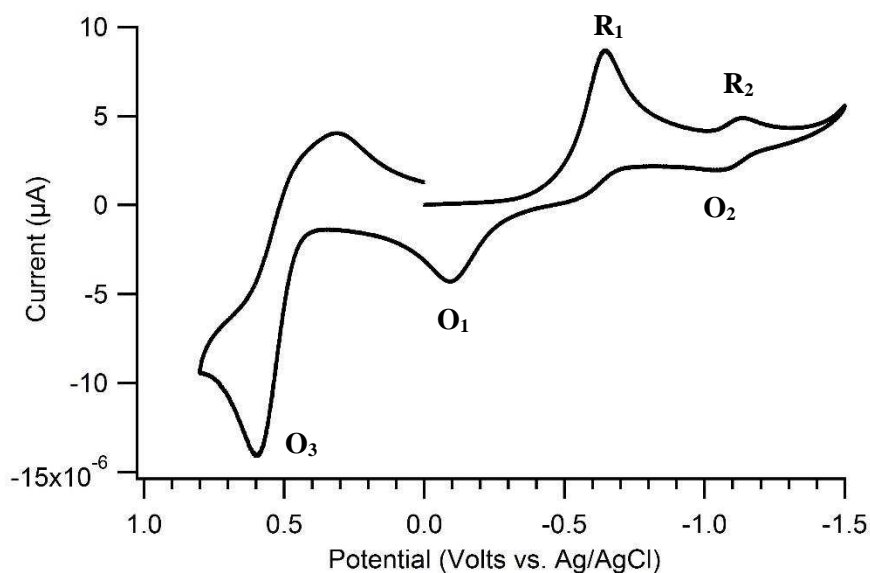


**Figure 2.18:** Half-Wave Potentials for Cobalt(II) Pre-Catalyst from Square Wave Voltammetry

Examining other pre-catalysts and their electrochemistry for comparison to the parent complex ( $\text{CoBr}_2 \cdot (\text{PCy}_3)_2$ ) also gives informative insight. The pre-catalyst  $\text{CoBr}_2 \cdot (\text{dppp})$ , which catalyzes the [2+2+2] cycloaddition in moderate yields, displays distinct electrochemical behavior (**Figure 2.19**). An initial cathodic sweep shows a large, irreversible reduction (**R<sub>1</sub>**). A subsequent anodic sweep reveals a broad oxidation event (**O<sub>1</sub>**), reminiscent of the electrode fouling observed by Périchon centered at -0.12 V vs Ag/AgCl. The large unimodal reduction wave **R<sub>1</sub>** is likely caused by the reduced species ( $\text{Co}^{\text{I}}$ ) undergoing rapid disproportionation. Therefore, distinct  $\text{Co}^{\text{II}}/\text{Co}^{\text{I}}$  and  $\text{Co}^{\text{I}}/\text{Co}^0$  half-waves are not distinguishable and appear as one broad wave. Undoubtedly, generation of cobalt(0) from the disproportionation causes the broad voltage separated oxidation **O<sub>1</sub>**. Although  $\text{CoBr}_2 \cdot (\text{dppp})$  is catalytically active, voltammetry suggests the dppp ligand is less stabilizing and possibly leads to the reduced yields observed.

The large anodic peak **O<sub>3</sub>** at +0.6 V and the well behaved redox couple (**R<sub>2</sub>/O<sub>2</sub>**) at -1.1 V also garnered interest. **O<sub>3</sub>** corresponds to oxidation of the dppp ligand and that the photo-catalyst can readily oxidize the phosphine ligand. This is undoubtedly another contributor to lower yields. Lastly, the redox couple at -1.1 V (**R<sub>2</sub>/O<sub>2</sub>**) is purportedly a bis-diphenylphosphinopropane cobalt(I)  $\{\text{Co}(\text{dppp})_2\text{X}\}$  formed by excess dppp present in solution via precipitation of insoluble metal(0) species.

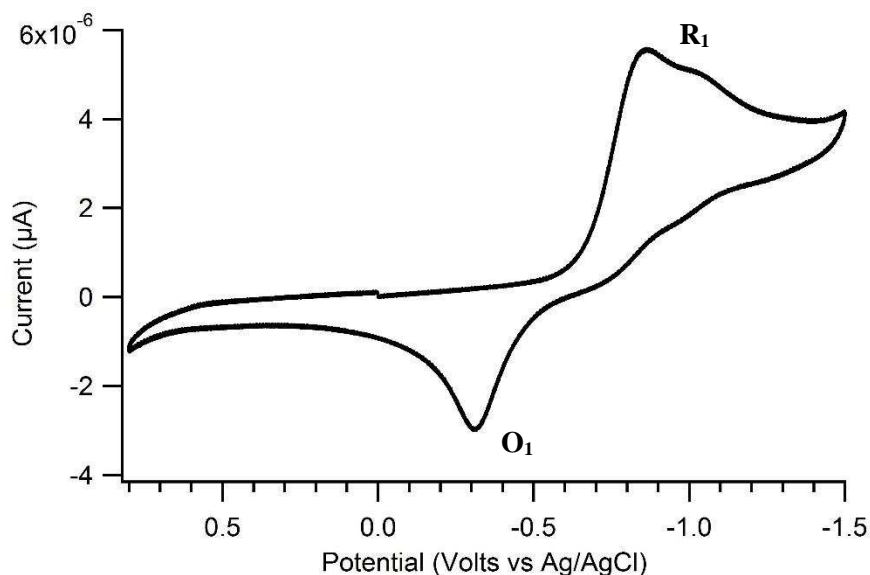




(5 mM in MeCN, 1-mm glassy carbon electrode, 200 mV/sec, leak-less Ag/AgCl reference)

**Figure 2.19:** Cyclic voltammetry on the pre-catalyst  $\text{CoBr}_2\cdot(\text{dppp})$

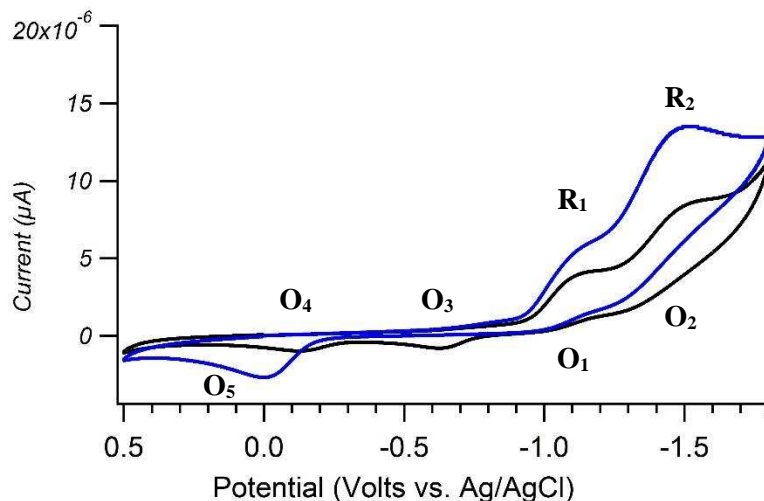
To correlate electrochemical differences to high, medium, and low reactivity pre-catalysts, we also performed voltammetry studies on  $\text{CoCl}_2\cdot(\text{PPh}_3)_2$  (**Figure 2.20**). Data suggests that the triphenylphosphine-containing complex is less stable relative to both  $\text{CoBr}_2\cdot(\text{dppp})$  and  $\text{CoBr}_2\cdot(\text{PCy}_3)_2$  after reduction. First, the broad cathodic wave (**R<sub>1</sub>**) and consequent **O<sub>1</sub>** again suggest high levels of disproportionation at cobalt(I). We propose the variation from bi-dentate to mono-dentate ligation leads to further destabilization and catalytically inactive decomposition products. As expected, the catalytic activity of each pre-catalyst qualitatively correlates to the instability reflected in the electrochemical experiments.



(5 mM in MeCN, 1-mm glassy carbon electrode, 200 mV/sec, leak-less Ag/AgCl reference)

**Figure 2.20:** Cyclic Voltammetry of  $\text{CoCl}_2 \cdot (\text{PPh}_3)_2$

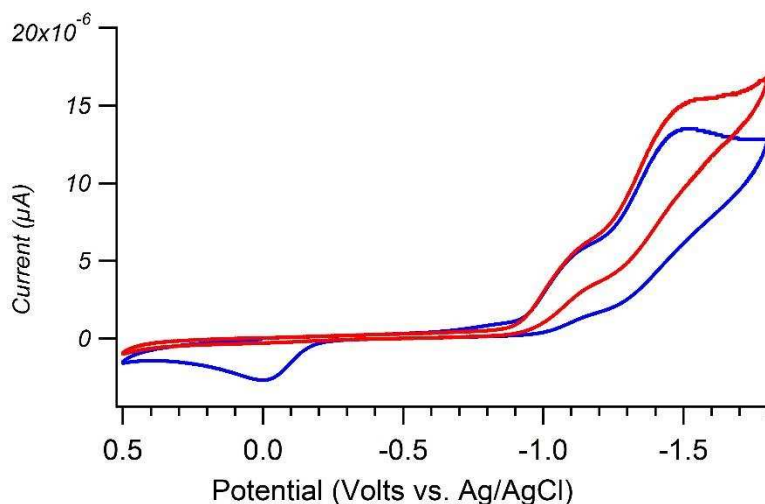
With a better understanding of the varying electrochemistry among pre-catalysts, we believed multicomponent voltammetry studies may provide mechanistic insight. To probe the validity of an oxidative cycloaddition with low-valent cobalt species, we conducted voltammetry experiments with the parent  $\text{CoBr}_2 \cdot (\text{PCy}_3)_2$  complex in the presence of 50 equivalents of bis-propargyl malonate ester **12** (**Figure 2.21**). Fascinatingly, voltammograms collected before and after substrate addition show increased cathodic current at **R1** and **R2**. This increase in current could be catalytic wave behavior; however, it could also be rationalized as increased analyte solubility due to diyne coordination. Furthermore, less current is observed at the  $\text{Co}^{\text{I}}/\text{Co}^0$  couple (**O2**) and the original anodic events **O3** and **O4** are no longer generated. We conclude these subtle changes in current suggest the diyne is intercepting the low valent cobalt—likely by an oxidative cyclization at cobalt(0).



(5 mM in MeCN, 50 eq. of diyne, 1-mm glassy carbon electrode, 200 mV/sec, leak-less Ag/AgCl reference)

**Figure 2.21:** Cyclic Voltammetry With Diyne Present

Appearance of the anodic wave (**O<sub>5</sub>**) centered around 0.00 V vs. Ag<sup>+</sup>/AgCl also supports an oxidative cyclization at cobalt(0). **O<sub>5</sub>** is only observed in the presence of the diyne substrate and has no corresponding cathodic wave (irreversibly oxidized). To confirm **O<sub>5</sub>** is generated by an EC mechanism, the same voltammogram is collected while stirring the vessel (**Figure 2.22**). Failure to observe **O<sub>5</sub>** supports an EC mechanism however, there are two caveats to bear in mind. 1) **O<sub>5</sub>** is a low valent cobalt species ligated and stabilized by diyne coordination and involves no oxidative cyclization, and 2) it could be the oxidative addition adduct to the terminal C-H bond of the alkyne functional group.



(5 mM in MeCN, 50 eq. of diyne, 1-mm glassy carbon electrode, 200 mV/sec, leak-less Ag/AgCl reference)

**Figure 2.22:** Stirred Voltammogram Suggests an EC Mechanism With Diyne

If an oxidative cyclization does occur, **O<sub>5</sub>** likely represent oxidation of a cobalt(II)cyclopentadiene to a cobalt(III)cyclopentadiene. Furthermore, upon oxidation the intermediate is immediately consumed by a chemical event or a reductive cheletropic extrusion. However, we cannot definitively conclude whether a cobalt(II) species would be the product of 1) an oxidative cyclization at cobalt(0), or 2) an oxidative cyclization at cobalt(I) followed by further reduction to cobalt(II) during the sweep to more negative potentials (**Figure 2.23**). To confirm either option, isolation of the species for further study would be required.

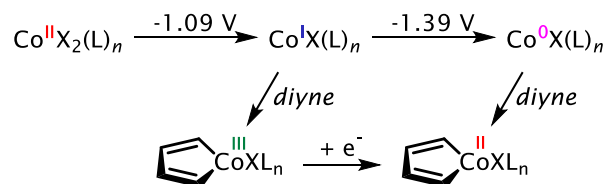
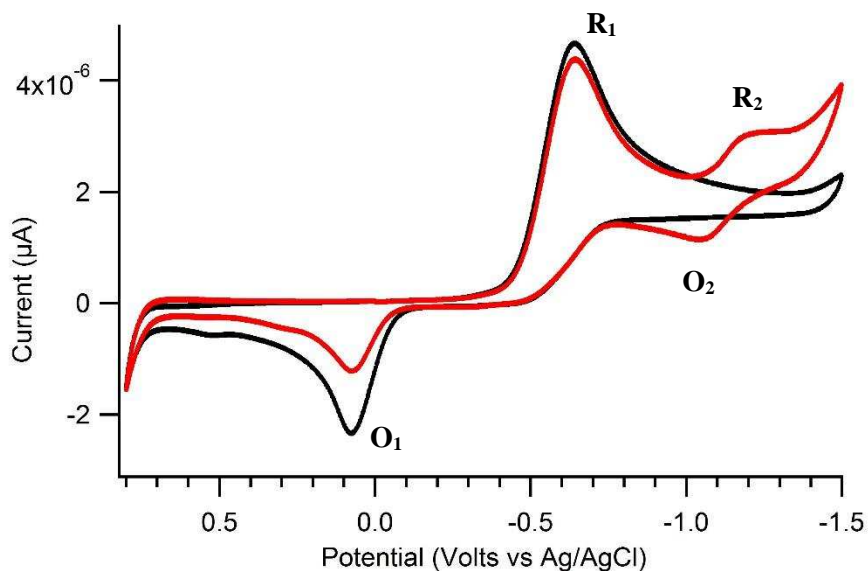


**Figure 2.23:** Possible Mechanism for Co(II) Intermediate

As a comparison to  $\text{CoBr}_2\cdot(\text{PCy}_3)_2$ , we also examined  $\text{CoBr}_2\cdot(\text{dppp})$  for any interaction with the diyne coupling partner (**Figure 2.24**). Shown in red, the voltammogram collected with 50 equivalents of diyne indicates little difference in current during the first reduction ( $\text{R}_1$ ). Interestingly, a new reversible redox couple, not observed when diyne is absent, now appears at -1.2 V vs. Ag/AgCl ( $\text{R}_2$ ). We believe this wave represents reduction of cobalt(I), but diyne coordination disfavors disproportionation. As a result the stabilized  $\text{Co}^{\text{I}}/\text{Co}^0$  displays a reversible and well behaved redox couple. In addition, with diyne present the extent of surface fouling is greatly diminished. This change is expected if diyne intercepts  $\text{Co}^{\text{I}}\text{Br}(\text{dppp})$  by oxidative addition. More broadly, chemical events are altered with diyne present. It is also conceivable that the  $\text{Co}^{\text{I}0}(\text{dppp})$  generated is not as susceptible to oxidative cyclization as well.



(5 mM in MeCN, 50 eq. of diyne, 1-mm glassy carbon electrode, 200 mV/sec, leakless Ag/AgCl reference)

**Figure 2.24:**  $\text{CoBr}_2\cdot(\text{dppp})$  Show No Cathodic Current Increase

Based on electrochemical data, it is our opinion that the pre-catalyst  $\text{CoCl}_2\cdot(\text{PCy}_3)_2$  stabilizes low valent cobalt the most effectively. This added stability allows the persistence of low-valent cobalt species in solution and ultimately leads to high product conversions. By comparison,

all other pre-catalysts which deliver lower product yields show greater amounts of low-valent disproportionation.

### 2.2.5 – Mechanistic Insight (Investigation of Light, Dark and Heat)

To continue investigation of the mechanism, we sought to learn more about the relationship between light radiation and thermal energy. We were interested to see whether the reaction can be conducted thermally, completely in the absence of light. Also, we wanted to determine if the reaction could be controlled with either light or heat after pre-catalyst reduction. Two experiments were conducted introducing heat and light at strategic reaction times to probe these questions. The first experiment starves the reaction of light. Without any light radiation the reaction provides no reactivity after being held at 80° C for 8 hours (**Figure 2.25**). This experiment undoubtedly demonstrates that pre-catalyst reduction cannot be done thermally and requires light radiation. In addition, this corroborates the voltammetry data which indicates pre-catalyst reduction potentials are thermodynamically accessible. With this data in hand, focus shifted to examining how thermal energy effects the reaction after the pre-catalyst is converted into an active catalyst by photo-reduction.

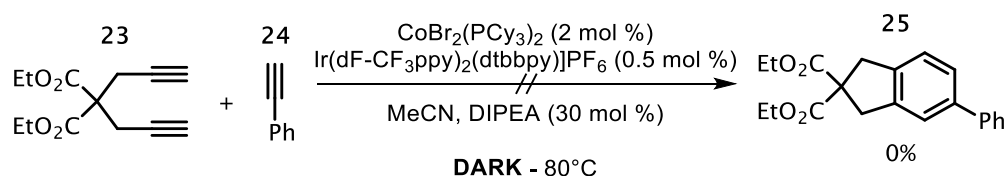


**Figure 2.25:** Strict Thermal Conditions Offer No Product

To probe whether this reaction can be driven thermally after pre-catalyst reduction, we conducted the experiment shown in **Figure 2.26**. Initial radiation for three minutes provides a yield of 46% which unambiguously indicates the pre-catalyst has been reduced. Removing light

radiation arrests catalysis and two reaction aliquots indicate little increase in product yield after 30 minutes of darkness. Next, the vessel was wrapped with aluminum foil to remove light and placed in a heating block at 80° C. After 15 minutes, the reaction yield increases from 46% to 79%. Surprisingly, after a second 15 minute period of heating no change in yield is observed. Despite reaction failure under thermal conditions, a subsequent three minute period of irradiation at room temperature restores catalysis and delivers a yield of 86%. We believe this data suggests an inhibited, on-cycle intermediate which requires either photo-catalyst *or* absorption of heat energy in order to proceed forward. However, thermal conditions eventually leads to decomposition and inactive intermediates—one of which is seemingly reactivated by photo-reduction.

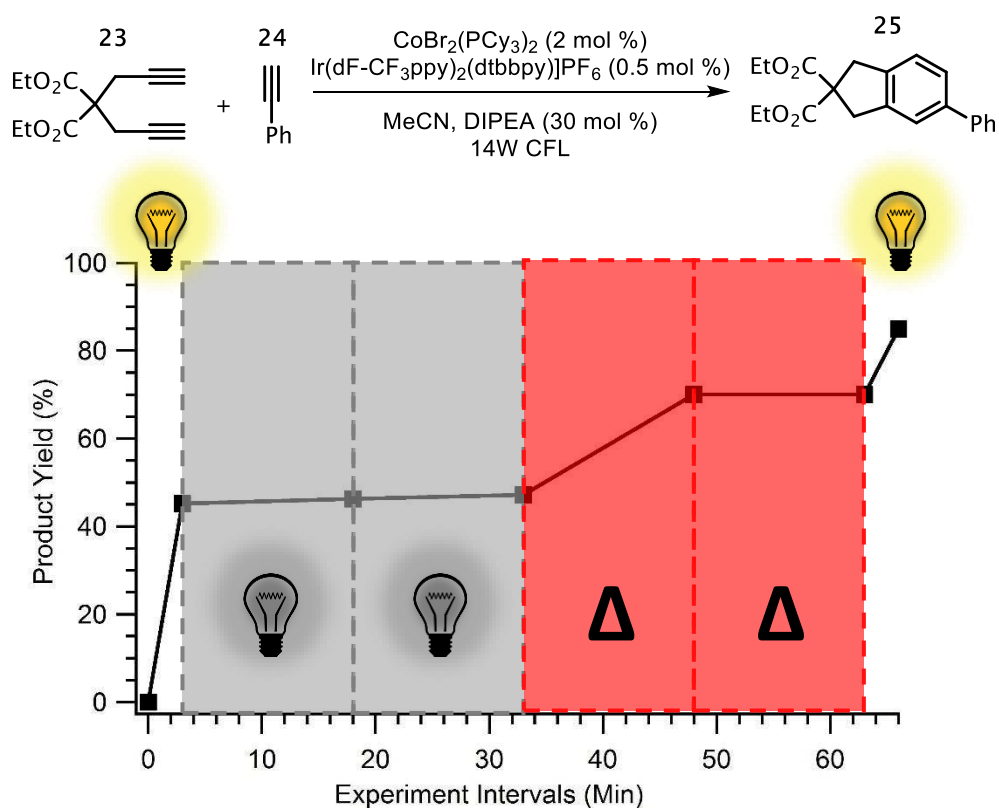


**Figure 2.26:** Determining the Reactions Dependence On Light, Darkness and Heat

## 2.2.6 – Proposed Catalytic Cycle

Based on the data collected, we conclude that the photo-catalyst not only plays an essential role in pre-catalyst activation, but is also involved in turning over the catalytic cycle. Thermal energy parallels the photo-catalyst's role within the catalytic cycle, but fails to reactivate catalysis after thermal decomposition of active species.

One plausible mechanism begins with excitation of the iridium photo-catalyst to  $\text{Ir}^{\text{III}*}$ . A subsequent reductive quench with diisopropylamine (DIPEA) delivers the highly reducing  $\text{Ir}^{\text{II}}$  species (**Figure 2.27, a**). Reduction of the cobalt pre-catalyst ( $E_{1/2}[\text{Co}^{\text{II}}/\text{Co}^{\text{I}}] = -1.14 \text{ V vs. SCE}$ ) by  $\text{Ir}^{\text{II}}$  ( $E_{1/2}[\text{Ir}^{\text{III}}/\text{Ir}^{\text{II}}] = -1.37 \text{ V vs SCE}$ ) is thermodynamically favored and gives cobalt(I) species **I**. Based on work by Leibeskind<sup>[10]</sup> with similar complexes, an oxidative cyclization with cobalt(I) furnishes a saturated, and likely unreactive, trigonal bipyramidal cobaltacyclopentadiene (**74**) intermediate **II** in the +3 oxidation state (**Figure 2.27, b**).<sup>[11]</sup>

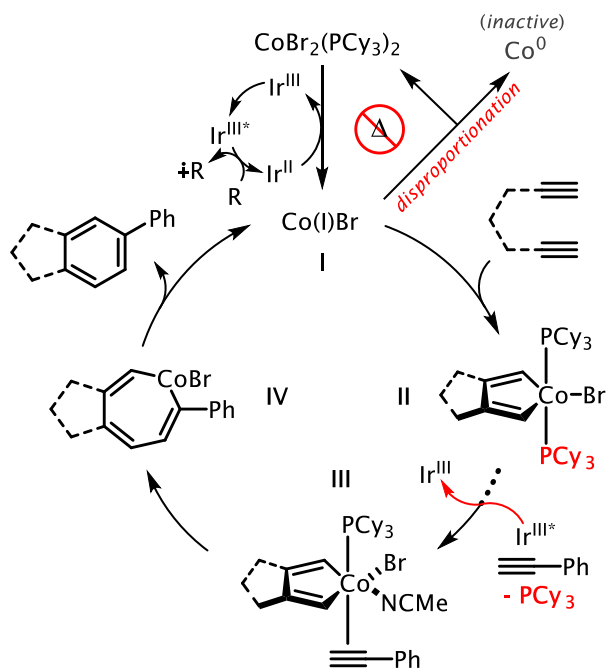


**Figure 2.27 (a):** Proposed Catalytic Cycle: Energy State Transfer



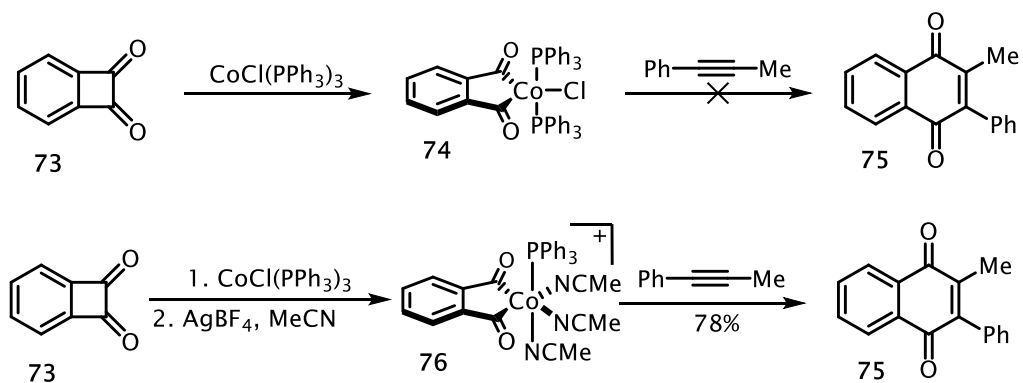


**Figure 2.27 (b):** Isolated Intermediates from Liebeskind

To proceed beyond saturated intermediate **II**, dissociation of a strongly bound phosphine ligand from the apical position is required to permit alkyne coordination. Data in **Figure 2.26** suggests this exchange is possible under thermal conditions; however, breaking the dative alkyl phosphine-cobalt bond requires elevated temperatures. Since photo-reduction is undeniably essential for entering the catalytic cycle and an active species must be available in the absence of light (limited thermal reactivity), we propose ligand dissociation is accomplished by the iridium photo-catalyst excited state via a Forster-type energy state transfer (61 kcal/mol).<sup>[12]</sup> An energy state transfer from  $\text{Ir}^{\text{III}*}$  to intermediate **II** would facilitate ligand dissociation to generate intermediate **III**. Subsequent reductive elimination from **IV** delivers the product and regenerates an active cobalt(I).

It is important to note in this case that quantum yield would undoubtedly exceed unity (~260% - experiment conducted by Ben Ravetz). After ligand ejection, catalysis proceeds without assistance of the photo-catalyst until the ligand re-inhibits the metal center. Moreover, the ligand effects observed in 1.2.3 **Figure 2.12** are possibly the result of  $\text{PEt}_3$  lacking the ability to effectively block the metal from alkyne coordination. Consequently, the bidentate ligand  $\text{dppp}$  likely adopts an entirely different metal geometry. Finally, the instability of cobalt(I) under strict

thermal conditions would only sustain catalysis until it disproportionates to an inactive species (potentially cobalt(II) and cobalt(0)). Hypothetically, the reaction “gate” remains open, catalyzing arene formation until light is removed and all active intermediates are re-ligated or funneled to inactive intermediates by thermal conditions.

Despite the possibility of energy state transfer from  $\text{Ir}^{\text{III}*}$  effecting ligand dissociation, another plausible mechanism exists. **Figure 2.28** illustrates a mechanism that proceeds by discreet electron transfer which also explains the “gating” effect observed. As previously proposed and supported by voltammetry, initial reduction of the cobalt(II) pre-catalyst to a cobalt(I) species is thermodynamically favored by 250 mV. Immediately following the cobalt intermediate **I-a** can be formed by direct reduction from the photo-catalyst or formation by disproportionation of cobalt(I). Given the decreased anodic current ( $\text{O}_2$ ) in the presence of diyne (**Figure 2.21**), it is also possible that **I-a** cyclizes to give the tetrahedral intermediate **II-a**. Interestingly, the cobalta(II)cyclopentadiene (**II-a**), which reacts slowly at room temperature and can be observed by CV, undergoes an irreversible oxidation to the cobala(III)cyclopentadiene (**III-a**) (0.00 V vs. Ag/AgCl by  $\text{Ir}^{\text{III}*}$   $E_{1/2}[\text{Ir}^{\text{III}*}/\text{Ir}^{\text{II}}] = +1.21$  V vs SCE). Coordination and insertion of the alkyne then furnishes intermediate **V-a** and subsequent reductive elimination affords cobalt(I).  $\text{Ir}^{\text{II}}$ , resulting from oxidation of **II-a** to **III-a**, then reduces the cobalt(I) species to cobalt(0) ultimately closing the catalytic cycle. It is also feasible that a disproportionation of cobalt(I) would generate an active cobalt(0), but in addition to an equivalent of thermally inactive cobalt(II).

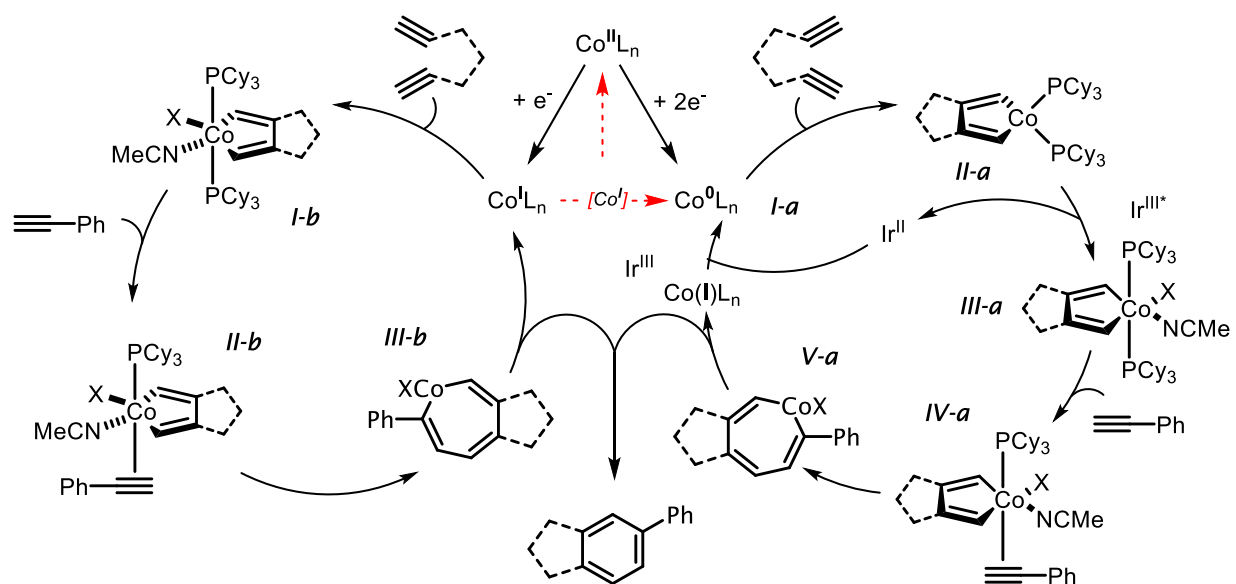


**Figure 2.28:** Proposed Catalytic Cycle Via Discrete Electron Transfer

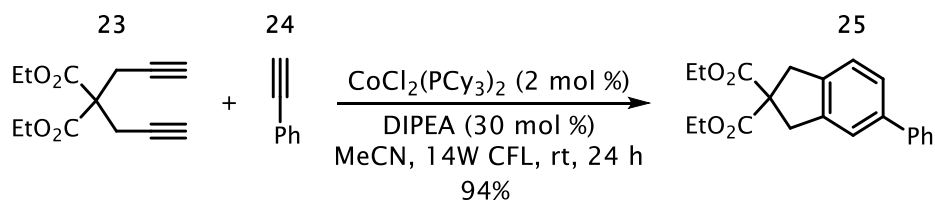
To rationalize the high thermal background reactivity, it is necessary to consider that cobalt(I) is active. However, cobalt(I) may be kinetically inferior toward oxidative cyclization and susceptible to disproportionation. Since oxidative cyclization at cobalt(I) could immediately generate the octahedral intermediate **I-b**, it is no surprise catalysis may take place in a  $\text{Co}^{\text{I/III}}$  cycle until cobalt(I) is converted to cobalt(0) or cobalt(II). In agreement with data, generation of cobalt(0) or cobalt(II) would lead to a gated catalytic cycle.

## 2.3 --- Photo-active Cobalt Species

### 2.3.1 – Reaction Development

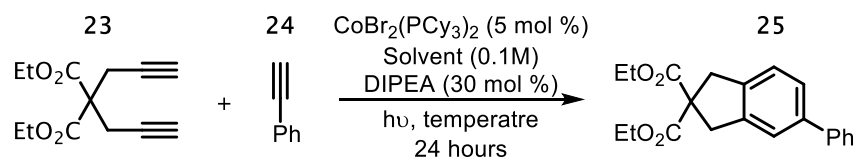
During reaction development, control studies illustrated that all reaction components were essential including a photo-redox catalyst, light, and sacrificial reductant. In fact, we found that several minutes were sufficient for a 14W CFL bulb to give high reaction yields. Without photo-catalyst, no measurable levels of product were detected after three hours of irradiation. Remarkably, we later found that extended periods of irradiation (16-24 hours) leads to high levels

of conversion (**Figure 2.29**). Although we originally suspected cross contamination of the iridium-based photo-catalyst, strict exclusion of any equipment in contact with the photo-catalyst delivered reactivity and product formation.



**Figure 2.29:** Additional Control Studies

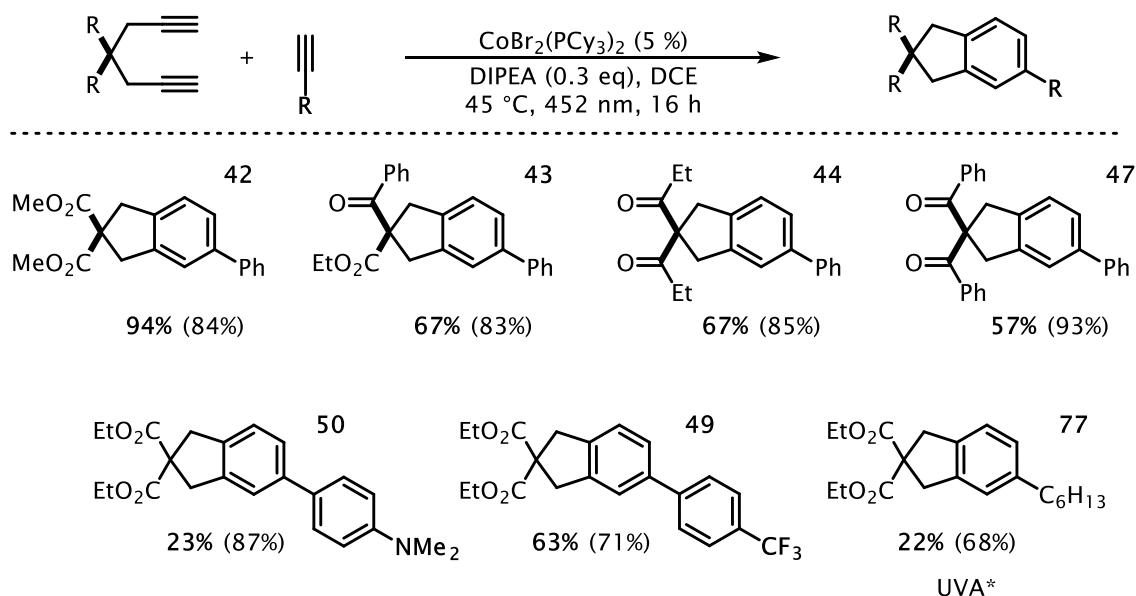
Reaction optimization shows that several variations are beneficial to the reaction (**Table 2.3**). Sufficient reactivity is achieved using dichloroethane as the solvent at elevated temperatures (**entry 1-4**). Substituting recrystallized pre-catalyst for crude pre-catalyst showed no impact on reactivity (**entry 5**). Use of distilled phenylacetylene also showed no positive effect (**entry 6**). These results rule out the suspicion that any minor reagent component is the active catalyst or pre-catalyst. Lastly, a 410 nm Kessel or UVA light provides the fastest reaction in the highest yield demonstrating that, without the iridium photo-catalyst, the reaction is heavily influenced by the light energy selected (**entry 7, 8**)

**Table 2.3:** Deviation from Standard Conditions

Entry	hv	temperature	solvent	yield
1	CFL	<b>21</b>	MeCN	10%
2	CFL	<b>35</b>	MeCN	22%
3	CFL	<b>35</b>	DCE	40%
4	CFL	<b>45</b>	DCE	71%
5 <sup>a</sup>	CFL	<b>45</b>	DCE	65%
6 <sup>b</sup>	CFL	<b>45</b>	DCE	73%
7	450	<b>45</b>	DCE	94%
8	410	<b>45</b>	DCE	98%
9 <sup>c</sup>	UVA	<b>45</b>	DCE	99%

a. Recrystallized pre-catalyst used. b. Distilled phenyl acetylene used.  
c. Reaction was complete after 1 hour of irradiation.

After a brief examination of standard conditions, we found the reaction scope is tolerant to a wide variety of diene substitution as their products are afforded in good to high yield (**Figure 2.30**). Interestingly, we noticed the reaction is sensitive to the alkyne coupling partner. While electron neutral and electron deficient aryl alkynes perform well, electron rich aryl alkynes (i.e. **50**) lead to poor yields. Similarly, attempts at coupling aliphatic alkynes (**77**) prove problematic. Using 452 nm light or a 14W CFL shows no reactivity. However, increasing light energy (UVA - >380 nm) provides yields up to 22%.



Note: Bold yields are without photo-catalyst (yield determined from isolated material). Yields in parenthesis are with iridium-photo-catalyst.

**Figure 2.30:** Preliminary Substrate Scope

### 2.3.2 – Proposed Mechanism

To gather evidence for a photoactive cobalt species, we conducted stoichiometric studies following pre-catalyst consumption with UV/Vis spectroscopy (**Figure 2.31**). The cobalt pre-catalyst (**40**), one equivalent of diyne (**23**), five equivalents of phenylacetylene (**24**), and ten equivalents of sacrificial reductant were dissolved in dichloromethane. The resulting solution was then placed in front of a 14W CFL and irradiated for 24 hours. Over time the solution drastically changed color from a light blue (pre-catalyst) to a dark green suggesting changes in the metal coordination environment. This was commonly observed during general reaction conditions as well.

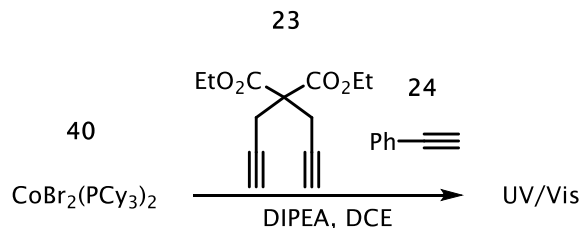


**Figure 2.31:** Monitoring pre-catalyst consumption by UV-Vis spectroscopy

Spectra taken at various time points and indicate the corresponding changes in the UV/Visible absorption (**Figure 2.32**). After initial combination of reagents the spectra reflect the expected charge transfer bands of a tetrahedral cobalt(II) complex in the yellow to yellow-orange wavelengths (570-620 nm). After initial irradiation, the low energy absorptions begin to fluctuate and a high energy absorption appears just beyond 350 nm. Collection of a final spectrum after irradiation and addition of a counter ion exchange reagent suggests complete consumption of the cobalt pre-catalyst. This spectrum also indicates formation of a new species with high energy electron transfer bands with a shoulder at 380-400 nm.

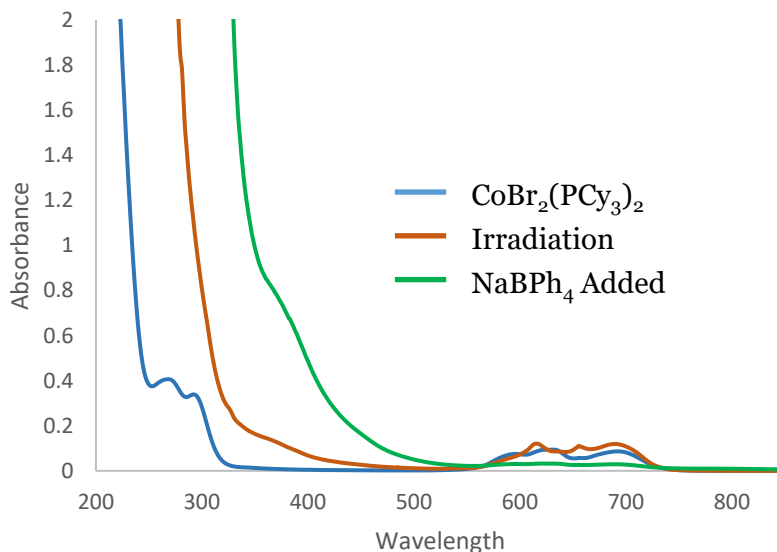


**Figure 2.32:** UV-Vis of Pre-catalyst Consumption

Fluorimetry studies corroborate the UV/Visible spectra as they show absorptions in similar wavelengths. Although the species still remains un-isolated, **Figure 2.33** suggests that a species generated during the experiment strongly absorbs wavelengths above 400 nm and emits violet-blue wavelengths.

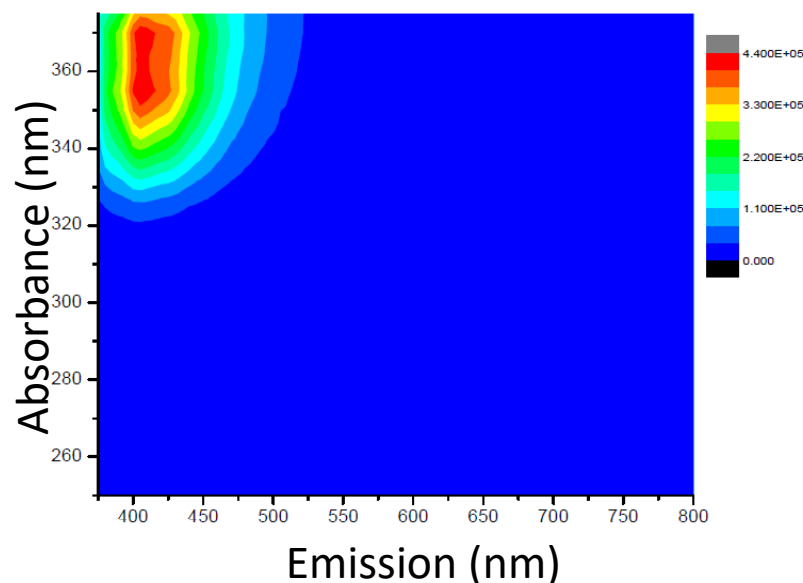


**Figure 2.33:** Fluorimetry of the Sample Suggests an Emissive Species

After learning of a potentially emissive cobalt species, it became clear why higher energy wavelengths were beneficial. Therefore, we proposed the mechanism shown in **Figure 2.34**. In the presence of a terminal aromatic alkyne under basic conditions, the cobalt pre-catalyst forms a photo-active cobalt acetylide (**I**).<sup>[13-15]</sup> After excitation, a reductive quench delivers a low-valent cobalt species **II** without the need for an exogenous photo-catalyst. Similar to the proposed mechanism in section 1.2.6, we propose an oxidative cycloaddition results in the similar cobaltacyclopentadiene species **III**. In the absence of a photo-catalyst, the acetylide contained in intermediate **III** facilitates photo-excitation by absorbing light energy to dissociate a phosphine ligand. This releases a ligand providing an open coordination site (**IV**). Insertion of the alkyne to



give **V**, followed by reductive elimination delivers arene the product and regenerates the low-valent cobalt acetylide **II**.

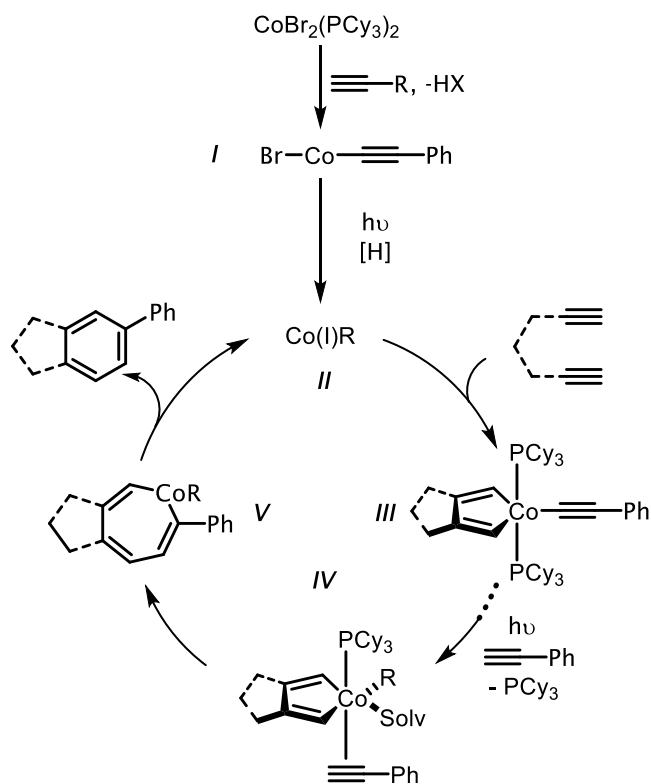


**Figure 2.34:** Proposed Mechanism of Photo-Catalyst Free [2+2+2] Cycloaddition

## 2.4 --- Pyridine Formation

In the initial [2+2+2] cycloaddition screening, several impurities were observed in small amounts by HPLC analysis. Analysis of the reaction wells by GC- and LC-MS revealed that one minor product formed is substituted pyridine **91** (**Figure 2.35**). An apparent conclusion is that a competing background reaction involves oxidative cyclization between two alkyne partners, followed by incorporation an equivalent of solvent (MeCN). Not all cobalt pre-catalysts, nor combinations of pre-catalyst and photo-redox catalyst, furnished pyridine products. When observed, pyridines were formed in low yields.

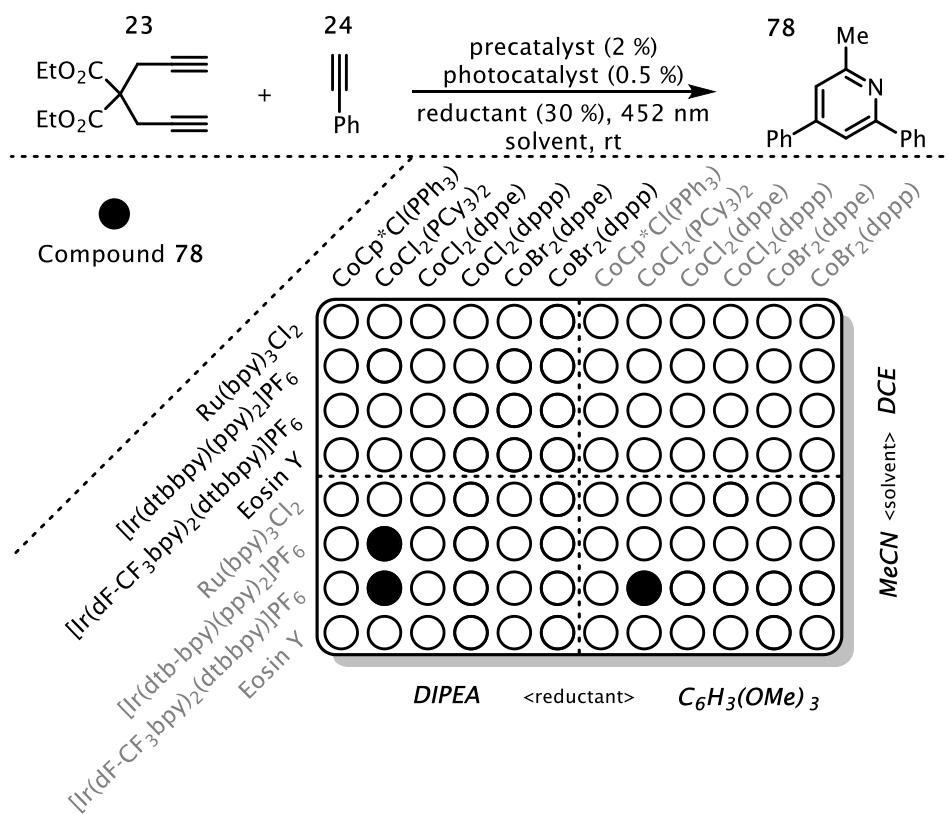


**Figure 2.35:** Initial Reaction Screening Showed Pyridine Formation

To confirm pyridine formation, we applied the reaction conditions to larger bench scale reactions. Given the nature of the pyridine observed (**78**), we excluded bis-propargyl ester **23** (**Figure 2.36**). Crude NMR analysis reveals **78** is formed in ~9% yield after 12 hours of irradiation. The mass balance of phenyl acetylene (**24**) is consumed by forming the trimer product **79**, which explains the low yields of pyridine product. In an effort to encourage diene **23** to participate in pyridine formation, we removed phenyl acetylene from the reaction leaving only acetonitrile available for incorporation. Interestingly, none of the expected pyridine product (**80**) is observed. LC-MS analysis however shows the major product is **81** indicating dimerization of the diene substrate. Despite a large equivalency bias, the reaction still favors a third equivalent of alkyne. In

fact, tethering the nitrile component (**82**) also provides no increase in reactivity for pyridine formation (**83**).

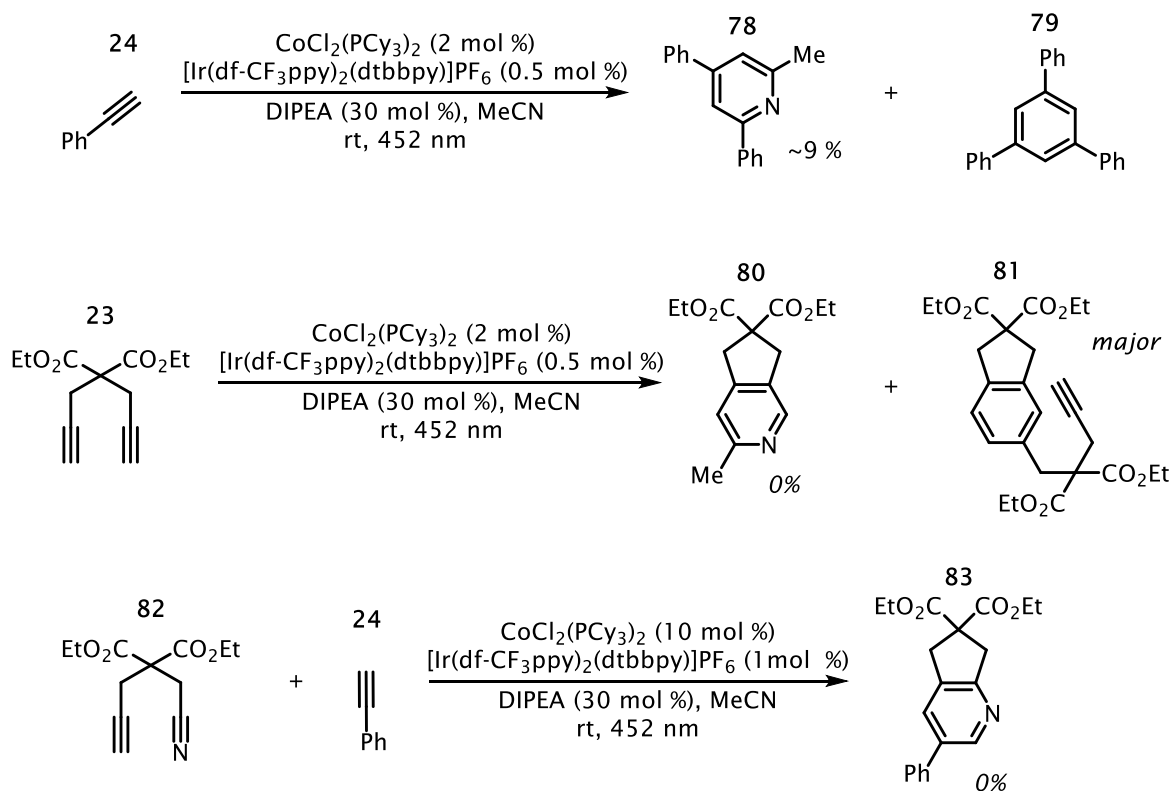


**Figure 2.36:** Reaction Scale-Up

The divergence in mechanism from the [2+2+2] cycloaddition mechanism is illustrated below in **Figure 2.37**. Reduction of the pre-catalyst to cobalt(I) and coordination of two equivalents of aryl alkyne lead to oxidative cyclization and formation of intermediate **II**. Energy state transfer (or discreet electron transfer from a cobalt(II)cyclopentadiene) removes a tightly bound phosphine ligand and allows coordination of acetonitrile giving intermediate **III**. A [4+2] cycloaddition (or insertion/reductive elimination) delivers the pyridine product and regenerates the active cobalt species.

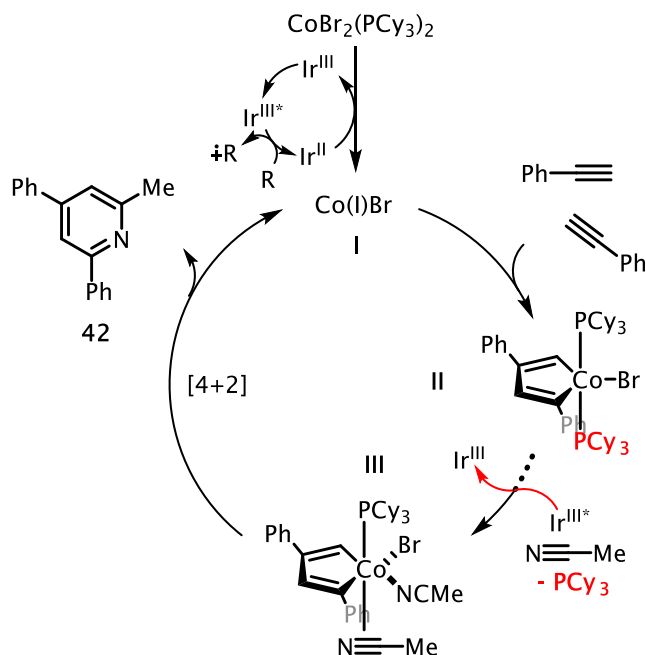


**Figure 2.37:** Proposed Mechanism

## 2.5 --- Summary

In conclusion, by combination of photo-redox and cobalt catalysis, we have discovered an efficient method for a light-controlled cobalt catalyzed [2+2+2] cycloaddition. This methodology affords high yields, rapid reaction rates, access to variety of substrates, and a unique control not commonly observed in transition metal catalysis. Mechanistically, evidence points to the iridium photo-catalyst serving two distinct roles in catalysis. Experiments suggest the photo-catalyst facilitates pre-catalyst reduction and we believe photo-catalyst is acting as an energy transfer reagent to dissociate a ligand. Evidence also supports that photo-catalysis may assist in performing discreet electron transfers from intermediates to promote catalysis by oxidation state changes. Furthermore, preliminary studies indicate this methodology will extend to catalyze pyridine formation. Since these early findings, a junior student in the group, Benjamin Ravetz, has explored this reaction and made large advances on the project. In addition, we are pursuing a photo-

controlled system free of any exogenous metal-based photo-catalysts. The following chapter will further explore “light-gated cobalt catalysis” and applications using light as an external stimulus for the [2+2+2] cycloaddition reaction.

## REFERENCES

- [1] Vollhardt, K. P. C. *Angew Chem.* **1984**, *23*, 539-556.
- [2] Lenges, C. P.; Brookhardt, M. *J. Am. Chem. Soc.* **1997**, *119*, 3165-3166.
- [3] a) Fallon, B. J.; Derat, E.; Amatore, M.; Aubert, C.; Chemla, F.; Ferreira, F.; Perez-Luna, A.; Petit, M. *J. Am. Chem. Soc.* **2015**, *137*, 2448-2451. b) Bolig, A. E.; Brookhardt, M. *J. Am. Chem. Soc.* **2007**, *129*, 14544-14545. c) Gandon, V.; Aubert, C.; Malacria, M. *Chem. Commun.* **2006**, 2209-2217.
- [4] a) Okamoto, S. *Heterocycles*, **2012**, *85*, 1579-1602 (and references therein). b) Saino, N.; Amemiya, F.; Tanabe, E.; Kase, K.; Okamoto, S. *Org. Lett.* **2006**, *8*, 1439-1442.
- [5] a) Chen, Q.-A.; Kim, D. K.; Dong, V. M. *J. Am. Chem. Soc.* **2014**, *136*, 3772-3775. b) Yang, J.; Seto, Yuan W.; Yoshikai, N. *ACS Catalysis*. **2015**, *5*, 3054-3057. c) Yang, J.; Yoshikai, N. *J. Am. Chem. Soc.* **2014**, *136*, 16748-16751.
- [6] Gao, K.; Yoshikai, N. *Acc. Chem. Res.* **2014**, *47*, 1208-1219.
- [7] Cismesia, M. A.; Yoon, T. P. *Chem. Sci.* **2015**, *6*, 5426-5434.
- [8] Buriez, O.; Labbé, E.; Périchon, J. *Journal of Electroanalytical Chemistry*. **2006**, *593*, 99-104.
- [9] a) Seka, S.; Buriez, O.; Périchon, J. *Chem. Eur. J.* **2003**, *9*, 3597-3603. b) Polleux, L.; Labbe, E.; Buriez, O.; Périchon, J. *Chem. Eur. J.* **2005**, *11*, 4678-4686.
- [10] Libesekind, L. S.; Baysdon, S. L.; South, M. S.; Iyer, S.; Leeds, J. P. *Tetrahedron*. **1985**, *41*, 5839-5853.
- [11] Bouayad, A.; Dartiguenave, M.; Menu, M. J.; Dartiguenave, Y. *Organometallics* **1989**, *8*, 629-637.
- [12] Farney, E. P.; Yoon, T. P. *Angew. Chem. Int. Ed.* **2013**, *53*, 793-797.

- [13] Cummins, D.; McKenzie, E. D.; Segnitz, A. *J. Organomet. Chem.* **1975**, 87, 19-21.
- [14] Zhou, G.-J.; Wong, W.-Y. *Chem. Soc. Rev.* **2011**, 40, 2541-2566.
- [15] Chatterjee, B.; Akin, F. A.; Jarrold, C. C.; Raghavachair, K. *J. Phys. Chem. A.* **2005**, 109, 6880-6886.

## CHAPTER THREE

### Introduction to Light-Gated Catalysis

#### 3.1 --- Light-Gated Catalysis

One of the leading goals in synthetic chemistry is to develop catalytic methods that form products rapidly, selectively, and efficiently. By using modular ligands, chemists can manipulate catalyst structure and quickly optimize reaction conditions.<sup>[1,2]</sup> However, some applications require more than just a high reaction rate and/or yield. The ability to control when and where catalysis takes place is attracting more attention among researchers. One successful strategy uses an external reaction stimulus to regulate catalysis; among the most effective are chemical force, redox agents, and light radiation.<sup>[3]</sup> Although many external stimuli work well, light's ubiquity and variability make it the quintessential stimuli. In addition, light radiation provides a range of reaction control, all of which can be categorized as light-gated catalysis.<sup>[4]</sup>

Compounds that irreversibly form an active species after absorbing light are considered to be light-caged catalysts. The transformations they catalyze can be categorized as induced or initiated reactivity. Even though caged reactions require light for initiation, continuous irradiation is not often necessary. One example from the Wang group demonstrates how a Bronsted base can act as a light-caged catalyst.<sup>[5]</sup> The protonated and inactive catalyst **1** is irradiated with UV light to irreversibly generate **2** (**Figure 3.1**). After the active catalyst (**2**) is released, it can perform the ring-opening polymerization of caprolactone (**3**). Because the catalyst formation is irreversible, polymerization will continue, even under dark conditions, until monomer is exhausted.



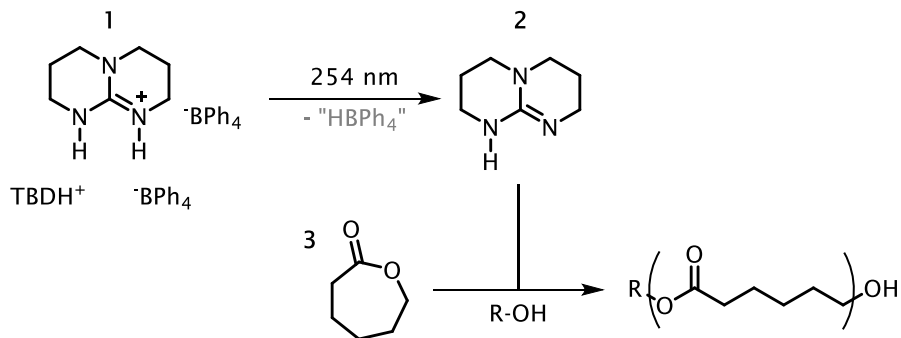


**Figure 3.1:** Light-Initiated Base Catalysis

Literature precedent indicates that light-caged catalysts are not limited to Bronsted bases. In the early 1980's, Vollhardt and co-workers demonstrated that irradiation of carbonyl-containing cobalt complexes increases the rate of a [2+2+2] cycloaddition reaction (**Figure 3.2**).<sup>[6, 7]</sup> When a carbonyl complex absorbs UV light, electrons are promoted to the metal-carbonyl antibonding orbitals. Consequently, this weakens the metal-ligand bond. The now labile carbonyl ligand can dissociate and open a coordination site on the metal; thus, the reactivity is enhanced.

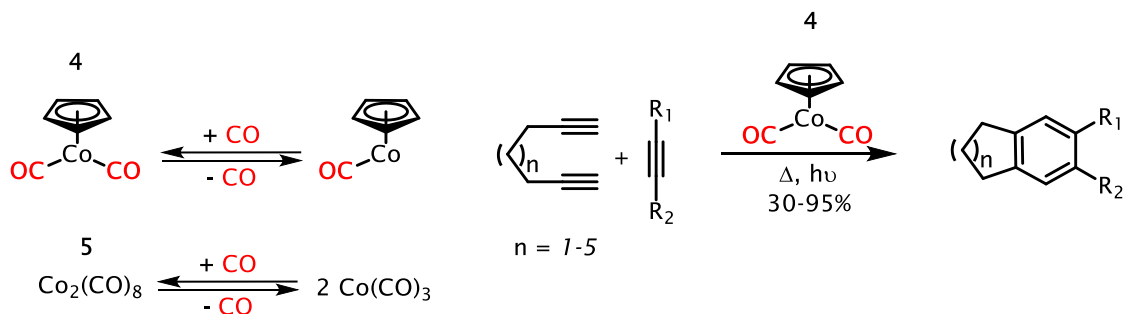


**Figure 3.2:** UV Radiation Assists Carbonyl Dissociation

Although many of these transformations benefit from constant irradiation, UV light cannot serve as the sole stimulus. Attempts to control reaction progress exclusively with UV irradiation have proven fruitless. This is because CO dissociation occurs thermally indicating that heat is responsible for high levels of product formation. In addition, thermodynamic wells in the catalytic

cycle also require elevated temperatures. As a consequence, heating the reactions to overcome these thermodynamic barriers further increases the thermal background rate.

Interestingly, light-induced ligand dissociation is an effective strategy to uncage several ruthenium-based ROMP catalysts. Mechanisms for light-initiated metathesis polymerizations have been reported by Muhlebach<sup>[8]</sup>, Noels<sup>[9]</sup>, Buchmeiser<sup>[10]</sup> and Grubbs<sup>[11]</sup> (**Figure 3.3**). Dissociation of a nitrile ligand (**A**) as well as an aromatic  $\pi$  ligand (**B, C**) have been used to gain reaction control. In a more intricate scenario, Grubbs and co-workers report a photo-acid induced ligand dissociation (**D**). Shining light on the photo-acid generator (PAG) releases a proton which, in turn, protonates the *tert*-butyl diketone ligand. In neutral form, the ligand's binding affinity is reduced and the ligand is lost releasing the active catalyst.

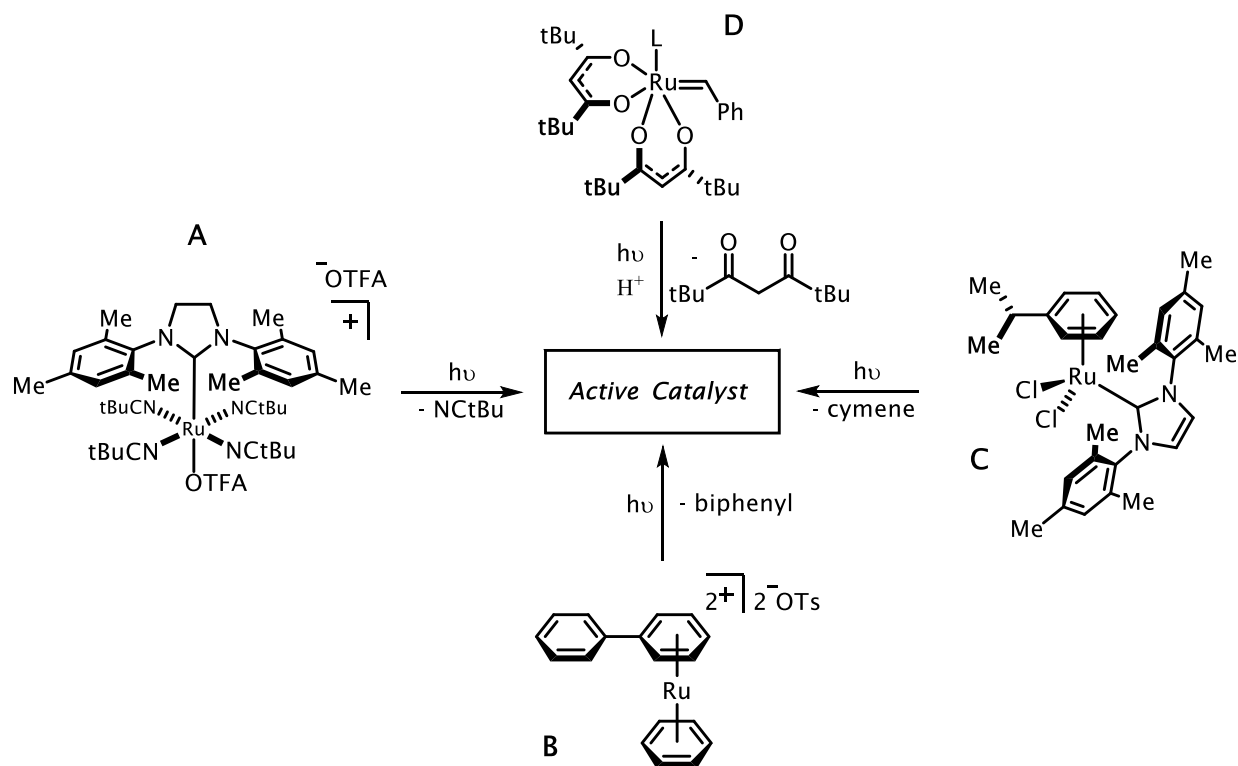


**Figure 3.3:** Catalyst Control Using Ligand Dissociation

A variety of light-caged metal catalysts can be activated directly by UV light. However, modern photo-catalysts also facilitate a similar process but do so with visible light energy.<sup>[12,13]</sup> Photo-catalysts absorb visible light and excite to a triplet state via a metal-to-ligand charge transfer (MLCT - See Chapter 1). This can then assist ligand dissociation from a saturated metal complex.<sup>[14]</sup> As a result, ligand exchange is drastically increased without UV light. By using a photo-catalyst (quantum yield less than unity,  $\phi < 1$ ) to dissociate a ligand, one would expect quantum yields for the controlled reaction to exceed unity ( $\phi > 1$ ). Since the catalyst is activated by a ligand release, it would continuously produce product until the ligand returns. Because re-coordination requires a bimolecular reaction to occur at low concentrations, it is conceivable this process may take several cycles to occur.

In contrast to light-caged catalysis, switchable catalysis uses a reversible gate with two distinct reaction states. Reactivity is on in the presence of light and off in the absence of light (or light of a longer wavelength).<sup>[4]</sup> Many reactions have been successfully gated and a variety of transformations are controlled with light radiation. The most common strategy employs a photochromic additive to create a switchable catalyst scaffold.<sup>[15]</sup>

One example of a switchable catalyst comes from the Inoue group. Here, they use an isomerizable vinyl pyridine ligand (**7**) to control an aluminum-based catalyst (**6**) (**Figure 3.4**).<sup>[16]</sup> Irradiating **7** with low energy light favors the *trans* alkene geometry. In the *trans* geometry, steric interactions between the *tert*-butyl group and the catalyst scaffold hinders coordination rendering the aluminum catalyst inactive (**6**) (OFF). Yet, irradiating with UV light isomerizes **7** to the *cis* geometry (**9**) allowing for the rotation of the *tert*-butyl group away from the catalyst scaffold. This decrease in sterics allows for coordination and gives an active catalyst (**8**) (ON). **8** then catalyzes the cyclization of carbon dioxide (**10**) and ethylene oxide (**11**) providing cyclic organic carbonate

**12.** Unlike initiated catalysis, the switchable aluminum catalyst can be cycled to achieve the desired level of product formation.

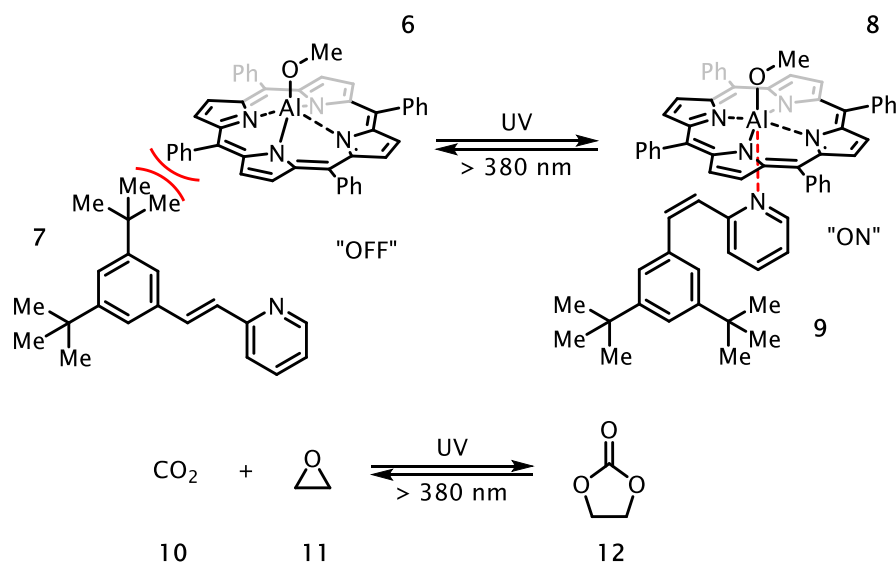


**Figure 3.4:** Photochromic Additive Controls Aluminum-Based Lewis Acid

### 3.2 – Temporally Controlled Catalysis

Harnessing reaction control with the flip of a light switch has extensive applications in materials and biological research. To achieve specific polymer molecular weights or alter a compound's concentration *in vivo*, scientists need ways of regulating reaction progress. Light-gated catalysis offers several strategies to obtain basic levels of temporal control (i.e. reactions that can be controlled with respect to time). The Bowman group has shown that an inactive copper(II) pre-catalyst can be uncaged with a photo-reductant (**15**) (**Figure 3.5**).<sup>[17]</sup> Photo-reduction irreversibly generates an active copper(I) species, which catalyzes a click reaction between an azide (**13**) and an alkyne (**14**). Although catalysis is merely initiated, careful selection of light exposure time enables a significant level of temporal control. Unsurprisingly, continuous irradiation provides the highest rate and yield of **16**. Five minute (green) or ten minute (red) cycles,

followed by darkness, both lead to different reaction rates and yields with a respectable level of temporal control.

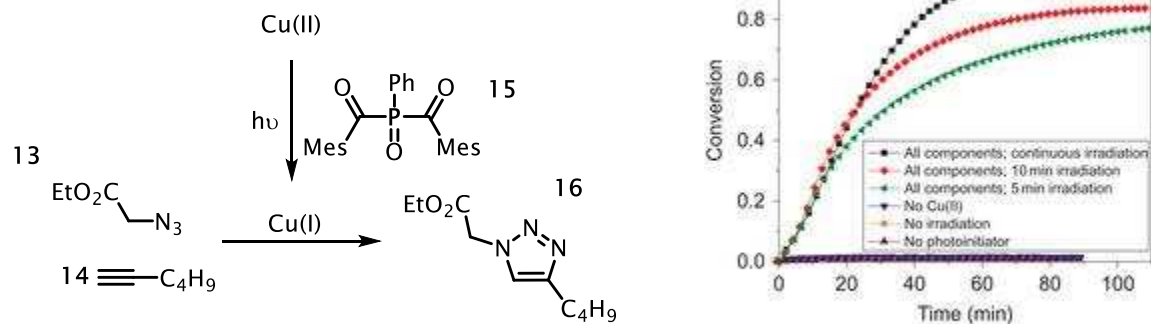


**Figure 3.5:** Light-Induced Click Reaction

The click reaction has garnered much attention due to its high bio-compatibility and orthogonality. Temporal control of the reaction holds great promise for *in vivo* labeling and tracking of biologically relevant compounds. In a similar respect, polymer performance relies on reproducible bulk properties, which are a function of molecular weight and polydispersity index (PDI). Therefore, strict reaction control during a polymerization is crucial to for the reliable production of polymers.

One example of a temporally-controlled polymerization is the light-controlled radical-based ATRP (atom-transfer radical polymerization).<sup>[18]</sup> Traditionally, ATRP is conducted with copper(I) salts, which have no opportunity for external regulation. With the advent of photocatalysis, ATRP is now easily controlled with visible light (**Figure 3.6**).<sup>[19]</sup> Photoexcitation of Ir(ppy)<sub>3</sub> (**19**) delivers the excited state [Ir(ppy)<sub>3</sub>]\*, a strong reductant ( $E_{1/2} = -1.73$  V vs. SCE). At this potential, reduction of alkyl halide initiator **18** is thermodynamically favored. The resulting fragmentation of the carbon-halide bond furnishes a bromide anion and the corresponding carbon radical. In the presence of monomer **17**, the radical forms a new carbon-carbon bond at the  $\beta$ -position and, in turn, propagates a new radical. Acrylate addition to the growing chain continues until it is terminated by a bromine atom (create by bromide oxidation). Hawker and Fors have

demonstrated that photo-controlled ATRP is effective for polymer synthesis as well as controlling molecular weight and PDI.

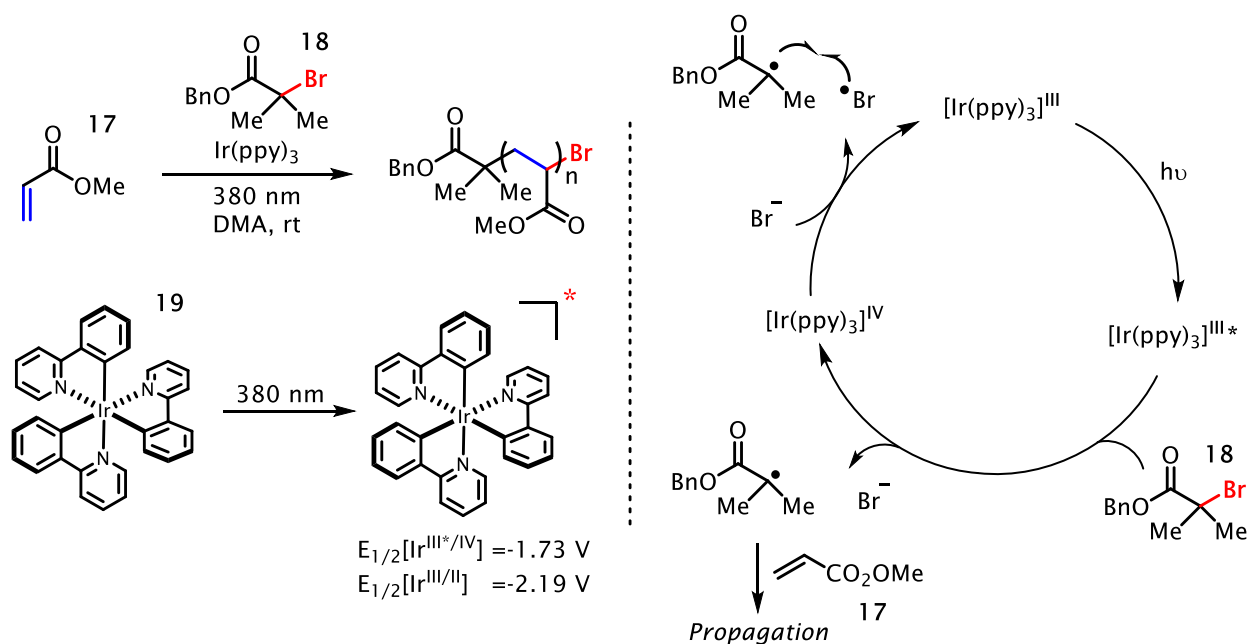


**Figure 3.6:** Temporally Controlled Atom-Transfer Polymerization

In many situations, polymers synthesized by ATRP inherently contain low levels of metal contaminants. To retain temporal control and minimize impurities, the Miyake group has developed highly reducing organic photo-redox catalysts to mediate ATRP (**Figure 3.7**).<sup>[20, 21]</sup> Similar to  $\text{Ir}(\text{ppy})_3$ , organic photo-catalyst **22** is a strong reductant ( $E_{1/2} = -2.24 \text{ V}$  vs SCE) capable of reducing the carbon-bromine bond in **20**. Propagation of the resulting radical with methylmethacrylate (**21**) delivers a polymer with high molecular weight and low PDI while maintaining complete temporal control.

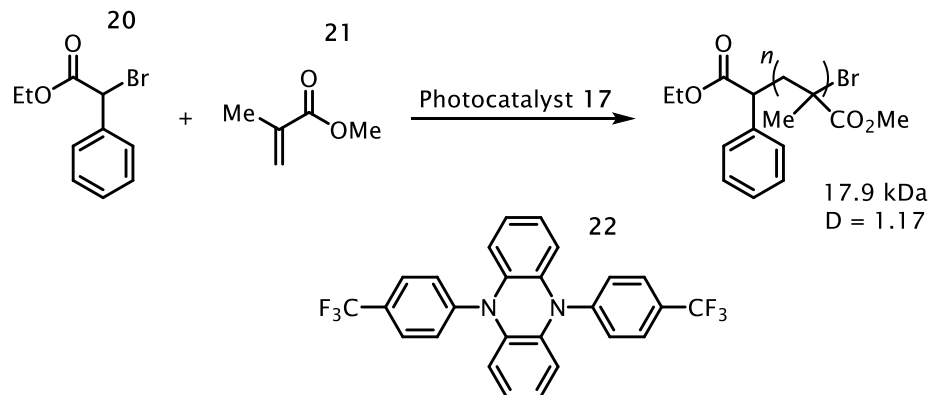


**Figure 3.7:** Organic Photo-redox Catalyst for Controlled ATRP

In addition to radical-based reactivity, several switchable catalysts also facilitate temporal control for a variety of polymerization reactions.<sup>[22]</sup> In 2001, Noels and colleagues reported a light-caged ruthenium-NHC ROMP catalyst in which a photo-labile *p*-cymene ligand creates a caged polymerization pre-catalyst (**23**) (**Figure 3.8**). Irradiating the catalyst dissociates the *p*-cymene ligand and induces the metathesis polymerization of cyclooctene (**24**). Although it is difficult to stop and start catalysis, data demonstrate that the polymerization can be conducted with predictable levels of temporal control.<sup>[9]</sup> Presently, a variety of light-caged ruthenium catalysts are effective to temporally control metathesis polymerizations.

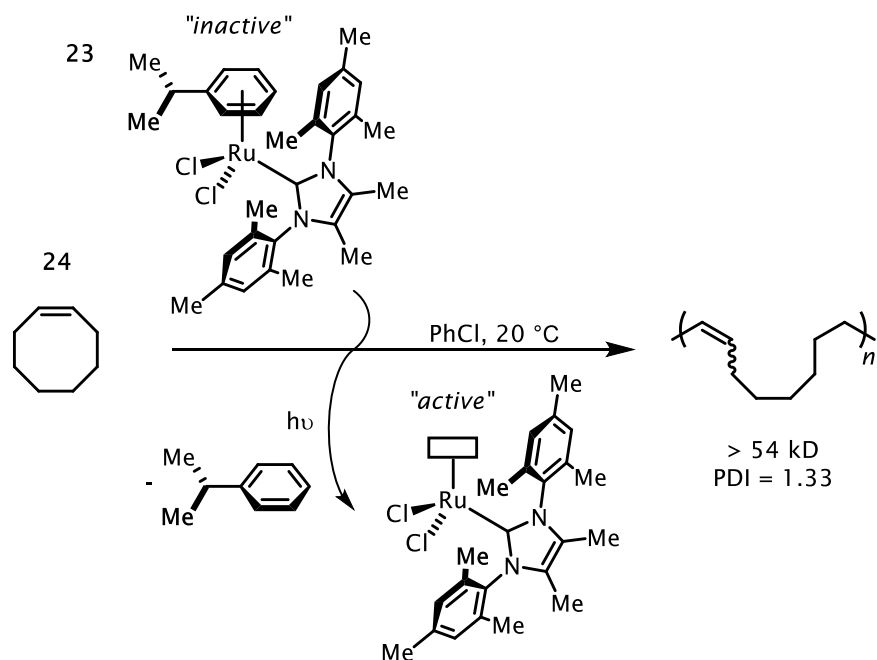


**Figure 3.8:** Light-Controlled ROMP

Moreover, even the delivery of a proton can be temporally controlled. Recently, Boyer and co-workers reported light-caged Bronsted acid catalyst **27** (Figure 3.9).<sup>[23]</sup> Exciting compound **27** with UV-light isomerizes the alkene to the *cis* geometry. In the *cis* geometry, a six-membered ring closure forms the spiro-aminal (**28**) and liberates an equivalent of acid. Once the proton is released, it catalyzes the ring opening polymerization of caprolactone **26**. Boyer adds that the proton release is reversible. Compound **28** can be re-protonated and the phenol reformed to remove H<sup>+</sup> from the solution which stops polymerization. With this reversibility the reaction can be continuously cycled until the desired polymer properties are achieved.



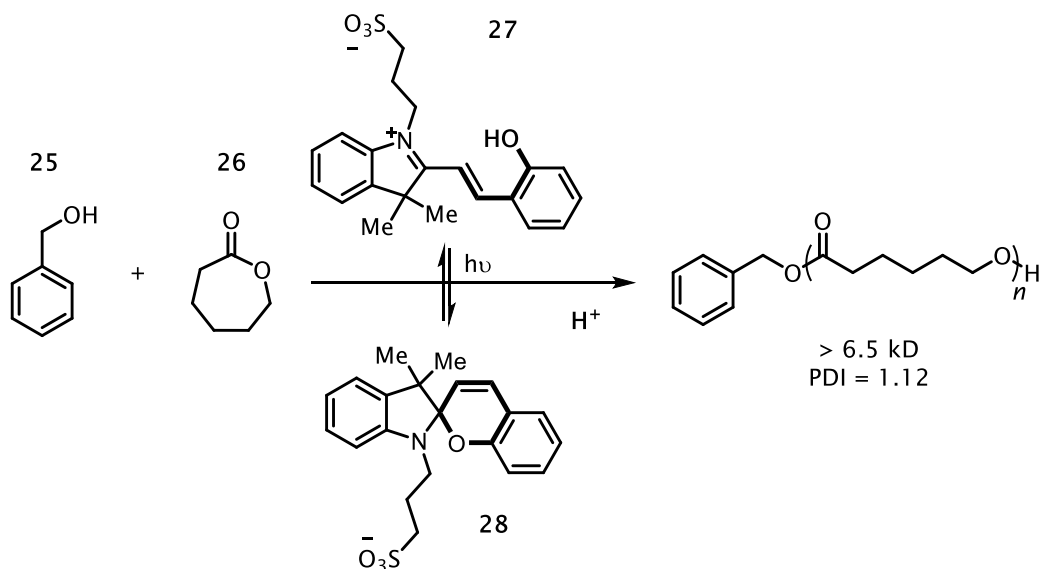


**Figure 3.9:** Acid-Controlled Ring Opening Polymerization

### 3.3 – Spatially Controlled Catalysis

Since the first computer was invented, an unwieldy machine that filled an entire room, electronic technology has continued to get smaller in size. Ongoing efforts to further miniaturize electronics cause many to question the limit of nanoscale fabrication. In light of Moore's Law, many believe computers will one day need to function on the atomic level to maximize data storage and computing output.<sup>[24]</sup> Although theory supports this idea, reaching this scale requires fabrication techniques that can deliver sub-nanoscale spatial resolution. Hence, to spatially control catalysis or to regulate where a reaction takes place, we must accurately deliver reagents or focus a reaction stimulus.

Ordinarily, spatially controlled reactivity involves the use of expensive and specialized equipment. Atomic force microscopy (AFM)<sup>[25]</sup>, dip-pen nano-lithography<sup>[26]</sup> and X-ray etching<sup>[27]</sup> are all competent methods to achieve spatial resolution. One of the first examples of direct-write nanolithography (i.e. pin-point reagent delivery) was reported by Mirkin in 1999 (**Figure 3.10**).<sup>[28]</sup>

Mirkin used an AFM cantilever to place alkanethiols on a gold film with 30-nanometers of spatial resolution. Even though this method is still far from the atomic level and restricted to gold's affinity for thiols, this method certainly pushes the current boundaries of nanoscale techniques.

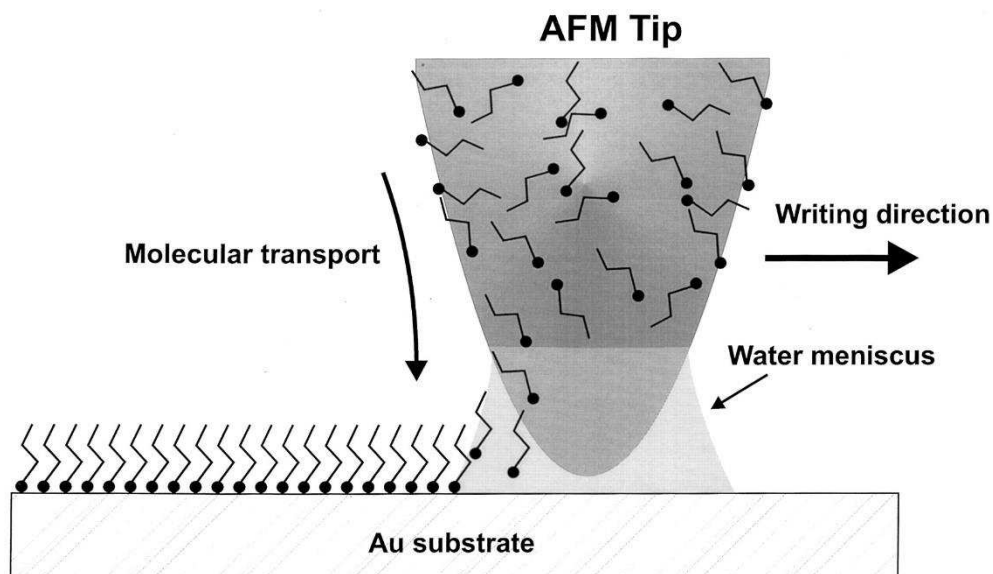


**Figure 3.10:** Dip-Pen Nanolithography for Alkanethiol Addition <sup>[28]</sup>

Directly placing a reagent is an attractive option for thiol-gold applications. Unfortunately, not every functionality is compatible with this technique. One approach that is not restricted to a gold substrate utilizes a preformed self-assembled monolayer (SAM) on nearly any desired substrate. Spatially removing or etching material from a surface ultimately provides the same outcome as direct delivery. Although AFM has been used to deliver reagents, it is also routinely used to remove material from a SAM (nanoshaving) (**Figure 3.11, A**).<sup>[29]</sup> High physical forces created by the cantilever tip are enough to break bonds and remove material. Interestingly, X-rays provide another way to spatially break covalent bonds and etch material from a SAM (**Figure 3.11, B**).<sup>[30]</sup> In this case, spatial resolution is a function of X-ray beam generation and focus.

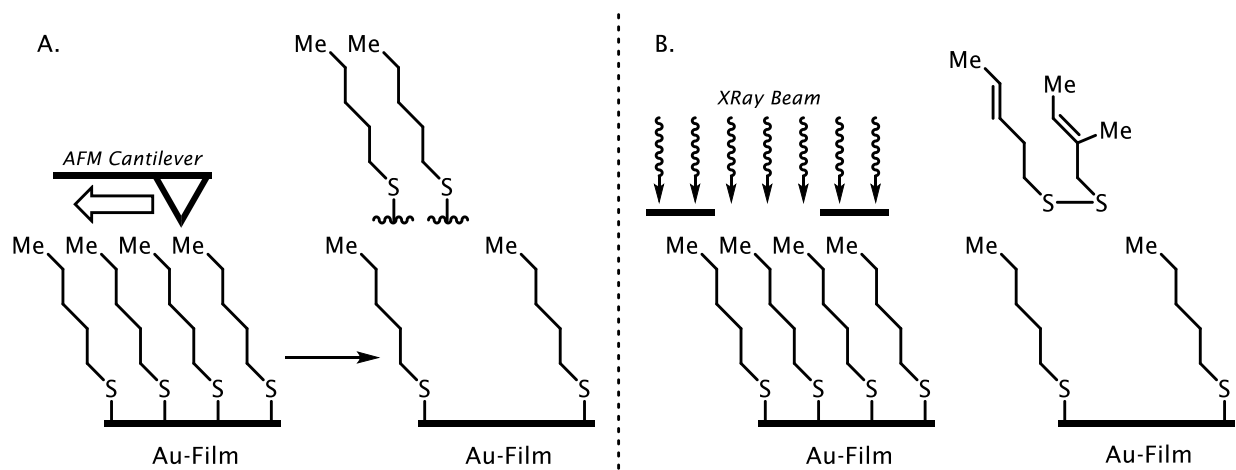


**Figure 3.11:** Example of AFM and X-Ray SAM Patterning

The specialized nature of AFM and X-ray equipment hinders their utility for surface modification techniques. Moreover, X-ray radiation is highly regulated due to the dangers associated with its use. One alternative that is now a large part of nanofabrication in materials and medical applications is photolithography.<sup>[31]</sup> UV light and inexpensive photomasks are both readily available and also craft an effective method to spatially modify SAM surfaces.<sup>[32]</sup> Wrighton and co-workers have applied this method to pattern a uniform monolayer of azide functional groups (**29**) (**Figure 3.12**).<sup>[33, 34]</sup> Placing the modified surface beneath a photomask and irradiating with UV light spatially controls azide activation. Areas that receive UV light through the photomask decompose in the presence of a secondary amine and give a capped unreactive surface. After areas of azide functionality are spatially capped, a subsequent azide-initiated polymerization furnishes spatially-resolved conducting polymers.

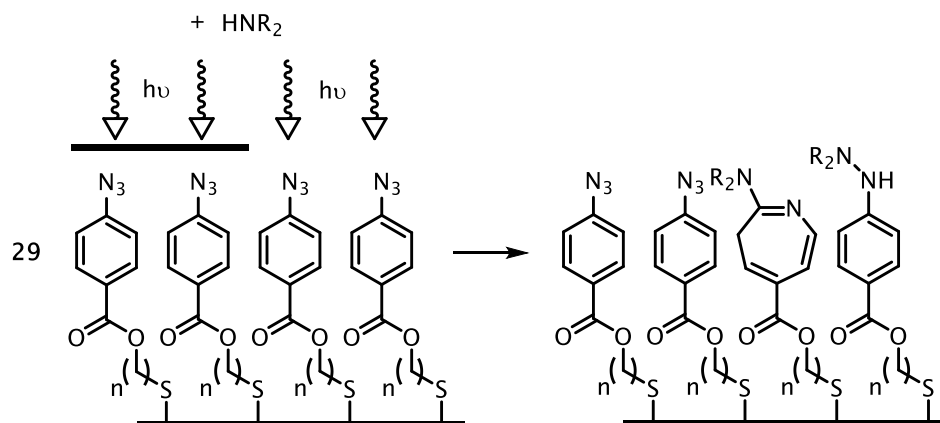


**Figure 3.12:** UV Light Photolithography on a SAM

In addition to spatially-controlled reagent delivery, bulk removal, or photo-etching, there is significant interest in spatially resolved catalytic methods. Although reagent equivalency is not a concern on small scale, many catalysts offer unique bond activations and formations. One catalyst delivery approach comes from the Coleman group and uses an AFM cantilever to spatially dose a platinum catalyst (**Figure 3.13**).<sup>[35]</sup> First, a uniform monolayer of catalyst-reactive functionality is constructed using the thiol-gold interaction. After covering the surface with reagents, a catalyst-coated AFM cantilever is used to add catalyst in the desire areas. Coleman and colleagues show that catalyst delivery is effective for both a Heck-type reaction as well as a Suzuki cross coupling.

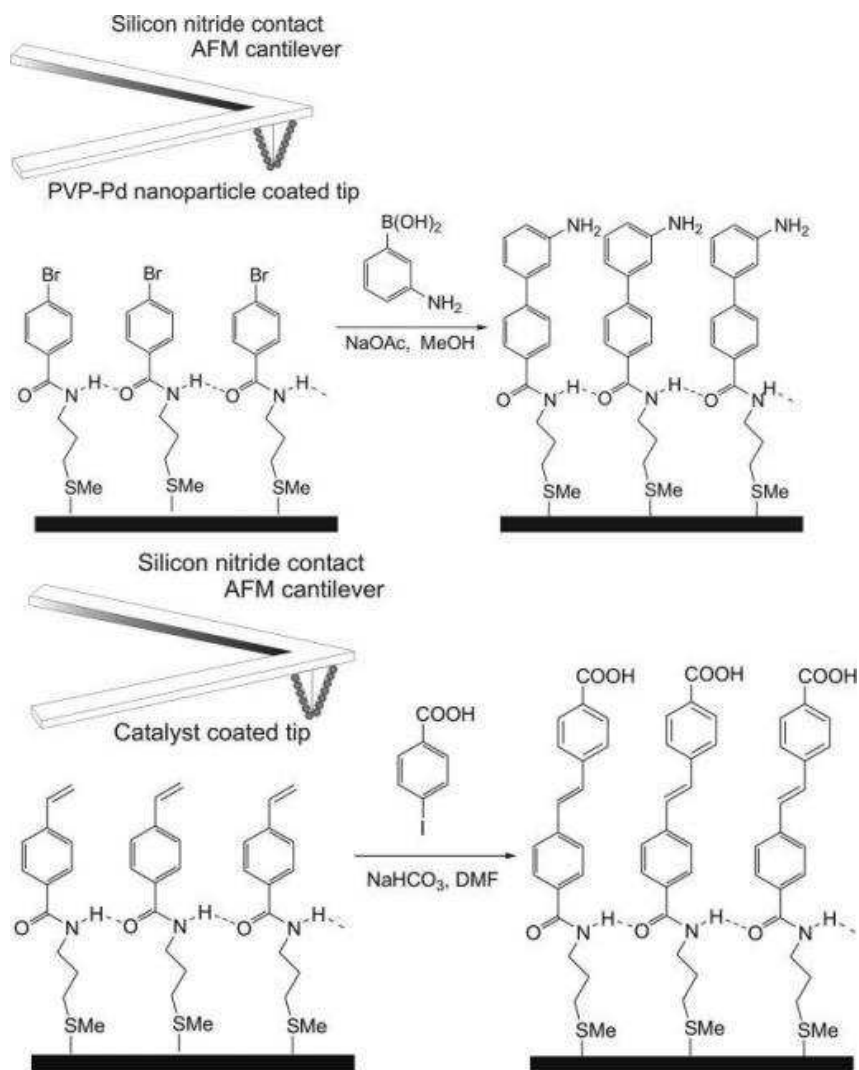
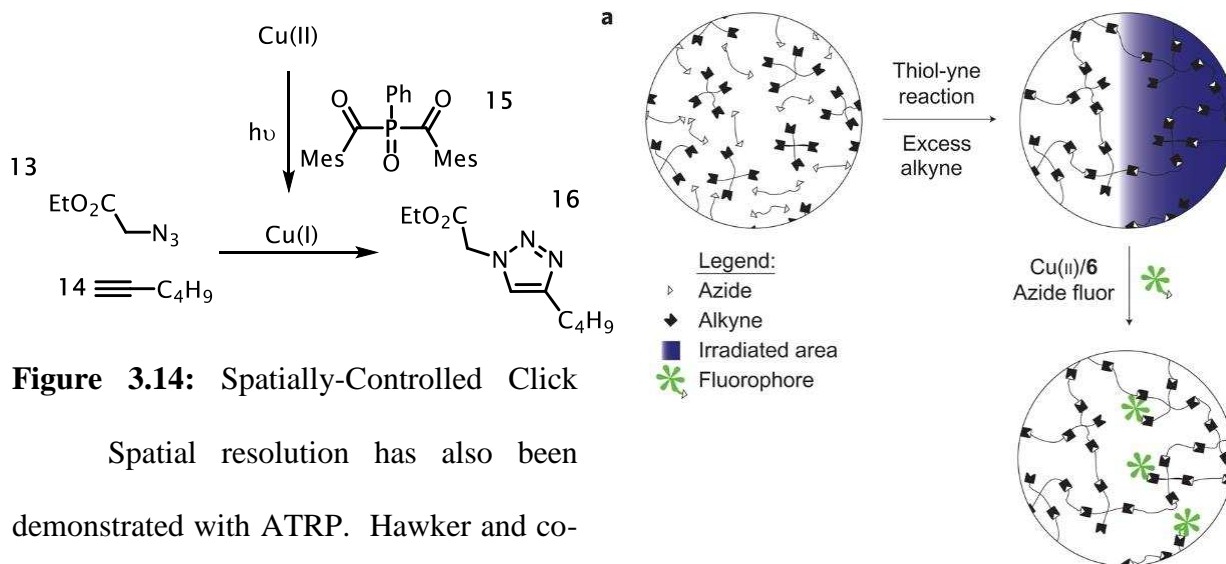


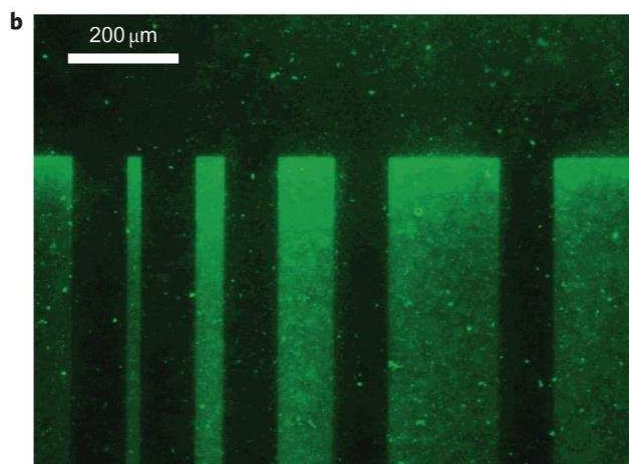
**Figure 3.13:** Catalyst Delivery Using AFM <sup>[35]</sup>

Similar to temporally resolved methodology, many chemists have avoided specialized equipment and explored light-gated catalysts to spatially regulate reactivity. Light's compatibility with lithography makes it a particularly attractive option. In 2011, the Bowman group showed that a light-induced click reaction provides high levels of spatial resolution (**Figure 3.14**). An alkyne-rich hydrogel is first swelled with fluorescent azide **13**, photo-reductant **14**, and a copper catalyst. The gel is then irradiated with light under a photo-mask. Afterward, the gel is thoroughly washed and imaged to reveal the spatially-controlled modification. Spatially-controlled click reactions are

especially appealing for *in vivo* biological applications. It is conceivable that, one day, it may allow for pin-point medical treatments and new ways to track compounds in metabolomics and proteomics.



Spatial resolution has also been demonstrated with ATRP. Hawker and co-workers previously demonstrated the photo-catalyst-controlled polymerization of acrylates (**Figure 3.6**). Experiments indicated the reaction could be controlled to increase molecular weight as a function of light. It is often the case that many temporally-controlled methods translate into



analogous spatially controlled methods. In 2013, Hawker and Fors reported a light-controlled ATRP to fabricate nano-brushes (**Figure 3.15**).<sup>[36]</sup> Immobilizing an alkyl-halide initiator to a surface is the first and foremost important element. A solution of photo-catalyst (**19**) and acrylate monomer (**17**) are placed on the modified surface underneath a photo-mask. Profilometry shows that with longer radiation times, polymer chains grow further from the surface as a result. Hawker adds that a gradient structure is easily generated by using a grayscale photomask. One end of the

mask transmits 100% of the light radiation but the opposing end is opaque and transmits 0%. This experiment clearly demonstrates that increasing amounts of photo flux leads to an increase in polymer length.

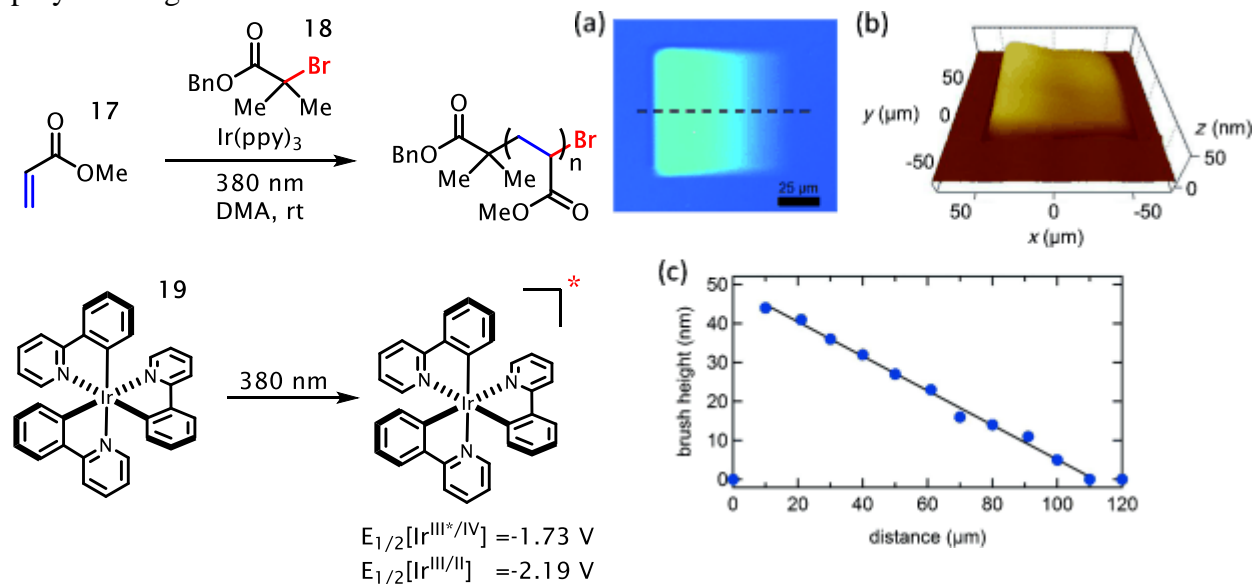


**Figure 3.15:** Spatially-Controlled Atom Transfer

Many metal-catalyzed cross couplings, alkyne-azide cycloadditions, and radical polymerizations have been demonstrated temporally and spatially. However, one catalyst does not have the ability to spatially and temporally control any desired functionality. Thus, exploring different catalytic methods and developing new light-gated catalysts is paramount. Given the unique control element disclosed in Chapter 1, we became interested in demonstrating temporal and spatial applications. To date, a genuine light-gated cobalt catalyst has not been reported.

## REFERENCES

- [1] Rovis, T. *Chem. Lett.* **2008**, 37, 2-7.
- [2] Harper, K. C.; Sigman, M.S. *Science.*, **2011**, 333, 1875-1878.
- [3] Leibfarth, F. A.; Mattson, K. M.; Fors, B. P.; Collins, H. A.; Hawker, C. J. *Angew. Chem. Int. Ed.* **2013**, 199-210.
- [4] Stoll, R. S.; Hecht, S. *Angew. Chem. Int. Ed.* **2010**, 49, 5054-5075.
- [5] Sun, X.; Gao, J. P.; Wang, Y. *J. Am. Chem. Soc.* **2008**, 130, 8130-8131.
- [6] Vollhardt, K. P. C. *Angew. Chem. Int. Ed.* **1984**, 23, 539-556.
- [7] Asinger, F.; Fell, B.; Collin, G. *Chem. Ber.* **1963**, 96, 716-735.
- [8] a) Karlen, T.; Ludi, A.; Muhlebach, A.; Bernhard, P.; Pharisa, C. J. *J. Polym. Sci. Part A* **1995**, 33, 1665-1674. b) Hafner, A.; van der Schaaf, P. A.; Muhlebach, A.; Bernhard, P.; Schaedeli, U.; Karlen, T.; Ludi, A. *Prog. Org. Coat.* **1997**, 32, 89-96.
- [9] a) Delaude, L.; Demonceau, A.; Noels, A. F. *Chem. Commun.* **2001**, 986-987. b) Delaude, L.; Szypa, M.; Demonceau, A.; Noels, A. F. *Adv. Synth. Catal.* **2002**, 344, 749-756.
- [10] Wang, D.; Wurst, K.; Knolle, W.; Decker, U.; Prager, L.; Naumov, S.; Buchmeiser, M. R. *Angew. Chem. Int. Ed.* **2008**, 47, 3267-3270.
- [11] Keitz, B. K.; Grubbs, R. H. *J. Am. Chem. Soc.* **2009**, 131, 2038-2039.
- [12] Serpone, N. S.; Emeline, A.; Ryabchuk, V.; *J. Photochem. Photobiol. A* **2000**, 130, 83-94.
- [13] Wrighton, M. *Chem. Rev.* **1974**, 74, 401-430.
- [14] Several examples of photo-catalyzed assisted catalysis have been reported by discrete electron transfers as well as via energy-state transfer processes.



- [15] a) Blanco, V.; Leigh, D. A.; Marcos, V. *Chem. Soc. Rev.* **2015**, 44, 5341-5370. b) Neilson, B. M.; Bielawski, C. W. *ACS Catal.* **2013**, 3, 1874-1885. c) Treator, A. J.; Lastovickova, D. N.; Bielawski, C. W. *Chem. Rev.* **2015**, 116(2), 1969-1992.
- [16] Sugimoto, H.; Kimura, T.; Inonue, S. *J. Am. Chem. Soc.* **1999**, 121, 2325-2326.
- [17] Adzima, B. J.; Tao, Y.; Kloxin, C. J.; DeForest, C. A.; Anseth, K. S.; Bowman, C. N. *Nature Chem.* **2011**, 3, 256-259.
- [18] Dadashi-Silab, S.; Tasdelen, M. A.; Yagci, Y. *J. Polymer Chem.* **2014**, 52, 2878-2888.
- [19] Treat, N. J.; Fors, B. P.; Kramer, J. W.; Christianson, M.; Chiu, C-Y.; Read de Alaniz, J.; Hawker, C. J. *ACS Macro Lett.* **2014**, 3, 580-584.
- [20] Trotta, J. T.; Fors, B. P. *Synlett.* **2016**, 27(5) 702-713.
- [21] Theriot, J. C.; Lim, C-H.; Yang, H.; Ryan, M. D.; Musgrave, C. B.; Miyake, G. M. *Science.* **2016**, 352, 1082-1086. Also see: Treat, N. J.; Sprafke, H.; Kramer, J. W.; Clark, P. G.; Barton, B. E.; Read de Alaniz, J.; Fors, B. P.; Hawker, C. J. *J. Am. Chem. Soc.* **2014**, 136, 16096–16101
- [22] Teator, A. J.; Lastovickova, D. N.; Bielawski, C. W. *Chem. Rev.* **2016**, 116, 1969-1992.
- [23] Fu, C.; Xu, J.; Boyer, C. *Chem. Comm.* **2016**, 52, 7126-7129.
- [24] Waldrop, M. M. *Nature* **2016**, 530, 144-147.
- [25] Rosa, L. G.; Liang, J. *J. Phys.: Condens. Matter* **2009**, 21 (48), 483001. (Review)
- [26] Salaita, K.; Wang, Y.; Mirkin, C. A. *Nature Nanotechnology* **2007**, 2, 145-155. (Review)
- [27] Sakdinawat, A.; Attwood, D. *Nature Photonics* **2010**, 4, 840-848. (Review)
- [28] Piner, R. D.; Zhu, J.; Xu, F.; Hong, S.; Mirkin, C. A. *Science* **1999**, 283 (5402), 661–663.
- [29] Hu, Y.; Das, A.; Hecht, M. H.; Scoles, G. *Langmuir* **2005**, 21 , 9103.
- [30] Golzhauser, A.; Geyer, W.; Stadler, V.; Eck, W.; Grunze, M.; Edinger, K.; Weimann, T.; Hinze, P. J. *Vac. Sci. Technol. B* **2000**, 18, 3414.

- [31] Li, N.; Tourovskaia, A.; Folch, A. *Crit. Rev Biomed Eng.* **2003**, 31, 423-488.
- [32] Dressick, W. J.; Calvert, J. M. *Jpn. J. Appl. Phys.* **1993**, 32, 5829-5839.
- [33] Rozsnyai, L. F.; Wrighton, M. S. *Langmuir* **1995**, 11, 3913-3920.
- [34] Ryan, D.; Parviz, B. A.; Linder, V.; Semetey, V.; Sia, S. K.; Su, J.; Mrksich, M.; Whitesides, G. M. *Langmuir* **2004**, 20, 9080-9088.
- [35] Davis, J. J.; Bagshaw, C. B.; Busuttill, K. L.; Hanyu, Y.; Coleman, K. S. *J. Am. Chem. Soc.* **2006**, 128, 14135-14141.
- [36] Poelma, J. E.; Fors, B. P.; Meyers, G. F.; Kramer, J. W.; Hawker, C. J. *Angew. Chem. Int. Ed.* **2013**, 52, 6844-6848.

## CHAPTER FOUR

### Applications of Light-Gated Cobalt Catalysis

#### **PART A:** *Light-Controlled [2+2+2] Cycloaddition Polymerization*

#### **4.1 - Background**

Step-growth monomers contain multiple reactive functional groups and every oligomer generated has an equivalent reactivity in the polymerization.<sup>[1]</sup> This means that, unlike chain-growth polymers, step-growth polymers do not grow exclusively from a leading chain end. Nylon and silicone are common examples of step-growth polymerizations (**Figure 4.1**). After two monomer units react the resulting dimer remains active in the polymerization. Although monomer is rapidly consumed at the outset of the polymerization, higher molecular weights are eventually achieved by reaction of higher order oligomers. Due to this growth mechanism, step-growth polymerizations that reach a high molecular weight often have high polydispersity indexes (PDIs).

Many controlled polymerizations are accomplished by exploiting a monomer functional group such as an alkyl halide bond (i.e. ATRP) (**Figure 4.1**). Without structural features to leverage for control, externally regulating a chain- or step-growth polymerization presents an interesting challenge. We felt that applying light-gated cobalt catalysis to temporally control a [2+2+2] polymerization would be an excellent demonstration of externally regulated cobalt catalysis.

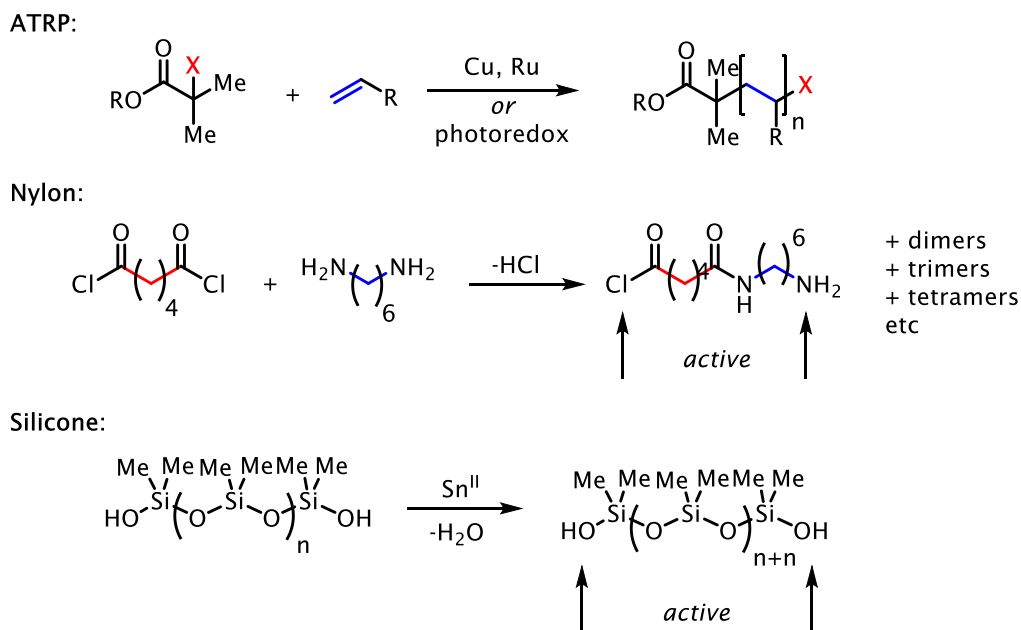


**Figure 4.1:** Comparison of ATRP to Step-Growth Polymerization

In 2011, Okamoto reported the first [2+2+2] cycloaddition polymerization (**Figure 4.2**).<sup>[2]</sup> In the presence of a cobalt(II) pre-catalyst and reductant, monomer **18** delivers a linear polymer with a high molecular weight and low PDI. Interestingly, the polymer linearity is influenced by the catalyst employed, and this effect is rationalized by the chain transfer mechanism also shown in **Figure 4.2**. Okamoto and associates propose that the incoming monomer coordinates to the metal center and directs the following oxidative cyclization to the tethered diyne in close proximity. This high fidelity of monomer addition reduces polymer branching and furnishes a highly linear polymer. They add that this reactivity enables a one-pot chain-growth block copolymer synthesis. The more reactive monomer **1** is rapidly consumed to construct the first half of the block polymer. The latter half of the co-polymer is then exclusively formed with monomer **2** which remained in solution. Although this reactivity exhibited in Okamoto's work is useful, it possesses no elements for external regulation.

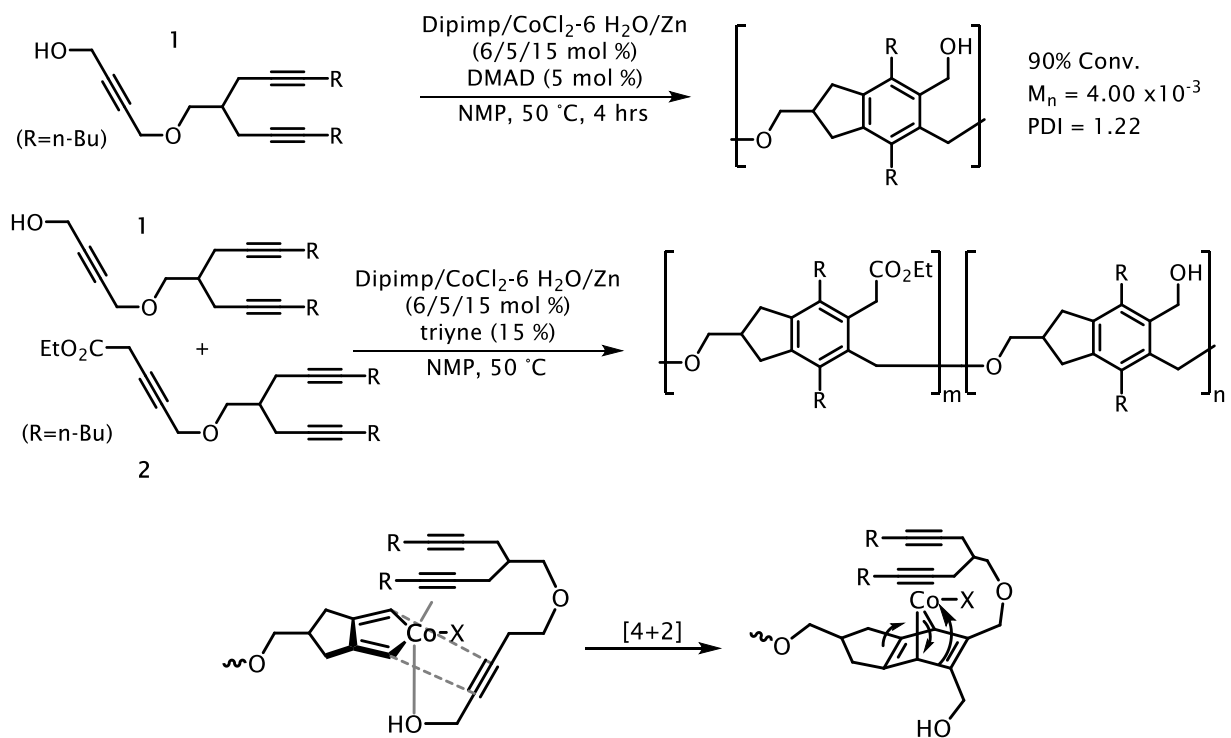


**Figure 4.2:** Okamoto's Chain-Growth [2+2+2] Cycloaddition Polymerization

With this knowledge we wanted to determine if our light-gated cobalt catalyst would control a [2+2+2] cycloaddition polymerization. We were specifically interested in the polymer's growth characteristics and the ability to regulate the polymer's molecular weight and PDI. To this point we already demonstrated our catalyst behaves as a light-switchable catalyst, so we began to examine a variety of [2+2+2] monomers and evaluate their reactivity towards polymerization.

## 4.2 – Results and Discussion

### 4.2.1 – Monomer Development

We began investigating externally-controlled cobalt-catalyzed polymerizations using para-diethynylbenzene (**3**) as a monomer.<sup>[3]</sup> Subjecting **3** to the standard reaction conditions led to a dark green/brown solution with a dark insoluble precipitate (**Figure 4.3**). Analyzing the

supernatant indicated that monomer consumption only reached 60%, and less than 20% of the material mass was isolated as a polymeric material. Additionally, preparing a sample for GPC analysis (Gel Permeation Chromatography) revealed that the polymer material was insoluble in most organic solvents. We hypothesized precipitation of the polymer from solution sequestered active catalyst and led to an incomplete monomer consumption. To address catalyst loss via polymer precipitation, we opted for a flexible monomer that we believed would increase polymer solubility.

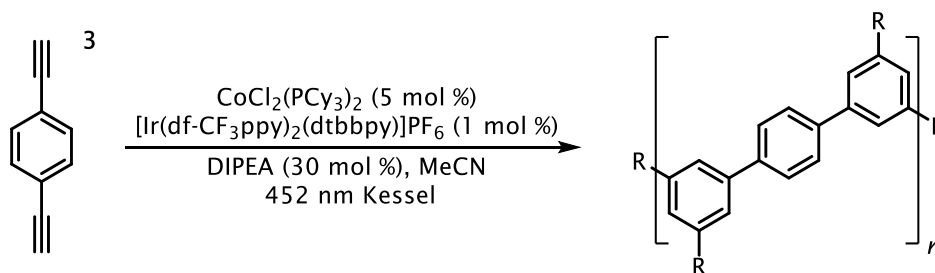


**Figure 4.3:** Attempted Polymerization of *p*-Diethynylbenzene

We continued our investigation with the *tris*-propargylated monomer **7**. As shown in **Figure 4.4**, the synthesis of **5** begins with a tri-alkylation of the commercially available mono ethyl ester malonic acid **4** with propargyl bromide. Initial alkylation delivers the mixed malonic ester which continues to react with propargyl bromide to afford compound **5** as a clear oil in 90% yield.

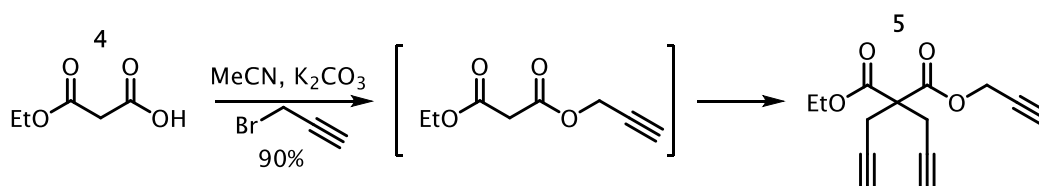


**Figure 4.4:** Synthesis of Aliphatic Monomer

With compound **7** in hand, we tested it as a monomer for the [2+2+2] cycloaddition polymerization. After 12 hours under the standard reaction conditions, a dark brown solution had formed an oily brown material (**Figure 4.5**). After several attempts, consumption of **5** never exceeded 40% and the yield of the polymer (**6**) was correspondingly low. In addition to the unreacted monomer, dimers and trimers were also identified by crude LC-MS. GPC analysis indicated **6** had a low average molecular weight (less 1000-1200 g/mol) below the instrument's calibration curve. Given the poor performance of **77** (Chapter 1), as well as the lower reactivity observed with aliphatic alkynes in Chapter 1, we believed monomer **7** was not reactive enough to achieve high molecular weights.

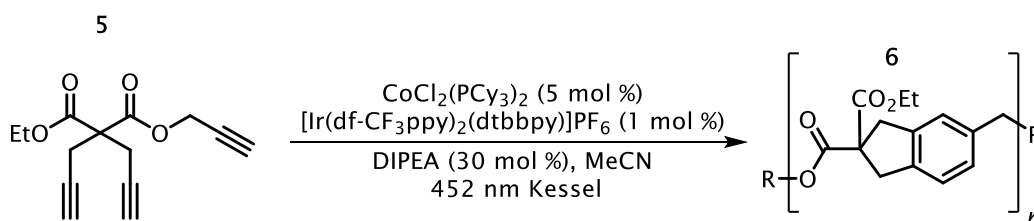


**Figure 4.5:** Attempted Polymerization with Aliphatic Monomer

After reviewing the reaction scope (Chapter 1, Figure 15), we felt introducing a quaternary carbon into the backbone of **7** would substantially increase reactivity. Synthesis of a test compound (**10**) to probe this hypothesis begins with bis-alkylation of malonate ester **7**. Mono-hydrolysis then furnishes the half-ester malonic acid **8** (**Figure 4.6**). To retain the quaternary carbon and introduce the p-ethynyl benzylic alcohol component (**9**), **5** is first converted to the corresponding acid chloride. At low temperature a solution of the acid chloride and triethylamine ( $\text{NEt}_3$ ) is added to the benzylic alcohol (**9**) drop-wise. After stirring for three hours at  $-10^\circ\text{C}$ , the compound is isolated and purified by column chromatography to give **10** as a white solid in 72% yield.

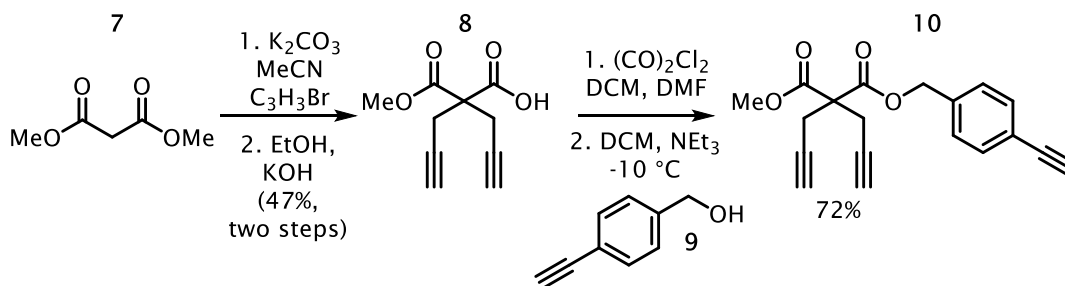


**Figure 4.6:** Synthesis of Monomer with Quaternary Carbon

Moving forward we found that **10** presented similar insolubility issues upon polymerization. After ten minutes of irradiation the reaction produced an insoluble polymer (**11a**). Significant amounts of unreacted monomer (**10**) remained in the supernatant and gel permeation chromatography (GPC) could not be performed on the isolated material (**Figure 4.7**). Although initial rates of monomer consumption was high, polymer precipitation sequestered the active catalyst from solution. Thus, we concluded that monomer **10** was sufficiently reactive but considered using additives to increase polymer solubility.

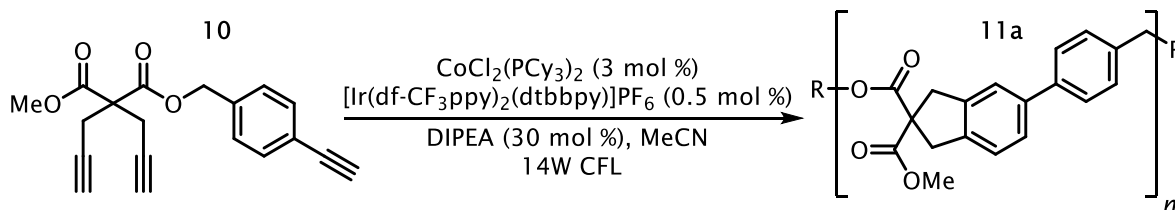


**Figure 4.7:** Reactive Monomer Still Suffers from Insolubility

We hypothesized that tri-ethynylbenzene (**12**), in small amounts, may significantly branch our polymer and form a dendrimer-type structure. Much to our excitement, the additive increases solubility and homogeneity of the polymerization reaction with loadings as low as 10% (**Figure 4.8**). After three hours, the reaction consumes **10** entirely and the polymer precipitates as an off-



white powder with the addition of methanol. GPC analysis indicates that polymer **11b** has a molecular weight of 1520 g/mol and a polydispersity index of 1.5 (PDI).

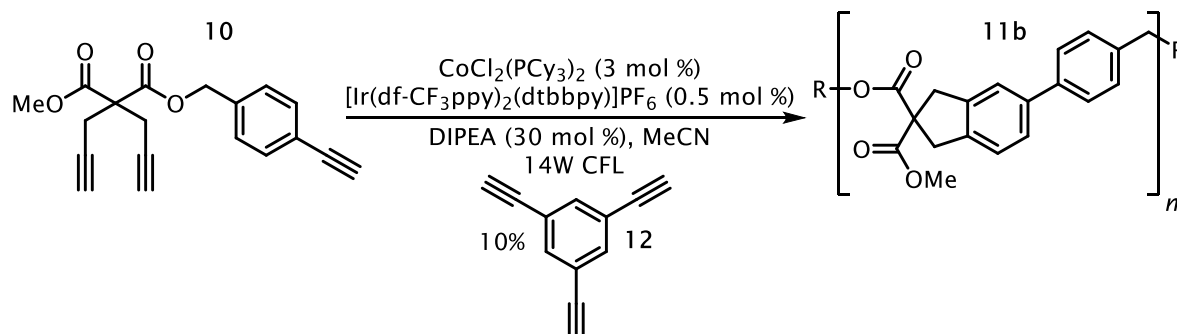


**Figure 4.8:** Tri-ethynylbenzene Increases Polymer Solubility

#### 4.2.2 – Monomer Consumption Experiments

A molecular weight of 1520 g/mol is low but provides an opportunity to determine if our light-gated catalyst enables a light-controlled polymerization. To test this proposal and track monomer consumption as a function of light irradiation, we conducted a polymerization in the presence of an internal standard. Gratifyingly, the consumption of **10** is easily controlled by adding or removing light radiation and in the first five minutes of irradiation monomer consumption reaches 55% (**Figure 4.9**). After the light is removed, the catalyst becomes dormant and **10** is no longer polymerized. The catalyst is then re-activated by reintroducing light and the polymerization is restarted. Remarkably, the reaction can be cycled continually and monomer disappears as a function of light radiation.

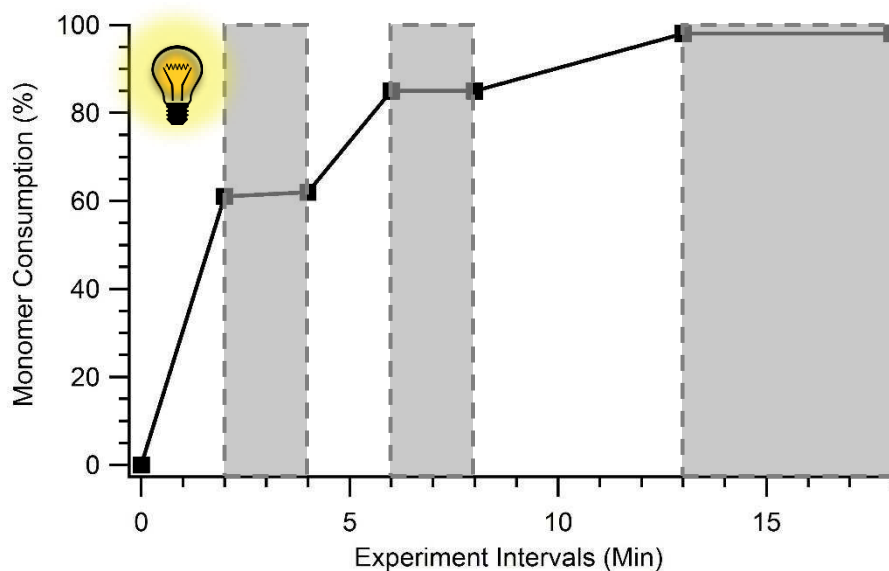
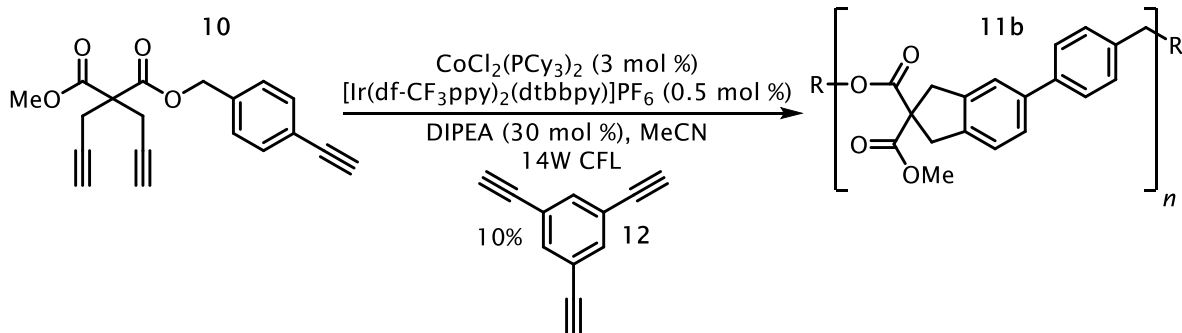


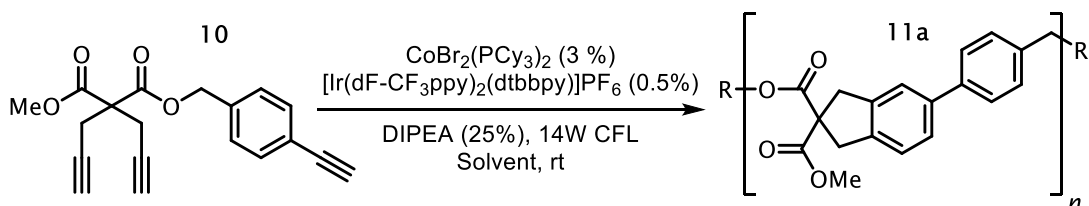
**Figure 4.9:** Initial Study of Monomer Consumption

#### 4.2.3 -- Polymer Optimization

Although monomer consumption responds to light radiation, light's effect on molecular weight remained speculative. Hence, we were eager to optimize the polymerization conditions and investigate the polymer's growth as a function of light radiation. Several changes to the standard conditions proved ineffectual but we observed that a mixed solvent using dichloromethane (DCE) and acetonitrile (MeCN) greatly enhances polymer solubility (**Table 4.1**, entry 2-4). In fact, by adding DCE, the TEB additive (**12**) could be removed from the reaction mixture. Furthermore, we found that pre-irradiating the pre-catalyst with certain additives was also beneficial to overall

performance. The pre-catalyst is dissolved in solution with photo-catalyst, sacrificial organic reductant and a sub-stoichiometric amount of an alkyne additive. This solution is irradiated for 15-30 minutes and then transferred to a solution of monomer. With this procedural change, molecular weights increase and we observe PDIs drop below 1.2 with acceptable molecular weights (**Table 4.1**, entry 5-9).

Conceivably, without this pre-irradiation sequence, slow and erratic pre-catalyst reduction leads to an inefficient polymer initiation. Polymerization reactions generally perform best with a rapid and clean initiation process and pre-irradiation with alkyne additives converts the pre-catalyst into an active but dormant species. After monomer addition, light radiation quickly activates the dormant catalyst and immediately begins to polymerize monomer. Ultimately, we consistently observe polymer yields in the high 80's, molecular weights in the 3-4kD range, and PDIs ranging from 1.18 to 1.30 (**Table 4.1**, entry 10, 11).

**Table 4.1:** Optimization of Polymerization Conditions

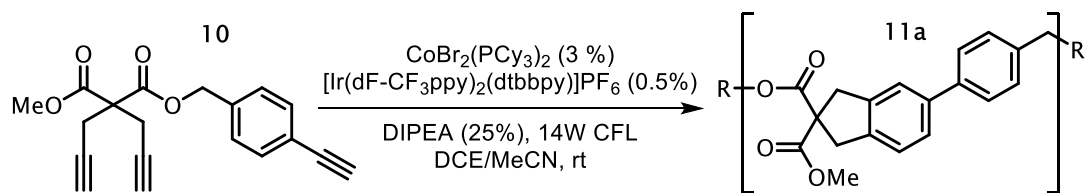
Entry	Solvent	[M]	Additive	Hr	Mn (kD)	PDI	Yield
1	MeCN	0.1	-----	16	---	---	45%
2	MeCN/DCE (1:5)	0.3	-----	16	4.7	2.17	90%
3	MeCN/DCE (1:5)	0.2	-----	16	3.7	1.51	83%
4	MeCN/DCE (1:5)	0.1	PhC <sub>2</sub> H (10%)	3.0	2.7	1.39	76%
5	DCE	0.1	PhC <sub>2</sub> H (10%)	3.0	3.2	1.35	72%
6	DMF	0.1	PhC <sub>2</sub> H (10%)	3.0	3.4	1.52	71%
7	DCE	0.1	PhC <sub>2</sub> H (10%)	16	2.9	1.38	85%
8	DCE	0.2	PhC <sub>2</sub> H (10%)	16	3.2	1.38	82%
9	MeCN/DCE (1:1)	0.2	Diyne (3%)	4	2.8	1.36	84%
<b>10</b>	<b>MeCN/DCE (1:1)</b>	<b>0.1</b>	<b>Diyne (3%)</b>	<b>4</b>	<b>3.3</b>	<b>1.28</b>	<b>82%</b>
11 <sup>a</sup>	MeCN/DCE (1:1)	0.1	Diyne (3%)	4	3.5	1.18	78%

After completion all reactions were concentrated under high vacuum, precipitated, and washed with MeOH for GPC analysis. a) Cobalt loading reduced to 1%

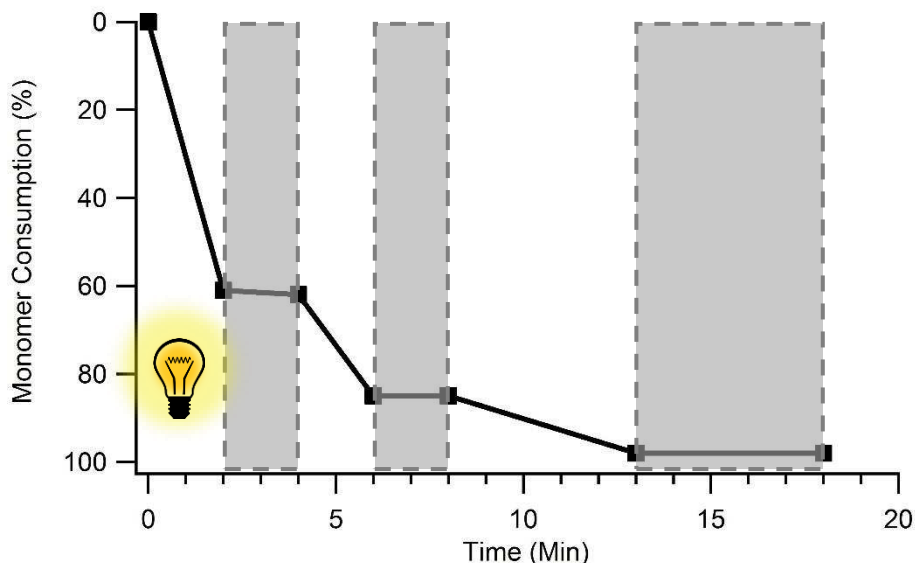
#### 4.2.4 – Polymer Growth Experiments

Although experiments suggest that light is intimately involved in monomer consumption, we were eager to determine light's impact on polymer growth and molecular weight. Following molecular weight as a function light would not only provide mechanistic information, but also confirm that monomer consumption is providing polymer and not just low molecular weight oligomers (dimers, trimers, etc.). To determine light's impact, we employed another ON/OFF experiment using alternating periods of light and darkness (**Figure 4.10**). LC and GPC analysis was used to determine monomer consumption and molecular weight over the entire reaction duration. Remarkably, in the first period of irradiation we see that monomer is consumed to 61%

and a 1.5 kD polymer is formed in solution (PDI = 1.07). As we expected, removing light deactivates the switchable cobalt catalyst and stops the polymerization. A second irradiation period reactivates the catalyst and continues to consume monomer which is echoed by an increase in molecular weight to 2.2 kD. Ultimately, a 3.0 kD polymer is isolated with a PDI of 1.5 is isolated at the end of the experiment. Without a doubt, this experiment suggests our switchable cobalt catalyst enables a light-controlled [2+2+2] cycloaddition polymerization and monomer consumption does in fact lead to polymer growth.



a.



b.

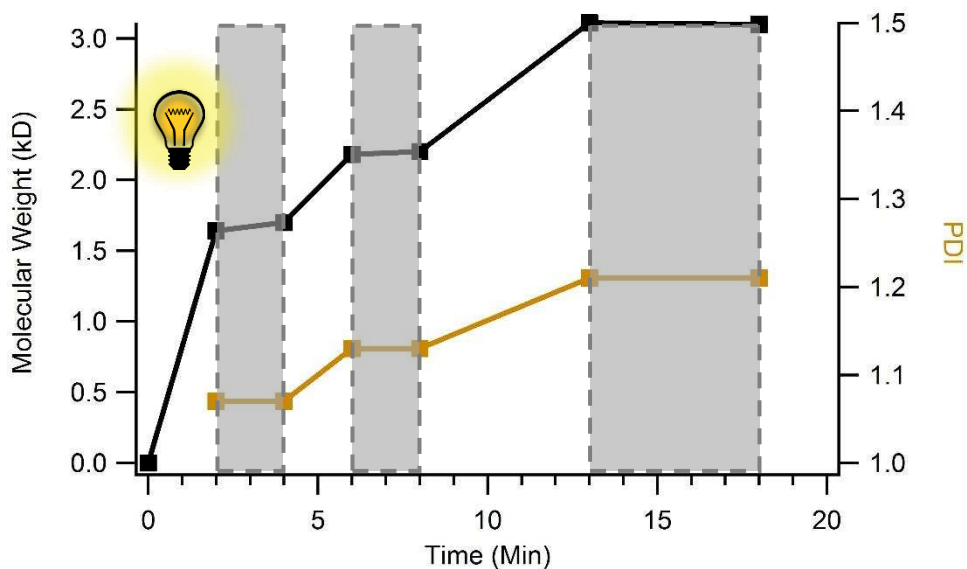


**Figure 4.10:** a) Monomer Consumption b) Molecular Weight and PDI

Step-growth polymerizations do not commonly afford appreciable molecular weights until monomer consumption reaches greater than 95%. Initial monomer consumption leads to formation of oligomers (dimers, trimers, etc.) first, but higher molecular weight requires extend reaction

times. Consequently, step-growth polymers generally deliver polymers with PDIs greater than 2.0. In contrast, chain-growth polymerizations achieve high molecular weights even in the presence of unconsumed monomer. Polymer growth occurs exclusively by addition of monomer units to the leading polymer end, and therefore, a chain-growth polymerization can furnish both high molecular weights and low PDIs without complete monomer consumption.

Although we initially assumed our [2+2+2] cycloaddition polymerization to proceed in a step-growth fashion, the rapid rise in molecular weight suggests that this may not be the case. An initial molecular weight of 1.5 kD and PDI of 1.07 after the first irradiation period suggests a modest level of chain-growth behavior. Inspection of the polymer by  $^1\text{H}$  NMR also reveals low levels of branching in the polymer due to cross reactivity between two diyne moieties (**Figure 4.11**). Although we cannot be certain, we believe the polymerization is predominately step-growth but intermittently proceeds via a chain-growth process.

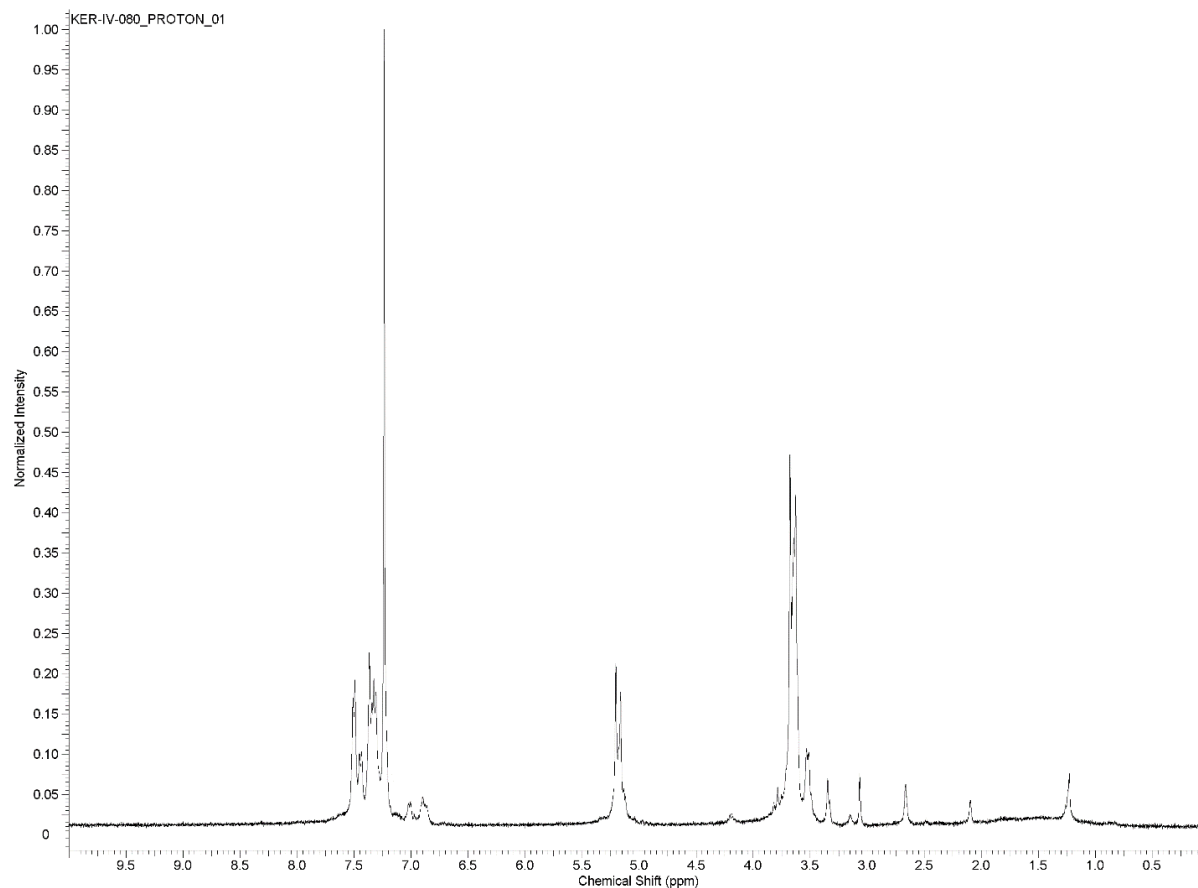


**Figure 4.11:** <sup>1</sup>H NMR of the [2+2+2] Cycloaddition Polymerization

### 4.3 Summary

Ultimately, our light-gated cobalt catalyst provides the first light-controlled [2+2+2] cycloaddition polymerization. Preliminary evidence suggests the polymerization proceeds mainly by a step-growth fashion but displays characteristics of a chain-growth polymerization. The polymer structure is not perfectly linear and shows low levels of branching due to diyne-diyne coupling. Conceivably, coordinating groups on the aryl alkyne may promote chain-growth behavior and increase polymer linearity. This system will be studied further to elucidate unique mechanistic aspects.



## PART B: Spatially Controlled Arene Formation

### 4.4 --- Background

Conjugated arenes comprise a unique class of compounds with numerous applications in materials chemistry. Overlapping, planar  $\pi$ -systems often give rise to unique HOMO-LUMO gaps which makes them distinct among many structural motifs. As a result, conjugated polymers (ie: **14**) are the foundation of many electrochemical devices including OLEDs, transistors and both chemical and biological sensory devices (**Figure 4.12**).<sup>[4]</sup> Many of these devices currently rely on precious and rare-earth metals which are not routinely recycled and repurposed. Replacing these sparse materials with carbon-based technology will increase the sustainability of technology and, ultimately, decrease the final cost extended to the consumer.

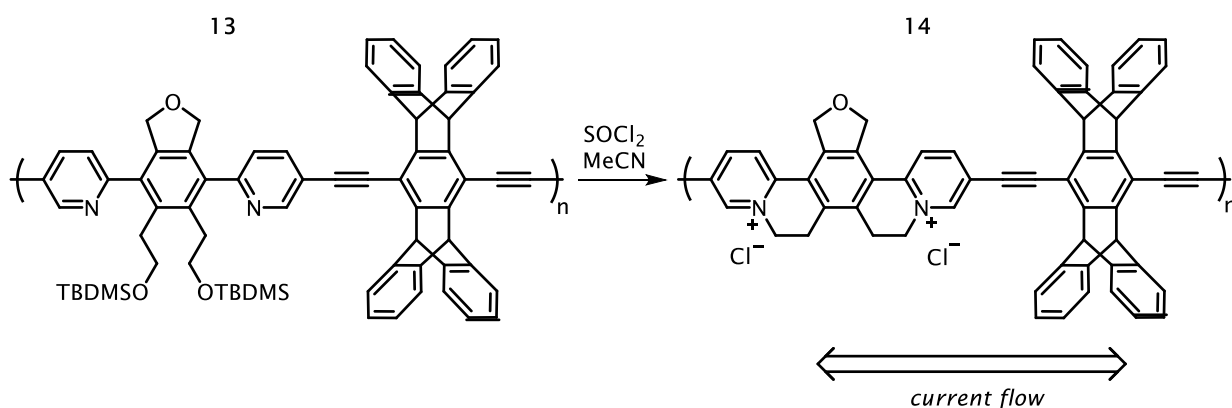


**Figure 4.12:** Conducting Polymer

Arranged in a monolayer, conjugated compounds are profoundly useful in many analytical and electrochemical applications.<sup>[5]</sup> However, constructing arene monolayers is an outstanding challenge especially in comparison to SAMs created on gold with alkanethiols.<sup>[6]</sup> The preferred method to form arene monolayers is by reduction of an aryl radical precursor (ie: **15**) at a conducting surface.<sup>[7]</sup> The high reactivity of arene radicals makes them versatile for bond

formation, but likewise renders them difficult to control. After formation of a uniform monolayer, the arene-rich surface remains exposed to radicals being generated at the surface (**Figure 4.13**). Further addition of arene radicals to the immobilized arene groups leads multi-layer formation which compromises overall performance.<sup>[8]</sup>

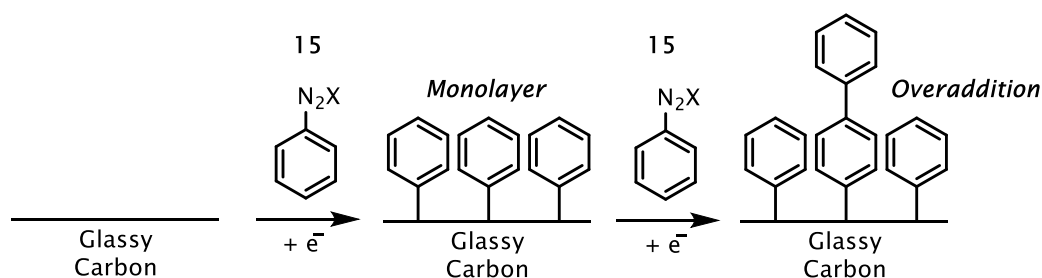


**Figure 4.13:** Aryl Diazonium Salts form Multi-layer on Surface

Fortunately, chemists have found ways to overcome this issue. In 2010, Hapiot and colleagues showed that substituting diazonium salts with bulky silane groups considerably decreases multi-layer formation (**Figure 4.14**).<sup>[9]</sup> Para-(silyl)ethynylbenzene diazonium salts (**16-18**) are easily synthesized from the corresponding anilines. A solution of the desired diazonium salt can then be prepared for a clean, polished glassy carbon electrode. Passing a reductive current then liberates nitrogen gas to generate an arene radical which forms a covalent bond with the surface. After a monolayer is formed, excess radicals will be blocked by the unreactive silanes. Therefore, a monolayer is exclusively formed. Hapiot adds that the silanes are easily de-protected with TBAF to give the unprotected and versatile alkyne functional group. Furthermore, larger silanes (ie: triisopropyl silane (TIPS)) provides a less dense arene monolayer and, respectively, smaller silanes give high density.<sup>[10]</sup>

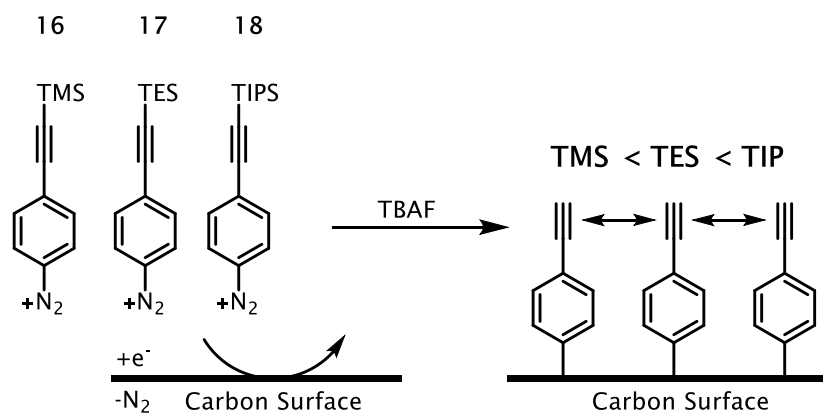


**Figure 4.14:** Bulky Groups Prevent Over-Addition

Alkyne functional groups provide a chemically versatile surface but the requisite silane groups restrict the diversity of applicable diazonium salts. Breton and co-workers report an alternative method that does not depend on a blocking group (**Figure 4.15**). Uniform nitro-arene monolayers are achieved by dissolving a radical scavenger in solution to intercept excess radicals.<sup>[11]</sup> 2-[4-(4-nitro)phenyl]-2-phenyl-1-picrylhydrazine (**20**) serves as the sacrificial radical scavenger to remove excess radical which generates compound **21**.

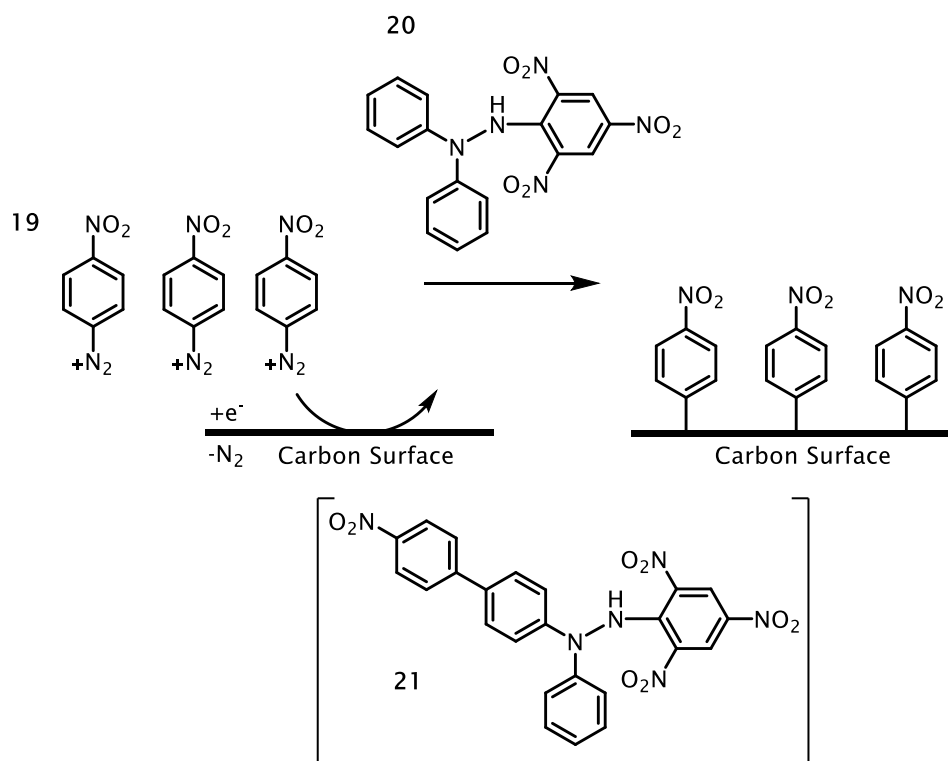


**Figure 4.15:** Radical Scavengers Prevent Over-Addition

Chemists have addressed multilayer formation with both bulky substituents and radical scavengers. However, the most efficient methods to create arene monolayers would be to form them directly via a [2+2+2]. Furthermore, arene monolayer formation via diazonium reduction leaves no opportunity for spatial control. We envisioned using light-gated cobalt catalysis to achieve arene monolayers with high levels of spatial control.

#### 4.5 – Results and Discussion

To initiate our surfaces studies with light-gated cobalt catalysis we first chose to work on glass since it is both inexpensive and widely available. In fact, alkyne-rich glass surfaces are commercially available from MicroSurfaces, Inc. In the first attempt, we treated the alkyne-rich glass slide with a solution containing cobalt pre-catalyst, photo-catalyst and diyne **22** (Figure

**4.16).** The solution was dispensed on the surface, covered with a glass cover slide and then irradiated. Afterward, the cover slide was removed and the surface was washed several times before being dried under vacuum. Analyzing the surface with X-ray photoelectron spectroscopy (XPS) before and after the modification indicated little change in surface composition. It is possible that XPS is not sensitive enough for such a thin surface modification or the chemistry itself was ineffective. However, recovering the reaction solution after irradiating and analyzing it by LC-MS suggested formation of a diyne dimer dominated the reaction in solution. This product, previously observed in reaction development, suggests the cobalt catalyst was active but interaction with the modified surface did not occur. It is logical to assume homogeneous catalysis would prevail over reaction with an immobilized reagent.

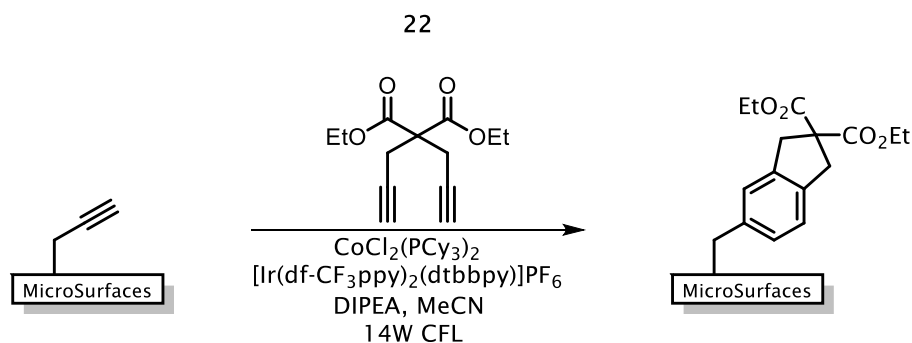


**Figure 4.16:** Initial Attempts at Surface Modification

We concluded that an immobilized aliphatic alkyne is not be reactive enough to participate in catalysis which is preferentially occurring in solution. To enhance the immobilized reagent's reactivity we believed that installation of an aromatic alkyne would offer higher catalyst affinity and reactivity.

Glass is comprised of repeating  $\text{SiO}_2$  units in a rigid network solid. Its surface can readily be oxidized with piranha solution ( $\text{H}_2\text{O}_2/\text{H}_2\text{SO}_4$ ) or with oxygen plasma to give a chemically

reactive and nucleophilic surface (**Figure 4.17**). To install a linker with an aromatic alkyne, we first created a maleimide-rich glass surface. A glass slide was oxidized with oxygen plasma and then immediately treated with APTES (aminopropyl ethoxysilane – **23**) to give a primary amine-rich surface. Treating this surface with a solution of **24** in DMSO forms an amide bond which anchors the dienophilic maleimide group to the glass surface.

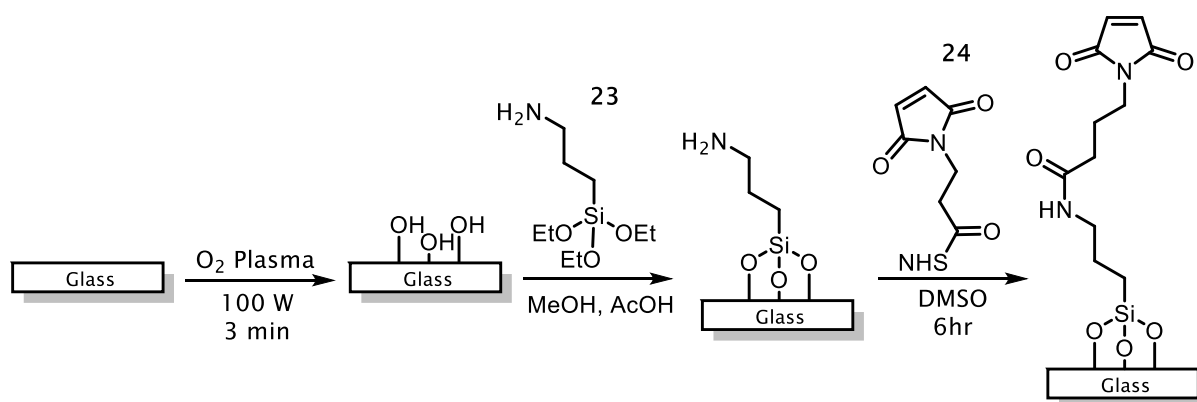


**Figure 4.17:** Glass Surface with an Aromatic Alkyne

Synthesis of the aromatic alkyne linker begins with commercially available TEG (tetraethyleneglycol – **25**) (**Figure 4.18**).<sup>[12]</sup> Mono-alkylation of **25** with 4-ethynylbenzyl bromide gives the mono-alcohol **26**. Tosylation of **26** with TsCl (tosyl chloride) under basic conditions and subsequent  $S_N2$  displacement with NaCP (sodium cyclopentadienide) furnishes the final linker (**27**). At this point, the linker is ready to be installed via a [4+2] cycloaddition reaction with the maleimide-rich surface.

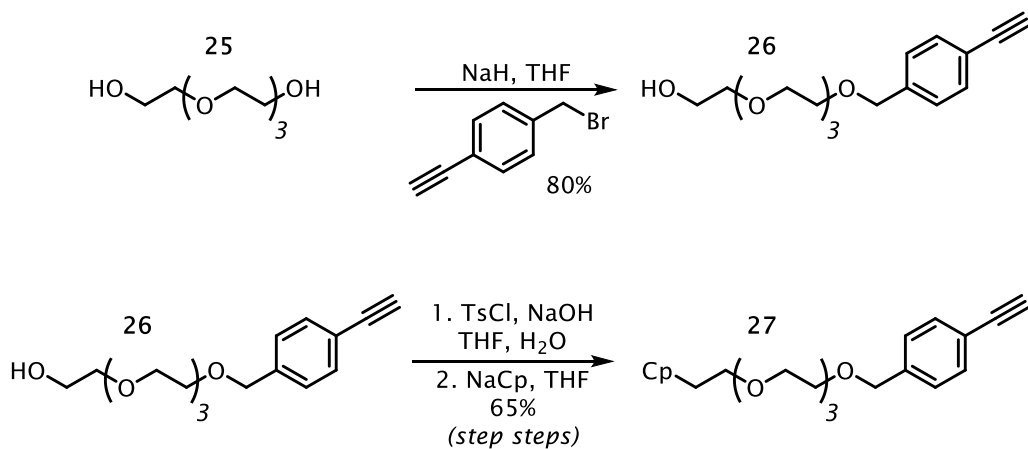


**Figure 4.18:** Synthesis of Aromatic Alkyne-Rich Surface

With the maleimide-rich glass surface and cyclopentadiene-containing linker in hand we then moved to install the linker (**Figure 4.19**). A solution of **27** was placed into a glass Petri dish and the maleimide functionalized glass slide was fully submerged. The Petri dish was covered in foil to minimize light exposure. After four hours the glass slide was removed, washed, and dried.

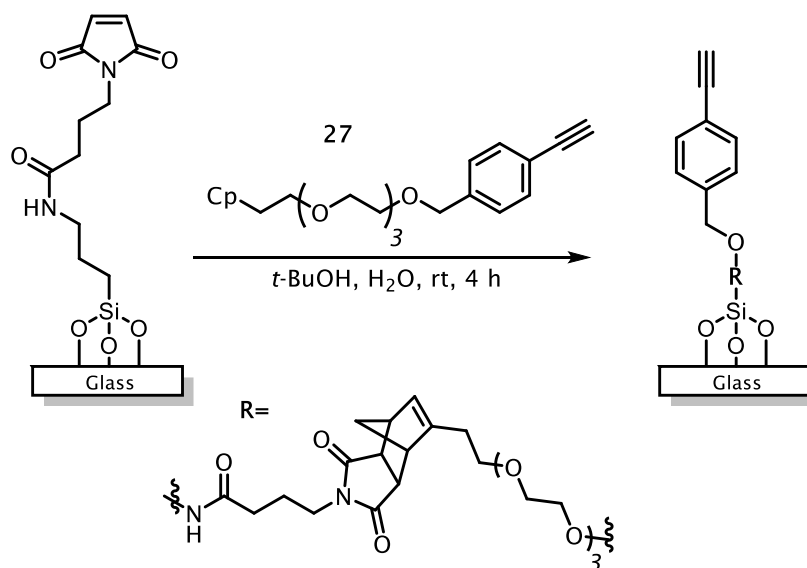


**Figure 4.19:** Attaching Aromatic Alkyne Linker to the Surface

Assuming the aromatic alkyne would be more reactive, we dissolved cobalt pre-catalyst, photo-catalyst and **22** in acetonitrile and placed it on the glass surface (**Figure 4.20**). After irradiating and cleaning the surface we conducted XPS analysis, however, we found no discernible differences between the various stages of chemical modification including the arene formation attempt. After failing to observe catalysis, yet again, we questioned the nature of our glass surface. We sought an adequate method to confirm alkyne functional groups on the surface and conclude why we were not observing reactivity.

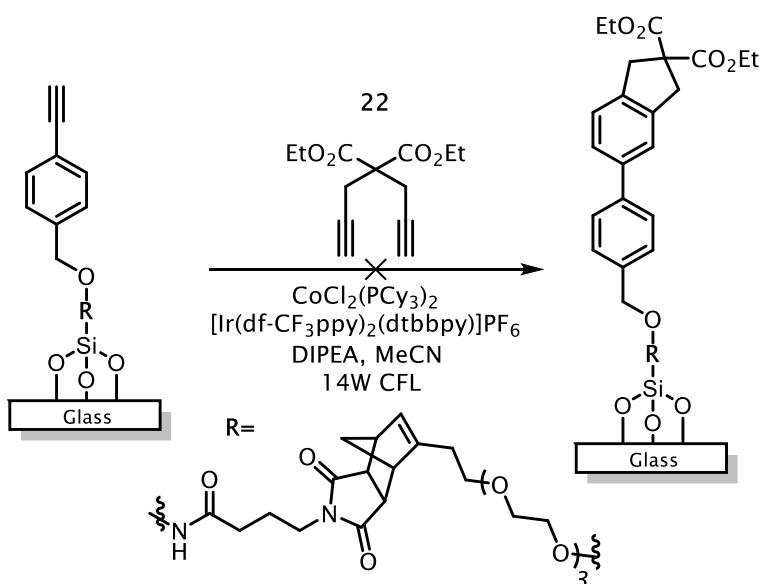


**Figure 4.20:** Attempt Surface Chemistry with Aromatic Alkynes

Fortunately, alkyne functional groups participate in a wide variety of transformations. Specifically, the robust nature of alkyne click chemistry and the availability to fluorescent azides makes it particularly attractive. We felt the Huisgen cycloaddition would allow us to qualitatively confirm alkynes on the glass surface. Initial click reactions with  $\text{Cu}(\text{SO}_4)_2$  and fluorescent azide **28** on the commercially available plates showed little to no reactivity. However, using a copper(I)acetonitrile complex with ligand **29** under anaerobic conditions gave us a positive



identification of alkynes by fluorescence microscopy (**Figure 4.21**). Although the fluorescence signal was weak, we qualitatively confirmed the presence of alkynes on the purchased substrates.

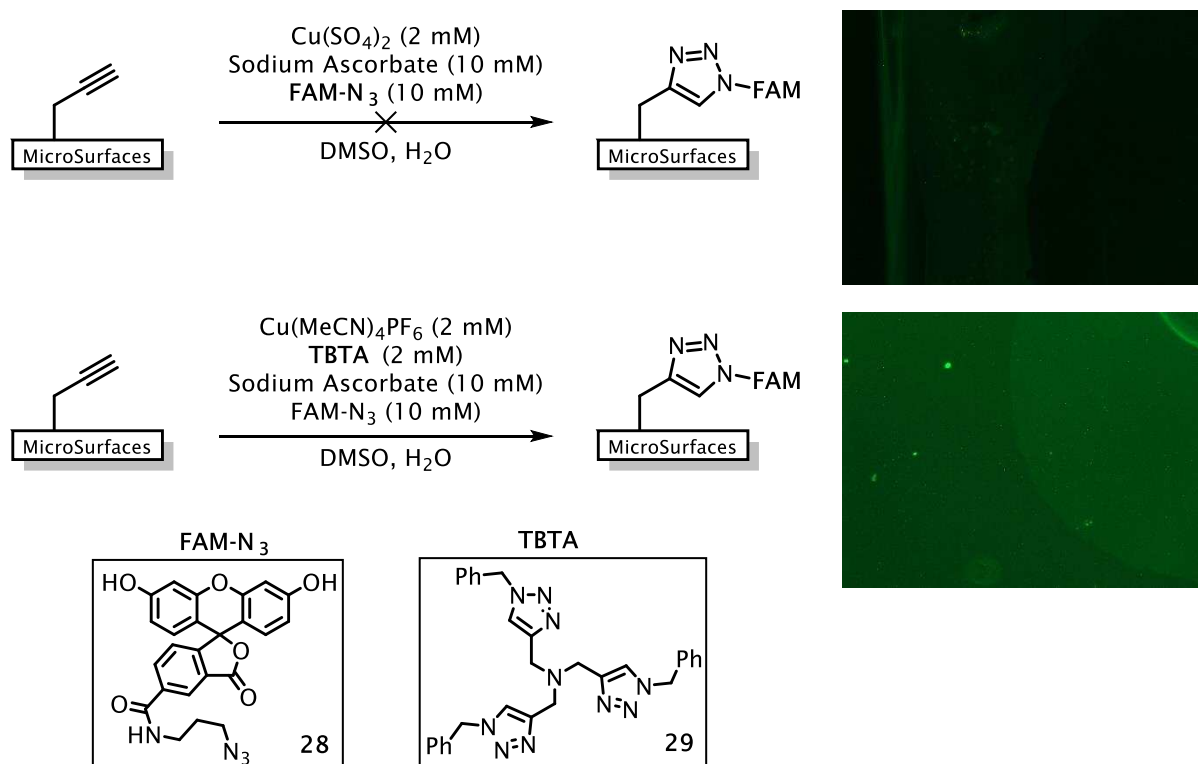


**Figure 4.21:** Optimizing Click Chemistry

After demonstrating that click-chemistry confirms the presence of alkyne functional groups, we revisited the previous glass surfaces. Although XPS analysis showed no changes in the aromatic alkyne surface, the click reaction suggests alkyne moieties are present (**Figure 4.22**). Confining the click control to a PDMS well on the substrate surface shows fluorescence only from the treated areas. As a negative control, the penultimate maleimide surface shows no observable amount of fluorescence after a click reaction.

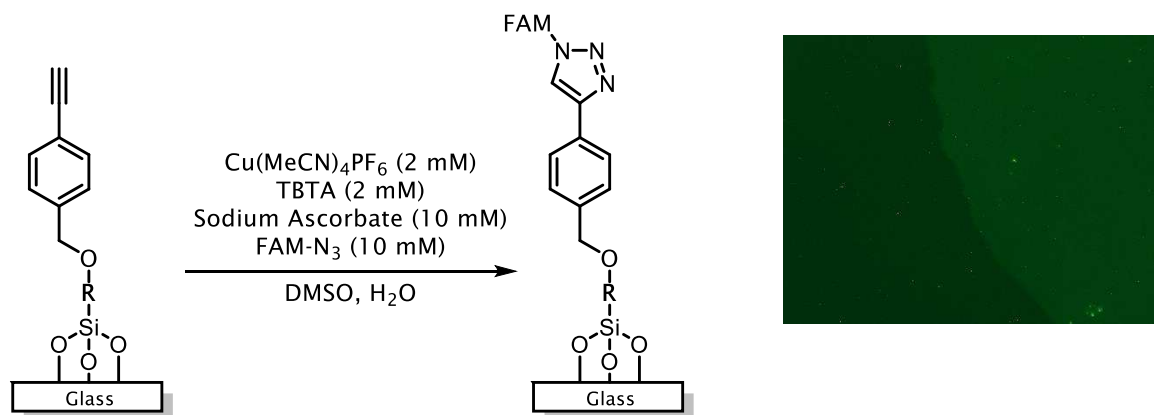


**Figure 4.22:** Positive Click Control on Aromatic Alkyne Surface

Insight from the controls led us to conclude that alkynes are present on the surface, but arene formation is likely not occurring. Considering the reaction mechanism, after the cobalt pre-catalyst is reduced in solution the following step requires an oxidative cyclization with the diyne substrate. In a surface application, oxidative cyclization must be followed by the intermediate diffusing to the surface followed by a subsequent coordination, insertion, and reductive elimination. This diffusion event, in competition with further reaction in solution, presents a large barrier to reactivity at the surface.

To increase the chance of surface coordination, and arene formation, we chose to immobilize diyne **32**. Ideally, attaching a diyne to the glass surface would increase catalyst coordination and promote reactivity at the surface. Unfortunately, attaching the bis-propargyl substrate (**32**) is difficult likely due large steric demands preventing reaction with the amine rich surface (**Figure 4.23**).

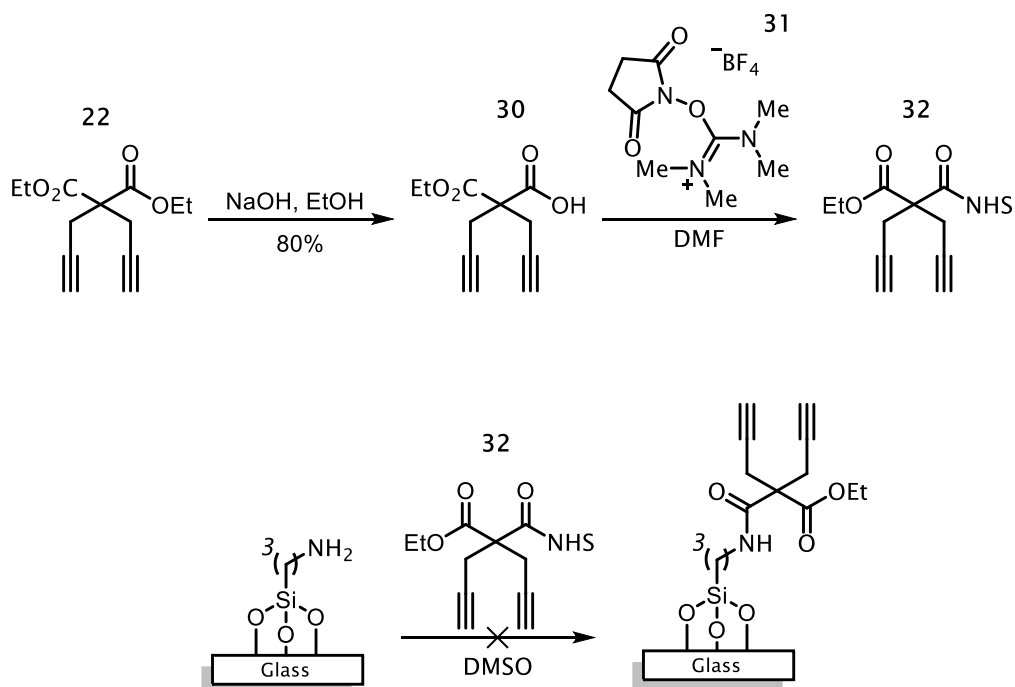


**Figure 4.23:** Attempts to Attach Diyne with Amide Bond

To extend the sterically crowded quaternary carbon away from the amide bond formation, we synthesized diene **34** (Figure 4.24). Treating **30** with oxalyl chloride gives the acid chloride and addition of beta-alanine provides the amide product **33** in high yield. Converting the corresponding acid (**33**) to the N-hydroxysuccinimide ester with TSTU (N,N,N',N'-Tetramethyl-O-(N-succinimidyl)uranium tetrafluoroborate) gives the final substrate **34**. Amidation of the amine-rich glass surface then proceeds smoothly in DMSO to give a diyne-rich surface. Fortunately, we observe a highly fluorescent surface after a click control suggesting that diynes were successfully attached to the glass surface.

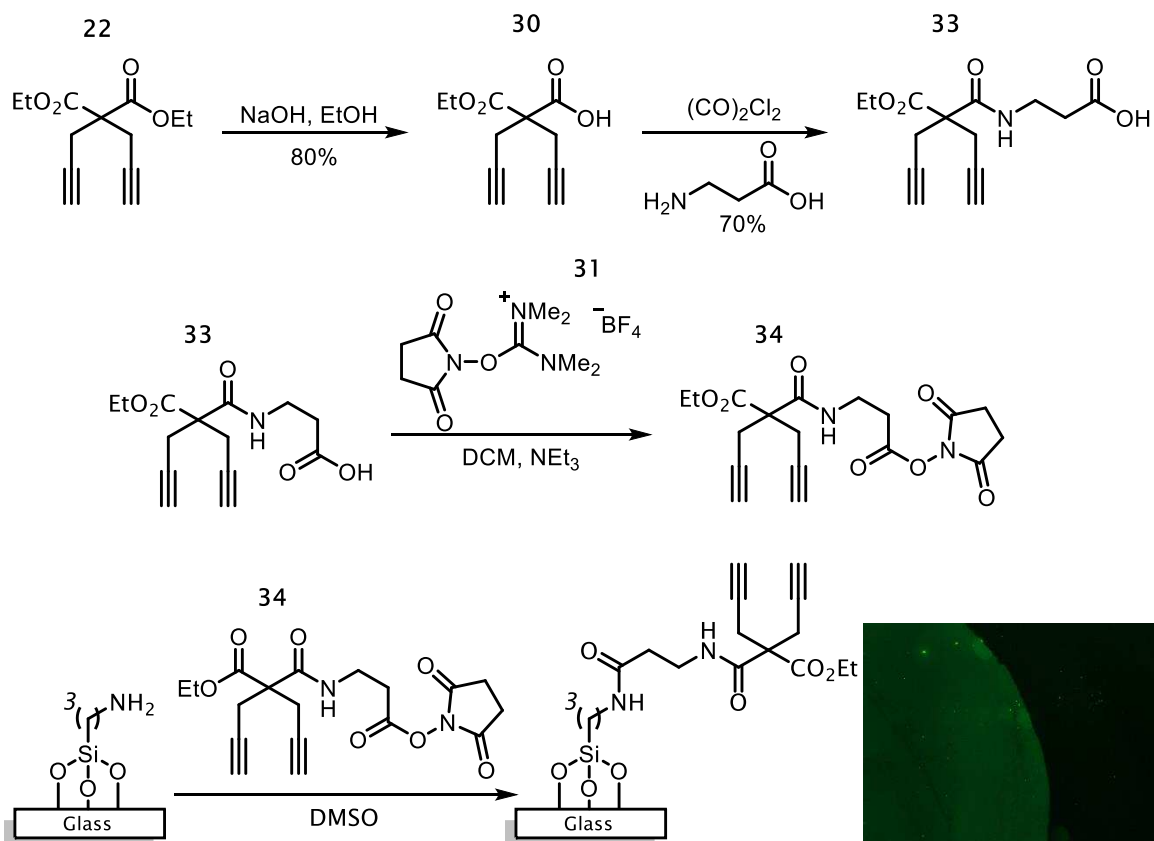
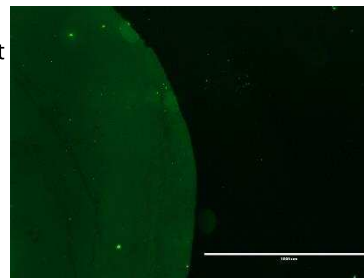


**Figure 4.24:** Addition of a Linker to the Diyne Substrate



With a confirmed diyne-rich glass surface in hand, we moved forward to arene formation (**Figure 4.25**). We initially treated the glass substrate with a solution of catalyst and two alkynes with different reactivity (aliphatic-**35** and aromatic alkyne-**36**). Each reaction was covered with a glass cover slide and irradiated with a 14W CFL for three different lengths of time (30, 60 and 90 minutes). After thoroughly washing the surface we collected XPS data, and we observed little to no change between modifications.

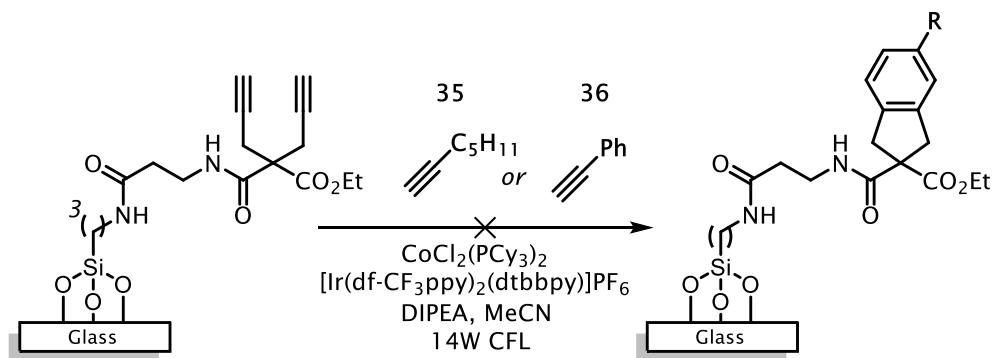
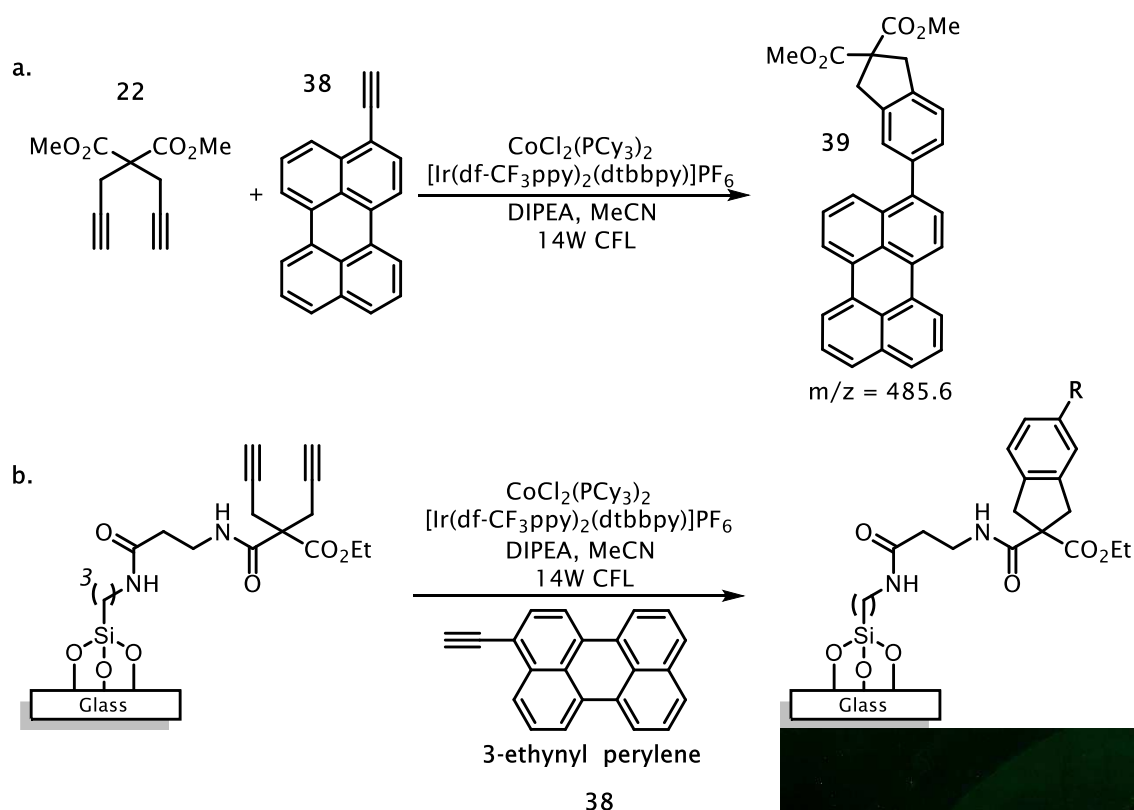


**Figure 4.25:** Attempt at Arene Formation Using Diyne

Following this study, a cursory search of the literature led us to believe XPS analysis may not be the best technique to confirm such a surface modification. Although XPS is fairly surface sensitive, structural information beyond the ratio of atomic elements is difficult to obtain. Given the success of the click controls on the surface we felt a method to visually confirm arene formation may be more fruitful. Fortunately, due to the wide availability of fluorescent click reagents, several fluorescent alkynes are available. In this scenario, if the [2+2+2] cycloaddition does form arenes, we can directly image the surface with fluorescence microscopy.

To determine the reactivity of the fluorescent alkyne (**38** - 3-ethynyl perylene) in a [2+2+2] cycloaddition we conducted a trial reaction at a larger scale in solution (**Figure 4.26**). **38** was combined with two equivalents of diyne substrate (**22**) and irradiated in solution with cobalt pre-catalyst and photo-catalyst. Although the alkyne's high molar absorptivity hinders reaction progress, monitoring the reaction by LC-MS reveals product **39** with a mass of 485.6 g/mol. After ensuring the alkyne was a competent substrate we wanted to test it on the diyne-rich surface. We used a PDMS barrier to create a well on the glass surface and contain the reaction components exclusively to one area. Afterward, the reaction solution is removed and the surface is thoroughly

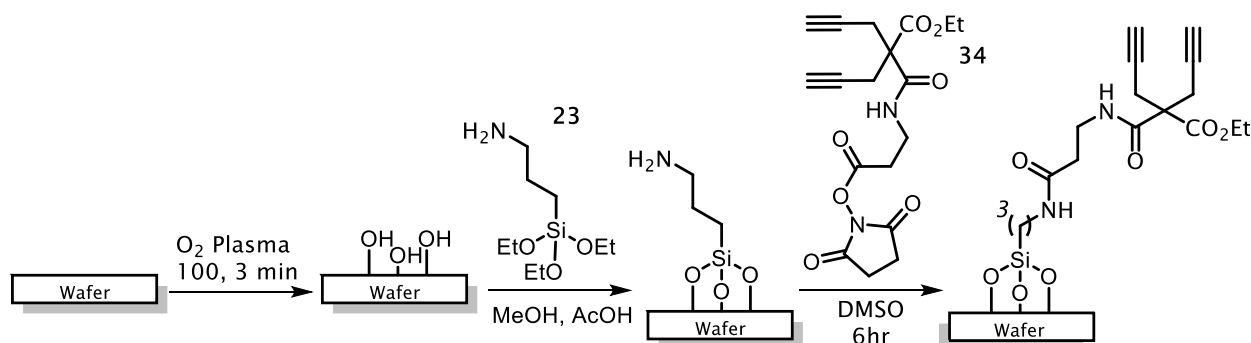
washed. Much to our excitement, fluorescence microscopy reveals fluorescence within the area restricted by the PDMS well.



**Figure 4.26:** a.) Test Reaction Ensures the Fluorescent Alkyne is Reactive b.) Attempts at Surface Modification.

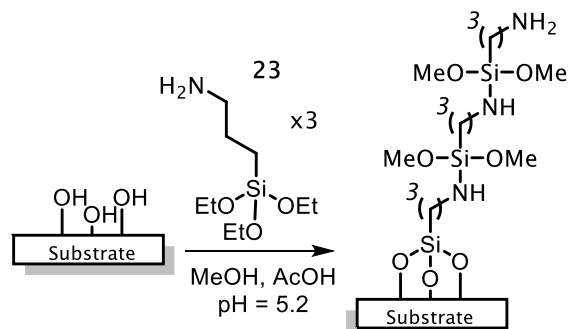
Although the root cause is unknown, these conditions did not provide reproducible results. Repeated attempts with various conditions suggests the glass substrate, the amination reaction, and diyne installation do not largely contribute to the irregularity. It is possible that an uncharacterized surface oddity on particular glass slides make them inherently more or less reactive to surface modifications. However, we realized a more severe issue exists. Internally reflected light within a clear glass slide would not be compatible with photolithographic techniques. With this we decided to abandon clear glass and continue investigations on a similar substrate—silicon wafers. Silicon wafers bear many similarities to glass and are compatible with similar chemical modifications. Unfortunately,

initial work on unmodified silicon wafers presented unfamiliar issues. Alternatively, we used thermally oxidized wafers that have a layer of SiO<sub>2</sub> (3000 Å) and which behave closer to glass (**Figure 4.27**). Still, the wafer substrates showed no observable fluorescence after treatment and irradiation with the fluorescent alkyne [2+2+2] cycloaddition.



**Figure 4.27:** Work on Silicon Wafers with Oxide Layer (SiO<sub>2</sub>)

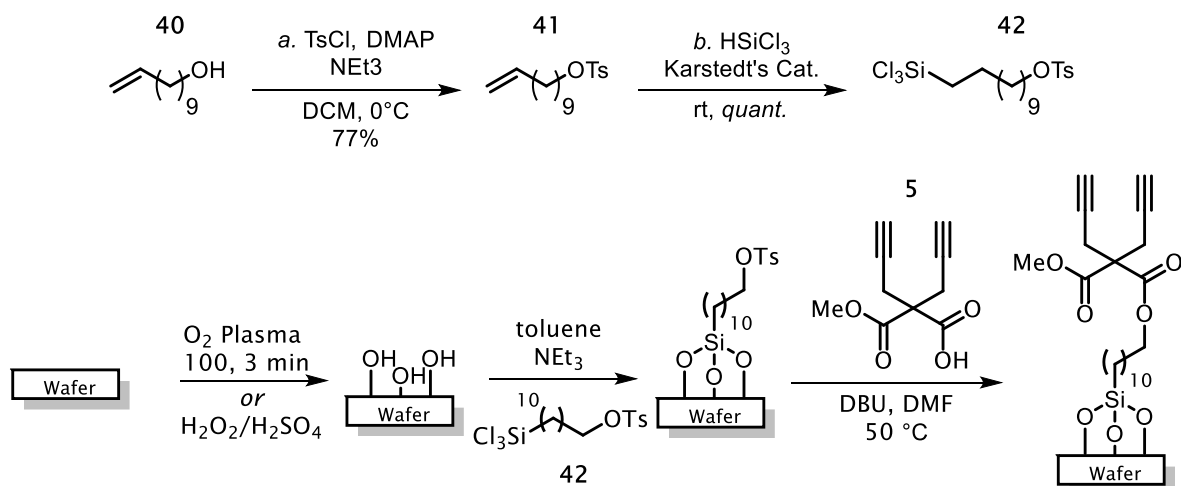
After working on three different substrates we were unable to reproducibly observe fluorescence on the surface. Reviewing procedures for aminating silicon-based substrates with APTES (**23**) revealed one potential cause for the reproducibility issues we encountered.<sup>[13]</sup> One large variability in surface modifications with APTES is the propensity to form multilayers and a thick substrate surface (**Figure 4.28**). It is conceivable that multilayer formation on the surface increases wettability and leads to superior interaction between the solution and solid phase. Although the low pH conditions used to install APTES limits the availability of nucleophilic nitrogen, irregular reaction times and changes in concentration may cause non-uniform layers.



**Figure 4.28:** Polymerization Can Occur at Amine-Rich Surfaces

With this possibility in mind we moved to a different linker in an attempt to increase surface wettability with organic solvents. Tosylation of 10-undecene-1-ol **40** with TsCl (tosyl chloride) gives the tosyl alkyne **41** (Figure 4.29). Hydrosilylation of **41** with Karstedt's catalyst and trichlorosilane quantitatively delivers the tosyl trichlorosilane **42**. Concurrently, treating the PDMS with oxygen plasma gives a surface of nucleophilic silanols suitable to react with the trichlorosilane (**42**). **42** and trimethylamine are dissolved in toluene and the wafer is fully submerged into the solution. A white precipitate of trimethylamine salts indicates that **42** is reacting with the surface. After aging overnight, the wafer is washed and transferred to a dimethylformamide (DMF) solution containing acid **5** and DBU. After twelve hours the surface is washed again to remove excess reagents and a click-control reveals the presence of the diyne on the surface.

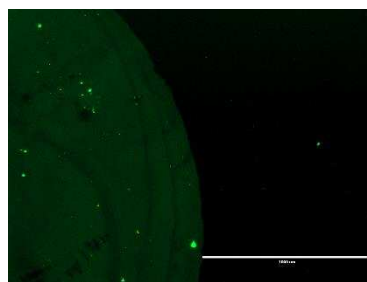


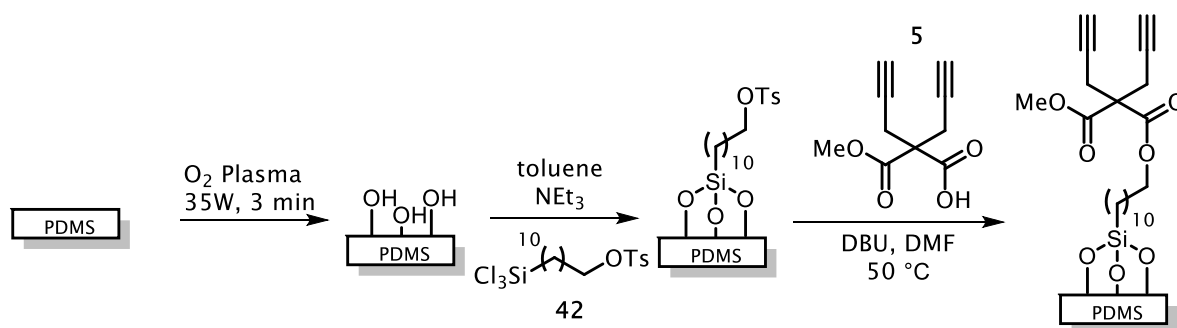


**Figure 4.29:** Synthesis of Long Aliphatic Linker

A longer linker lead to more reproducible results for the surface [2+2+2] cycloaddition but the resulting modifications were difficult to image due to weak fluorescence. However, we were encouraged by the marginal increase in performance and decided to use the longer aliphatic linker on a similar silicon containing substrate, PDMS (polydimethylsiloxane).

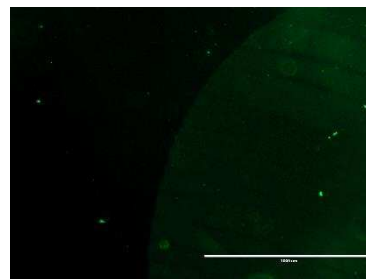
PDMS is a silicon-based polymer, similar to glass and silicon wafers, and is best characterized as a hydrophobic soft material. PDMS readily absorbs organic solvents<sup>[14]</sup> and is the foundation of many microfluidic devices.<sup>[15]</sup> We began working with PDMS using the aliphatic linker **42** to install the diyne substrate onto the surface (**Figure 4.30**). Oxygen plasma is first used to oxidize the PDMS surface. Swelling the oxidized PDMS in toluene and treating with trichlorosilane (**42**) then gives a tosyl-rich surface. Finally, an  $S_N2$  substitution of the tosyl group with acid **5** gives the diyne rich surface confirmed by a click control.





**Figure 4.30:** Installation of Linker and Diyne on the Surface

With alkyne-rich PDMS substrate in hand, we set out to test the [2+2+2] cycloaddition on the surface. To prevent wrinkling, modified PDMS is first swollen in a solution containing pre-catalyst, photo-catalyst and fluorescent alkyne for six to twelve hours under rigorously dark conditions (**Figure 4.31**). Working under argon and red light, the swelled substrate is removed from the solution placed on a piece of clean silicon wafer. A photomask was placed in direct contact with the functionalized surface and a light was placed 1-2 feet above the photomask. After irradiating for 8-15 minutes the photomask was removed and the PDMS was placed in a vial of THF wrapped in foil. To remove excess reagents from the PDMS, several washes were completed using THF and MeCN. Finally the substrate was placed in a  $100^\circ C$  oven for ten minutes to remove any remaining solvent. Imaging the substrate with the fluorescence microscope revealed the photomask pattern is reflected on the surface of the PDMS.



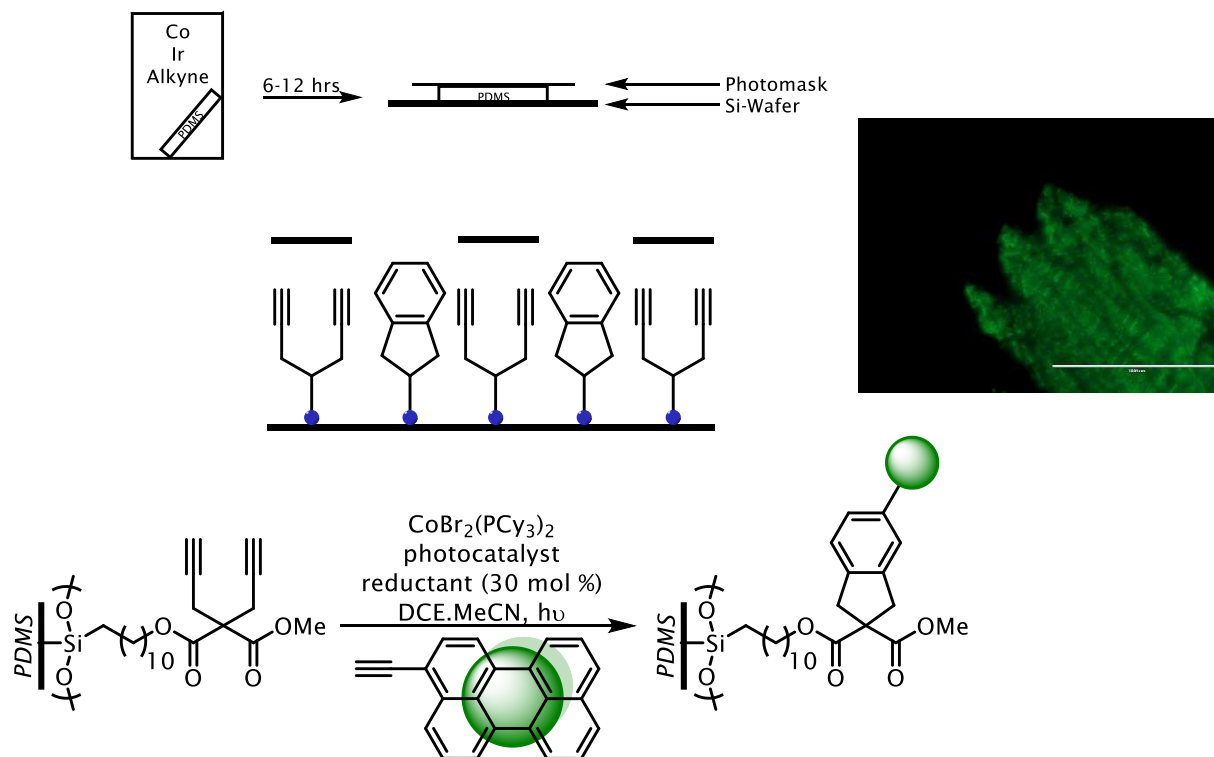


**Figure 4.31:** Printing Arenes on the Surface of PDMS

With conditions in hand, we wanted to test various photomasks and determine the limits of printing on PDMS with light-gated cobalt catalysis. Indeed, a wide variety of intricate patterns can be printed into the PDMS substrate (**Figure 4.32**). The smallest features printable on the surface measure 20-25 microns which is an excellent demonstration of control.

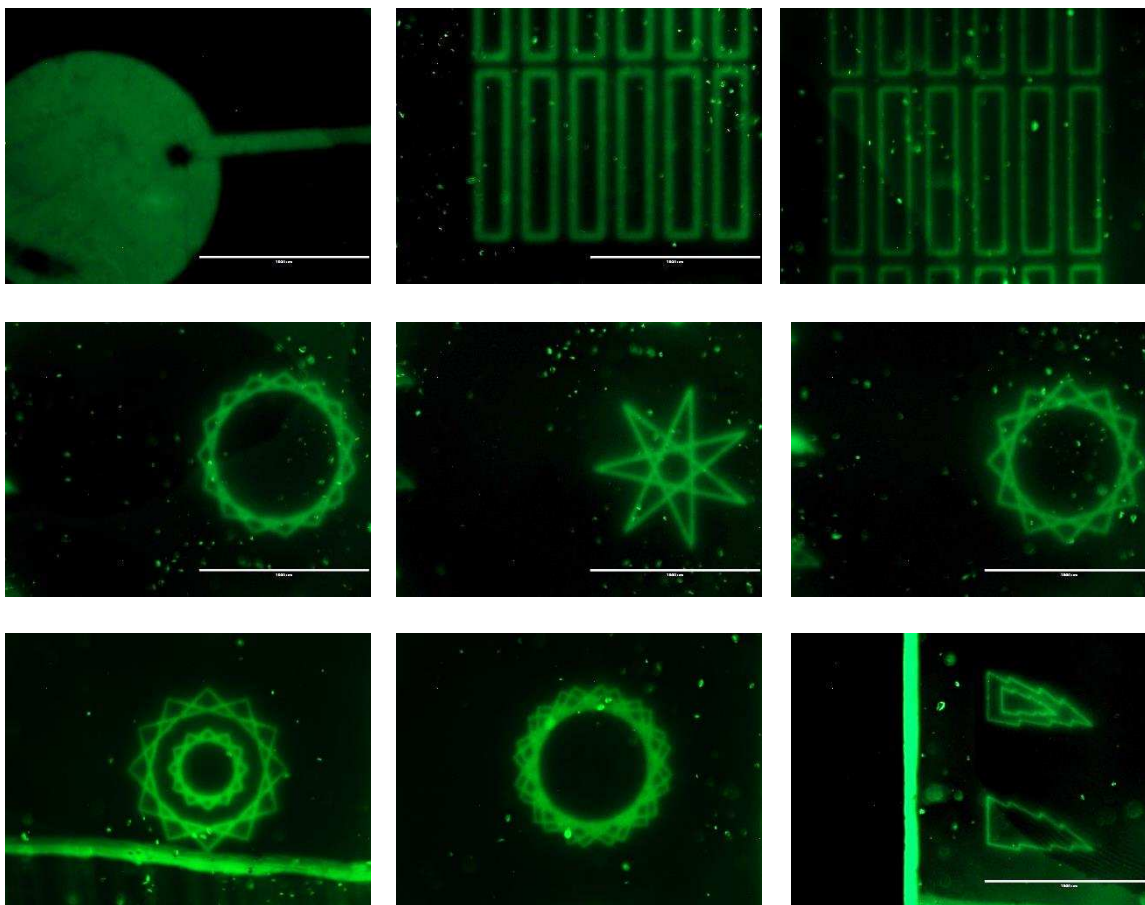


**Figure 4.32:** Patterns Printed on Functionalized PDMS

Beyond binary photomasks, grayscale photolithography requires an additional level of spatial and temporal control. In theory, a light-controlled technique should provide higher levels of functional density with higher doses of light radiation. Hawker and Fors have demonstrated this is the case with photo-redox-controlled ATRP when constructing complex features on the surface of silicon wafers using grayscale photomasks.<sup>[16]</sup> To probe our control over arene density on the surface of PDMS, we conducted the light-gated [2+2+2] cycloaddition using grayscale masks (**Figure 4.33**). We found the extent of arene formation on the surface of PDMS is controllable through light dosage. Heavily shaded areas of the photomask correspond to less surface fluorescence and areas of high light transmission results in high surface fluorescence.

Plotting the average fluorescence levels across the image in **Figure 4.33** gives rise to the data shown on the right. From the area of highest light transmission to the least, a linear decrease in fluorescence is observed which suggests a higher level of photo flux leads to an increase in arene density on the surface of PDMS.

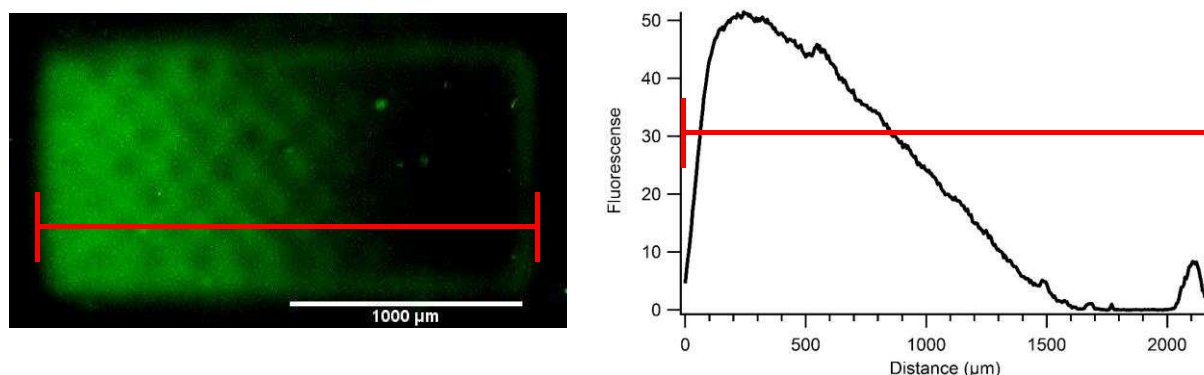


**Figure 4.33:** Grayscale Photolithography

#### 4.6 – Summary

In conclusion, in part A of this chapter we demonstrated that light-gated cobalt catalysis controls a [2+2+2] cycloaddition polymerization reaction. Interestingly, the polymerization is a unique example of a light-controlled [2+2+2] cycloaddition polymerization with characteristics of a chain-growth polymerization. The reaction can be stopped and started by adding or removing light radiation which is an excellent demonstration of temporal control. Ultimately, the reaction delivers good molecular weights and low PDIs.

In addition, we showed that light-gated cobalt catalysis is effective for spatially controlling arene formation. Despite several materials being problematic, a ubiquitous soft material, PDMS, is easily functionalized with the [2+2+2] cycloaddition reaction using simple photolithographic photomasks. The fluorescence images obtained show high spatial control and features as small as 20-25 microns can be routinely printed. Furthermore, we found that light-gated cobalt catalysis is

compatible with grayscale photolithography. We conclude this experiment indicates we can not only control where arenes are formed, but to what extent arenes are constructed in a specific area.

## REFERENCES

- [1] Polymer Science and Technology. Third Edition. Joel R. Fried. 2014.
- [2] Sugiyama, Y-K.; Kato, R.; Sakurada, T.; Okamoto, S. *J. Am. Chem. Soc.* **2011**, 133, 9712-9715.
- [3] a) Zhan, X.; Xu, S.; Yang, M.; Lei, Z. *Catal. Lett.* **2002**, 80, 59-61. b) Zhan, X.; Yang, M.; Lei, Z. *J. Mol. Catal. A.: Chem.* **2002**, 184, 139-145.
- [4] Rochat, S.; Swager, T. M. *J. Am. Chem. Soc.* **2013**, 135, 17703-17706.
- [5] Devadoss, A.; Chidsey, C. E. D. *J Am. Chem. Soc.* **2007**, 129, 5371 and references therein.
- [6] McCreery, R. L. *Chem. Rev.* **2008**, 108, 2646.
- [7] Pinson, J.; Podvorica, F. *Chem. Soc. Rev.* **2005**, 34, 429.
- [8] Brooksby, P. A.; Downard, A. J. *Langmuir* **2004**, 20, 5038-5045.
- [9] Leroux, Y. R.; Fei, H.; Noel, J-M; Roux, C.; Hapiot, P. *J. Am. Chem. Soc.* **2013**, 132, 14039-14041.
- [10] Leroux, Y. R.; Hapiot, P. *Chem. Mater.* **2013**, 25, 489-495.
- [11] Menanteau, T.; Levillain, E.; Breton, T. *Chem. Mater.* **2013**, 25, 2905-2909.
- [12] Sun, X-L.; Yang, L.; Chaikof, E. L. *Tet. Lett.* **2008**, 49, 2510-2513.
- [13] Kim, J.; Seidler, P.; Wan, L. S.; Fill, C. *J. Colloid Interface Sci.* 2009, 329, 114-119.
- [14] Lee, J. N.; Park, C.; Whitesides, G. M. *Anal. Chem.* **2003**, 75, 6544-6554.
- [15] a) Wong, I.; H. C-M. *Microfluid Nanofluid.* **2009**, 7, 291-306. b) Zhou, J.; Khodakov, D. A.; Ellis, A. V.; Voelcker, N. H. *Electrophoresis.* **2012**, 33, 89-104. c) Kuddannaya, S.; Chuah, Y. J.; Lee, M. H. A.; Menon, N. V.; Kang, Y.; Zhang, Y. *ACS Appl. Mater. Interfaces* **2013**, 5, 9777-9784.

[16] Fors, B. P.; Poelma, J. E.; Menyo, M. S.; Robb, M. J.; Spokoyny, D. M.; Kramer, J. W.; Waite, J. H.; Hawker, C. J. *J. Am. Chem. Soc.* **2013**, *135*, 14106-14109.



## APPENDIX ONE

### Merging Photo-Redox and Cobalt Catalysis: Experimental

#### A 1.1 --- General Methods and Materials

All reactions were conducted in anhydrous solvents and performed under air free conditions unless specifically noted. For air free applications, schlenk equipment or a glove box (MBraun MB 200G) were used. Anhydrous, degassed acetonitrile (MeCN), dichloroethane (DCE) and diisopropylethylamine (DIPEA) were purchased from Sigma Aldrich in Sure-Seal bottles, opened under an inert nitrogen atmosphere and used without further purification. Tetrahydrofuran (THF), dichloromethane (DCM), and diethyl ether (Et<sub>2</sub>O) were degassed with a stream of argon for fifteen minutes and then passed through two columns of neutral alumina before use. Anhydrous ethanol was purchased from Sigma-Aldrich, stored over molecular sieves after opening and degassed with a stream of argon before it was used. Thin layer chromatography was conducted on SiliCycle® 250 µm 60 Å (glass-backed) and column chromatography was performed on SiliCycle® Silica Flash ® 40-63 µm 60Å. Anhydrous cobalt halide salts were purchased from Sigma Aldrich or Strem Chemicals and stored under a nitrogen atmosphere. N,N-dipropargyl-p-toluenesulfonamide is available from TCI America or easily prepared from tosyl amine and propargyl bromide. 1,6-Heptadiyne was purchased from Sigma Aldrich and used without further purification. Alkyne coupling partners were purchased via Sigma-Aldrich, Oakwood Chemicals, or Alfa Aesar. Any alkynes not commercially available were prepared via literature procedures. Light sources used include: a 410 nm 35W Kessil LED, 450 nm 35W Kessil LED and a standard household 14 W CFL. The photo-catalysts [Ir(dF-CF<sub>3</sub>ppy)<sub>2</sub>(dtbbpy)]PF<sub>6</sub>, [Ir(ppy)<sub>2</sub>(dtbbpy)]PF<sub>6</sub>,

and Ru(bpy)<sub>3</sub>Cl<sub>2</sub> were purchased from Strem Chemicals or prepared using known literature procedures.

### **A 1.2 --- Instrumentation**

Voltammetry experiments were performed on a CH Instruments Model 1232B bipotentiostat using a 1-mm disk glass carbon working electrode (EDAQ), leakless Ag/AgCl reference electrode (EDAQ) and a platinum gauze as a counter electrode (VWR). All voltammetry measurements were conducted in dry, degassed acetonitrile (Sigma Aldrich) using tetrabutylammonium hexafluorophosphate (TBAF, 0.1 M) as electrolyte and at a scan rate of 100 mV/s unless otherwise noted. Liquid chromatography (LC) was performed on an Agilent Technologies 1260 Infinity. Mesitylene (1, 3, 5-trimethylbenzene) was used as an intern standard for any yields not obtained from isolated material. Proton NMR were collected on a Varian 300 or 400 MHz spectrometer and data is reported as follows: in CDCl<sub>3</sub> (7.26 ppm); multiplicity (s = singlet, bs = broad singlet, d = doublet, t = triplet, q = quartet, and m = multiplet), coupling constants (Hz). Carbon NMR spectra were collected on a Varian 300 or 400 MHz spectrometer and all chemical shifts are reported in reference to CDCl<sub>3</sub> (77.2 ppm).

### **A 1.3 --- General Procedure for Cobalt Pre-Catalysts Synthesis**

A flame-dried round bottom flask was equipped with a stir bar and charged with the desired cobalt halide (1 equivalent). The flask was evacuated (three minutes under vacuum) and backfilled with argon three times. A second flame-dried round bottom flask was charged with a stir bar and the appropriate phosphine ligand (mono-dentate ligand use 1.05 equivalents, bi-dentate ligand use 2.05 equivalents). The flask was then placed under an inert atmosphere by evacuation (three

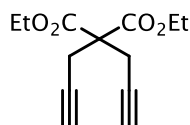
minutes under vacuum) and backfilled with argon (repeated three times). Both vessels were then charged with degassed, anhydrous ethanol and vigorously stirred until a homogenous solution was observed (cobalt halide solution: ~0.3M, phosphine solution: ~0.1M). *Note:* Phosphine solutions commonly required mild heating (~50-60 °C) to obtain homogenous solution. To maintain an inert atmosphere, the phosphine solution was transferred to the cobalt halide solution via cannula over a period of three minutes. The resulting solution generally changed color and produced a precipitate. The vessel was stirred overnight (12-16 hours) at room temperature and under an argon atmosphere. After stirring overnight, the flask was opened to the air and the precipitate was quickly collected on a glass frit. The solid was washed with cold ethanol followed by diethyl ether and then dried *in vacuo* to give a powder. *Note:* Most complexes have a moderate to high shelf-life under ambient conditions, but storage under argon is recommended for long term storage. For electrochemical measurements, complexes were purified via vapor diffusion recrystallization using DCM or MeCN as pro-solvents and pentane or diethyl ether as anti-solvents.

#### **A 1.4 --- General Procedures for Diyne Substrate Synthesis**

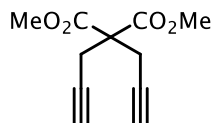
**A 1.4.1 -- Procedure A:** A flame-dried flask was charged with a stir bar and dicarbonyl compound (1 equivalent) under ambient conditions. Anhydrous acetonitrile (0.25 M in dicarbonyl) was then added to the flask and the vessel was gently stirred. In one portion, vacuum dried potassium carbonate (3.5 equivalents) and propargyl bromide (2.5 equivalents – 80% solution in toluene) was added to the flask and the vessel was vigorously stirred. After stirring 24 hours the reaction was examined by TLC to confirm starting material was fully consumed. *Note:* Some reactions were heated to reflux to shorten reaction times. After starting materials were consumed by TLC the reaction was concentrated *in vacuo* and the residue was immediately suspended in

ethyl ether. The resulting solution was then filtered to remove inorganic salts and the filtrate was added directly to a separatory funnel. The organic layer was washed two times with water, one time with brine and then dried over magnesium sulfate. After twenty minutes the drying agent was removed by vacuum filtration and the organic layer was concentrated again *in vacuo*. The compound was then purified by column chromatography using an ethyl acetate:hexane and gradient (0-25%) unless otherwise noted. *Note:* many compound were not visible by UV light and were visualized with KMnO<sub>4</sub>.

**A 1.4.2 -- Procedure B:** Alternatively, some dicarbonyl compounds were more efficiently alkylated with a slightly modified version of procedure A. Anhydrous acetone (distilled from Drierite) was substituted for acetonitrile and potassium carbonate was substituted with cesium carbonate (Cs<sub>2</sub>CO<sub>3</sub>).

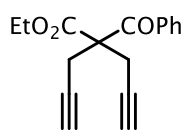


**(Diethyl 2,2-di(prop-2-yn-1-yl)malonate (23):** The synthesis of this compound has been reported previously.<sup>[1]</sup> General procedure **A** was followed and compound **23** was recrystallized from hot ethyl acetate and hexane to furnish translucent white crystals. A <sup>1</sup>H NMR has been included for reference. <sup>1</sup>H NMR (400 MHz, CDCl<sub>3</sub>): δ 4.20 (q, J = 7.0 Hz, 4H), 2.97 (d, J = 2.7 Hz, 4H), 2.00 (t, J = 2.7 Hz, 2H), 1.24 (t, J = 7.0, 6H) ppm. Compound characterization matched spectra reported in the literature.

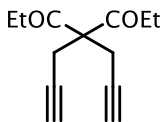


**(Dimethyl 2,2-di(prop-2-yn-1-yl)malonate (42d):** The synthesis of this compound has been reported.<sup>[1]</sup> General procedure **A** was used and compound **42d** was recrystallized from hot ethyl acetate and hexane to furnish translucent white crystals after cooling. A <sup>1</sup>H NMR has been included for reference. <sup>1</sup>H NMR (400 MHz, CDCl<sub>3</sub>): δ 3.77 (s, 6H),

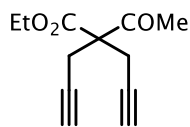
3.01 (d,  $J = 2.3$  Hz, 4H), 2.04 (t,  $J = 2.3$  Hz, 2H) ppm. Compound characterization matched spectra reported in the literature.



**Ethyl 2-benzoyl-2-(prop-2-yn-1-yl)pent-4-ynoate (43d):** The synthesis of this compound has been reported in the literature.<sup>[2]</sup> General procedure **B** was used and compound **43d** was purified via column chromatography on a Teledyne ISCO automated column running an ethyl acetate:hexane gradient (0-30%) to afford a white solid. A  $^1\text{H}$  NMR has been included for reference.  $^1\text{H}$  NMR (400 MHz,  $\text{CDCl}_3$ ):  $\delta$  7.86-7.83 (m, 2H), 7.60-7.55 (m, 1H), 7.48-7.43 (m, 2 H), 4.24 (q,  $J = 7.15$  Hz, 2H), 3.17 (m, 4H), 2.04 (t, 2.57 Hz, 2H), 1.18 (t,  $J = 7.15$  Hz, 3H) ppm. Compound characterization matched spectra reported in the literature.

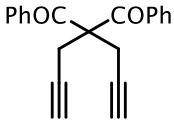


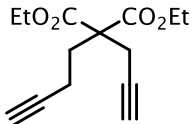
**4,4-Di(prop-2-yn-1-yl)heptane-3,5-dione (44d):** This compound was prepared using procedure **B**. Crude compound **44d** was purified via column chromatography on a Teledyne ISCO automated column running an ethyl acetate:hexane gradient (0-30%) to afford a white solid in 67%.  $^1\text{H}$  NMR (400 MHz,  $\text{CDCl}_3$ ):  $\delta$  2.94 (m, 4H), 2.43 (q,  $J = 7.34$  Hz, 4H), 2.00 (t,  $J = 2.45$  Hz, 2H), 1.03 (t,  $J = 7.34$  Hz, 6H) ppm.  $^{13}\text{C}$  NMR (101 MHz,  $\text{CDCl}_3$ ):  $\delta$  205.49, 79.02, 72.08, 69.15, 31.90, 21.10, 7.77 ppm. IR (ATR): 3285, 2986, 2947, 2895, 1704  $\text{cm}^{-1}$ . MS (ESI, pos):  $m/z = 205.2$   $[\text{M}]^+$



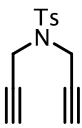
**Ethyl 2-acetyl-2-(prop-2-yn-1-yl)pent-4-ynoate (46d):** The synthesis of this compound has been reported in the literature.<sup>[3]</sup> General procedure **B** was used and compound **46d** was purified via column chromatography on a Teledyne ISCO automated column running an ethyl acetate:hexane gradient (0-30%) to afford a white solid. A  $^1\text{H}$  NMR has

been included for reference.  $^1\text{H NMR}$  (400 MHz,  $\text{CDCl}_3$ ):  $\delta$  4.26 (q,  $J = 7.1$  Hz, 2H), 2.97 (dq,  $J = 14.92$  Hz,  $J = 2.69$  Hz, 4H), 2.22 (s, 3H), 2.04 (t,  $J = 2.69$  Hz, 2H), 1.29 (t,  $J = 7.1$  Hz, 3H) ppm. Compound characterization matched spectra reported in the literature.

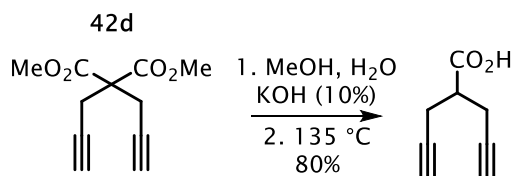
 **1,3-Diphenyl-2,2-di(prop-2-yn-1-yl)propane-1,3-dione (47d):** The synthesis of this compound has been reported. <sup>[2]</sup> General procedure **B** was used and compound **47d** was purified via column chromatography on a Teledyne ISCO automated column running an ethyl acetate:hexane gradient (0-30%) to afford a white solid. A  $^1\text{H NMR}$  has been included for reference.  $^1\text{H NMR}$  (400 MHz,  $\text{CDCl}_3$ ):  $\delta$  7.87-7.84 (m, 4H), 7.54-7.50 (m, 2H), 7.41-7.37 (m, 4H), 3.31 (s, 2H), 3.30 (s, 2H), 2.04 (t,  $J = 2.57$  Hz, 2H) ppm. Compound characterization matched spectra reported in the literature.

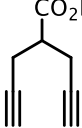
 **Diethyl 2-(but-3-yn-1-yl)-2-(prop-2-yn-1-yl)malonate (48d):** The synthesis of this compound has been reported. <sup>[4]</sup> Compound 48d was prepared using a procedure modified from the synthesis of a similar compound. <sup>[5]</sup> A large portion of sodium hydride (NaH, 60% dispersion in mineral oil) was pre-washed with hexane under an inert atmosphere (glove box). In a glove box, a flame-dried flask was charged with clean, dry NaH (1.5 equivalent) and a stir bar. The flask was then sealed, removed from the glove box, and placed onto an argon line. Dry THF was added via syringe (0.2 M final reaction concentration) and the flask was cooled to 0 °C. While vigorously stirring the flask to suspend the insoluble NaH, diethyl 2-(prop-2-yn-1-yl)malonate (purchased from TCI America and distilled under vacuum –  $^1\text{H NMR}$  included below) was added drop-wise to the NaH suspension. The reaction was allowed to stir for one hour at 0 °C, then butynyl bromide (1.2 equivalents) was added in one portion. The reaction was allowed to

warm to room temperature overnight. After ~8 hours the reaction was quenched with brine and transferred to a separatory funnel. The aqueous layer was extracted thrice with dichloromethane, the organic layers were combined, and dried over magnesium sulfate (MgSO<sub>4</sub>). The crude compound was purified via column chromatography using an ethyl acetate:hexane gradient (0-15%) to give a light yellow oil (~30%). Compound characterization matched spectra reported in the literature but was impure. A <sup>1</sup>H NMR has been included below for reference.

 **4-Methyl-N,N-di(prop-2-yn-1-yl)benzenesulfonamide (61d):** The synthesis of this compound has been reported. <sup>[4]</sup> A <sup>1</sup>H NMR has been included for reference. **<sup>1</sup>H NMR** (300 MHz, CDCl<sub>3</sub>): δ 7.73-7.69 (m, 2H), 7.30-7.27 (m, 2H), 4.16 (s, 2H), 4.15 (s, 2H), 2.41 (s, 3H), 2.14 (t, J = 1.76, 2H) ppm. Compound characterization matched spectra reported in the literature.

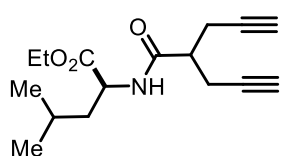
#### A 1.4.3 -- Preparation of Compound 63d:



 **2-(prop-2-yn-1-yl)pent-4-ynoic acid:** The synthesis of this compound has been reported. <sup>[7]</sup> We used a modified procedure. A 500 ml round bottom flask was charged with a stir bar followed by compound **42d** (10g, 1.0 equivalents). The flask was then charged with methanol (125 mL, ~0.3M in **42d**) and stirred until a homogenous solution was formed. An aqueous solution of potassium hydroxide (13.4 g, 5.0 equivalents) was prepared with a minimal amount of water and added to the methanol solution. The reaction was allowed to stir overnight at room temperature. At this time the reaction was concentrated *in vacuo* to dryness. The solid, crude

material was suspended in diethyl ether, filtered on a glass frit and washed with excess diethyl ether. The filter cake was collected, dissolved in 1M HCl, and transferred to a separatory funnel where the aqueous layer was extracted thrice with dichloromethane (DCM). The organic layers were combined and dried over magnesium sulfate. The dry solution was then concentrated *in vacuo* to give the di-acid intermediate as a pure white solid (8.13 g, 94%) and used without further purification.

Crude di-acid was transferred into a flame-dried 25 mL flask and placed under an argon atmosphere. The flask was then lowered into an oil bath at 135 °C for approximately three hours until the neat liquid had ceased bubbling. The flask was cooled and the brown material was flushed through a plug of silica eluting with DCM. The solvent was removed *in vacuo* and the oily, light yellow compound was used without further purification (4.91 g, 80% yield). A <sup>1</sup>H NMR has been included for reference. <sup>1</sup>H (300 MHz, CDCl<sub>3</sub>): δ 2.81 (m, 1H), 2.05 (m, 4H), 2.04 (s, 2H) ppm. Compound characterization matched spectra reported in the literature.



**3-methyl-1-(2-(prop-2-yn-1-yl)pent-4-ynamido)butyl propionate**

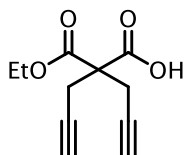
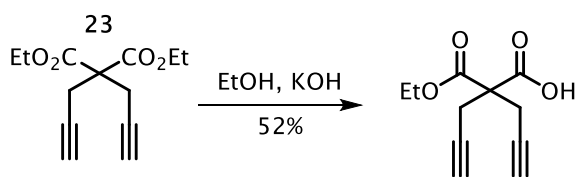
**(63d):** A flame-dried 25 mL round bottom flask was charged with 2-(prop-2-yn-1-yl)pent-4-ynoic acid (450 mg, 1.0 equivalents) and anhydrous

dichloromethane (0.2M in acid). Oxalyl chloride (353 uL, 1.5 equivalents) was slowly added, followed by 1-2 drops of anhydrous dimethylformamide and the reaction immediately began to bubble. After bubbling ceased the reaction was concentrated, redissolved in dichloromethane (0.1M), and chilled to 0°C. To the chilled solution, isoleucine ethyl ester HCl salt (970 mg, 1.5 equivalents) was added in one portion and trimethylamine (1.4 mL, 2.0 equiv.) was added dropwise to keep the reaction temperature at 0°C. After starting material was consumed, the



reaction was warmed to room temperature, diluted with dichloromethane, and washed with 1M HCl (3x). The organic layer was dried over magnesium sulfate and purification was accomplished via flash chromatography using a 0-50% ethyl acetate:hexane gradient which afforded **63d** a white solid (70%). **<sup>1</sup>H NMR** (400 MHz, CDCl<sub>3</sub>): δ 6.27 (d, J = 8.2 Hz, 1H), 4.63 (qt, J = 5.50Hz, 3.5Hz, 1H), 4.17 (q, J = 7.0 Hz, 2H), 2.60-2.45 (m, 5H), 2.04 (m, 2H), 1.75-1.51 (m, 4H), 1.27 (t, J = 7.0 Hz, 3H), 0.93 (dd, J = 6.3 Hz, 6H) ppm. **<sup>13</sup>C NMR** (101 MHz, CDCl<sub>3</sub>): δ 172.8, 171.7, 81.2, 81.0, 70.8, 70.6, 61.3, 50.9, 45.0, 41.9, 24.8, 22.8, 21.9, 20.9, 20.8, 14.1 ppm. **IR** (ATR): 3324, 3263, 2956, 2925, 2873, 2115, 1712, 1634, 1275, 1205 cm<sup>-1</sup>. **MS** (ESI, pos): m/z = 278.2 [M+H]<sup>+</sup>; 299.8 [M+Na]<sup>+</sup>

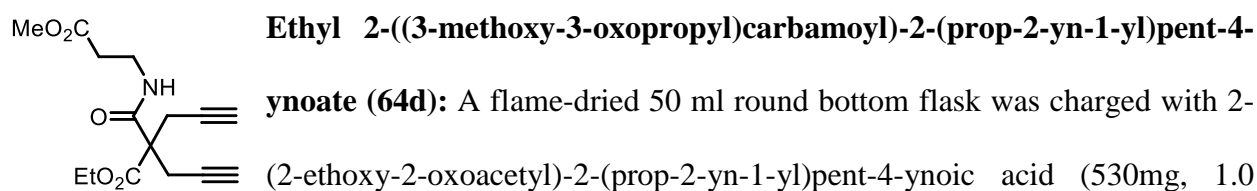
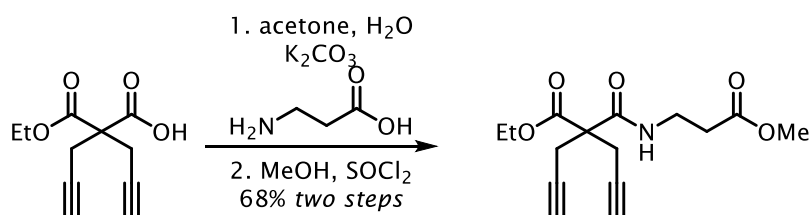
#### 1.4.4 -- Preparation of Compound 64d:



**2-(2-ethoxy-2-oxoacetyl)-2-(prop-2-yn-1-yl)pent-4-ynoic acid:** The synthesis of this compound has been reported and we used a modified procedure.<sup>[1]</sup> A flame-dried 50 mL round bottom flask was charged with compound **23** (750 mg,

1.0 equivalents) and potassium hydroxide (196 mg, 1.1 equivalents). Anhydrous ethanol (15 mL, ~0.2M) was then added to the flask and the reaction was stirred overnight at 50 °C. Over 12 hours the solution became heterogeneous and the suspension was concentrated *in vacuo* to dryness. The precipitated crude material was then suspended in diethyl ether, filtered, and washed with excess diethyl ether to remove unreacted starting material. The solid was immediately dissolved in 1M HCl and transferred to a separatory funnel. The aqueous layer was extracted thrice with dichloromethane (DCM), the organic layers were combined, and dried over magnesium sulfate.

Concentration of the organic layers afforded an off white solid pure by  $^1\text{H NMR}$  in 52% yield. A  $^1\text{H NMR}$  has been included for reference.  $^1\text{H NMR}$  (300 MHz,  $\text{CDCl}_3$ ):  $\delta$  4.26 (q,  $J = 7.04$  Hz, 2H), 3.00 (m, 4H), 2.05 (t,  $J = 2.93$  Hz, 2H), 1.28 (t,  $J = 7.04$  Hz, 3H) ppm. Compound characterization matched spectra reported in the literature.

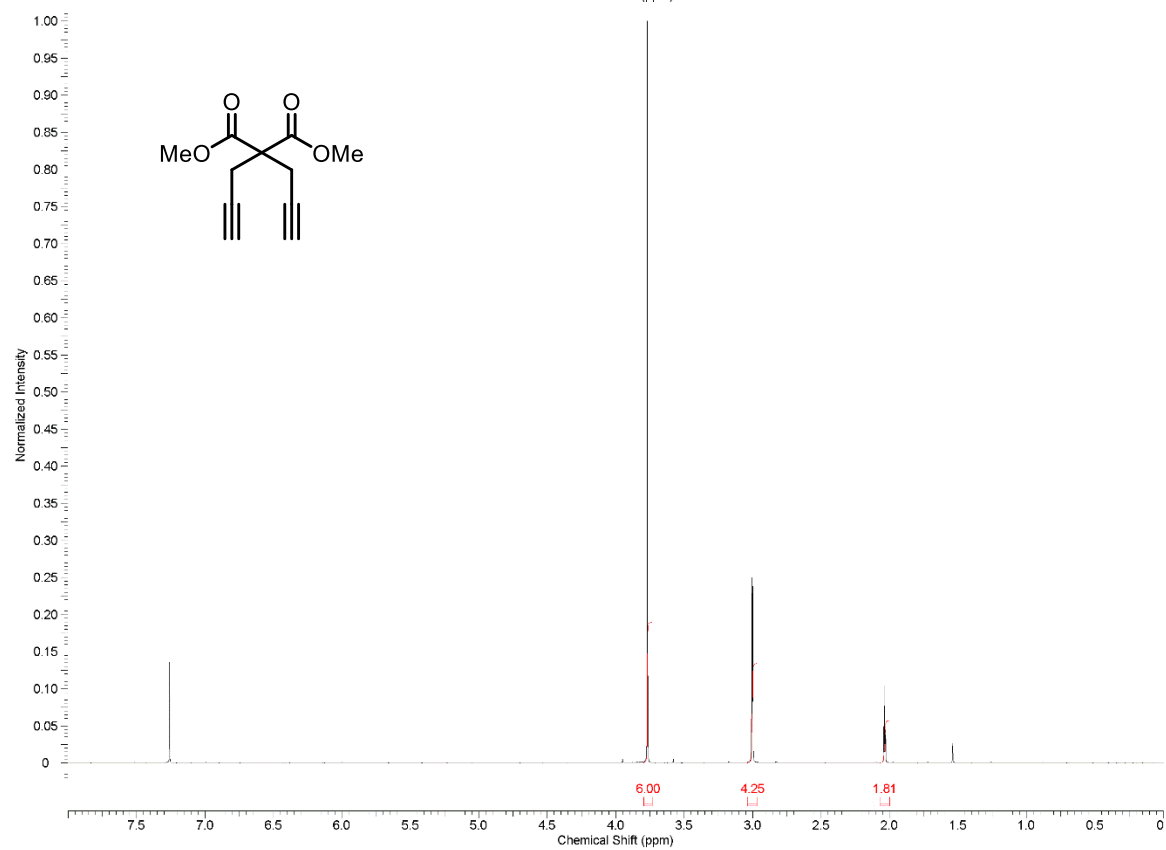
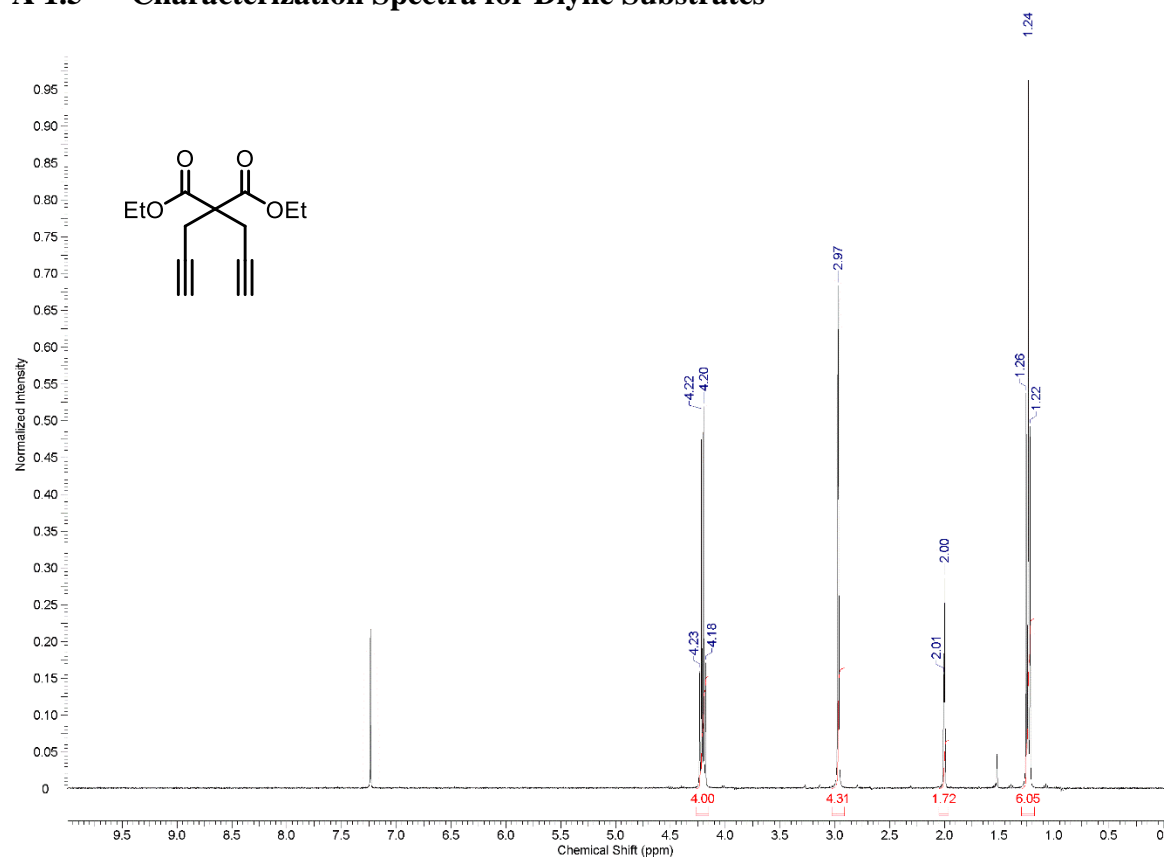


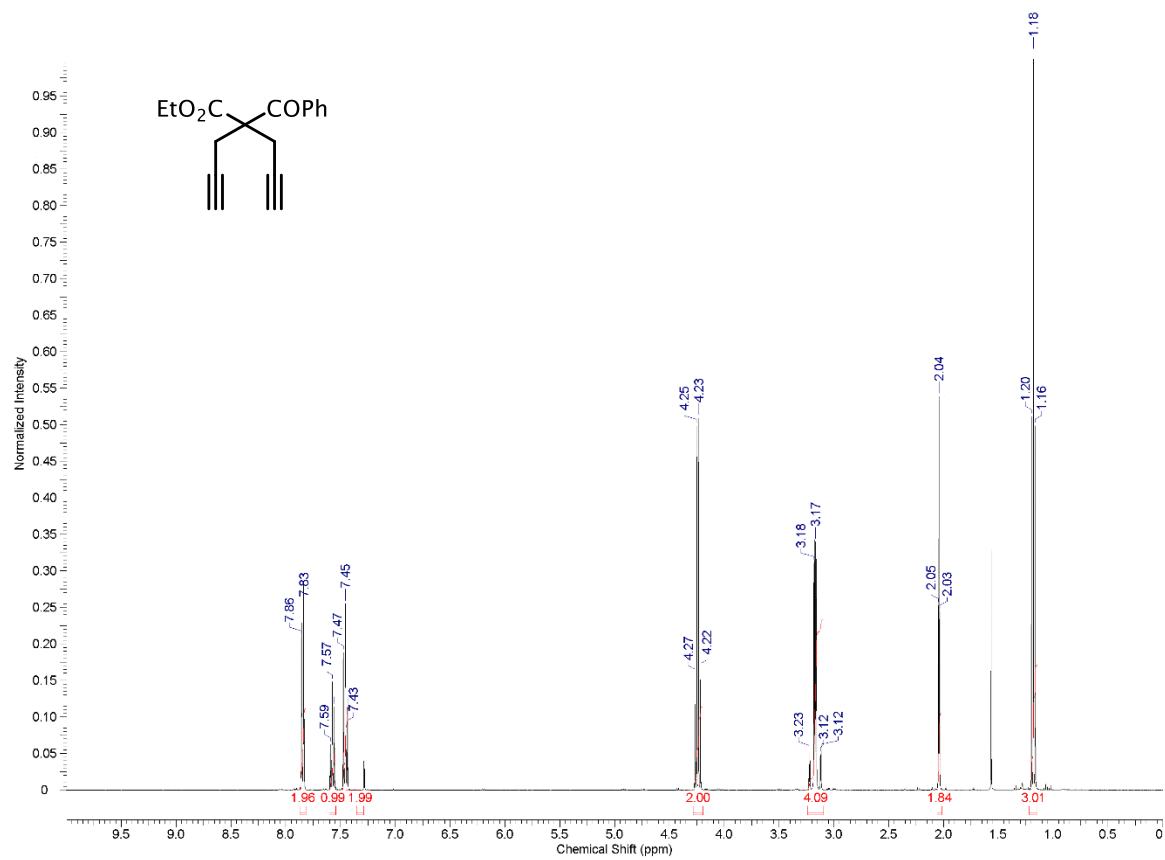
equivalents) followed by anhydrous dichloromethane (13 mL, ~0.2M). Dimethylformamide (2-3 drops) was then added to the flask followed by oxalyl chloride (261  $\mu\text{L}$ , 1.2 equivalents) in one portion. After the reaction had stopped releasing gas, the reaction was concentrated *in vacuo* and the crude oil was re-dissolved in dry acetone. A second flask 25 mL round bottom flask was charged with beta-alanine (227 mg, 1.0 equivalents) and potassium carbonate (1.06g, 3.0 equivalents). Enough water was added to dissolve the reagents and the acetone solution was added in one portion. The reaction was allowed to stir overnight (12 hours) and then the volatile solvents were removed *in vacuo*. The remaining aqueous layer was extracted with diethyl ether three times and dried over sodium sulfate. Concentration of the dried organic layers gave 540 mg of crude acid material (~76%).

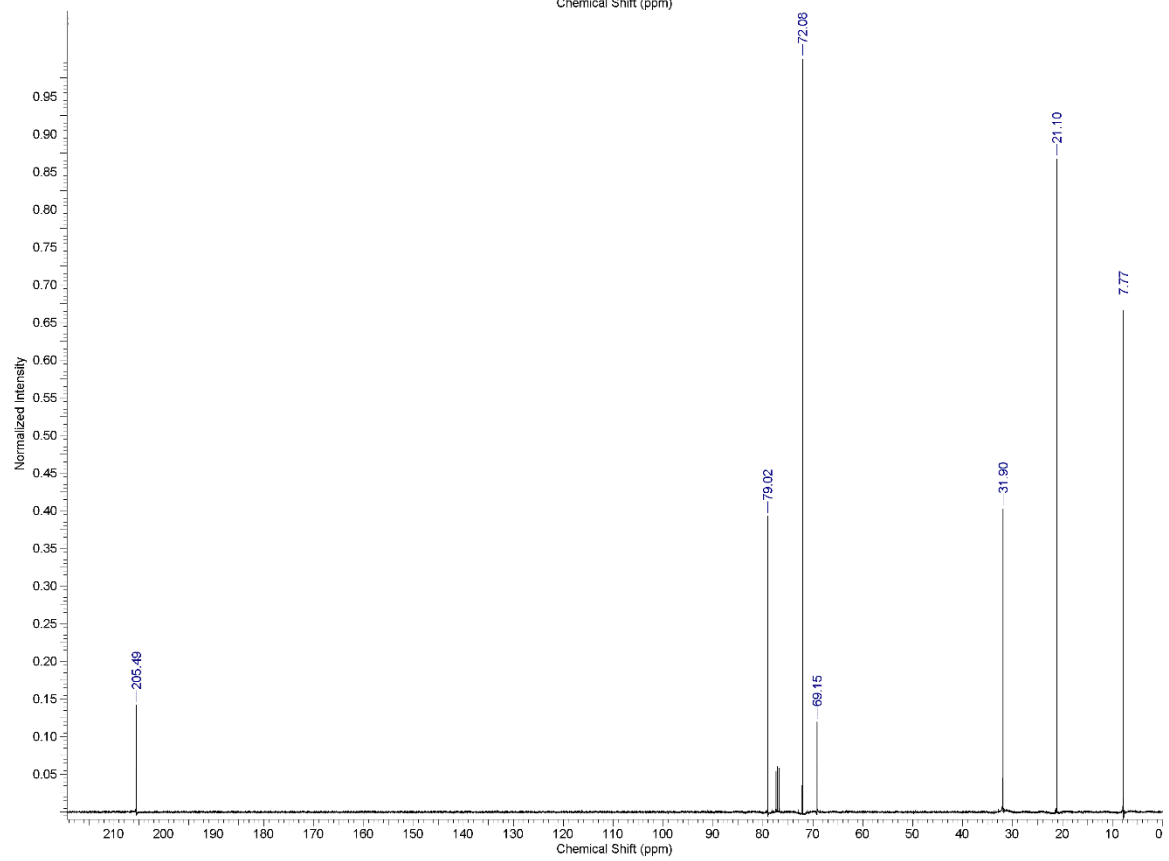
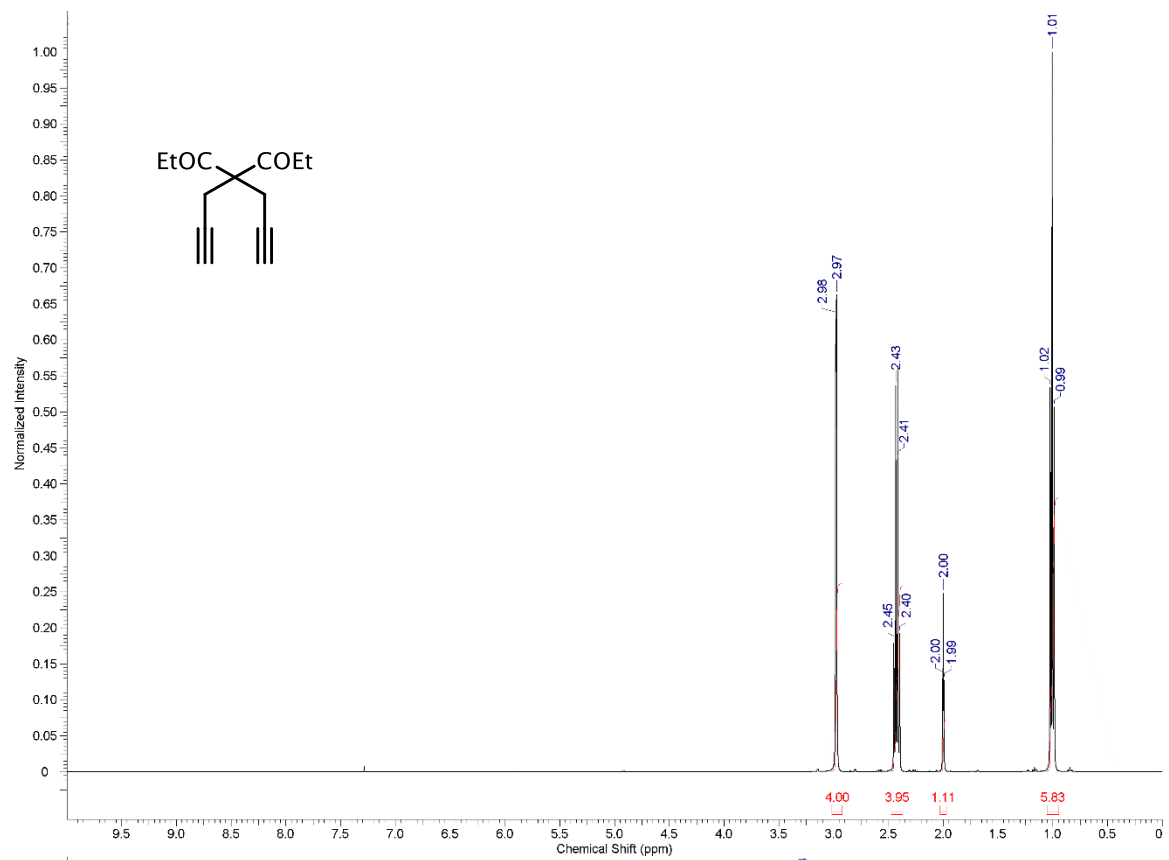
This crude material was immediately dissolved in anhydrous methanol and chilled to  $0^\circ\text{C}$ . Thionyl chloride was added (145  $\mu\text{L}$ , 1.05 equivalents) at  $0^\circ\text{C}$  and the reaction was allowed to

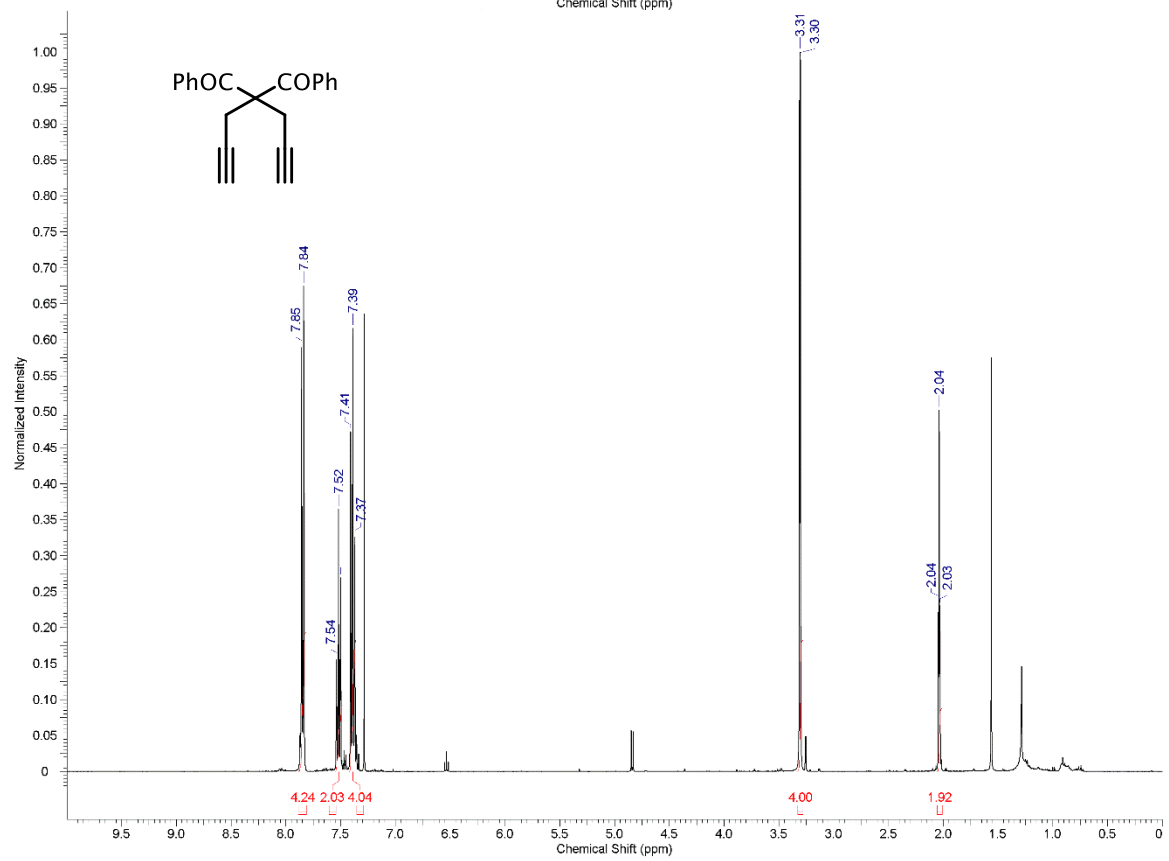
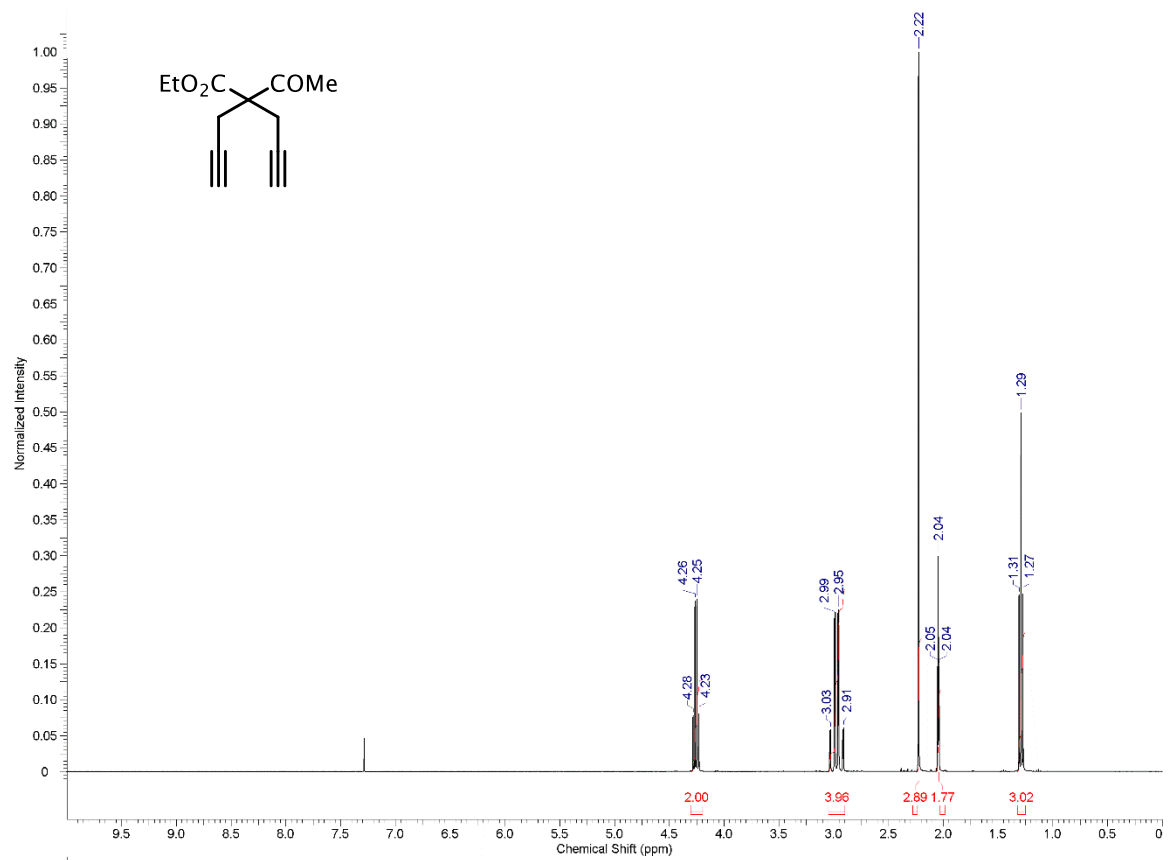
warm to room temperature. Once the reaction reached room temperature, the reaction was concentrated and purified by column chromatography eluting with an ethyl acetate:hexane mixture (25%) to afford 508 mg of **64d** as a white solid in 90% yield (68% yield over two steps). **<sup>1</sup>H NMR** (400 MHz, CDCl<sub>3</sub>): δ 7.04 (bs, 1H), 4.25 (q, J = 7.0 Hz, 2H), 3.69 (s, 3H), 3.55 (q, J = 5.87 Hz, 2H), 2.92 (m, 4H), 2.52 (t, J = 6.26 Hz, 2H), 2.02 (t, J = 2.74 Hz, 2H), 1.28 (t, 7.0 Hz, 3H) ppm. **<sup>13</sup>C NMR** (101 MHz, CDCl<sub>3</sub>): δ 172.8, 170.6, 167.7, 78.9, 71.6, 62.3, 56.4, 51.8, 35.3, 33.4, 23.9, 13.9 ppm. **IR** (ATR): 3393, 3302, 3237, 2956, 2925, 2995, 2852, 1721, 1673, 1526, 1184, 1218 cm<sup>-1</sup>. **MS** (ESI, pos): m/z = 293.9 [M+H]<sup>+</sup>; 315.8 [M+Na]<sup>+</sup>

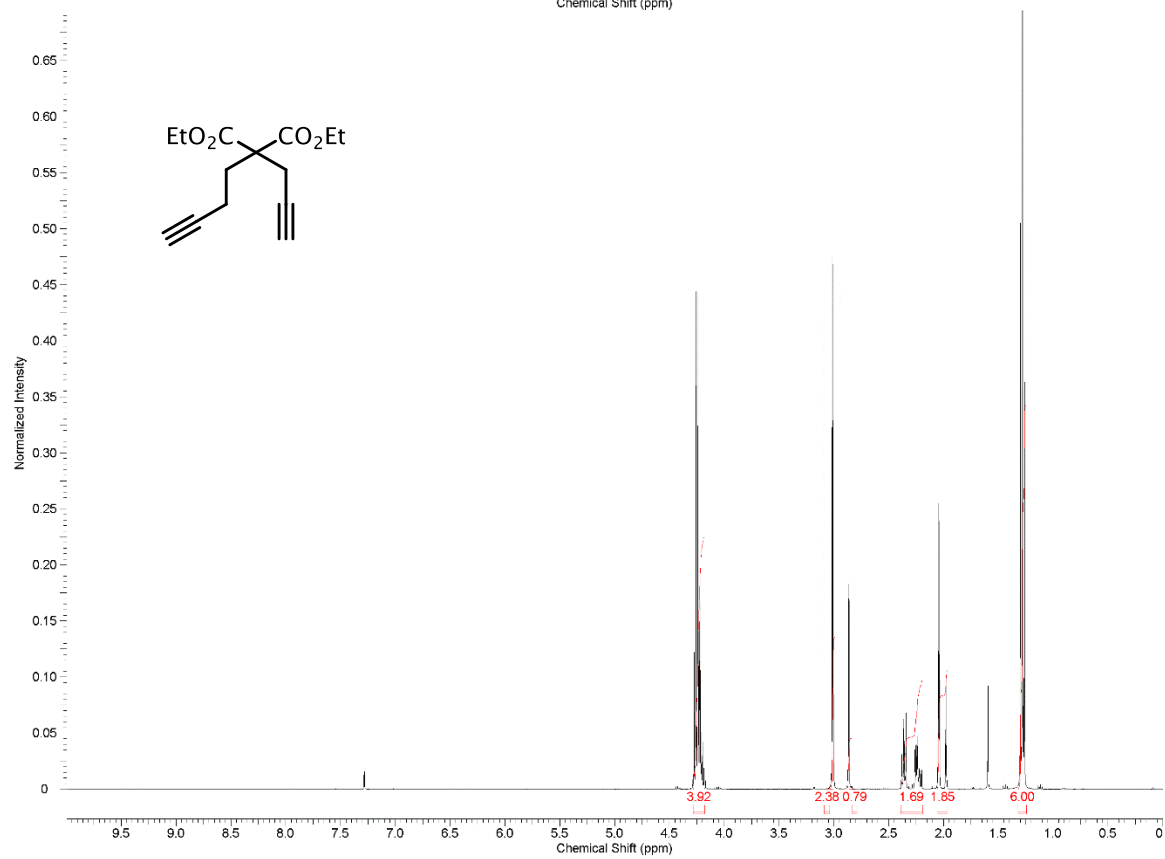
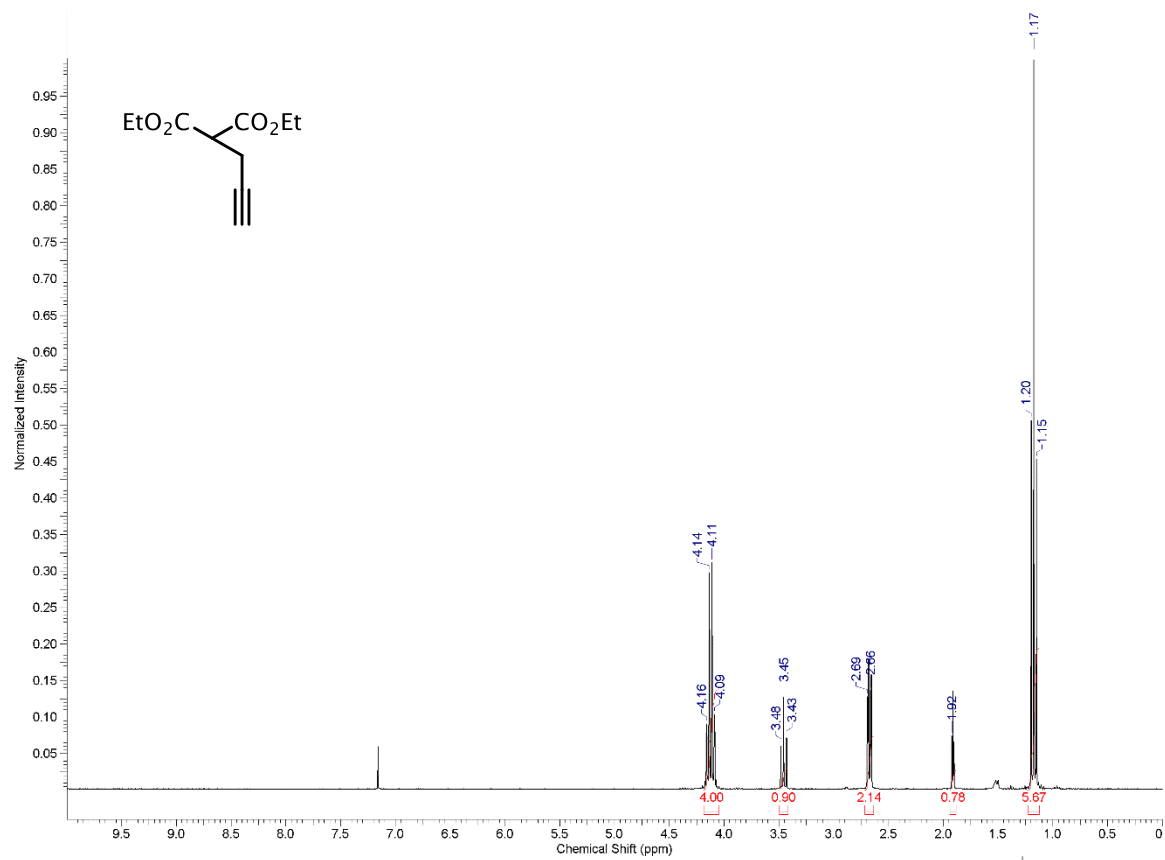
## A 1.5 --- Characterization Spectra for Diyne Substrates



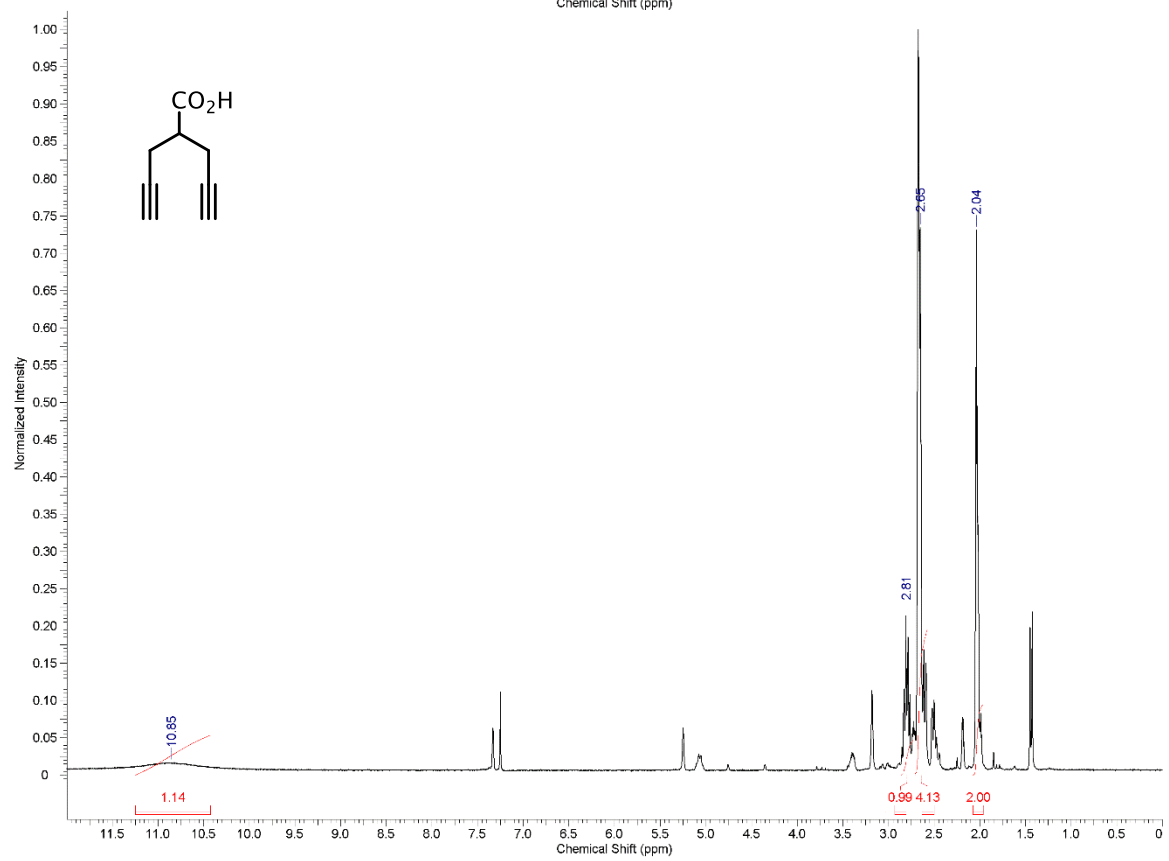
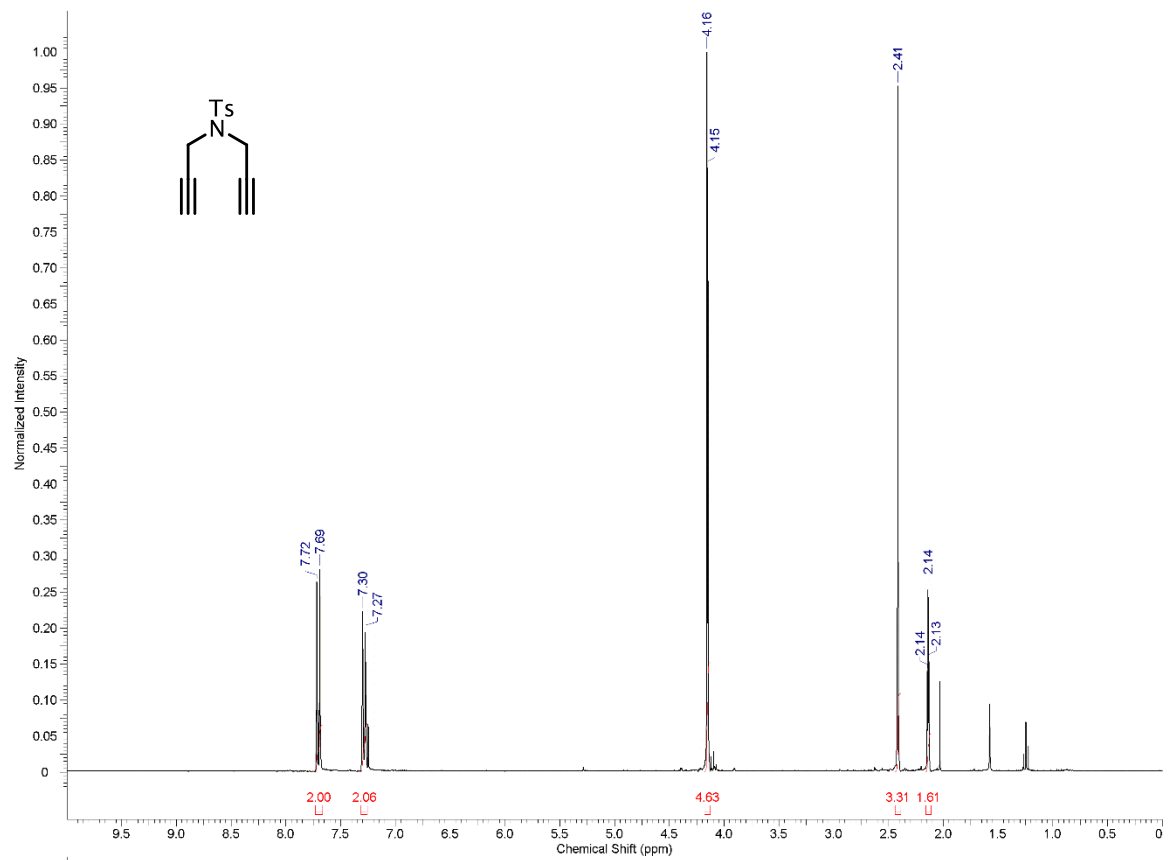


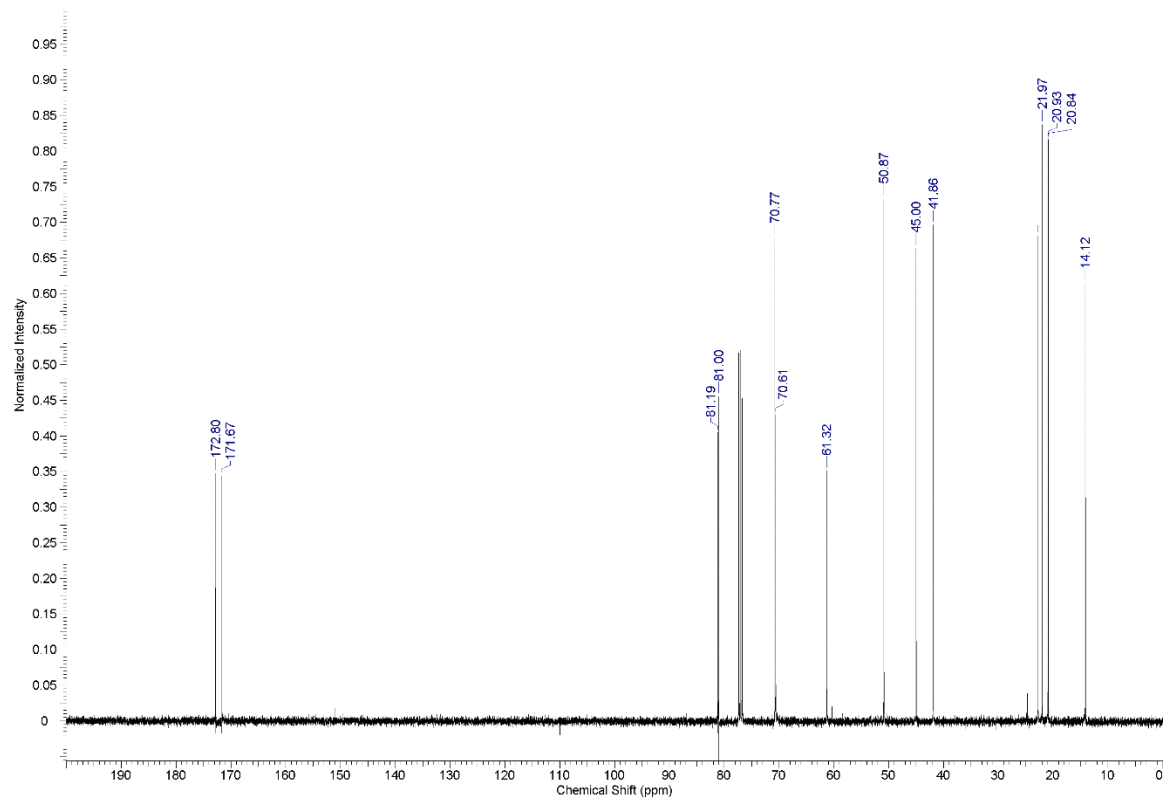
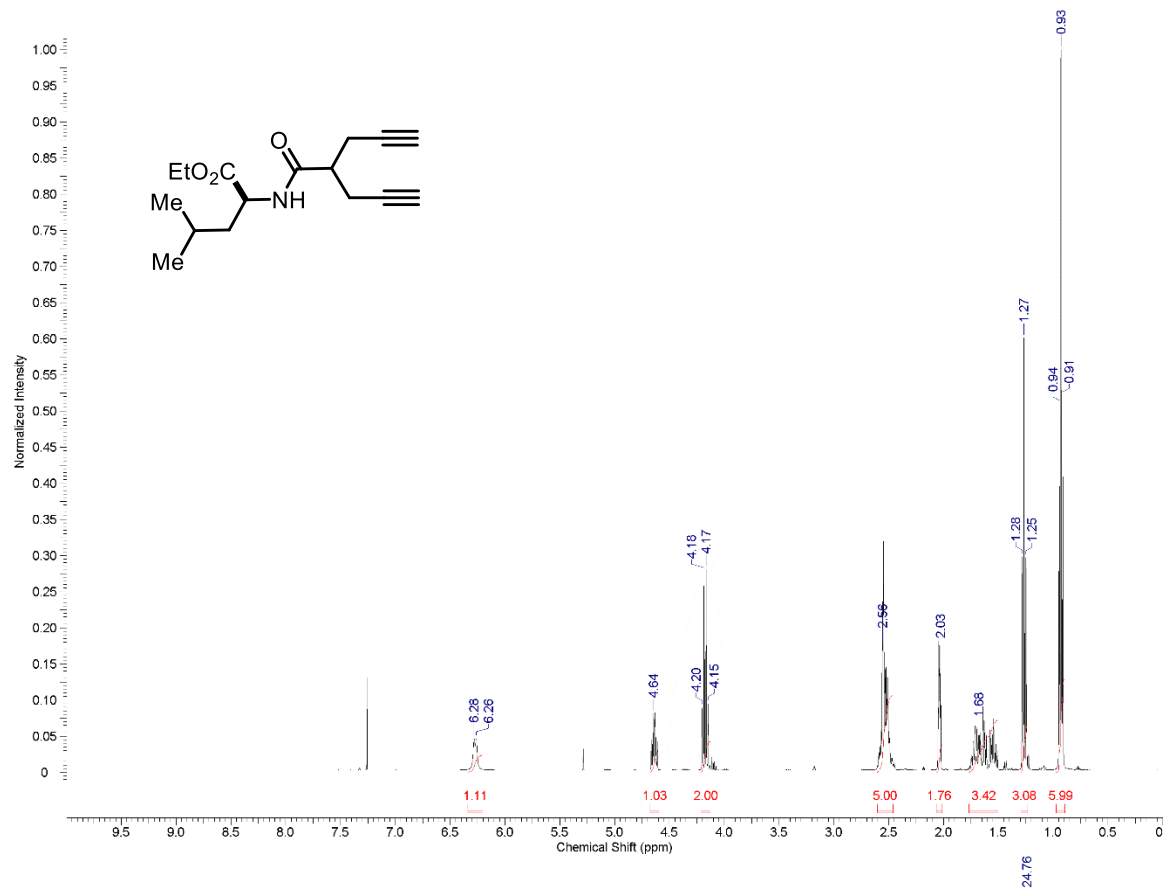


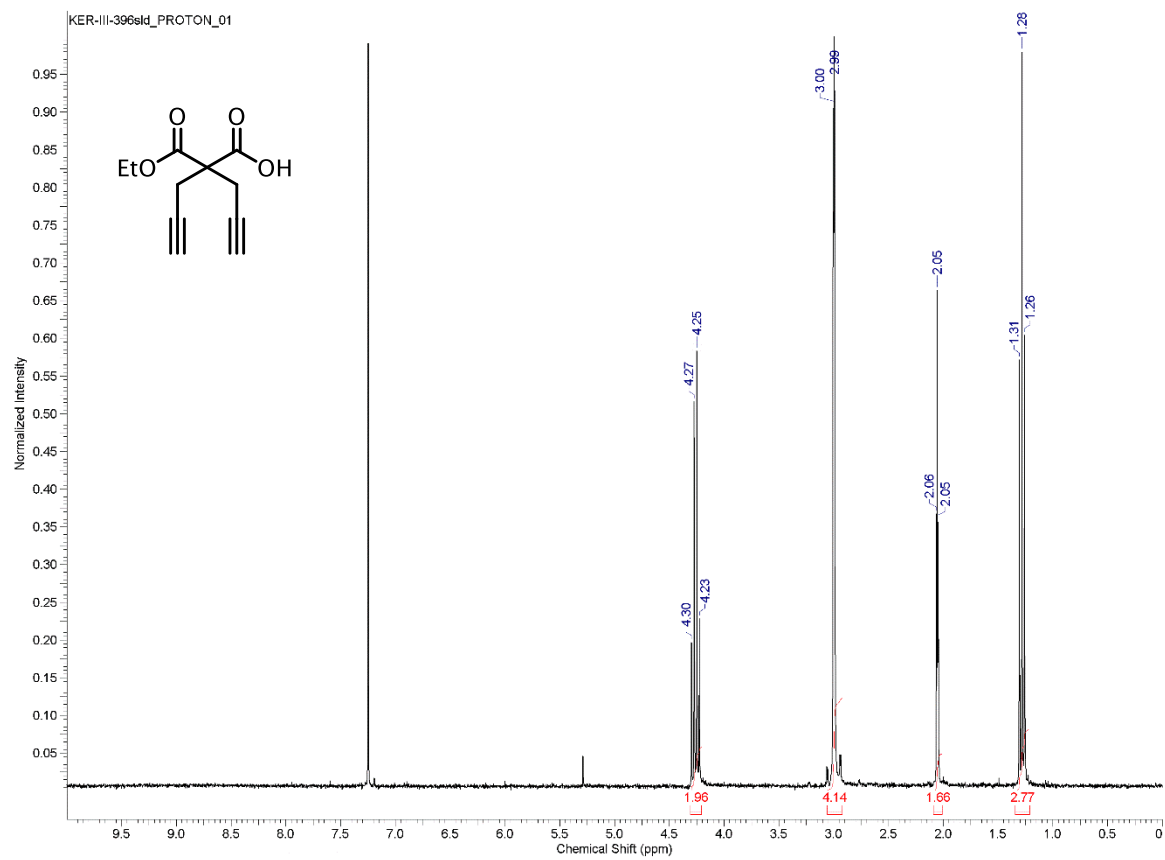


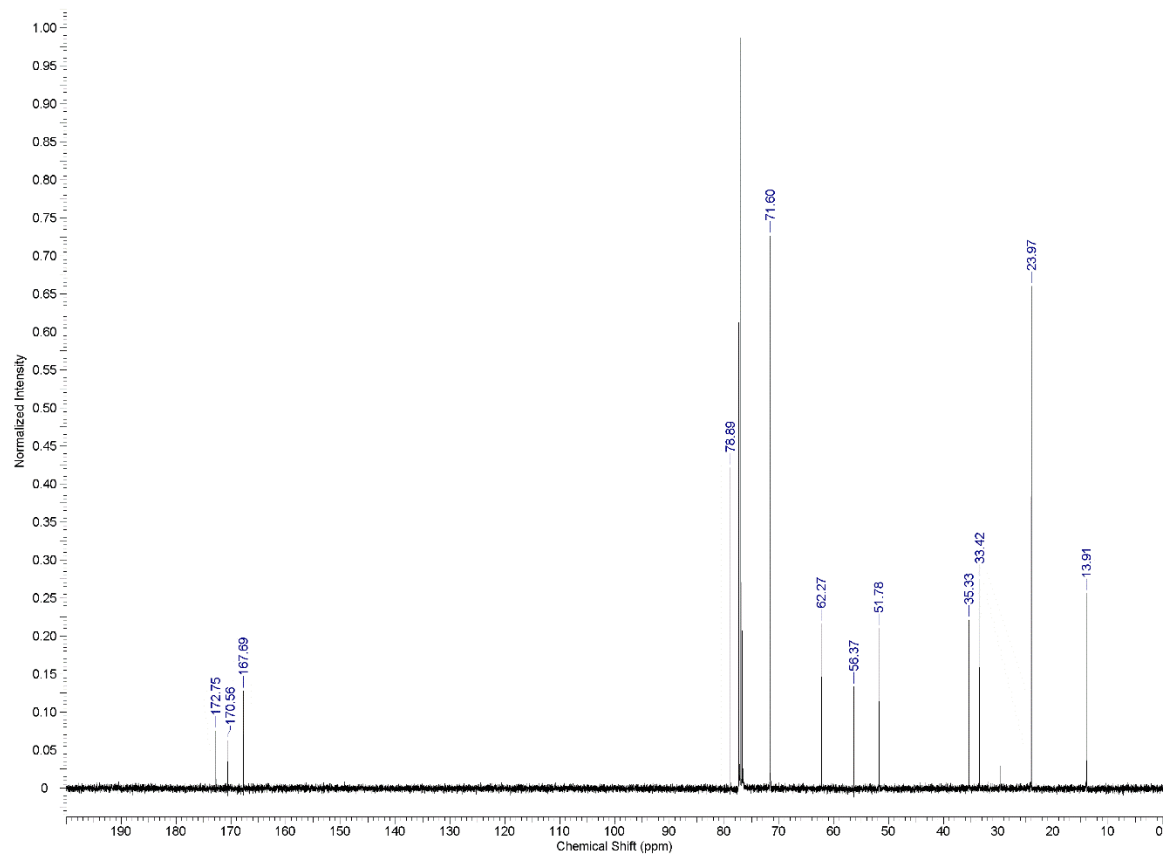
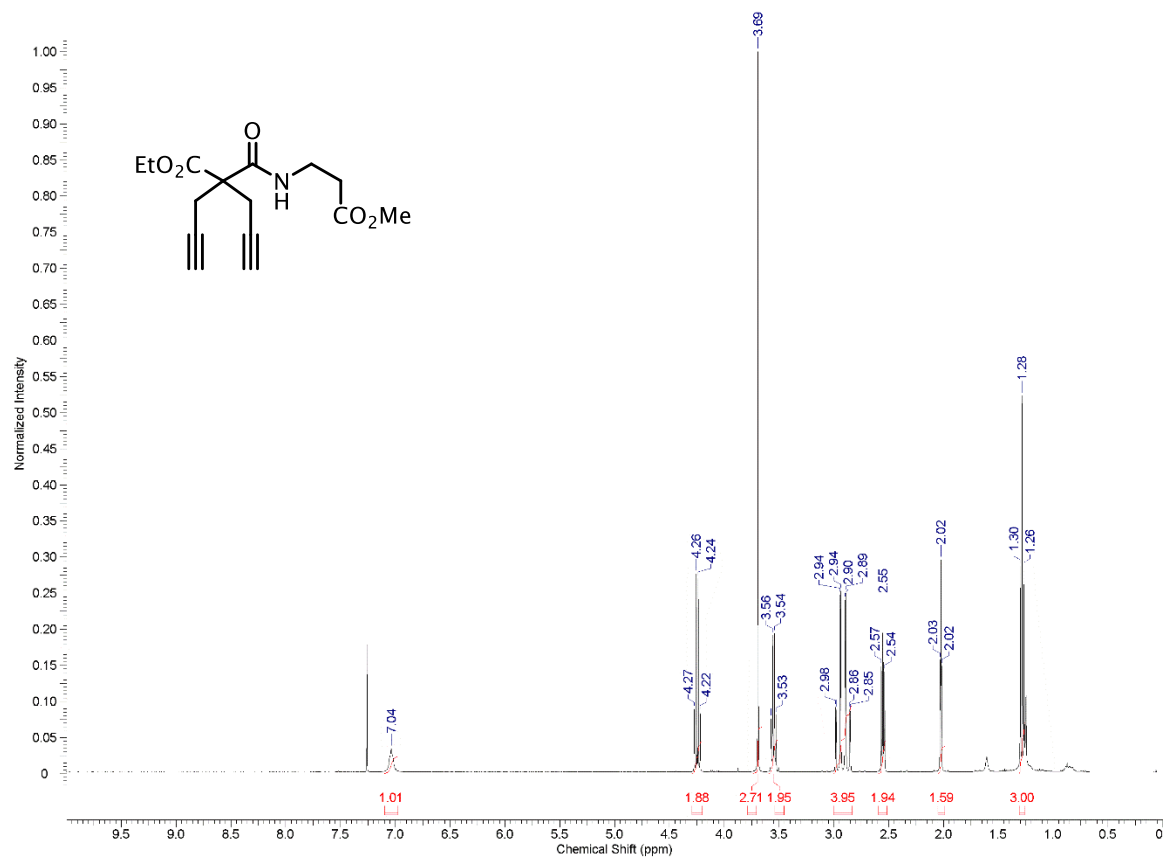






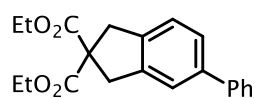




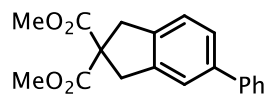


## A 1.6 --- General [2+2+2] Cycloaddition Procedure

Under ambient conditions, an oven dried 1-dram vial was charged with a stir bar. Diyne (0.3 mmol, 1.0 equivalent), cobalt pre-catalyst (0.006 mmol, 0.02 equivalents) and iridium photocatalyst (0.003, 0.01 equivalents) were weighed directly into the vial and then the vial was fitted with a teflon cap. The vial was then pumped into the glove box and charged with degassed acetonitrile (0.1 M), alkyne coupling partner (0.6 mmol, 2.0 equivalents) and diisopropylamine (DIPEA – 0.075 mmol, 0.25 equivalents). The vial was then firmly sealed, removed from the glove box, and placed in front of the desired light source (~16 inches for Kessil LED and ~6 inches for 14W CFL). After an allotted reaction time (1-16 hours), or complete consumption of starting materials, celite was added to the reaction and the solvent was removed *in vacuo*. After being deposited on celite the compound was loaded onto a column and eluted with an ethyl acetate:hexane gradient from 0-20%.

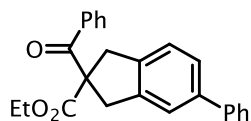


**Diethyl 5-phenyl-1,3-dihydro-2H-indene-2,2-dicarboxylate(40):** This compound was prepared with the general procedure and has been reported in the literature.<sup>[1]</sup> Compound **40** was isolated as an off-white solid in 92% yield. A <sup>1</sup>H NMR has been included for reference. <sup>1</sup>H NMR (400 MHz, CDCl<sub>3</sub>): δ 7.55 (m, 2H), 7.43-7.39 (m, 4H), 7.34-7.30 (m, 1H), 7.27-7.25 (m, 2H), 4.22 (q, J = 7.04 Hz, 4H), 3.65 (s, 2H), 3.63 (s, 2H), 1.27 (t, J = 7.04 Hz, 6H) ppm.



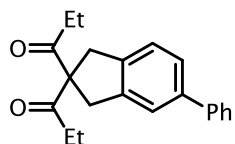
**Dimethyl 5-phenyl-1,3-dihydro-2H-indene-2,2-dicarboxylate (42):** This compound was prepared with the general procedure and has been reported.<sup>[1]</sup> Compound **42** was isolated as an off-white solid in 84% yield. A <sup>1</sup>H NMR has been

included for reference.  $^1\text{H NMR}$  (400 MHz,  $\text{CDCl}_3$ ):  $\delta$  7.54 (m, 2H), 7.40 (m, 4H), 7.31 (m, 1H), 7.25 (d,  $J = 7.8$  Hz, 1H), 3.78 (s, 6H), 3.63 (s, 2H), 3.63 (s, 2H) ppm.



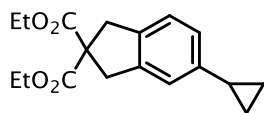
**Ethyl 2-benzoyl-5-phenyl-2,3-dihydro-1H-indene-2-carboxylate (43):**

This compound was prepared using the general procedure and isolated as a white solid in 83% yield.  $^1\text{H NMR}$  (400 MHz,  $\text{CDCl}_3$ ):  $\delta$  7.93 (d,  $J = 7.63$  Hz, 2H), 7.58- 7.53 (m, 3H), 7.48-7.38 (m, 6H), 7.33-7.25 (m, 2H), 4.13 (q,  $J = 7.0$  Hz, 2H), 3.92-3.73 (m, 4H), 1.04 (t,  $J = 7.0$  Hz, 3H) ppm.  $^{13}\text{C NMR}$  (101 MHz,  $\text{CDCl}_3$ ):  $\delta$  194.60, 173.73, 141.37, 140.60, 140.44, 139.07, 134.81, 133.08, 128.08, 128.73, 128.69, 127.17, 127.10, 126.28, 124.55, 123.07, 63.81, 61.88, 40.93, 40.67, 13.81 ppm. **IR** (ATR): 3060, 3029, 2977, 2934, 2852, 1730, 1686, 1483, 1448, 1266, 1244, 1201  $\text{cm}^{-1}$ . **MS** (ESI, pos):  $m/z = 371. 2 [\text{M}+\text{H}]^+$



**1,1'-(5-phenyl-2,3-dihydro-1H-indene-2,2-diyl)bis(propan-1-one) (44):**

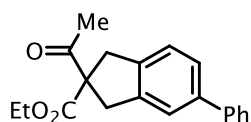
This compound was prepared using the general procedure and isolated as a white solid in 85% yield.  $^1\text{H NMR}$  (400 MHz,  $\text{CDCl}_3$ ):  $\delta$  7.56-7.53 (m, 2H), 7.43-7.38 (m, 4H), 7.34-7.30 (m, 1H), 7.26-7.24 (m, 1H), 3.57 (s, 2H), 3.55 (s, 2H), 2.48 (q,  $J = 7.04$  Hz, 4H), 1.07 (t,  $J = 7.04$  Hz, 6H) ppm.  $^{13}\text{C NMR}$  (101 MHz,  $\text{CDCl}_3$ ):  $\delta$  207.7 (2), 141.17, 140.58, 140.41, 139.02, 128.69, 127.10, 127.08, 126, 19, 124.60, 123.12, 74.62, 37.78, 37.50, 32.27, 8.30 ppm. **IR** (ATR): 2980, 1714, 1697  $\text{cm}^{-1}$ . **MS** (ESI, pos):  $m/z = 307.2 [\text{M}+\text{H}]^+$



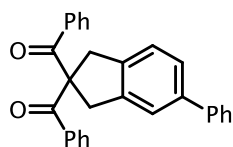
**Diethyl 5-cyclopropyl-1,3-dihydro-2H-indene-2,2-dicarboxylate (45):**

This compound was prepared with the general procedure and has been reported previously. <sup>[8]</sup> Compound **45** was isolated as a white solid in 66% yield. Spectral data has

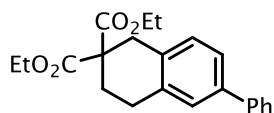
been included for reference.  $^1\text{H NMR}$  (400 MHz,  $\text{CDCl}_3$ ):  $\delta$  7.06 (d,  $J = 7.4$  Hz, 1H), 6.90-6.87 (m, 2H), 4.19 (q,  $J = 7.4$  Hz, 4H), 3.53 (s, 4H), 1.89-1.82 (m, 1H), 1.25 (t,  $J = 7.4$  Hz, 6H), 0.93-0.89 (m, 2H), 0.66-0.63 (m, 2H) ppm.  $^{13}\text{C NMR}$  (101 MHz,  $\text{CDCl}_3$ ):  $\delta$  171.69, 142.78, 140.13, 137.06, 124.60, 123.89, 121.40, 61.62, 60.50, 40.39, 40.10, 15.24, 14.01, 9.01 ppm. **MS** (ESI, pos):  $m/z = 303.1$   $[\text{M}+\text{H}]^+$



**Ethyl 2-acetyl-5-phenyl-2,3-dihydro-1H-indene-2-carboxylate (46):** This compound was prepared using the general procedure and isolated as a white solid in 91% yield.  $^1\text{H NMR}$  (400 MHz,  $\text{CDCl}_3$ ):  $\delta$  7.56-7.54 (m, 2H), 7.44-7.39 (m, 4H), 7.34-7.30 (m, 1H), 7.27-7.24 (m, 1H), 4.24 (q,  $J = 7.04$  Hz, 4H), 3.58 (m, 4H), 2.26 (s, 3H), 1.28 (t,  $J = 7.04$  Hz, 3H) ppm.  $^{13}\text{C NMR}$  (101 MHz,  $\text{CDCl}_3$ ):  $\delta$  202.65, 172.34, 141.23, 140.52, 140.39, 138.97, 128.76, 128.67, 127.76, 127.10, 127.07, 126.19, 124.54, 123.07, 67.01, 61.88, 38.98, 38.73, 26.13, 14.03 ppm. **MS** (ESI, pos):  $m/z = 309.2$   $[\text{M}+\text{H}]^+$

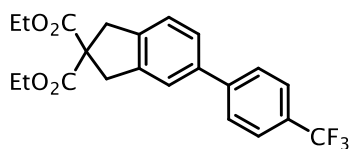


**(5-phenyl-2,3-dihydro-1H-indene-2,2-diyl)bis(phenylmethanone) (47):** This compound was prepared with the general procedure and isolated as a white solid in 93% yield.  $^1\text{H NMR}$  (300 MHz,  $\text{CDCl}_3$ ):  $\delta$  7.88 (d,  $J = 7.6$  Hz, 4H), 7.53 (d,  $J = 7.6$  Hz, 2H), 7.47-7.27 (m, 12H), 4.04 (s, 2H), 4.02 (s, 2H) ppm.  $^{13}\text{C NMR}$  (101 MHz,  $\text{CDCl}_3$ ):  $\delta$  197.21, 140.52, 138.98, 135.47, 133.25, 129.47, 128.71, 127.18, 127.06, 126.35, 124.61, 123.12, 70.02, 41.26, 41.01 ppm. **IR** (ATR): 3029, 3064, 2852, 2921, 1660, 1262, 1262, 1240  $\text{cm}^{-1}$ . **MS** (ESI, pos):  $m/z = 403.2$   $[\text{M}+\text{H}]^+$



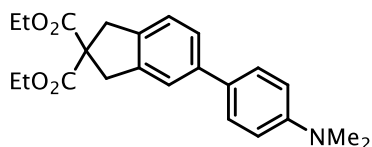
**Diethyl 6-phenyl-3,4-dihydronaphthalene-2,2(1H)-dicarboxylate (48):**

This compound was prepared using the general procedure and isolated as a white solid in 75% yield.  $^1\text{H NMR}$  (400 MHz,  $\text{CDCl}_3$ ):  $\delta$  7.58 (m, 2H), 7.44 (m, 4H), 7.34 (m, 1H), 7.29 (m, 1H), 4.24 (q,  $J = 7.2$  Hz, 4H), 3.68 (s, 2H), 3.66 (s, 2H), 2.88 (d,  $J = 2.75$  Hz, 1H), 2.38 (m, 1H), 2.25 (m, 1H), 2.03 (m, 1H) ppm.  $^{13}\text{C NMR}$  (101 MHz,  $\text{CDCl}_3$ ):  $\delta$  171.66, 141.33, 140.73, 139.20, 129.08, 128.70, 127.14, 127.08, 126.15, 124.47, 123.03, 68.94, 61.80, 61.75, 60.54, 56.17, 40.52, 40.24, 30.08, 22.95, 14.07, 14.01, 13.89 ppm. **IR** (ATR): 2934, 2986, 2847, 1734, 1266, 1244, 1184  $\text{cm}^{-1}$ . **MS** (ESI, pos):  $m/z = 403$ . 2  $[\text{M}+\text{H}]^+$



**Diethyl 5-(4-(trifluoromethyl)phenyl)-1,3-dihydro-2H-indene-2,2-dicarboxylate (49):**

This compound was prepared with the general procedure and isolated as a white solid in 71% yield.  $^1\text{H NMR}$  (400 MHz,  $\text{CDCl}_3$ ):  $\delta$  7.66 (m, 4H), 7.41 (m, 2H), 7.29 (d,  $J = 7.8$  Hz, 1H), 4.23 (q,  $J = 7.0$  Hz, 4H), 3.66 (s, 2H), 3.64 (s, 2H), 1.27 (t,  $J = 7.0$  Hz, 6H) ppm.  $^{13}\text{C NMR}$  (101 MHz,  $\text{CDCl}_3$ ):  $\delta$  171.51, 144.79, 141.02, 140.26, 138.81, 129.60, 129.27, 128.95, 128.63, 126.24, 125.59, 124.69, 123.10, 61.79, 60.47, 40.43, 40.22, 14.02 ppm. **IR** (ATR): 2982, 2934, 2852, 1730, 1158, 1240, 1158, 1062, 1106, 1062  $\text{cm}^{-1}$ . **MS** (ESI, pos):  $m/z = 406$ . 2  $[\text{M}]^+$

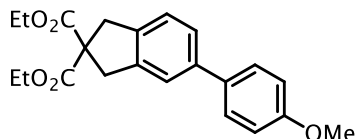


**Diethyl 5-(4-(dimethylamino)phenyl)-1,3-dihydro-2H-indene-2,2-dicarboxylate (50):**

This compound was prepared using the general procedure and isolated as an off-white, light yellow solid in 90% yield.  $^1\text{H NMR}$  (400 MHz,  $\text{CDCl}_3$ ):  $\delta$  7.45 (d,  $J = 9.0$  Hz, 2H), 7.35 (m, 2H), 7.21 (d,  $J = 7.4$  Hz, 1H), 6.79 (d,  $J = 9.0$  Hz, 2H), 4.22 (q,  $J = 7.0$  Hz, 4H), 3.63 (s, 2H), 3.61 (s, 2H), 2.98 (s,

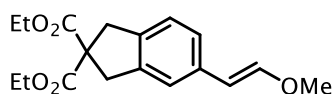


6H), 1.27 (t, J = 7.0 Hz, 6H) ppm.  $^{13}\text{C}$  NMR (101 MHz,  $\text{CDCl}_3$ ):  $\delta$  171.72, 149.83, 140.53, 140.32, 137.78, 129.42, 127.66, 125.29, 124.29, 122.10, 112.7, 61.66, 60.53, 40.58, 40.53, 40.19, 14.03 ppm. IR (ATR): 2977, 2934, 2886, 2800, 1730, 1244, 1153, 1179  $\text{cm}^{-1}$ . MS (ESI, pos):  $m/z$  = 381.2  $[\text{M}]^+$ ; 382.2  $[\text{M}+\text{H}]^+$



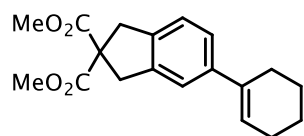
**Diethyl 5-(4-methoxyphenyl)-1,3-dihydro-2H-indene-2,2-dicarboxylate (51):** This compound was prepared using the general

procedure and has been reported.<sup>[9]</sup> Compound **51** was isolated as an off-white, light yellow solid in 83% yield. Spectral data has been included for reference.  $^1\text{H}$  NMR (400 MHz,  $\text{CDCl}_3$ ):  $\delta$  7.49-7.47 (m, 2H), 7.35 (m, 2H), 7.23 (m, 1H), 6.95 (m, 2H), 4.22 (q, J = 7.04 Hz, 4H), 3.84 (s, 3H), 3.63 (s, 2H), 3.61 (s, 2H), 1.26 (t, J = 7.04 Hz, 6H) ppm.  $^{13}\text{C}$  NMR (101 MHz,  $\text{CDCl}_3$ ):  $\delta$  171.66, 141.77, 141.65, 140.64, 139.91, 138.92, 138.50, 133.92, 133.86, 128.10, 125.70, 124.38, 124.38, 122.57, 114.11, 61.70, 60.51, 55.32, 40.49, 40.18, 14.03 ppm. MS (ESI, pos):  $m/z$  = 369.2  $[\text{M}+\text{H}]^+$



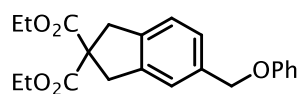
**Diethyl (E)-5-(2-methoxyvinyl)-1,3-dihydro-2H-indene-2,2-dicarboxylate (52):** This compound was prepared with the general

procedure and isolated as a white solid in 85% yield.  $^1\text{H}$  NMR (300 MHz,  $\text{CDCl}_3$ ):  $\delta$  7.45 (s, 1H), 7.31 (d, J = 7.8 Hz, 1H), 7.09 (d, J = 7.8 Hz, 1H), 6.08 (d, J = 7.04 Hz, 1H), 5.17 (d, J = 7.04 Hz, 1H), 4.19 (q, J = 7.0 Hz, 4H), 3.76 (s, 3H), 3.56 (s, 2H), 3.53 (s, 2H), 1.24 (t, J = 7.0 Hz, 6H) ppm.  $^{13}\text{C}$  NMR (101 MHz,  $\text{CDCl}_3$ ):  $\delta$  172.19, 147.51, 139.87, 137.36, 134.84, 127.23, 123.87, 123.83, 105.68, 60.63, 60.53, 52.92, 40.62, 40.43 ppm. IR (ATR): 3003, 3034, 2951, 2839, 1734, 1270, 1249, 1073  $\text{cm}^{-1}$ . MS (ESI, pos):  $m/z$  = 319.2  $[\text{M}+\text{H}]^+$



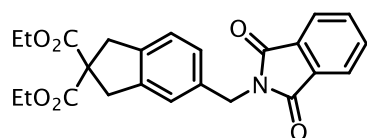
**Diethyl 5-(cyclohex-1-en-1-yl)-1,3-dihydro-2H-indene-2,2-dicarboxylate (53):** This compound was prepared using the general

procedure and has been previously been reported.<sup>[10]</sup> Compound **53** was isolated as a viscous oil which solidified upon cooling in 72% yield. A <sup>1</sup>H NMR has been included for reference. <sup>1</sup>H NMR (400 MHz, CDCl<sub>3</sub>): 7.12 (m, 2H), 7.02 (d, J = 7.8 Hz, 1H), 5.98 (m, 1H), 3.67 (s, 6H), 3.50 (s, 2H), 3.49 (s, 2H), 2.30 (m, 2.0H), 2.11 (m, 2H), 1.69 (m, 2H), 1.57 (m, 2H) ppm.



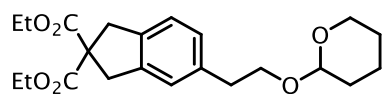
**Diethyl 5-(phenoxymethyl)-1,3-dihydro-2H-indene-2,2-dicarboxylate (54):** This compound was prepared with the general

procedure and isolated as an off-white, light yellow solid in 67% yield. <sup>1</sup>H NMR (400 MHz, CDCl<sub>3</sub>): δ 7.31-7.19 (m, 5H), 6.99-6.94 (m, 3H), 5.01 (s, 2H), 4.21 (q, J = 7.04 Hz, 4 H), 3.60 (s, 2H), 3.59 (s, 2H), 1.26 (t, J = 7.04 Hz, 6H) ppm. <sup>13</sup>C NMR (101 MHz, CDCl<sub>3</sub>): δ 171.56, 158.79, 140.53, 139.93, 135.83, 129.43, 126.48, 124.28, 123.53, 120.87, 114.79, 69.95, 61.72, 60.47, 40.37, 40.24, 14.01 ppm. **MS** (ESI, pos): m/z = 369. 2 [M+H]<sup>+</sup>



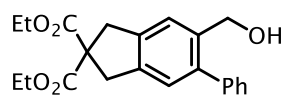
**Diethyl 5-(((1,3-dioxoisindolin-2-yl)methyl)-1,3-dihydro-2H-indene-2,2-dicarboxylate (55):** This compound was prepared

using the general procedure and isolated as a white solid in 90% yield. <sup>1</sup>H NMR (400 MHz, CDCl<sub>3</sub>): δ 7.85-7.83 (m, 2H), 7.71-7.69 (m, 2H), 7.25 (m, 2H, overlapping with 7.26 - CHCl<sub>3</sub>), 7.12 (m, 1H), 4.79 (s, 2H), 4.18 (q, J = 7.04 Hz, 4H), 3.54 (s, 2H), 3.53 (s, 2H), 1.23 (t, J = 7.04 Hz, 6H) ppm. <sup>13</sup>C NMR (101 MHz, CDCl<sub>3</sub>): δ 171.54, 168.04, 140.60, 139.75, 135.92, 132.14, 127.57, 124.56, 123.31, 61.69, 60.38, 41.46, 40.30, 40.17, 13.99 ppm. **MS** (ESI, pos): m/z = 422. 2 [M+H]<sup>+</sup>



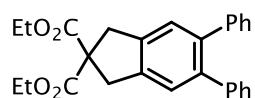
**Diethyl 5-(2-((tetrahydro-2H-pyran-2-yl)oxy)ethyl)-1,3-dihydro-2H-indene-2,2-dicarboxylate (56):** This compound was

prepared using the general procedure and has been reported in the literature.<sup>[11]</sup> Compound **56** was isolated as a light brown viscous oil in 82% yield and spectra were consistent with the literature report.



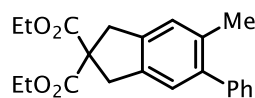
**Diethyl 5-(hydroxymethyl)-6-phenyl-1,3-dihydro-2H-indene-2,2-dicarboxylate (57):** This compound was prepared using the general

procedure and has been reported in the literature.<sup>[9]</sup> Compound **57** was isolated as an off white solid in 82% yield. A <sup>1</sup>H NMR has been included for reference. <sup>1</sup>H NMR (400 MHz, CDCl<sub>3</sub>): δ 7.42-7.32 (m, 6H), 7.10 (s, 1H), 1.95 (s, 2H), 4.22 (q, J = 7.4 Hz, 4H), 3.64 (s, 2H), 3.61 (s, 2H), 1.27 (t, J = 7.4 Hz, 6H) ppm. MS (ESI, pos): m/z = 351. 2 [M-OH]<sup>+</sup>



**Diethyl 5,6-diphenyl-1,3-dihydro-2H-indene-2,2-dicarboxylate (58):**

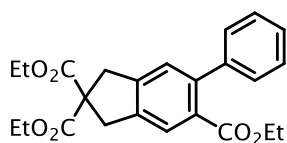
This compound was prepared using the general procedure and has been reported in the literature.<sup>[11]</sup> Compound **58** was isolated as white solid in 65% yield. A <sup>1</sup>H NMR has been included for reference. <sup>1</sup>H NMR (400 MHz, CDCl<sub>3</sub>): δ 7.25 (s, 2H), 7.18-7.16 (m, 6H), 7.11-7.08 (m, 3H), 4.24 (q, J = 7.0 Hz, 4H), 3.68 (s, 4H), 1.28 (t, J = 7.0 Hz, 6H) ppm. MS (ESI, pos): m/z = 415. 2 [M+H]<sup>+</sup>



**Diethyl 5-methyl-6-phenyl-1,3-dihydro-2H-indene-2,2-dicarboxylate (59):** This compound was prepared using the general procedure and has been

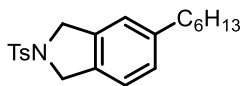
reported in the literature.<sup>[12]</sup> Compound **59** was isolated as white solid in 64% yield. A <sup>1</sup>H NMR

has been included for reference. **<sup>1</sup>H NMR** (400 MHz, CDCl<sub>3</sub>): δ 7.41-7.37 (m, 2H), 7.33-7.27 (m, 3H), 7.10 (s, 1H), 7.05 (s, 1H), 4.22 (q, J = 7.04 Hz, 4H), 3.60 & 3.59 (overlapping singlets, 2H), 2.21 (s, 3H), 1.27 (t, J = 7.04 Hz, 6H) ppm. **MS** (ESI, pos): m/z = 353. 2 [M+H]<sup>+</sup>



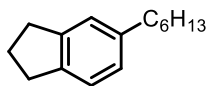
**Triethyl 6-phenyl-1,3-dihydro-2H-indene-2,2,5-tricarboxylate (60):**

This compound was prepared using the general procedure and has been reported in the literature.<sup>[12]</sup> Compound **60** was isolated as an off-white solid in 92% yield. A <sup>1</sup>H NMR has been included for reference. **<sup>1</sup>H NMR** (400 MHz, CDCl<sub>3</sub>): 7.64 (s, 1H), 7.33 (m, 3H), 7.25 (d, J = 7.4 Hz, 2H), 7.17 (s, 1H), 4.20 (q, J = 7.0 Hz, 4H), 3.62 (s, 2H), 3.61 (s, 2H), 3.57 (s, 3H), 1.25 (t, J = 7.4 Hz, 6H) ppm.



**5-hexyl-2-tosylisoindoline (61):** This compound was prepared using the general procedure and has been reported previously.<sup>[13]</sup> Compound **61** was

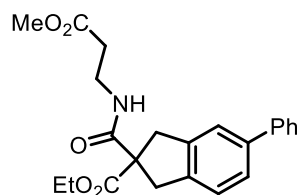
isolated as a tan solid in 68% yield. A <sup>1</sup>H NMR has been included for reference. **<sup>1</sup>H NMR** (400 MHz, CDCl<sub>3</sub>): δ 7.77 (d, J = 8.2 Hz, 2H), 7.30 (d, J = 8.2 Hz, 2H), 7.05 (m, 2H), 6.98 (s, 1H), 4.58 (s, 4H), 2.55 (t, J = 7.4 Hz, 2H), 2.40 (s, 3H), 1.54 (m, 2H), 1.27 (m, 6H), 0.87 (t, J = 6.3 Hz, 3H) ppm.



**5-hexyl-2,3-dihydro-1H-indene (62):** This compound was prepared using the general procedure and has been reported in the literature.<sup>[14]</sup> Compound **62** was

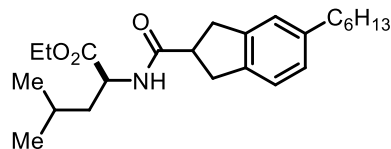
isolated as a clear oil in 60% yield. A <sup>1</sup>H NMR has been included for reference. **<sup>1</sup>H NMR** (400 MHz, CDCl<sub>3</sub>): δ 7.15 (d, J = 7.8 Hz, 1H), 7.07 (s, 1H), 6.97 (d, J = 7.8 Hz, 1H), 2.90 (qt, J = 4.3

(3), 3.1 (3) Hz, 4H), 2.59 (t, J = 7.4 Hz, 2H), 2.08 (quin, J = 7.4 Hz, 2H), 1.61 (m, 2H), 1.33 (m, 6H), 0.91 (t, J = 6.7 Hz, 3H) ppm.



**Methyl 2-((3-methoxy-3-oxopropyl)carbamoyl)-5-phenyl-2,3-dihydro-1H-indene-2-carboxylate (63):** This compound was prepared using the general procedure and compound **63** was isolated as an off-

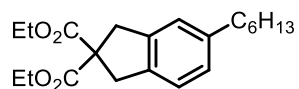
white solid in 74% yield. **<sup>1</sup>H NMR** (400 MHz, CDCl<sub>3</sub>): δ 7.55 (m, 2H), 7.41 (m, 4H), 7.32 (tt, J = 7.4, 2.0 Hz, 1H), 7.25 (d, J = 7.0 Hz, 1H), 6.74 (t, J = 5.5 Hz, 1H), 4.20 (ddt, J = 7.4 Hz, 2H), 3.69 (s, 3H), 3.67-3.52 (m, 6H), 2.54 (t, J = 5.9 Hz, 2H), 1.25 (t, J = 7.4 Hz, 3H) ppm. **<sup>13</sup>C NMR** (101 MHz, CDCl<sub>3</sub>): δ 173.3, 172.8, 170.2, 141.3, 140.9, 140.3, 139.3, 128.7, 127.09, 127.04, 126.1, 124.4, 123.0, 62.1, 61.7, 51.8, 40.6, 40.3, 35.5, 33.6, 13.9 ppm. **IR** (ATR): 3285, 2949, 2988, 1735, 1644, 1541, 1192 cm<sup>-1</sup>. **MS** (ESI, pos): m/z = 396.1 [M+H]; 418.2 [M+Na<sup>+</sup>]



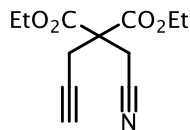
**1-(5-hexyl-2,3-dihydro-1H-indene-2-carboxamido)-3-methylbutyl propionate (64):** This compound was prepared using the general procedure and isolated as an off-white solid in

64% yield as a 1:1 mixture of diastereomers. **<sup>1</sup>H NMR** (400 MHz, CDCl<sub>3</sub>) δ 7.10 (d, J = 7.8Hz, 1H), 7.02 (s, 1H), 6.97 (d, J = 7.8Hz, 1H), 5.88 (d, J = 7.4Hz, 1H), 4.66 (qt, J = 5.1Hz, 3.91Hz, 1H), 4.19 (q, J = 7.0Hz, 2H), 3.19 (m, 5H), 2.56 (t, J = 7.4Hz, 2H), 1.69-1.51 (m, 5H), 1.36-1.26 (m, 9H), 0.94 (m, 6H), 0.88 (t, J = 6.7 Hz, 3H) ppm. **<sup>13</sup>C NMR** (101 MHz, CDCl<sub>3</sub>) δ 174.6, 173.2, 141.8, 141.7, 141.6, 141.5, 138.8, 138.7, 126.84, 126.83, 124.35, 124.31, 124.03, 124.00, 61.3, 50.7, 45.8, 41.8, 36.6, 36.4, 36.3, 35.8, 31.8, 31.7, 29.0, 24.9, 22.8, 22.6, 22.0, 14.14, 14.09 ppm.

**IR** (ATR): 3293, 2951, 2925, 2856, 1734, 1656, 1543, 1192, 1149  $\text{cm}^{-1}$ . **MS** (ESI, pos):  $m/z = 388.4$   $[\text{M}+\text{H}]$ ;  $410.4$   $[\text{M}+\text{Na}^+]$

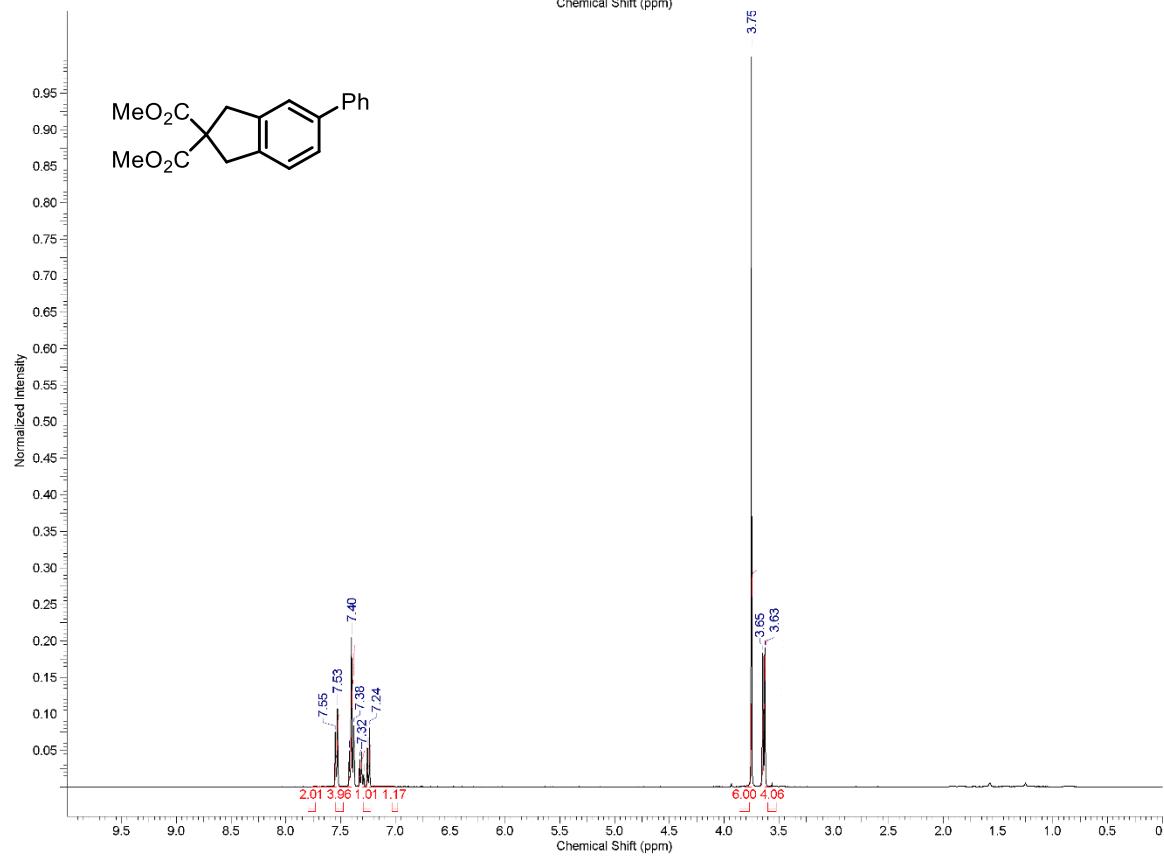
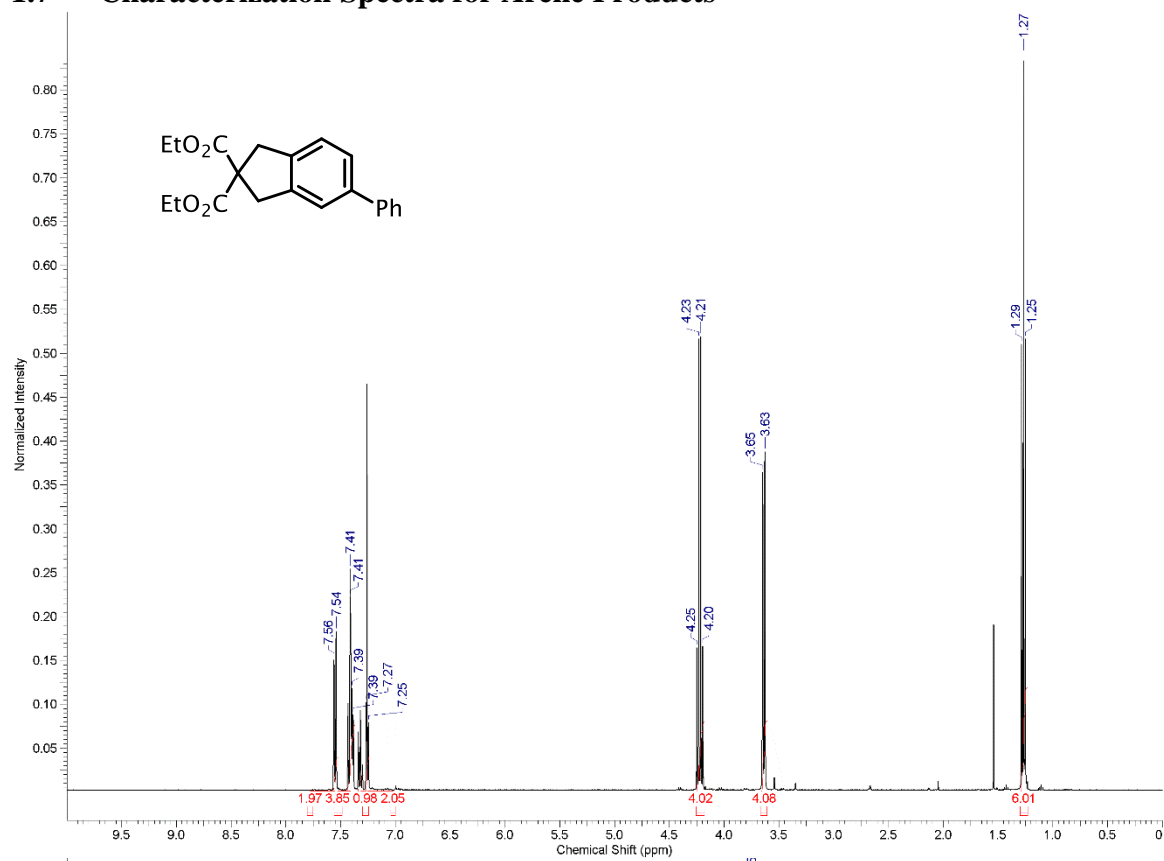


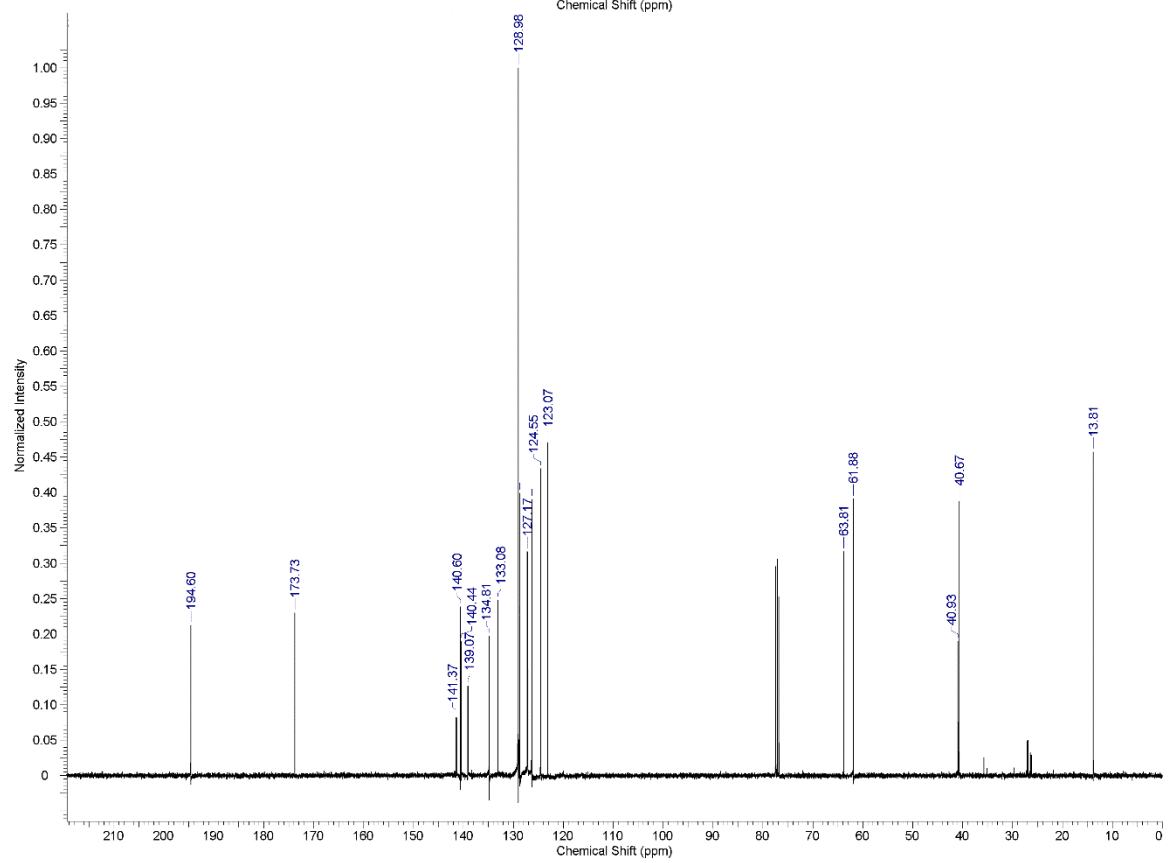
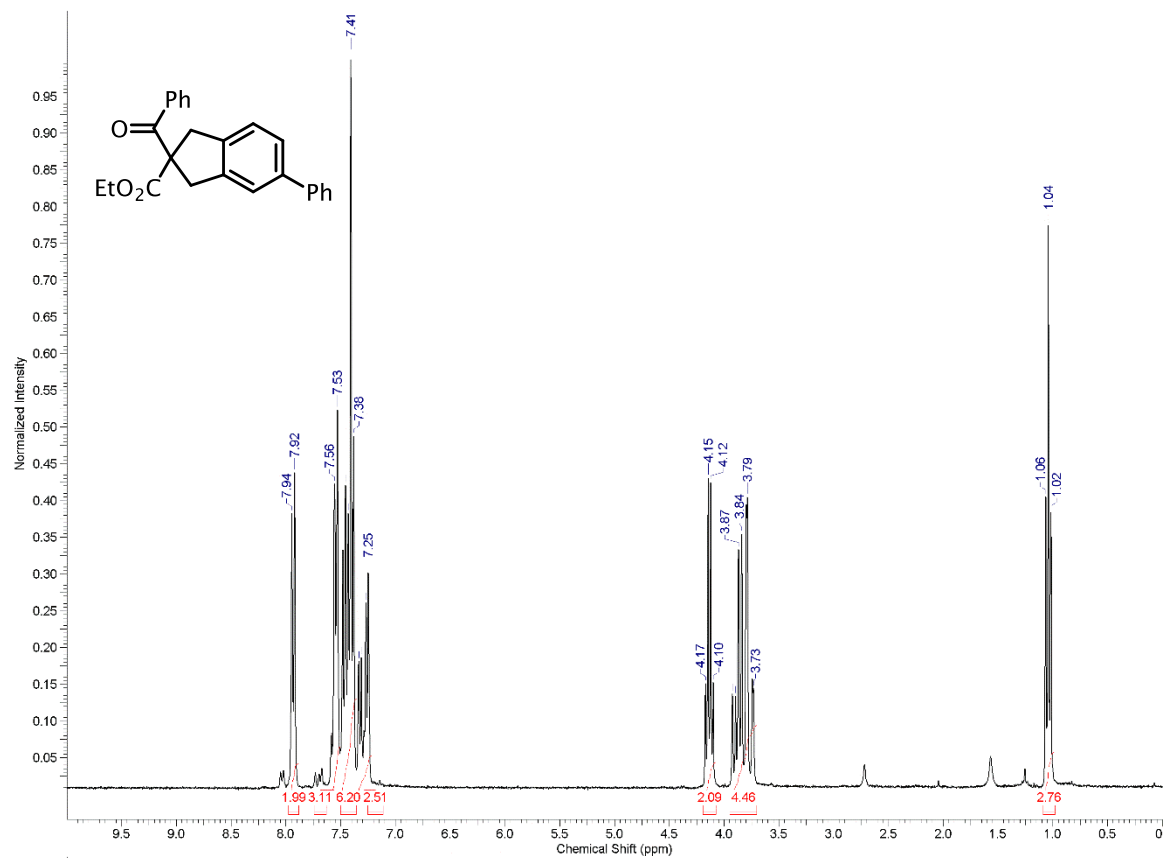
**Diethyl 5-hexyl-1,3-dihydro-2H-indene-2,2-dicarboxylate (77)**: This compound was prepared with the general procedure and has been previously been reported.<sup>[12]</sup> Compound **77** was isolated as a clear oil in 60% yield. A  $^1\text{H}$  NMR has been included for reference.  $^1\text{H}$  NMR (400 MHz,  $\text{CDCl}_3$ ):  $\delta$  7.09 (d,  $J = 7.8\text{Hz}$ , 1H), 7.01 (s, 1H), 6.97 (d,  $J = 7.8\text{ Hz}$ , 1H), 4.2 (q,  $J = 7.4\text{ Hz}$ , 4H), 3.55 (s, 2H), 3.56 (s, 2H), 2.55 (t,  $J = 7.4\text{Hz}$ , 2H), 2.31 (m, 2H), overlapping 1.30 (m, 6H) and 1.25 (t,  $J = 7.4\text{ Hz}$ , 6H), 0.88 (t,  $J = 6.7\text{Hz}$ , 3H) ppm.



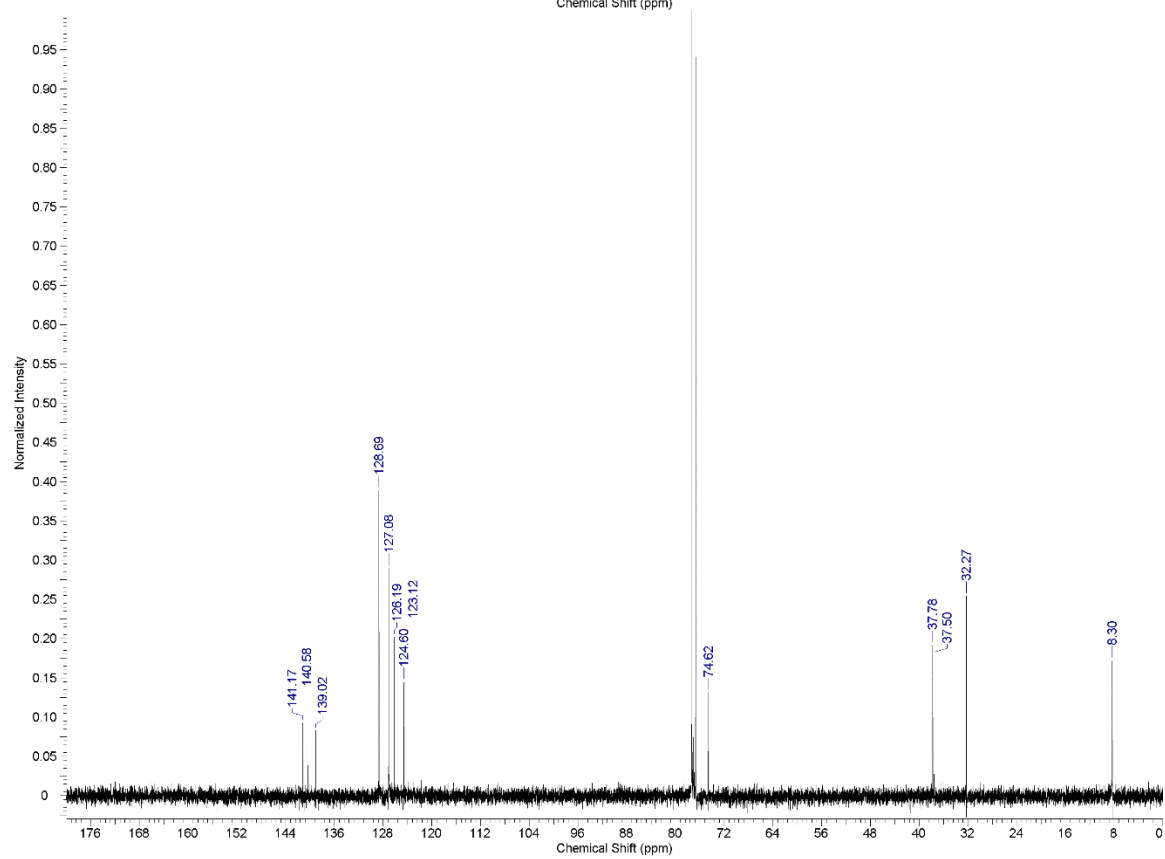
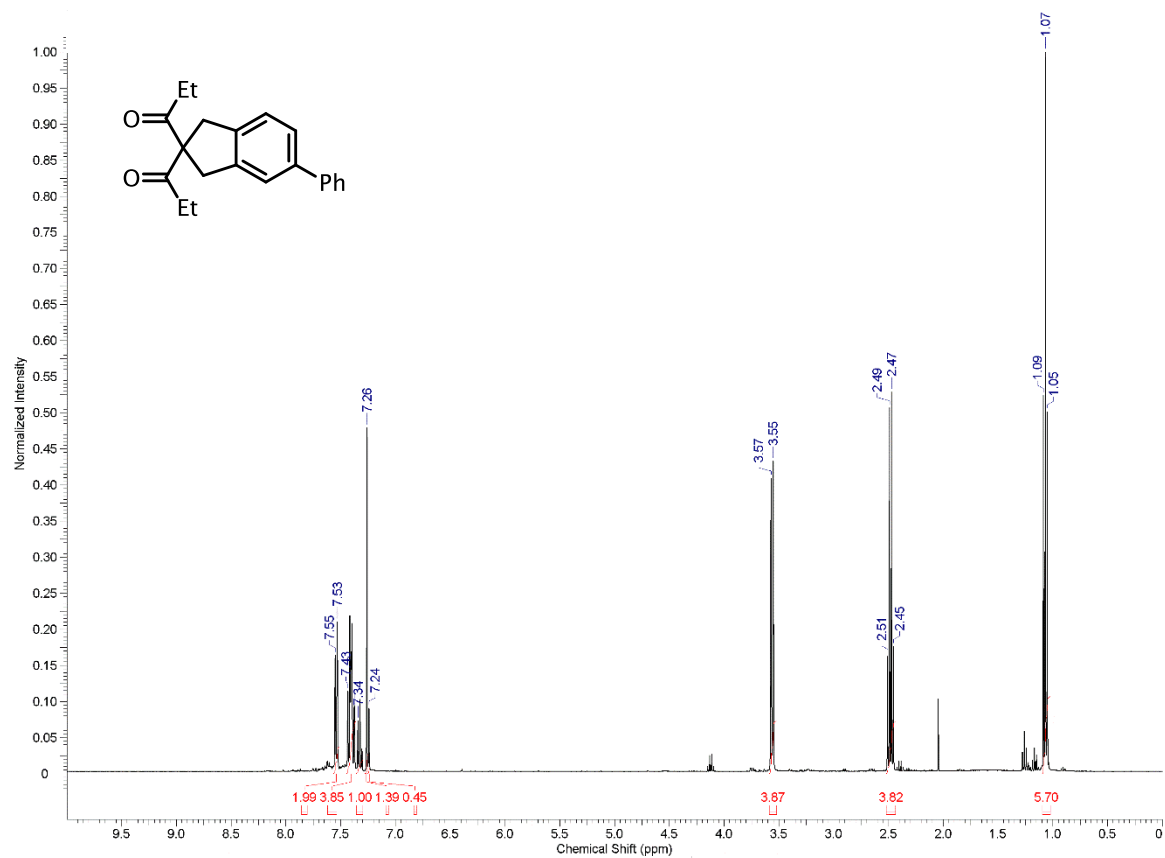
**Diethyl 2-(cyanomethyl)-2-(prop-2-yn-1-yl)malonate (82)**: This compound was prepared accord to the literature procedure.<sup>[12]</sup> A  $^1\text{H}$  NMR has been included for reference.  $^1\text{H}$  NMR (300 MHz,  $\text{CDCl}_3$ ):  $\delta$  4.26 (q,  $J = 7.0\text{ Hz}$ , 4H), 3.12 (s, 2H), 3.00 (m, 2H), 2.10 (t,  $J = 2.35\text{ Hz}$ , 1H), 1.28 (t,  $J = 7.0\text{ Hz}$ , 6H) ppm.

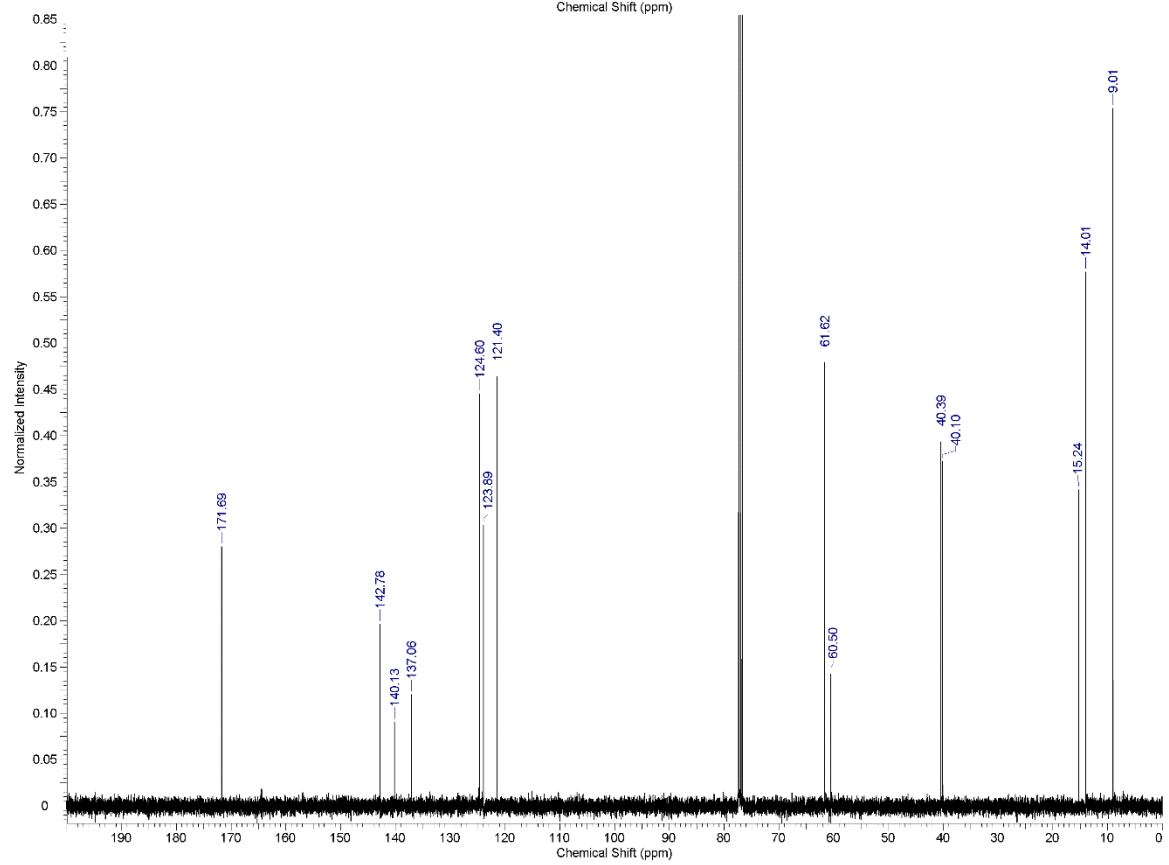
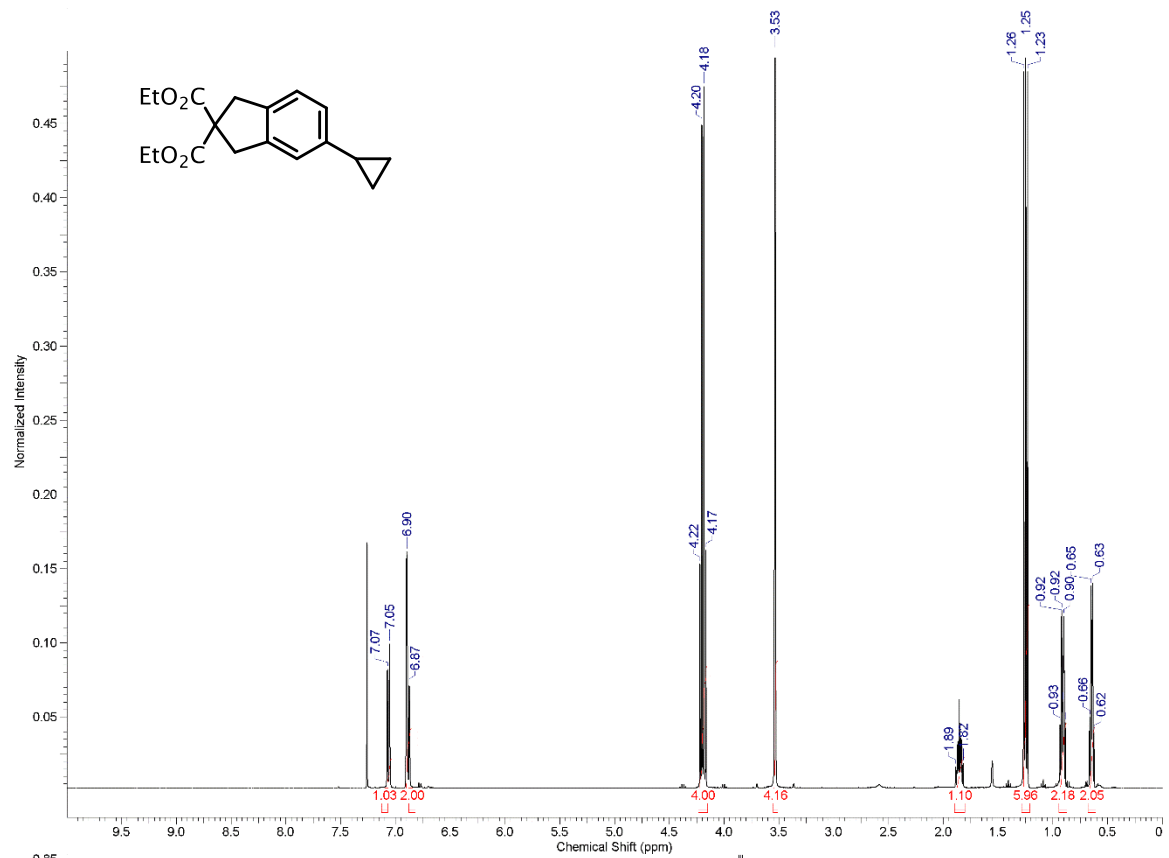
## 1.7 --- Characterization Spectra for Arene Products

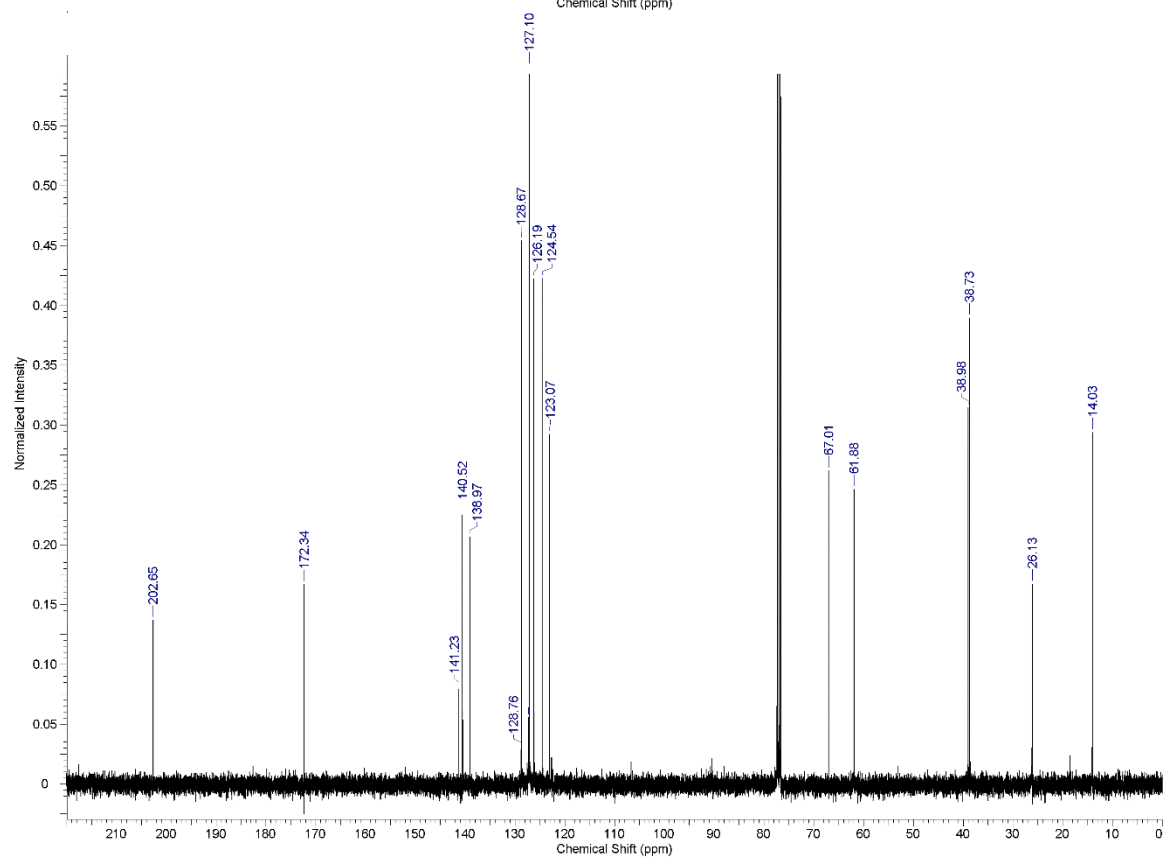
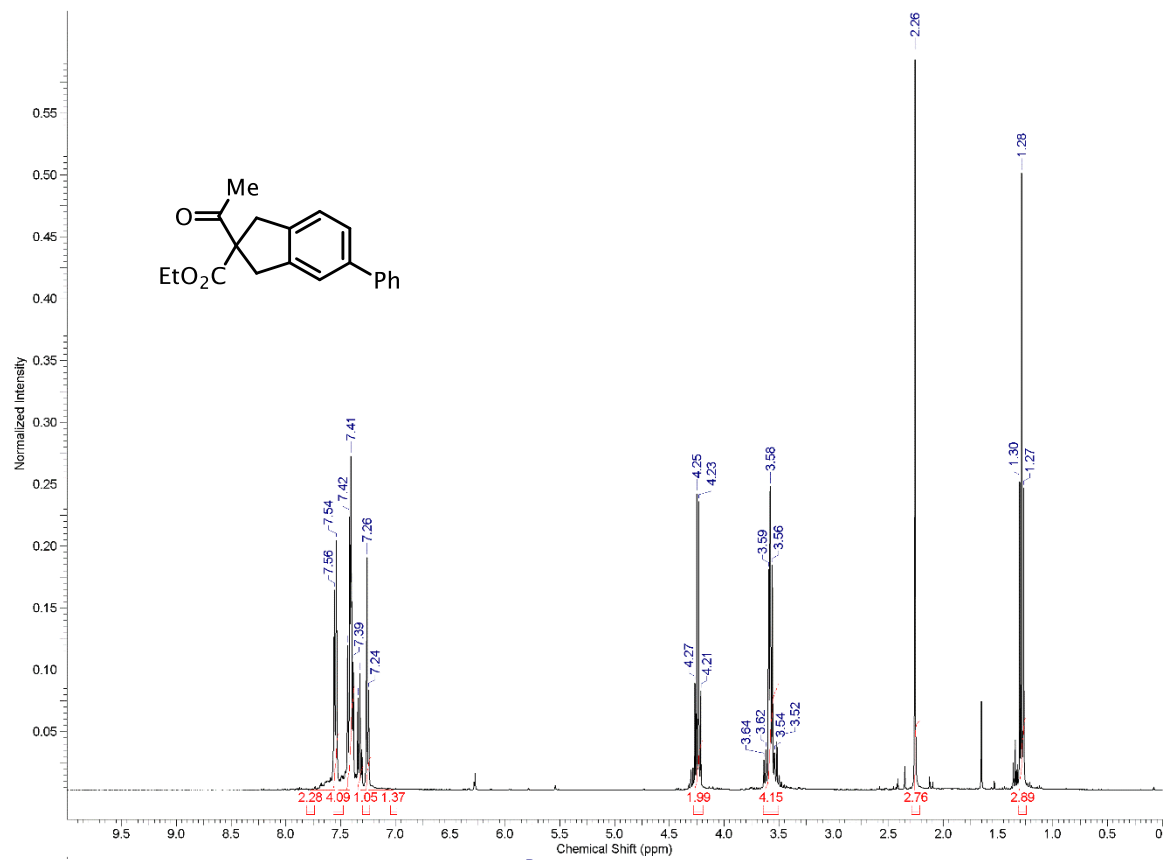


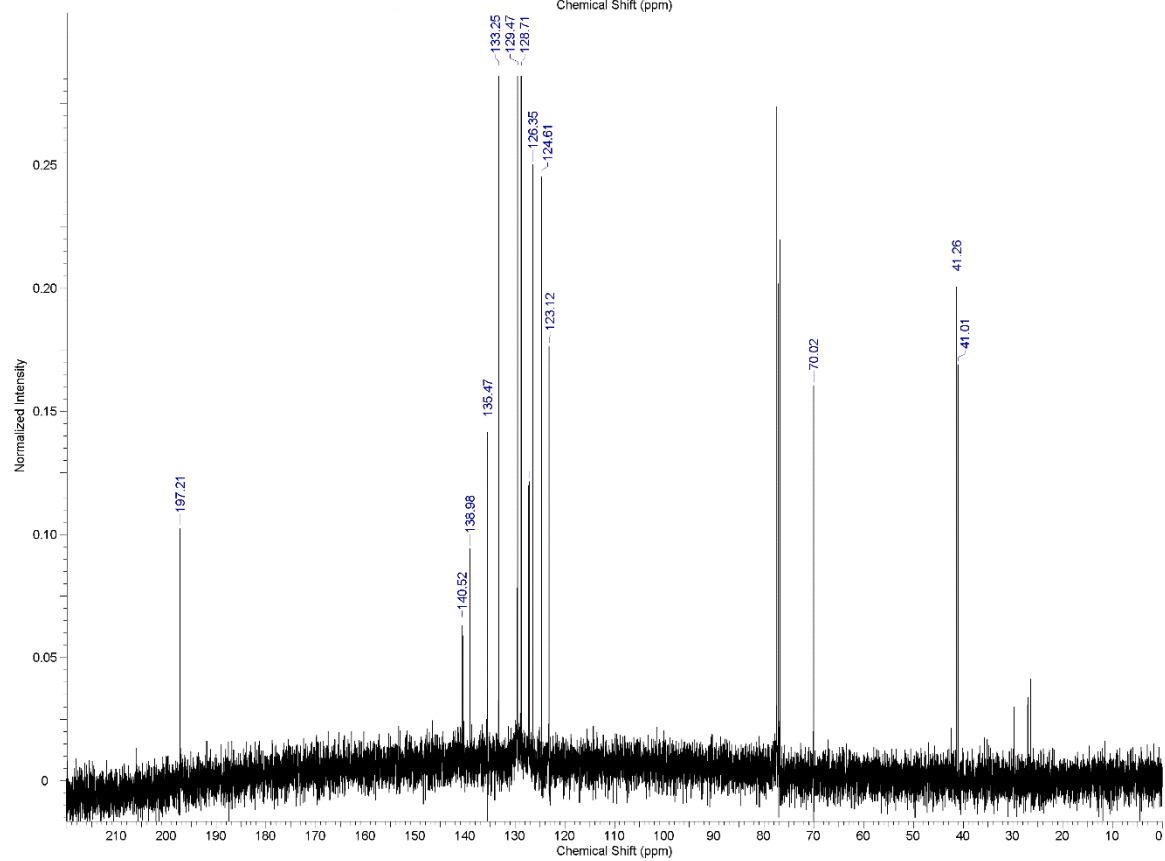
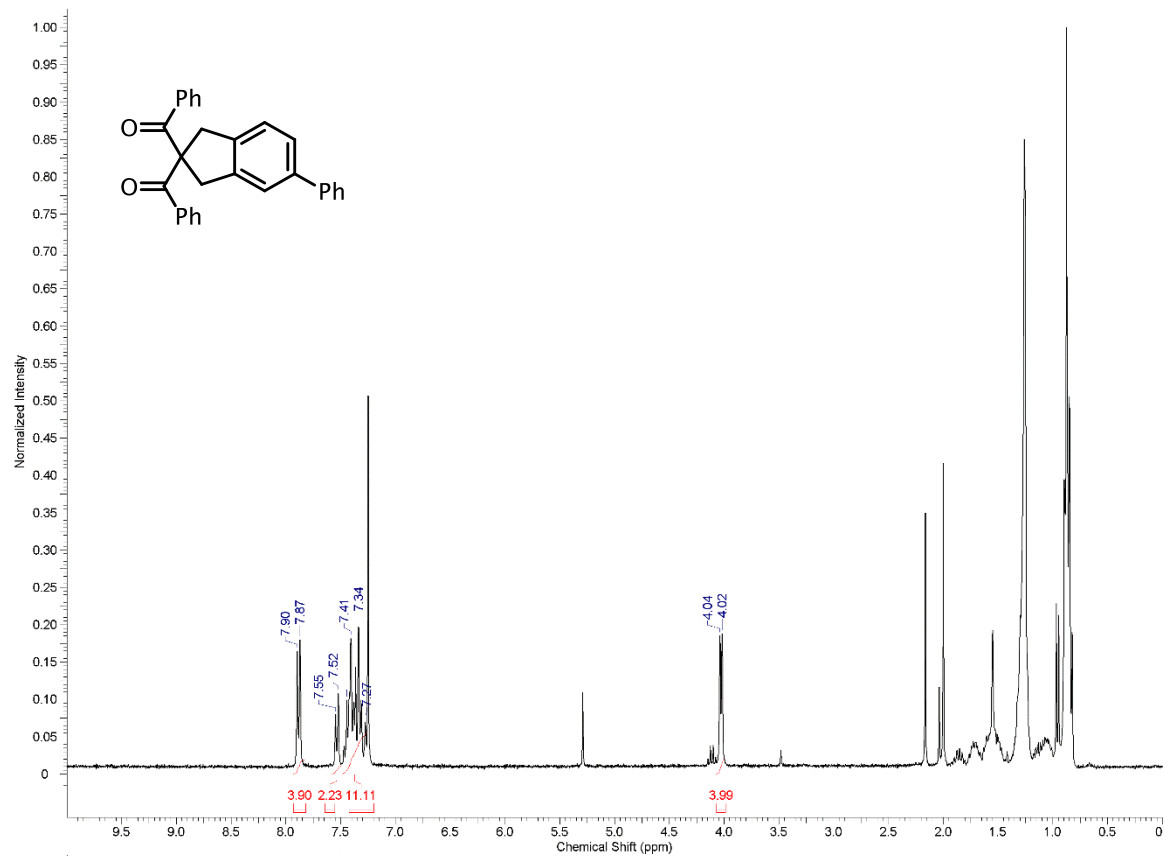


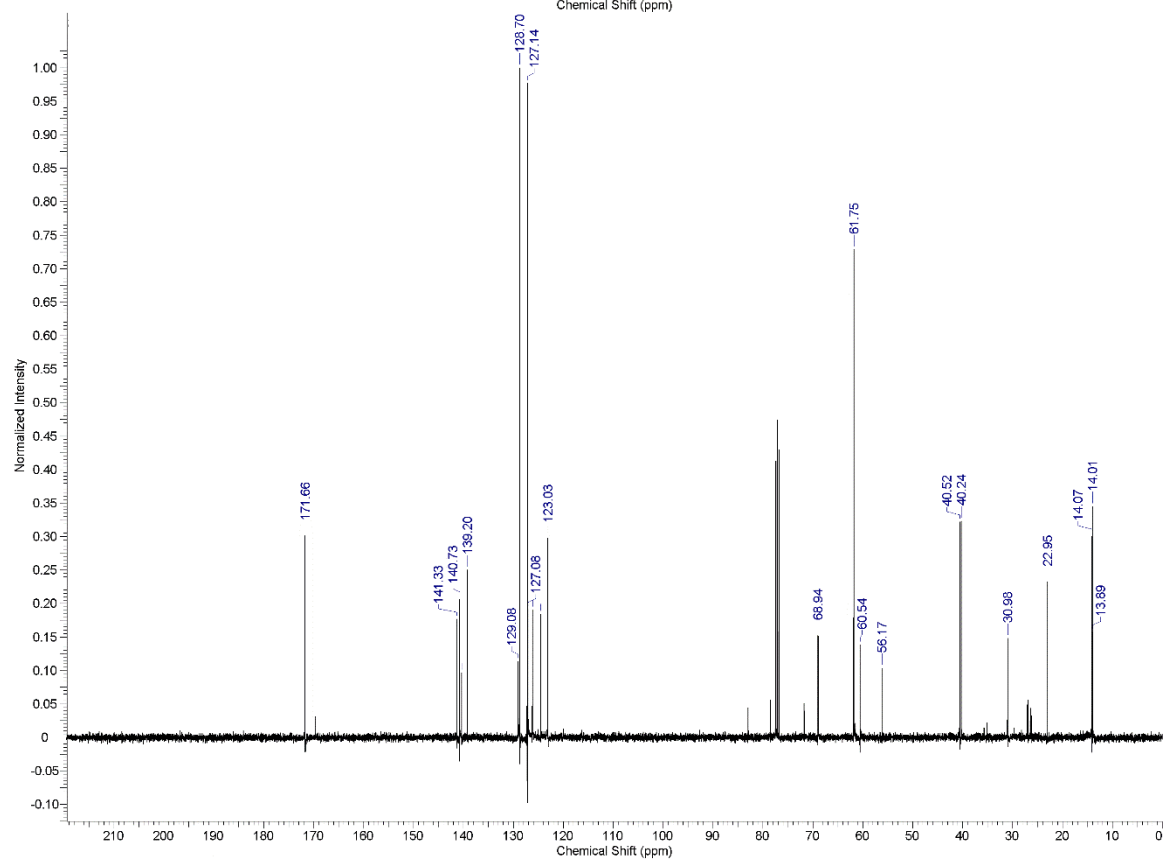
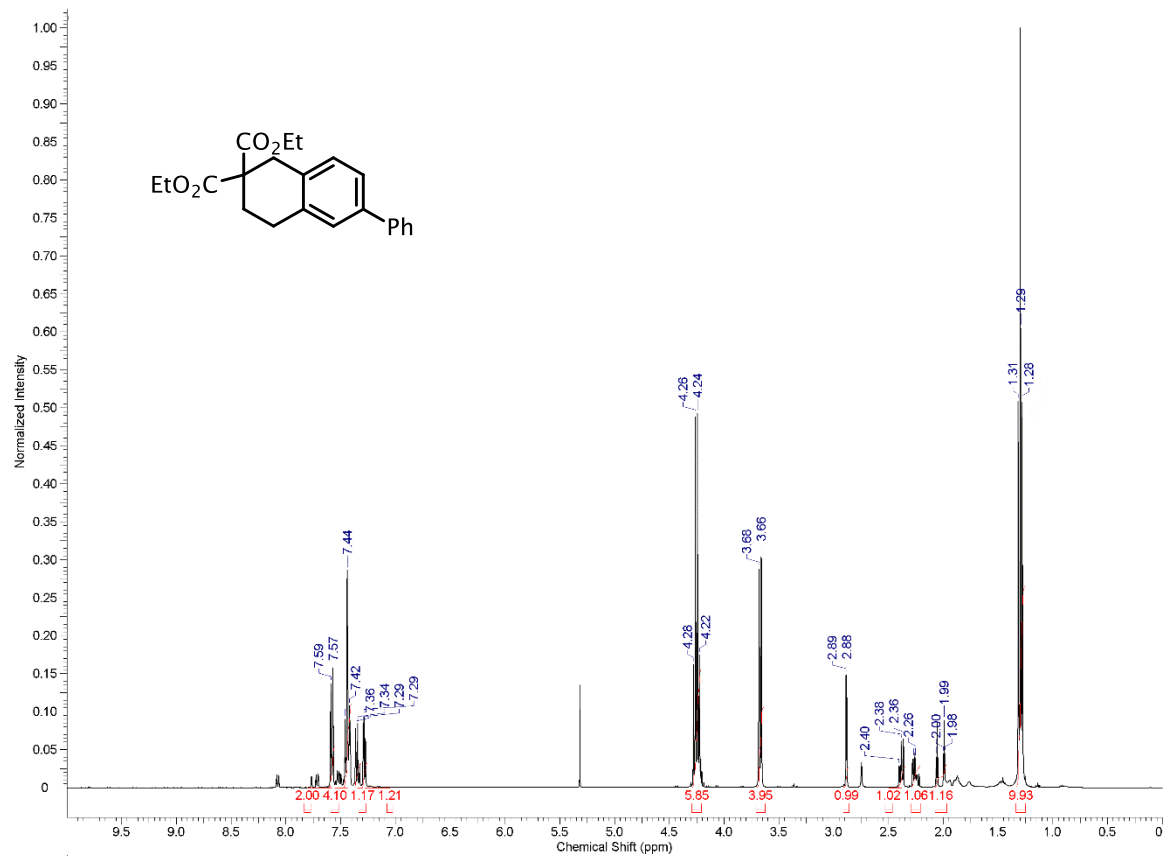


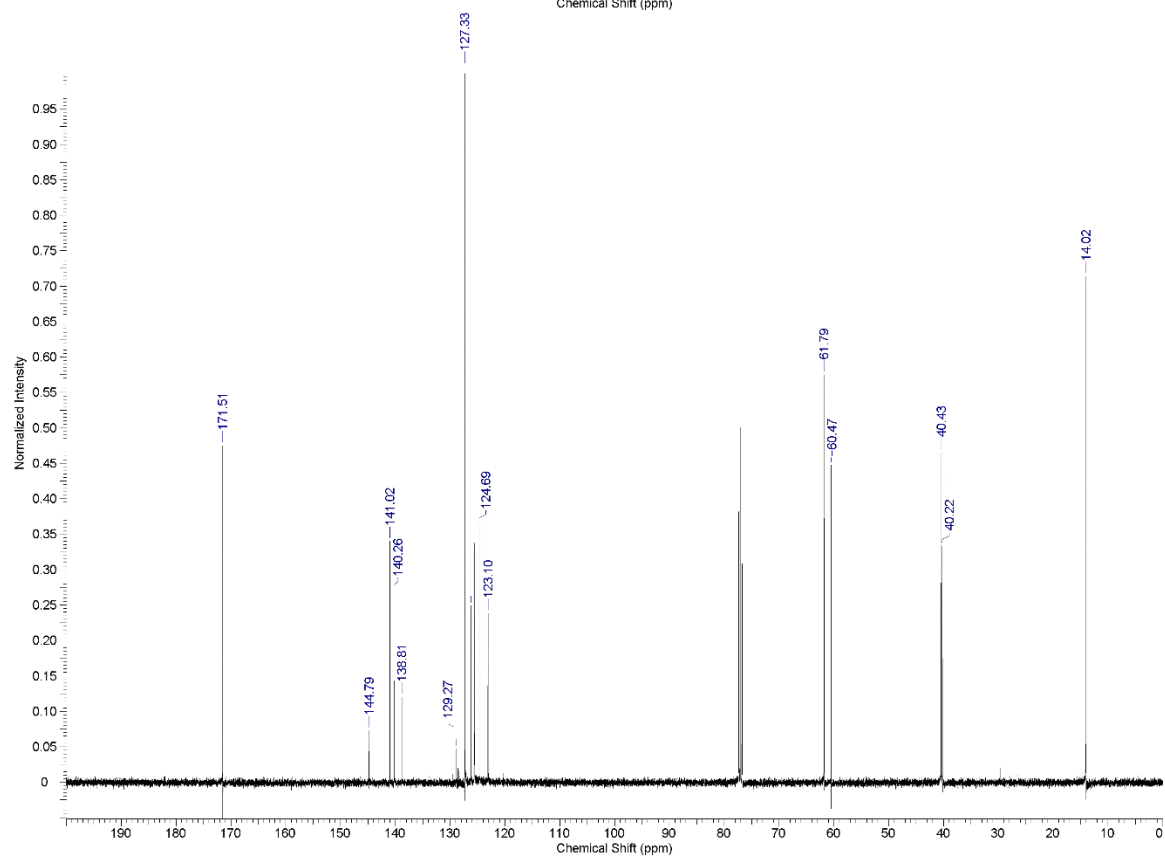
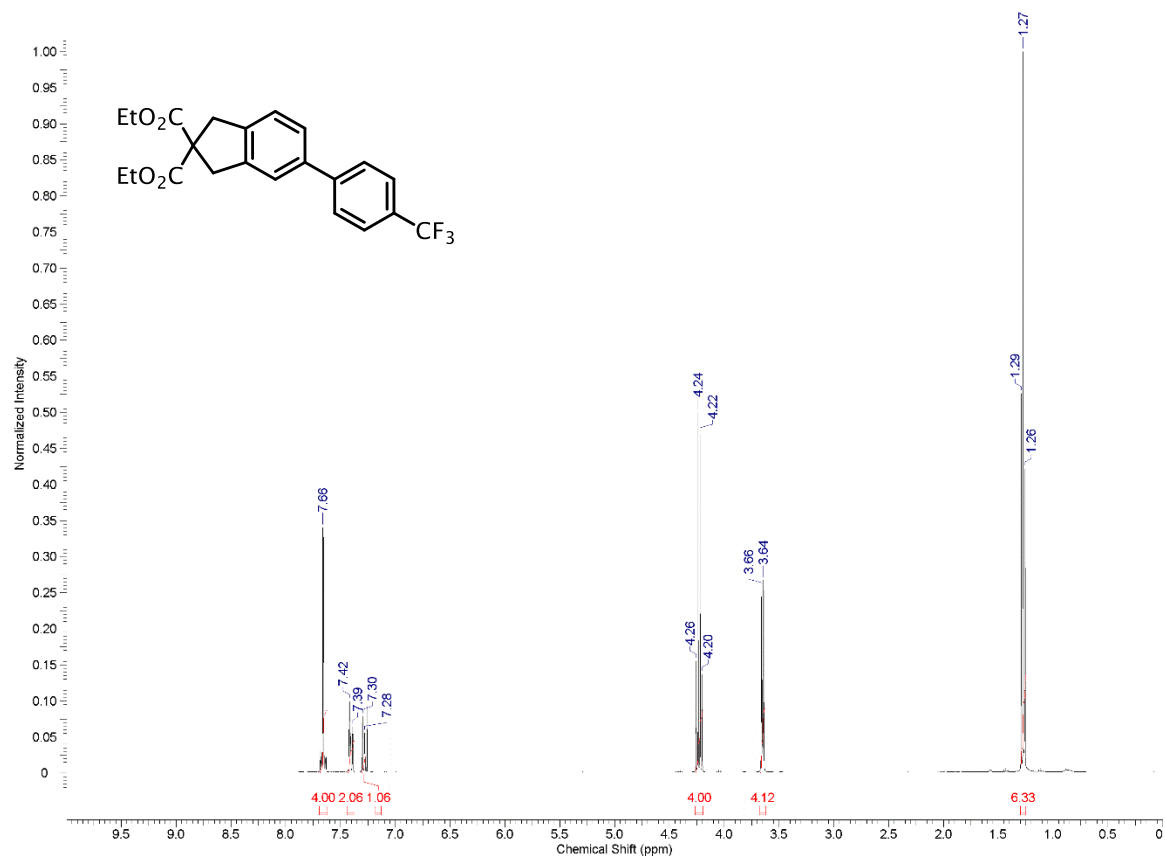


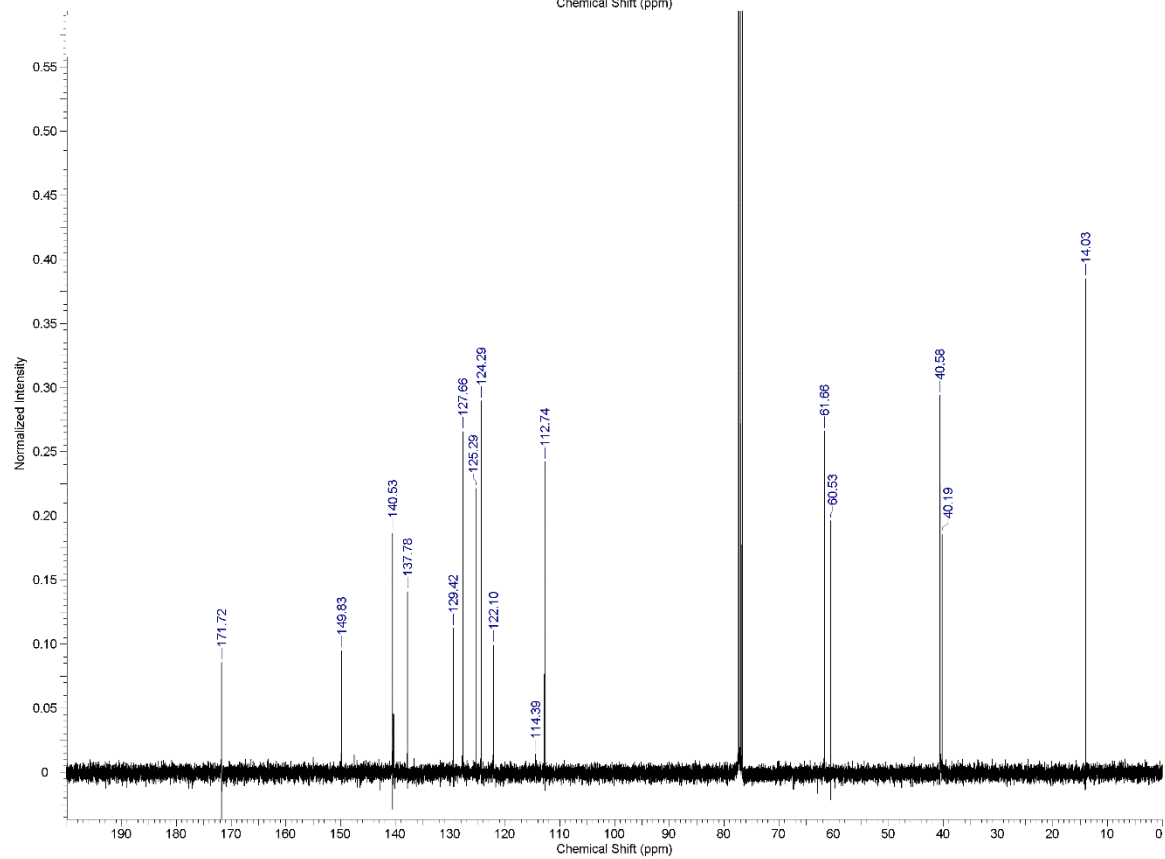
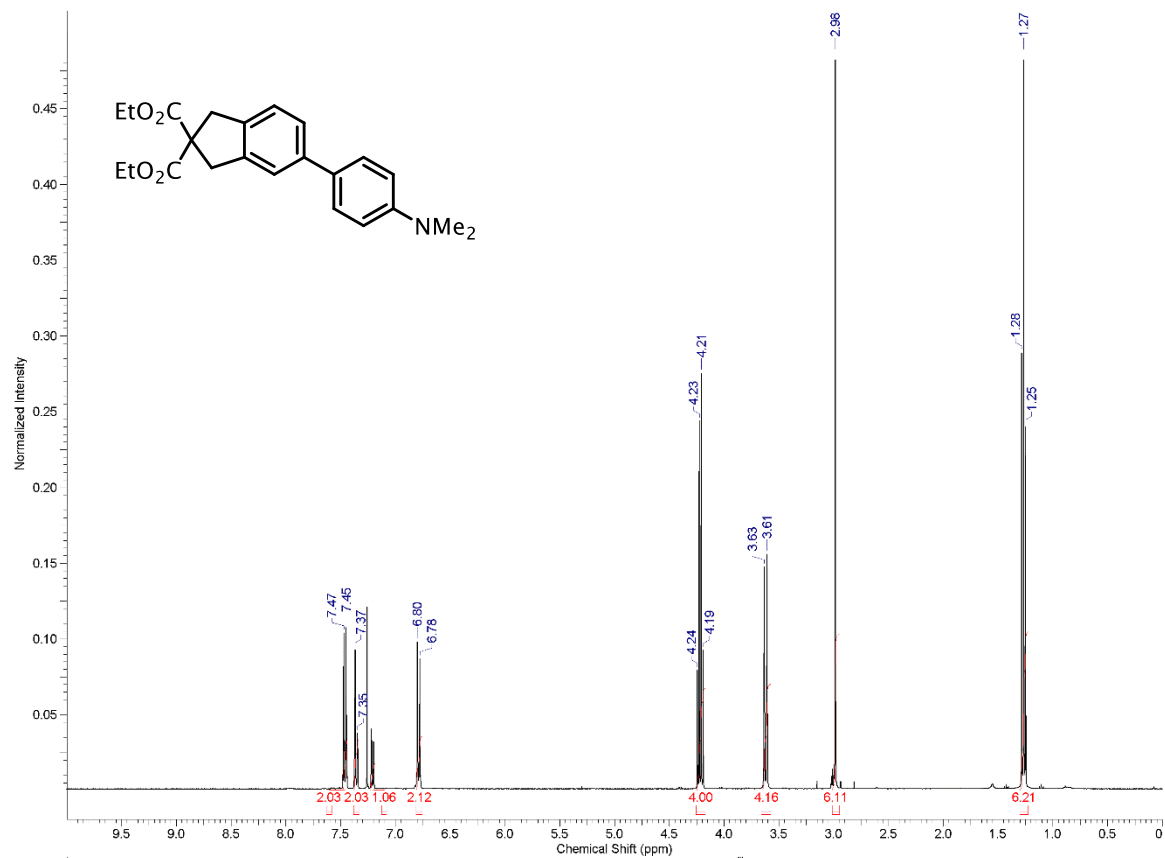


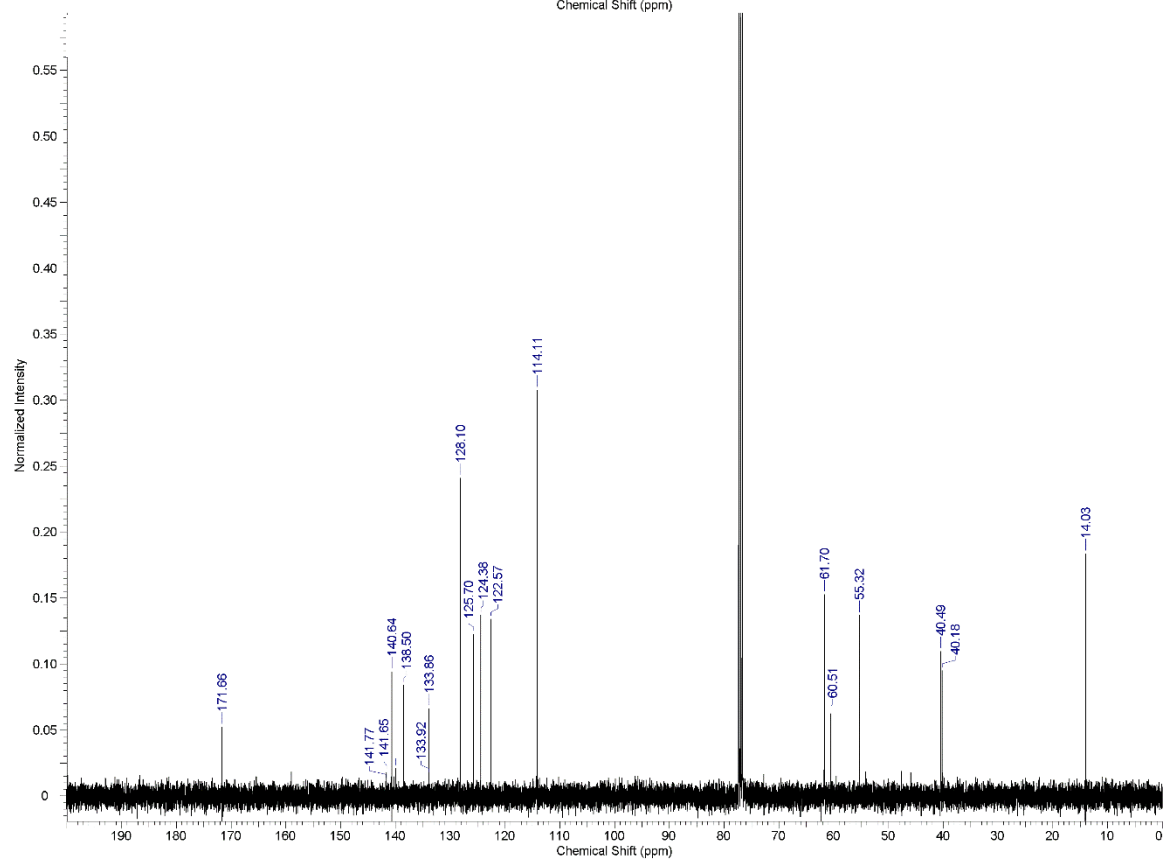
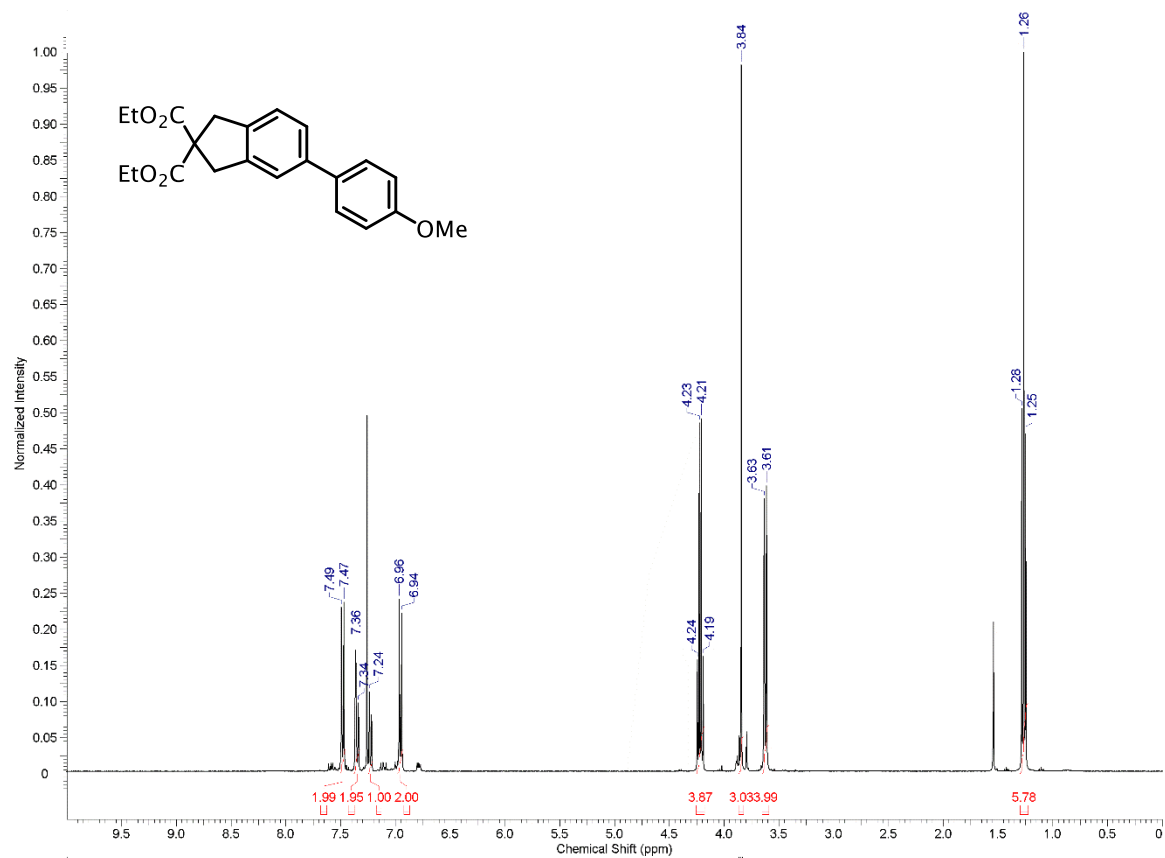




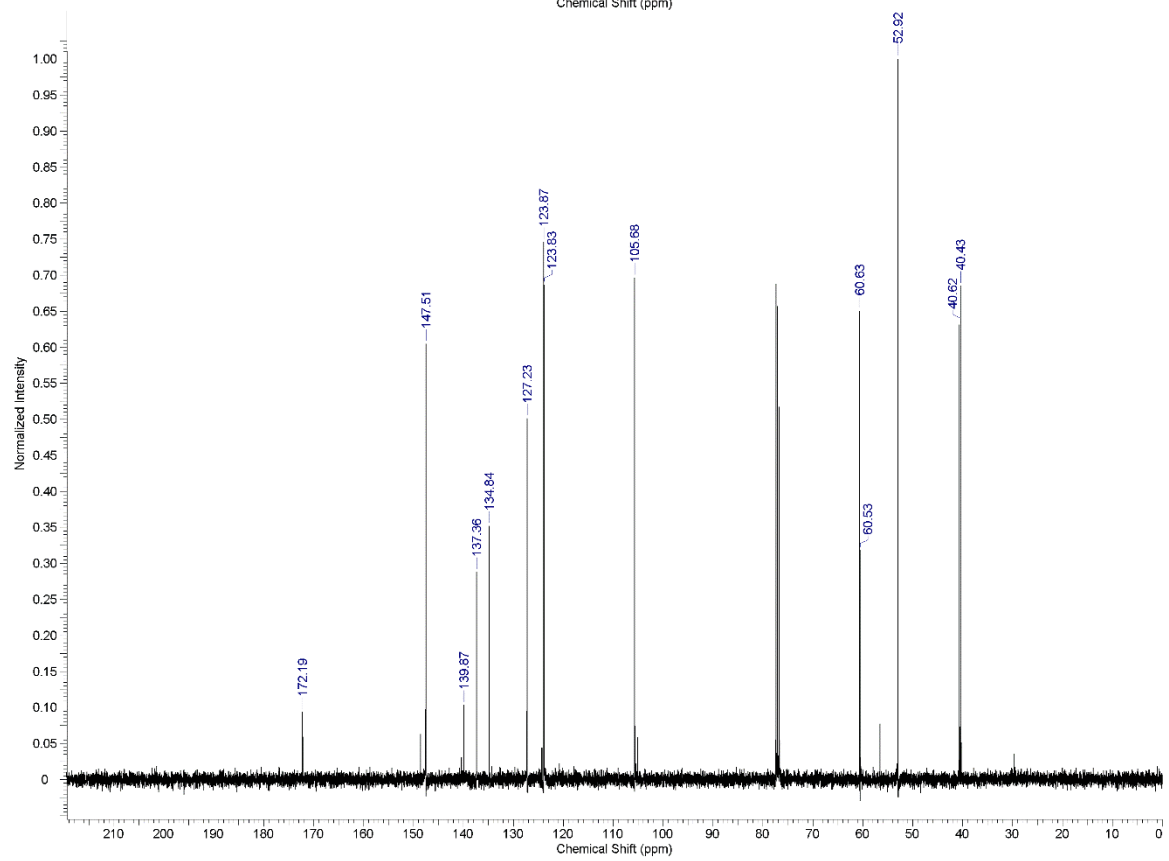
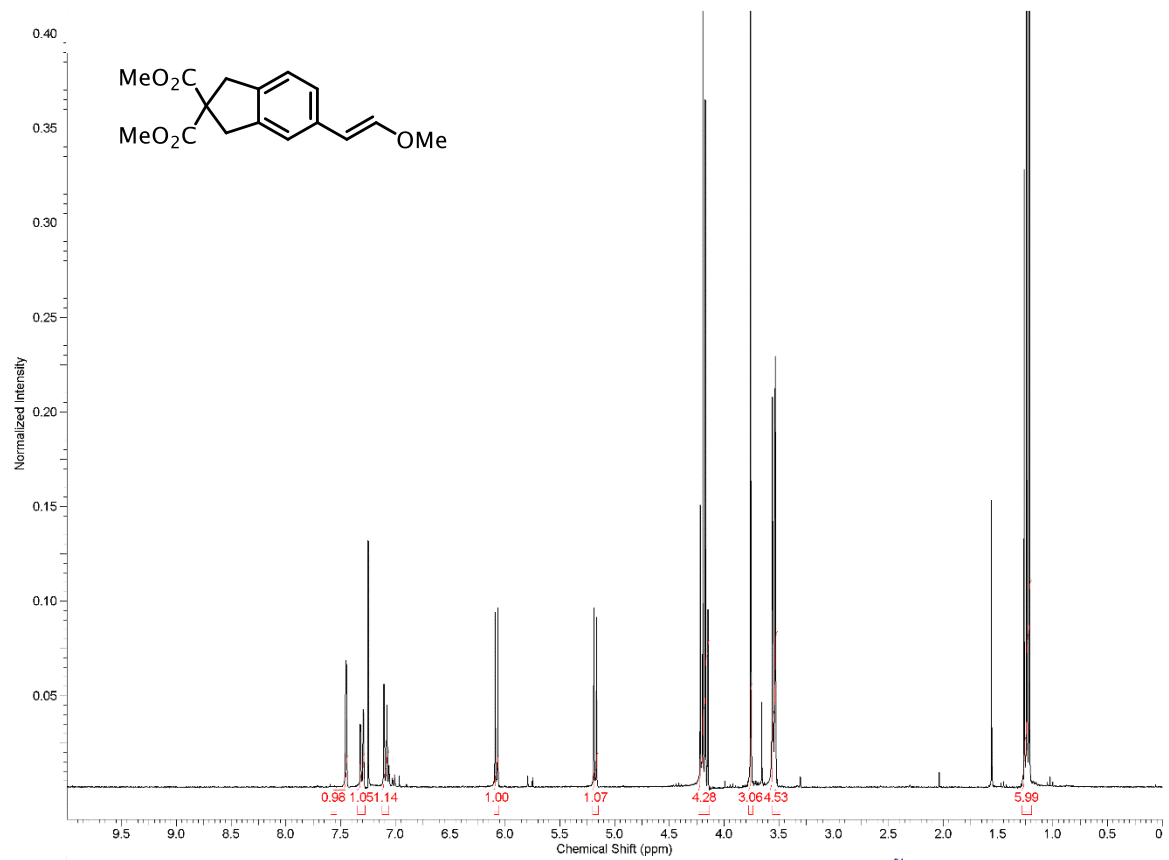


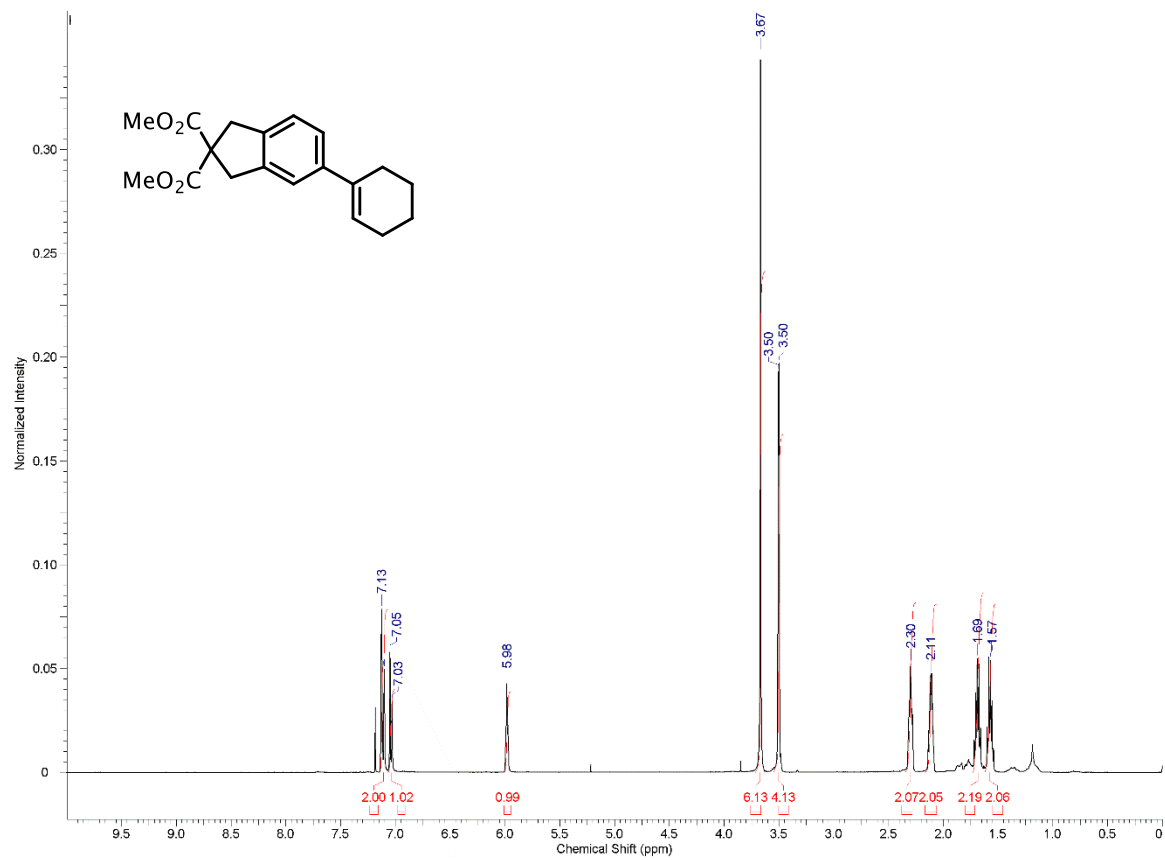


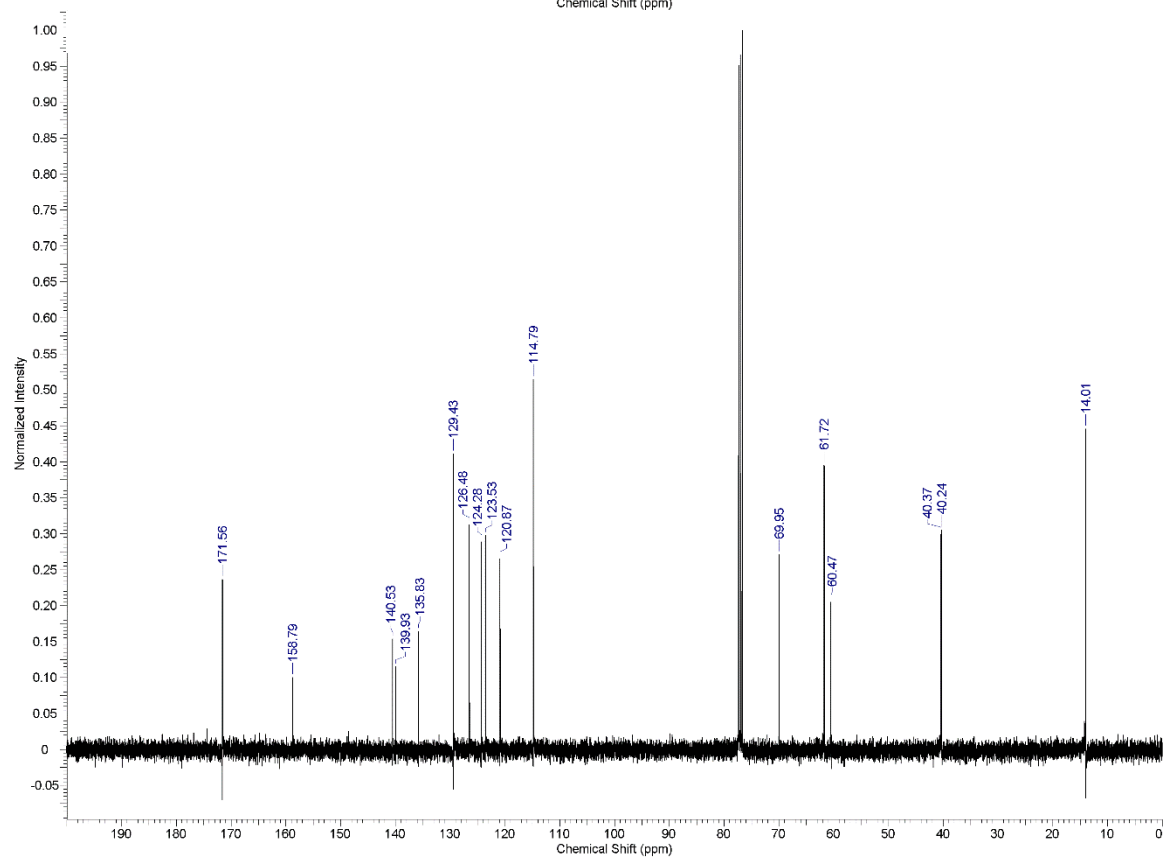
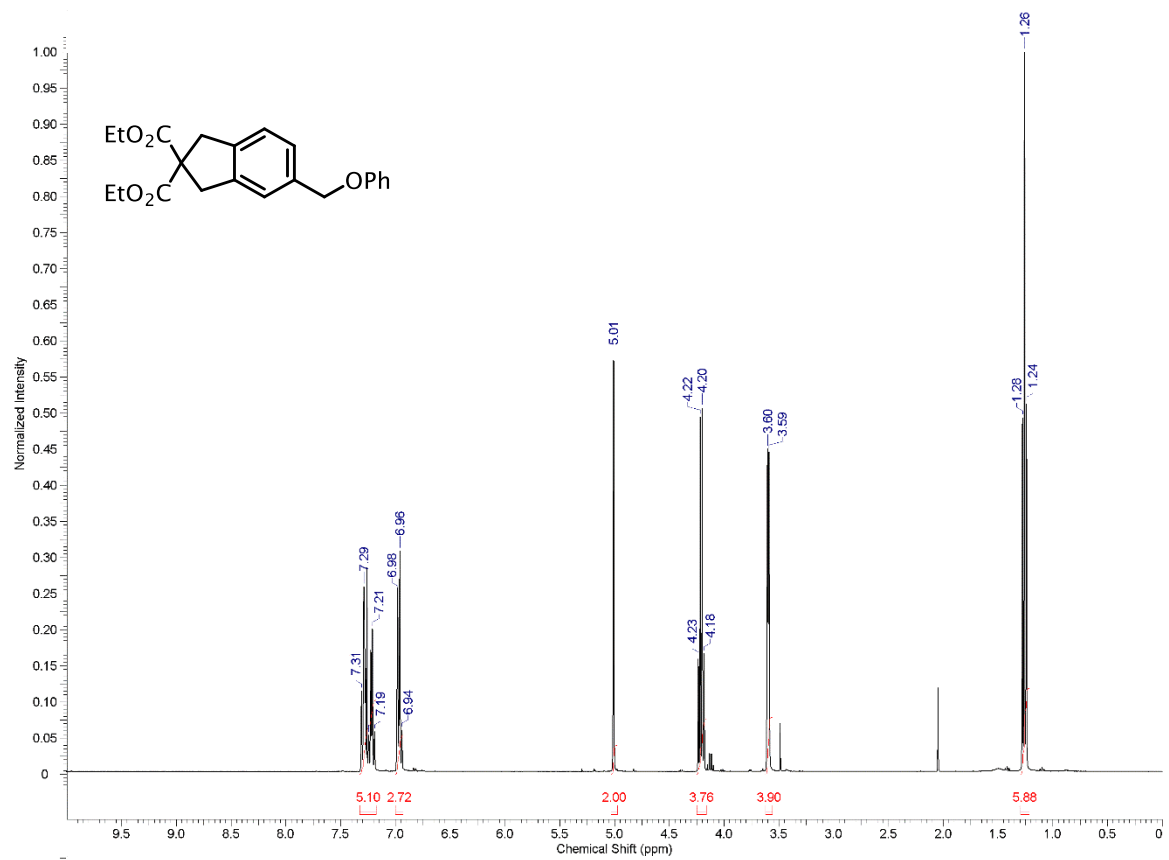


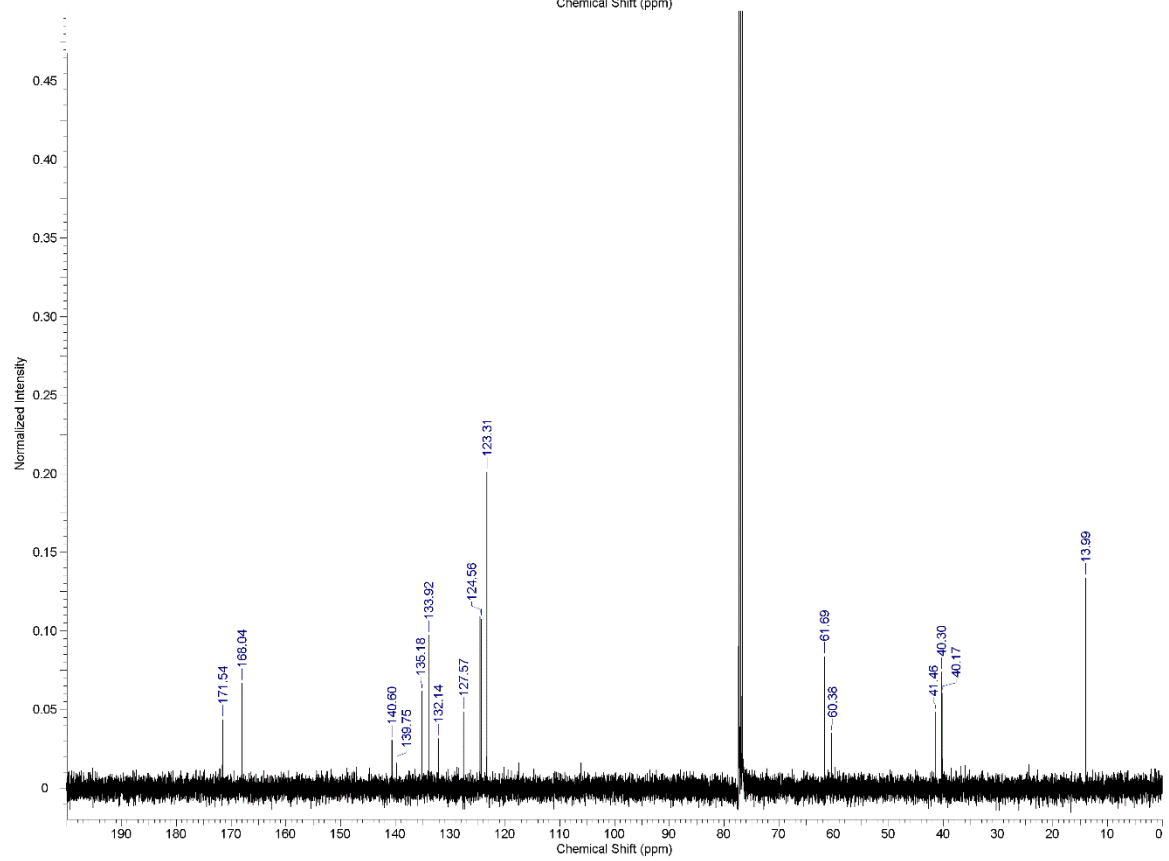
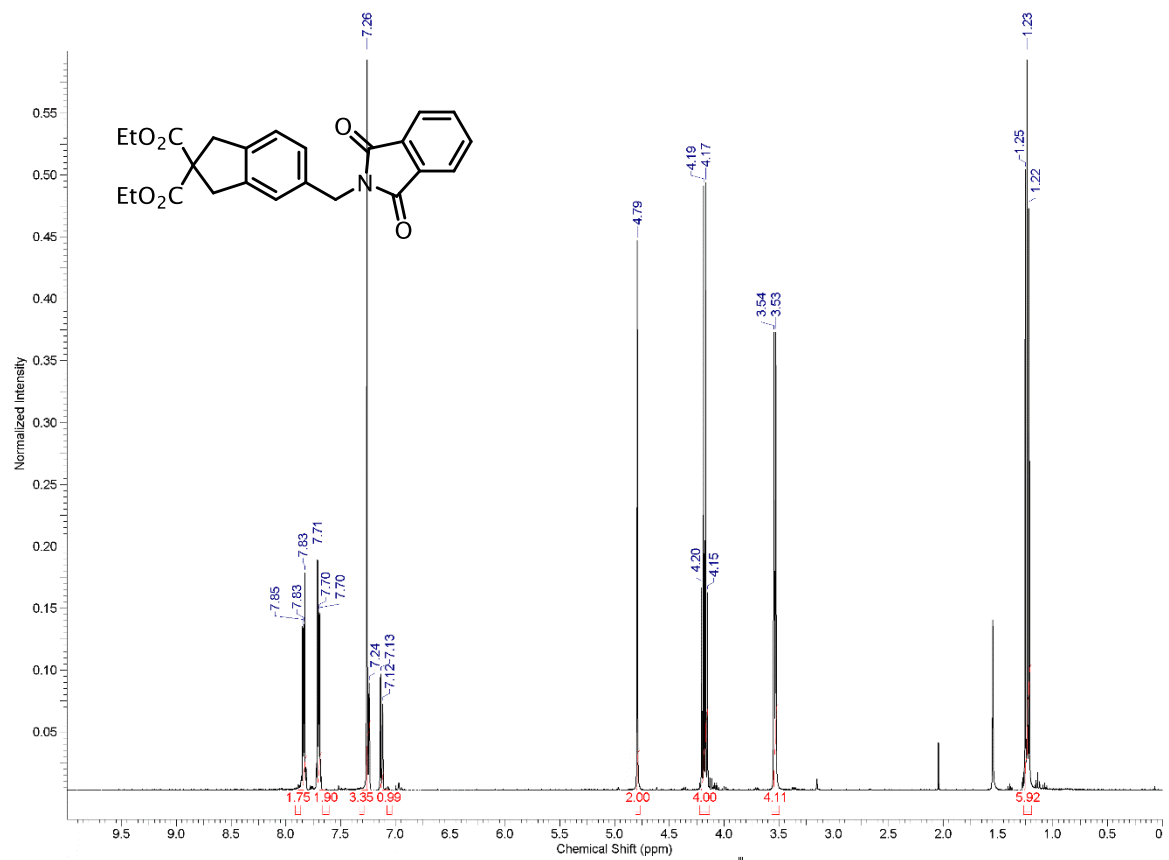


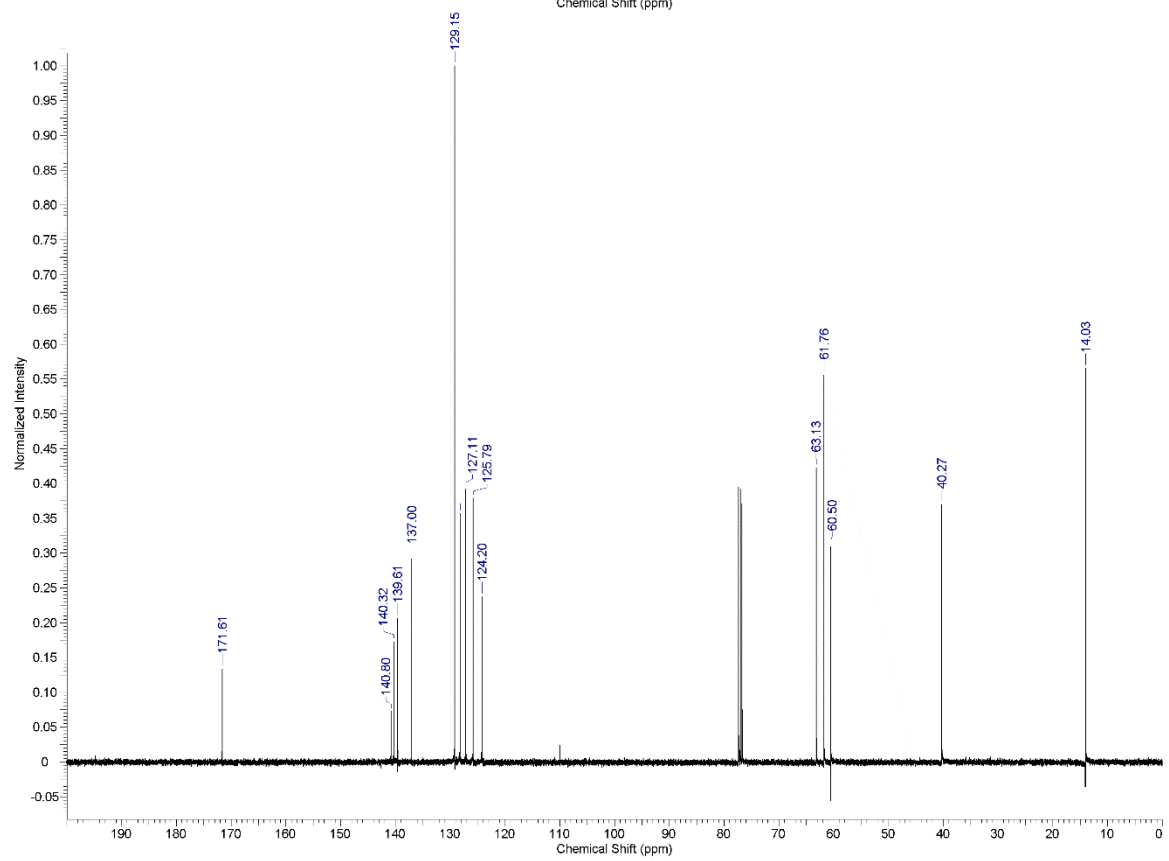
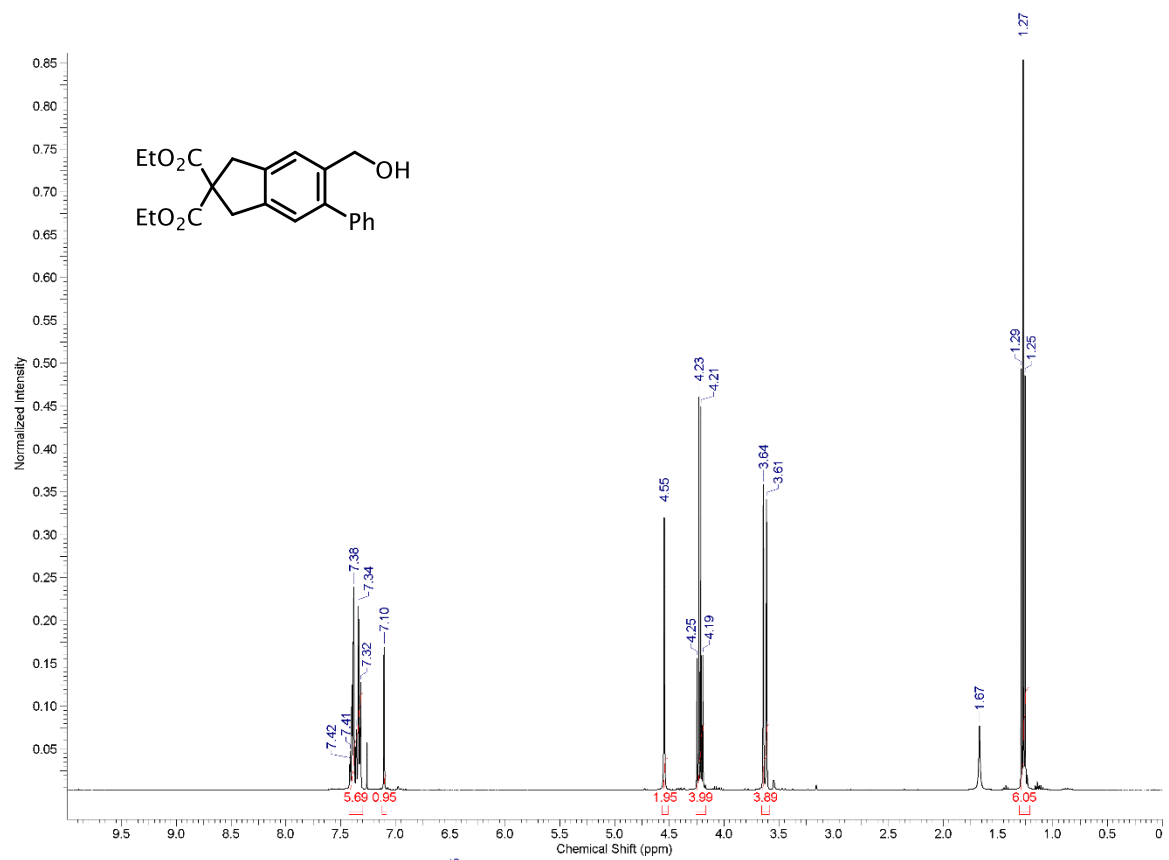


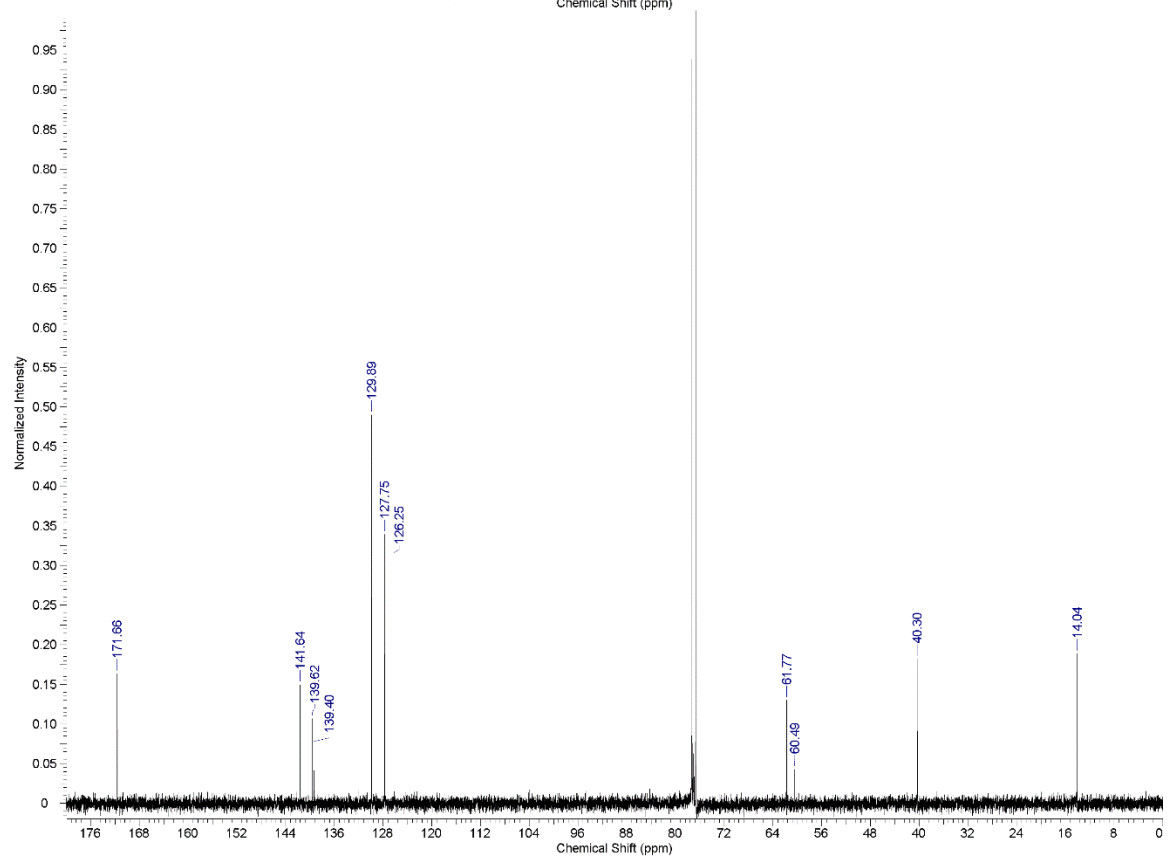
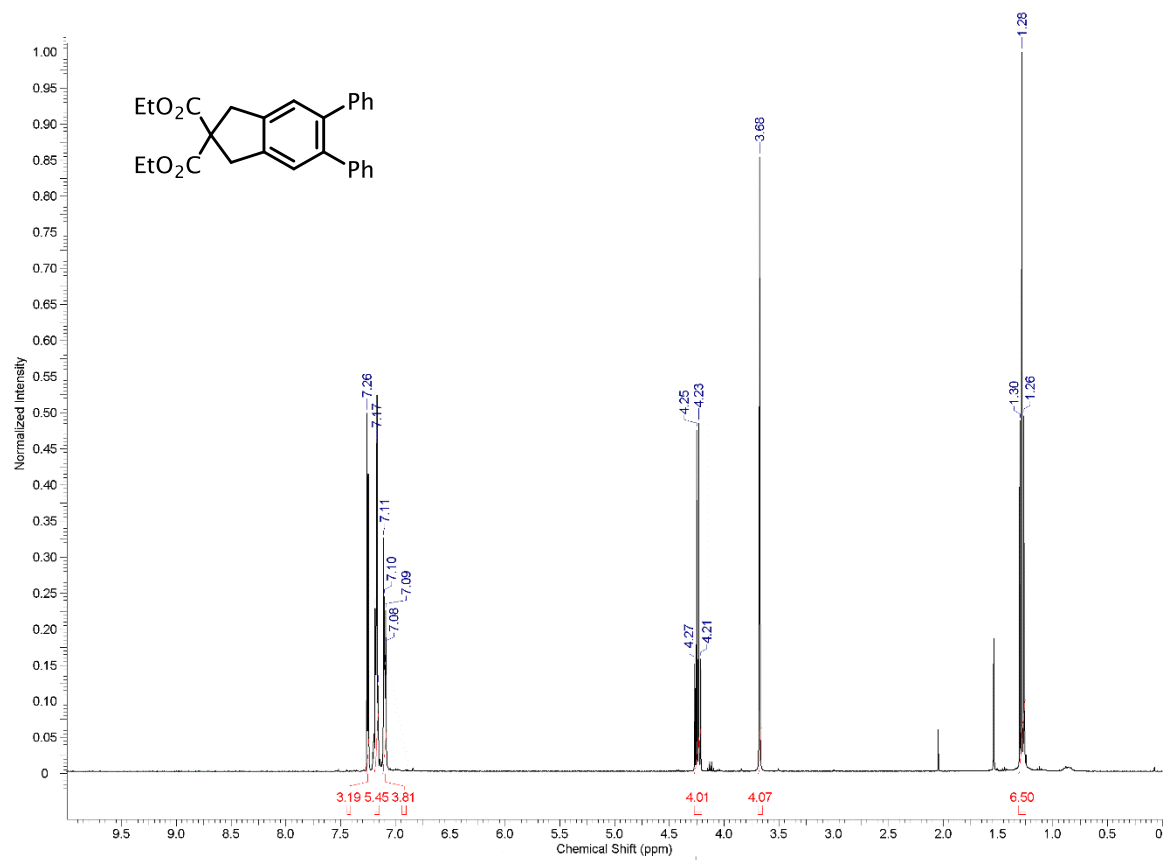


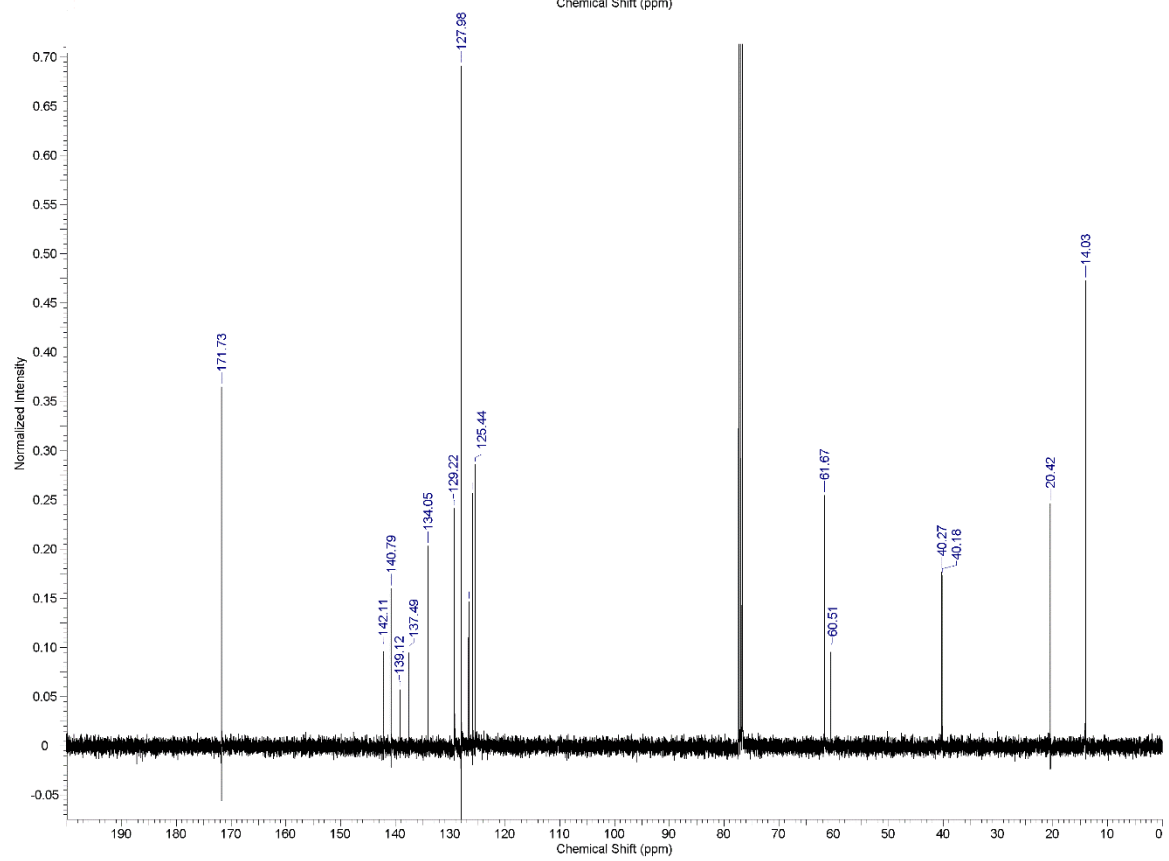
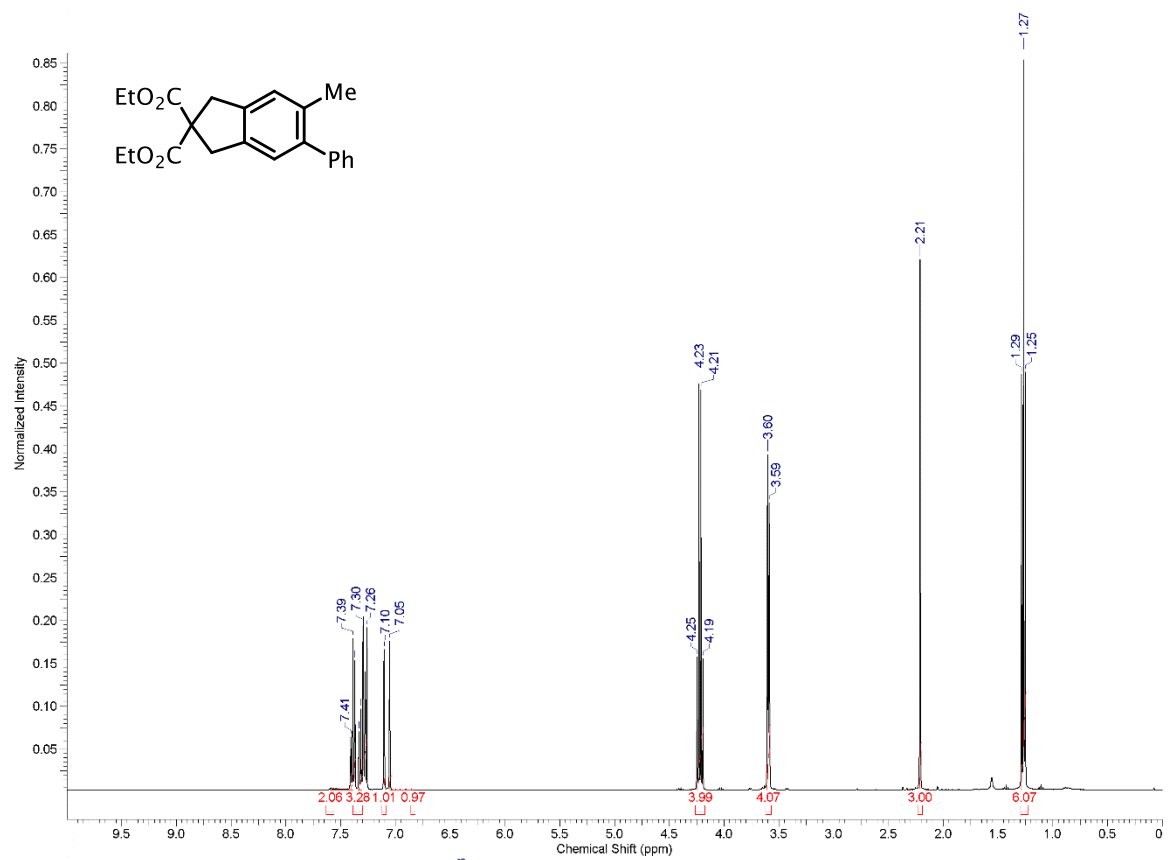


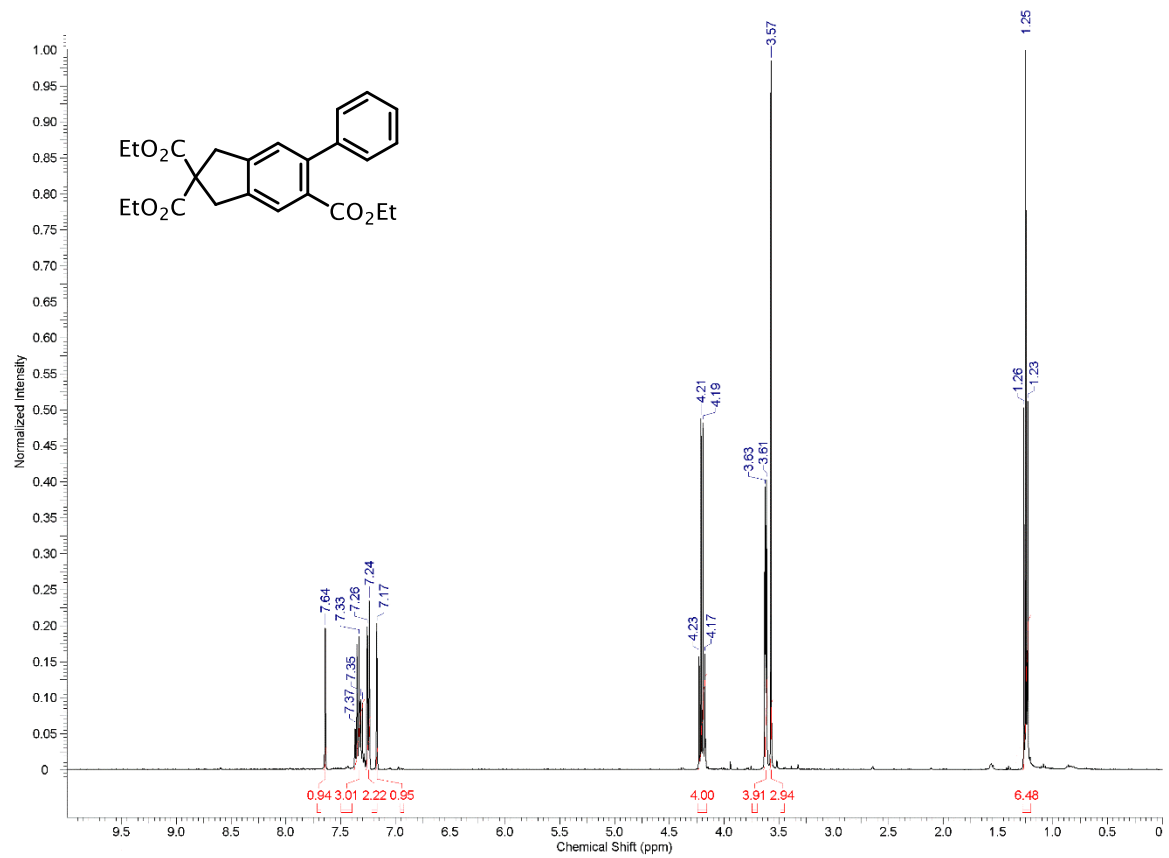




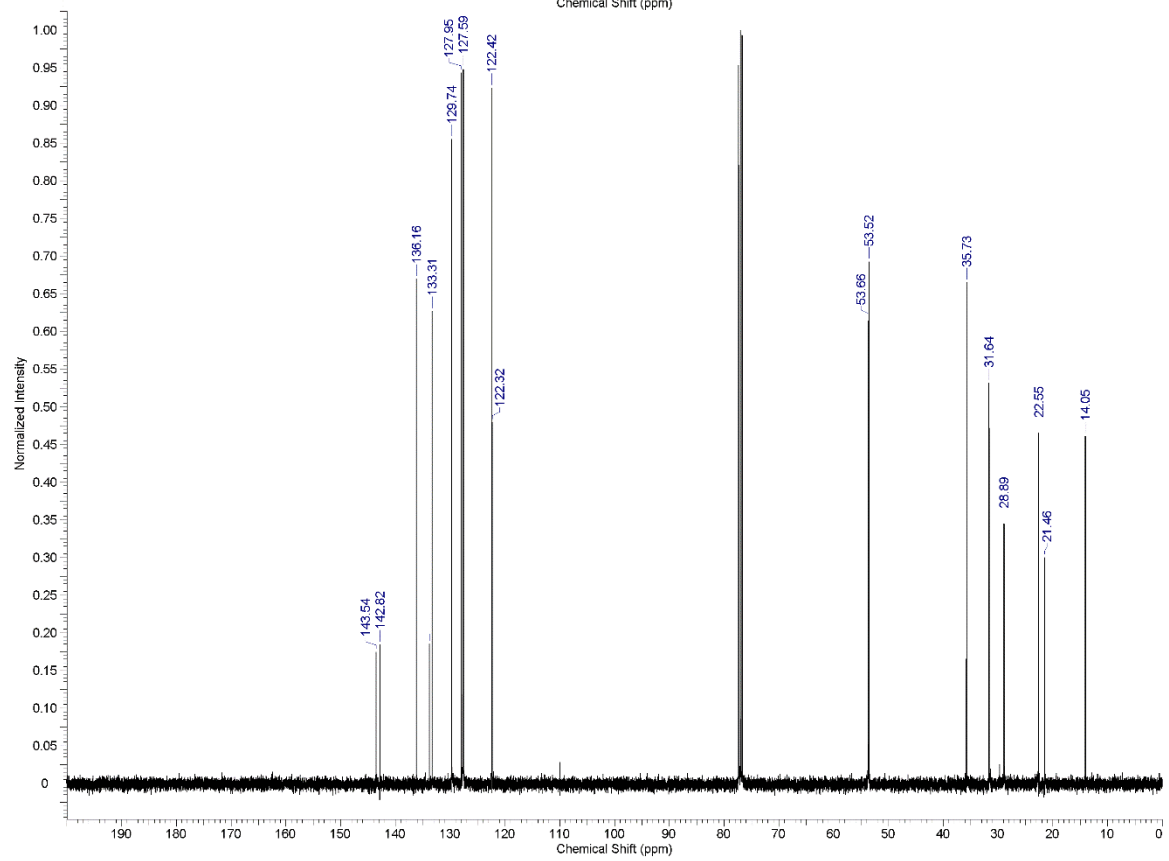
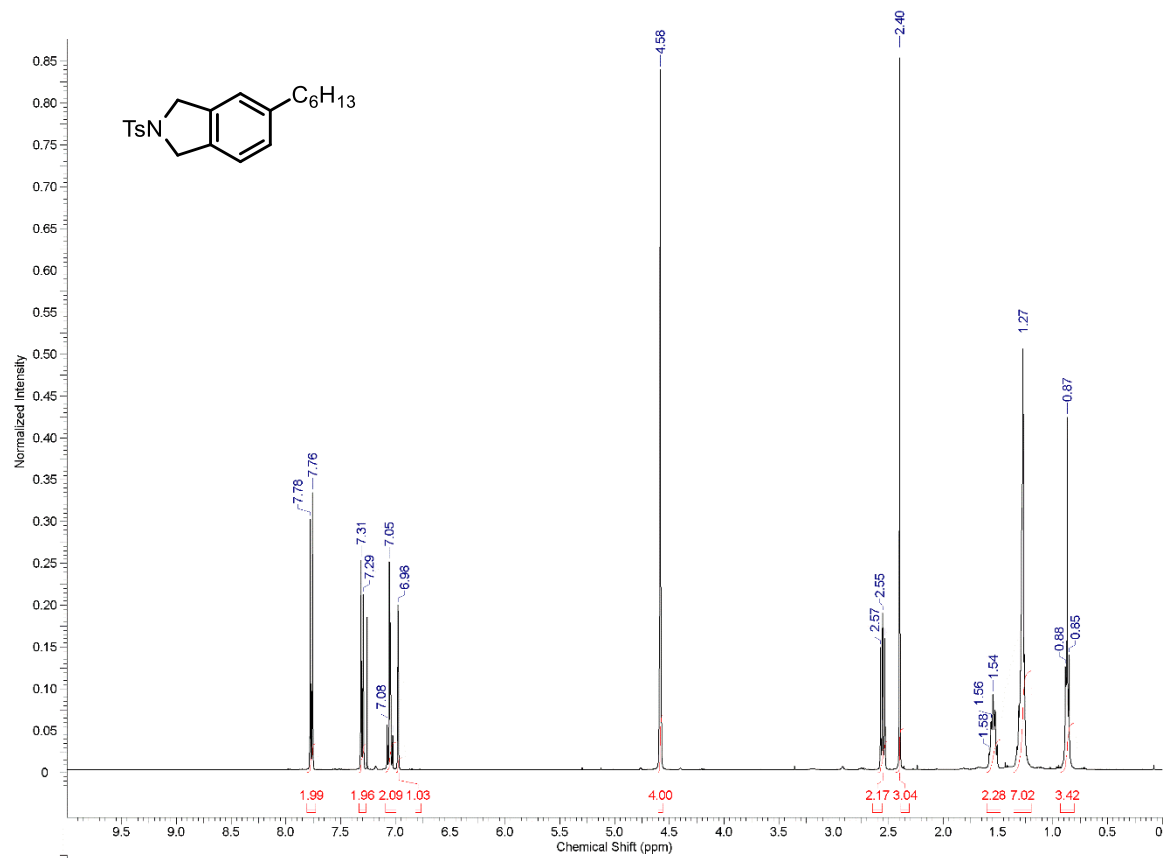


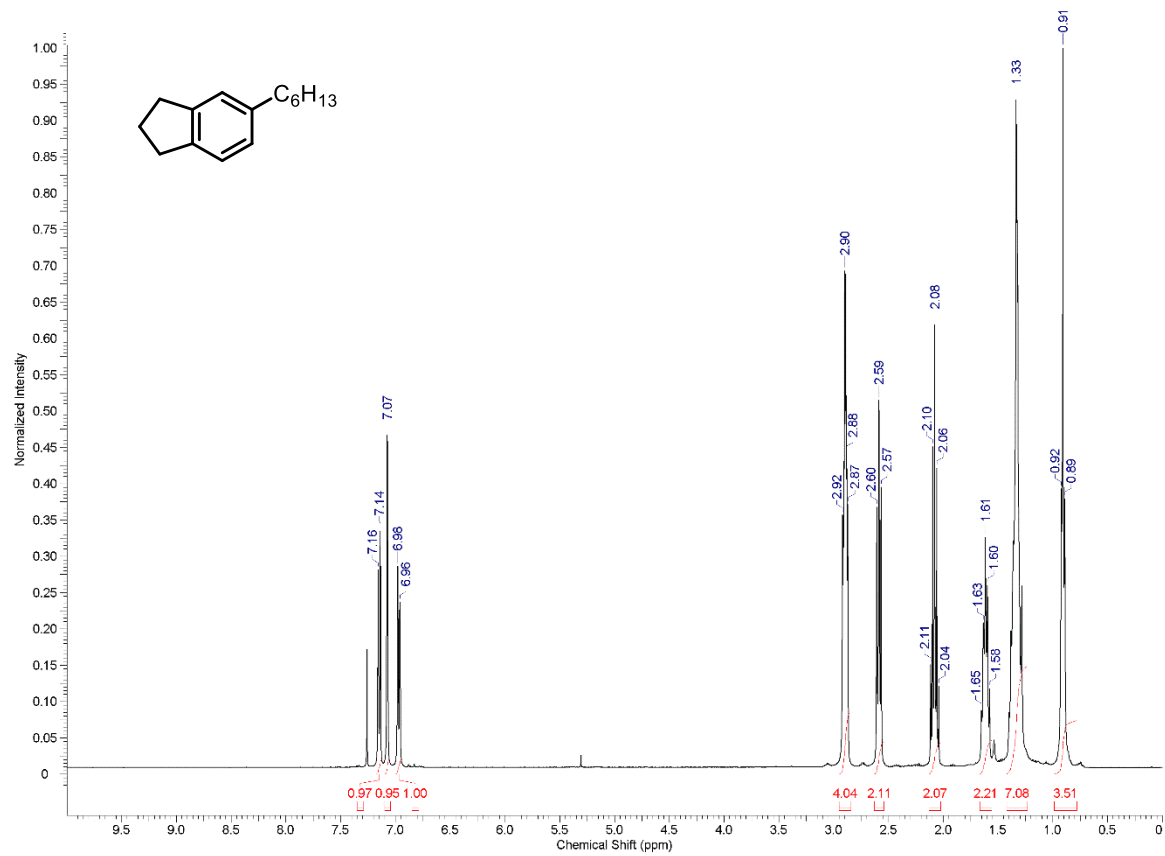


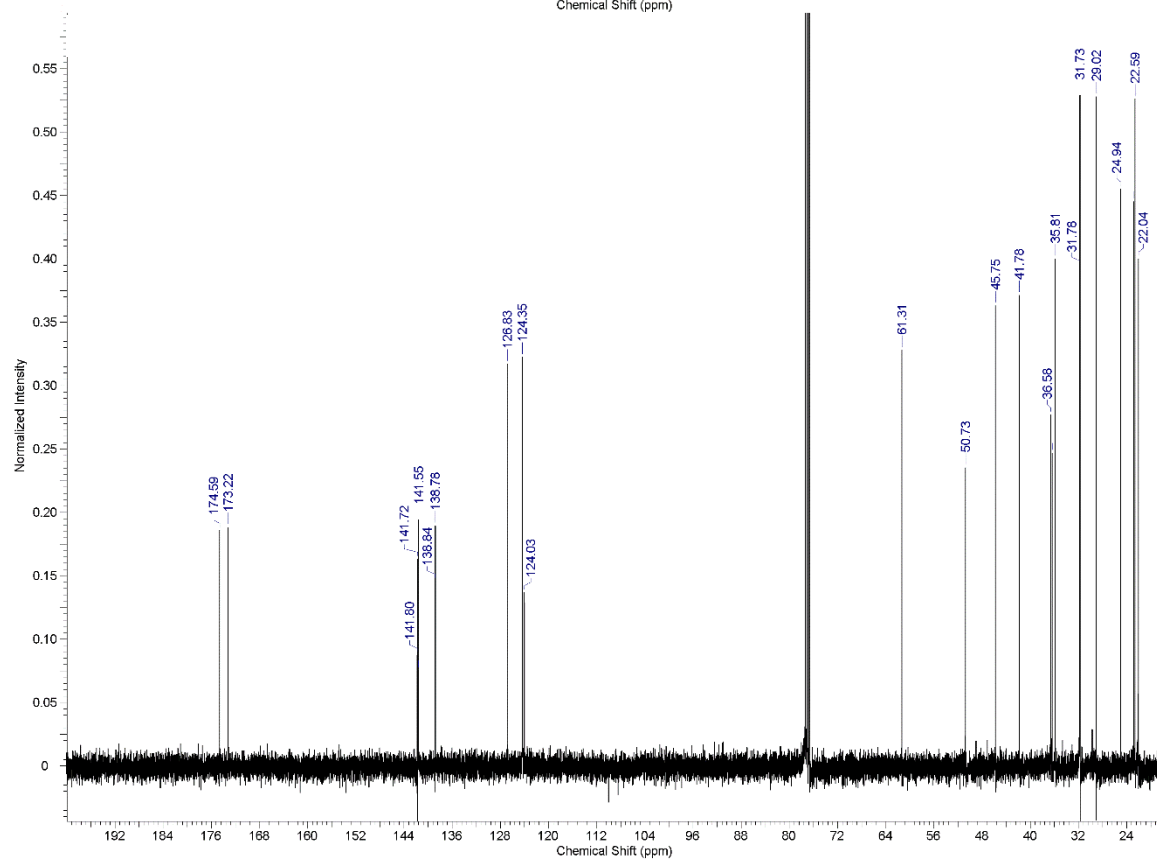
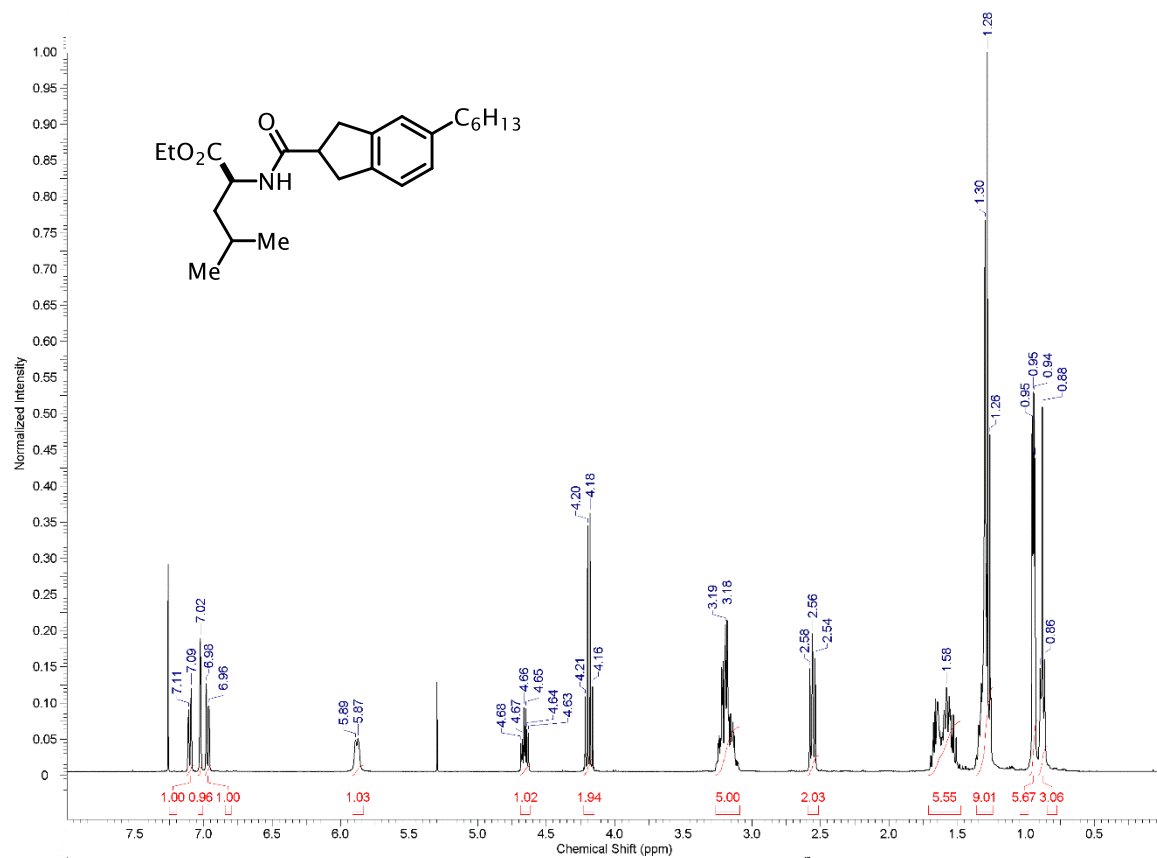


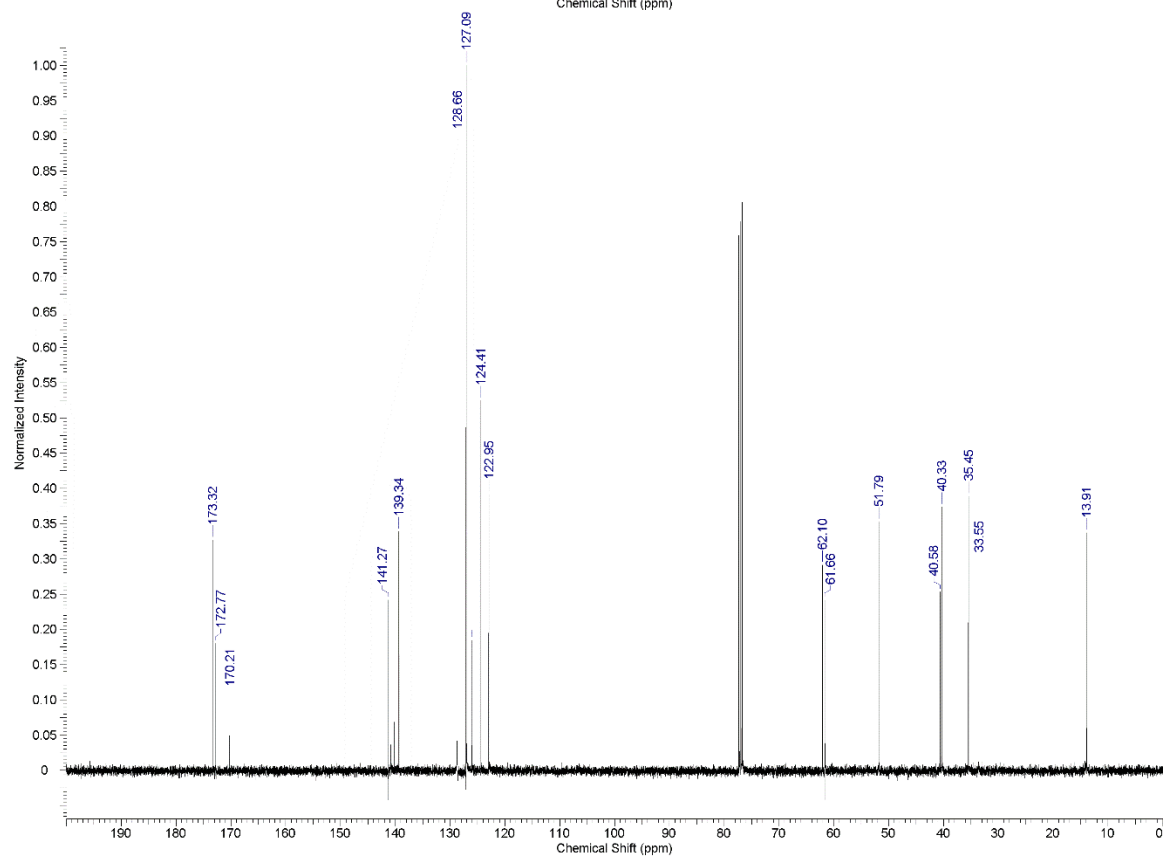
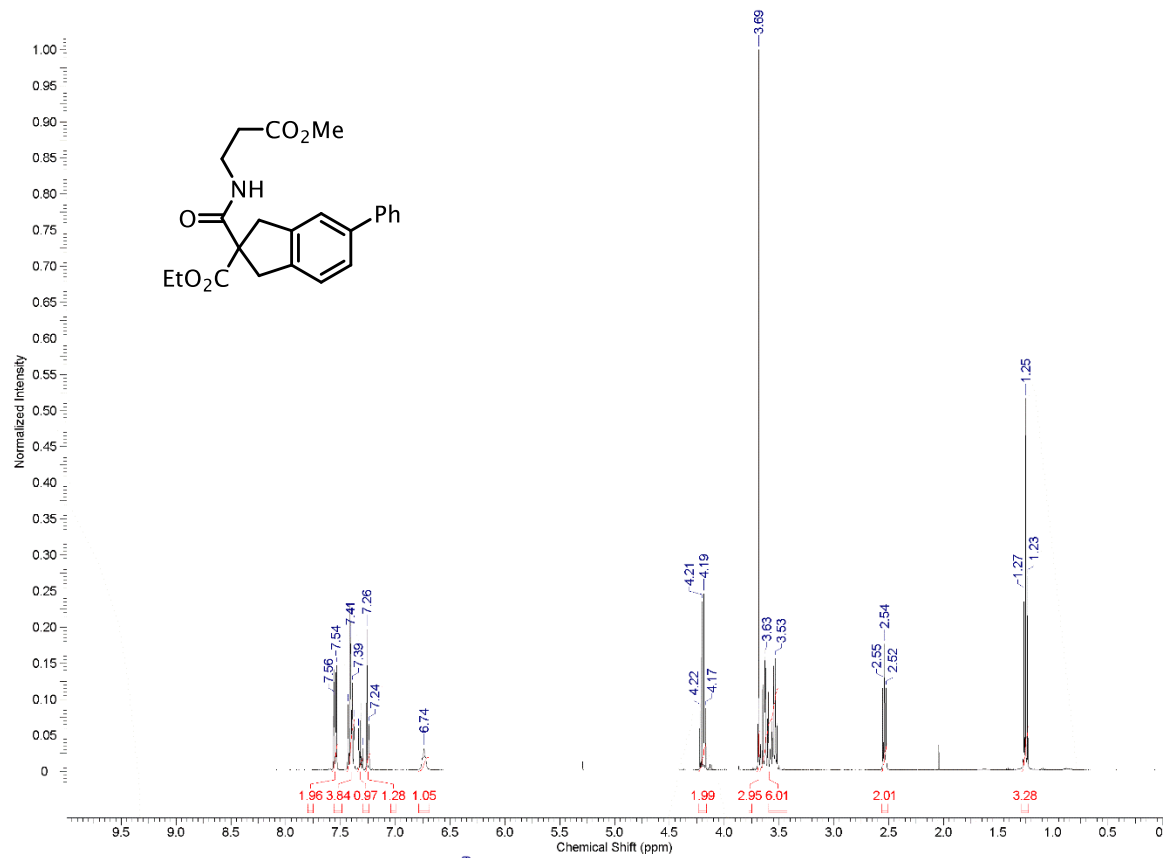


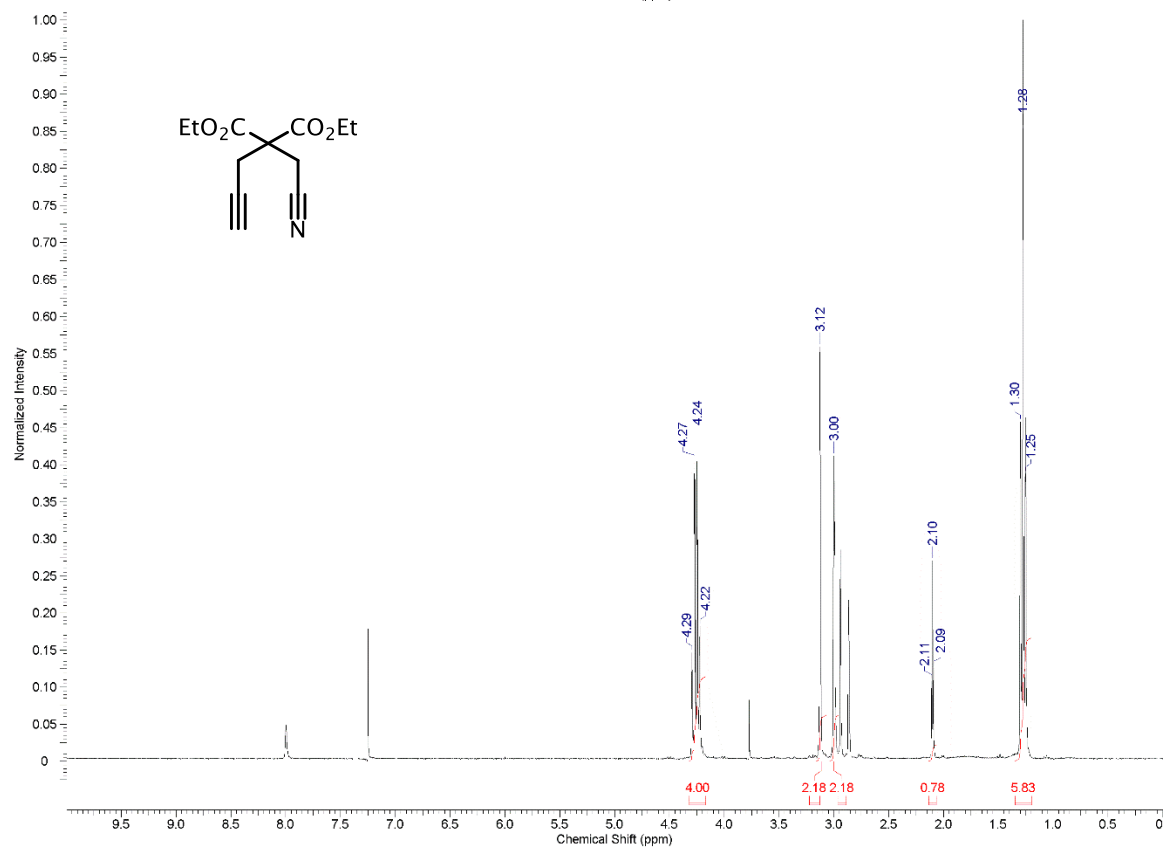
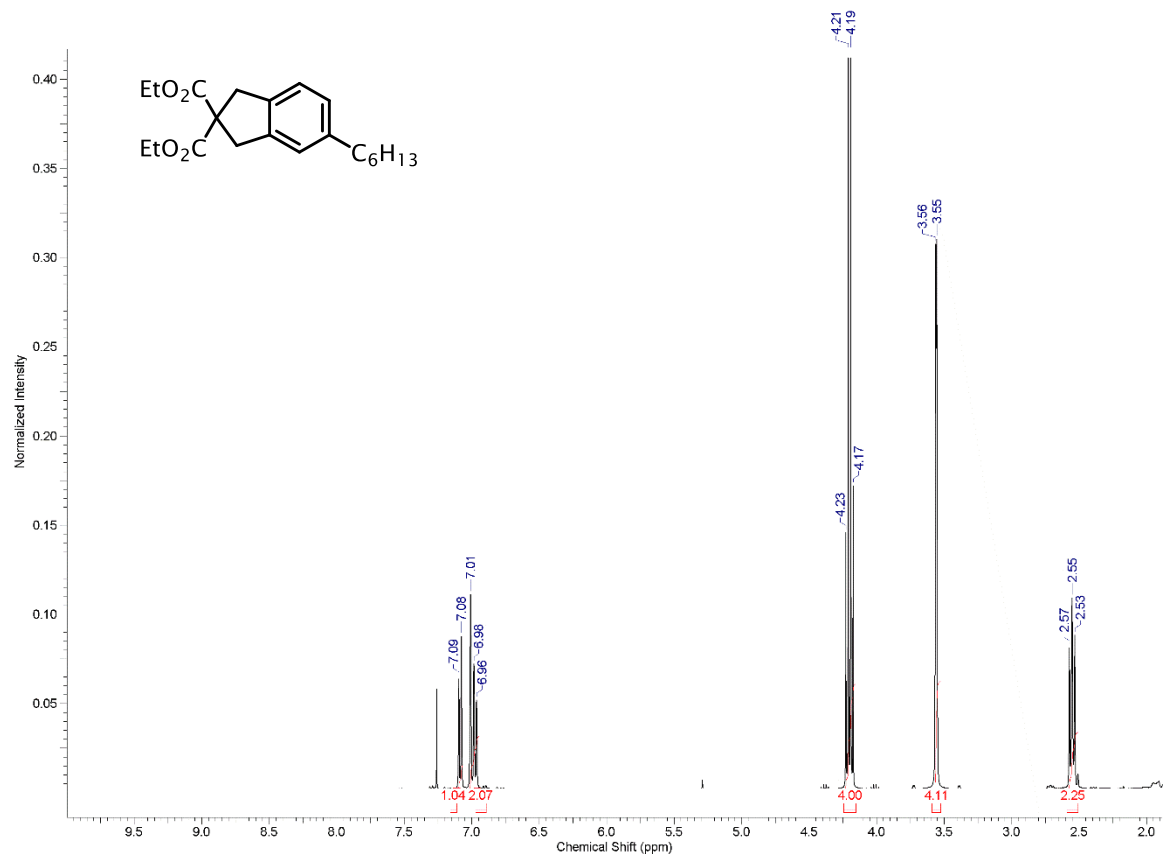












## REFERENCES

- [1] Wilking, M.; Mück-Lichtenfeld, C.; Daniliuc, C. G.; Hennecke, U. *J. Am. Chem. Soc.* **2013**, 135, 8133-8136.
- [2] Nakajima, K.; Takata, S.; Sakata, K.; Nishibayashi, Y. *Angew. Chem. Int. Ed.* **2015**, 54, 7597-7601.
- [3] Sankar, U.; Raju, C.; Uma, R. *Current Chemistry Letters* **2013**, 1, 123-132.
- [4] Song, J.-A.; Park, S.; Kim, T.-S.; Choi, T.-L. *ACS Macro Letters* **2014**, 3, 795-798.
- [5] Lee, I.; Kang, E.-H.; Park, H.; Choi, T. *Chem. Sci.* **2012**, 3, 761-765.
- [6] Kothandaraman, P.; Zhao, Y.; Lee, B. R.; Le Ng, C. J.; Lee, J. Y.; Ayers, B. J.; Chan, P. W. H. *Adv. Synth. Catal.* **2016**, 358, 1385-1391.
- [7] Lancaster, T. M.; Butters, R.; Choodnovskiy, N. R.; Zion, T. C. WO 2011-US44989.
- [8] Auvinet, A.-L.; Ez-Zoubir, M.; Bompard, S.; Vitale, M. R.; Brown, J. A.; Michelet, V.; Ratovelomanana-Vidal, V. *ChemCatChem* **2013**, 5, 2389-2394.
- [9] Saino, N.; Amemiya, F.; Tanabe, E.; Kase, K.; Okamoto, S. *Org. Lett.* **2008**, 8, 1439-1442.
- [10] Kezuka, S.; Tanaka, S.; Ohe, T.; Nakaya, Y.; Takeuchi, R. *J. Org. Chem.* **2006**, 543-552.
- [11] Bhatarah, P.; Smith, E. H. *J. Chem. Soc., Perkin Trans. 1* **1990**, 9, 2603-2603.
- [12] Yoshida, K.; Morimoto, I.; Mitsudo, K.; Tanaka, H. *Tetrahedron.* **2008**, 5800-5807.
- [13] Yun-Hua Wang, Shao-Hsien Huang, Tze-Chiao Lin, Fu-Yu Tsai. *Tetrahedron.* **2010**, 7136-7141.
- [14] Hillard, R. L.; Vollhardt, K. P. C. *J. Am. Chem. Soc.* **1977**, 99, 4058-4069.

## APPENDIX TWO

### Applications of Light-Gated Cobalt Catalysis: Experimental

#### **Part A:** *Light-Controlled [2+2+2] Cycloaddition Polymerization*

##### **A 2.1 --- General Methods and Materials**

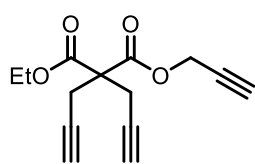
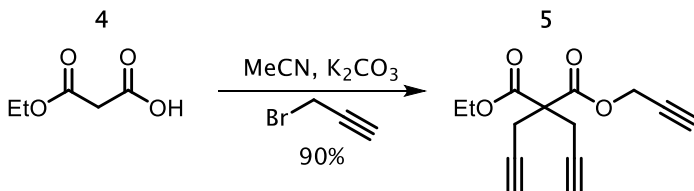
All reactions were carried out in anhydrous solvents and performed under ambient conditions unless otherwise noted (glove box: MBraun MB 200G or Schlenck techniques). Anhydrous, degassed acetonitrile (MeCN), dichloroethane (DCE) and diisopropylethylamine (DIPEA) were purchased from Sigma Aldrich in Sure-Seal bottles, opened under an inert nitrogen atmosphere and used without further purification. Tetrahydrofuran (THF), dichloromethane (DCM), and diethyl ether (Et<sub>2</sub>O) were degassed with a stream of argon and passed through two columns of neutral alumina before use. Thin layer chromatography was conducted on SiliCycle® 250 µm 60 Å (glass-backed) and column chromatography for isolated compounds was performed on SiliCycle® Silica Flash® 40-63 µm 60Å. Anhydrous cobalt halide salts were purchased from Sigma Aldrich or Strem Chemicals and stored under inert conditions. (4-ethynylphenyl)methanol (**9**) is available from Sigma Aldrich or easily prepared by LAH reduction of methyl 4-ethynylbenzoate (from AK Scientific). Undec-10-en-1-ol was purchased from Sigma-Aldrich and used without further purification. Light sources used include a 410 nm 35W Kessil LED, 450 nm 35W Kessil LED or a standard household 14W CFL. The photo-catalyst [Ir(dF-CF<sub>3</sub>ppy)<sub>2</sub>(dtbbpy)]PF<sub>6</sub> was synthesized according to literature procedures or purchased from Strem Chemicals.

## A 2.2 --- Instrumentation

GPC analysis was performed using a Viscotek GPCMax and TDA302 Tetradelector Array (refractive index) with three Olexis columns (Agilent) calibrated using polystyrene standards (500 to 1.2E<sup>6</sup>). Washed and dried samples were dissolved and eluted using HPLC grade (Burdock and Jackson) DMF (1mL/min). NMR spectra were collected on a Varian 300 or 400 MHz spectrometer and data is reported as follows: in CDCl<sub>3</sub> (7.26 ppm); multiplicity (s = singlet, bs = broad singlet, d = doublet, t = triplet, q = quartet, and m = multiplet), coupling constants (Hz). Carbon NMR spectra were collected on a Varian 300 or 400 MHz spectrometer. Chemical shifts are reported in reference to CDCl<sub>3</sub> (77.2 ppm). Non-polymeric compounds and polymer spectra were conducted in CDCl<sub>3</sub> at room temperature.

## A 2.3 --- Synthesis of Step-Growth Monomers

### A 2.3.1 -- Synthesis of Compound 5:

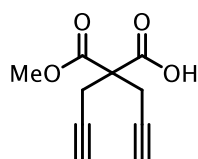
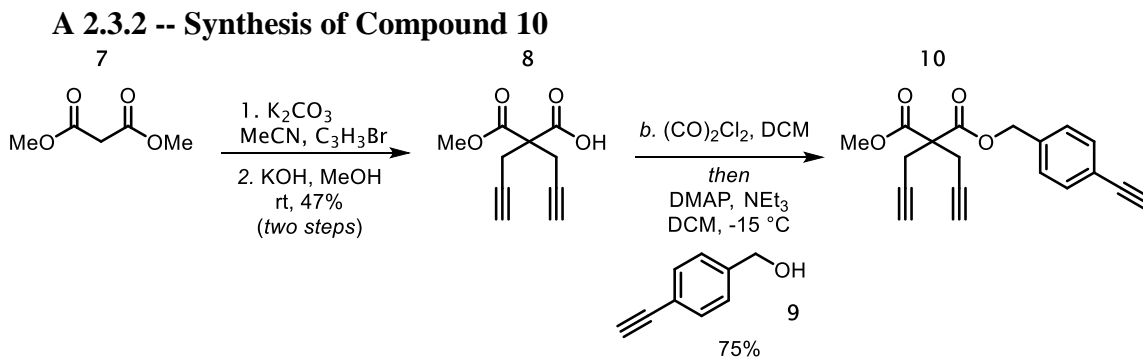


**1-ethyl 3-(prop-2-yn-1-yl) 2,2-di(prop-2-yn-1-yl)malonate (7):** A 50 ml

flame-dried round bottom flask was charged with a stir bar, monoethyl malonic acid **4** (3.0g, 1.0 equivalents), and potassium carbonate (16 g, 5.0 equivalents). Anhydrous acetonitrile (130 mL, ~0.2M) was added to the flask followed by propargyl bromide (80% in toluene, 7.10 mL, 3.5 equivalents), and the reaction was aggressively stirred overnight. After 12 hours the reaction was filtered through a glass frit and the filtrate was concentrated *in vacuo*. The crude material was loaded directly onto a silica gel column and eluted with a 0-25% ethyl acetate:hexane gradient to afford compound **5** in 90% as a translucent solid.



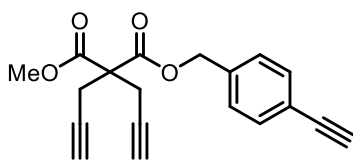
**<sup>1</sup>H NMR** (300 MHz, CDCl<sub>3</sub>) δ 4.74 (d, J = 2.35 Hz, 2H), 4.22 (q, J = 7.0 Hz, 2H), 3.00 & 2.99 (overlapping singlets, 4H), 2.47 (t, J = 2.35 Hz, 1H), 2.03 (m, 2H), 1.25 (t, J = 7.0 Hz, 3H) ppm. **<sup>13</sup>C NMR** (101 MHz, CDCl<sub>3</sub>) δ 167.97, 167.87, 78.03, 77.44, 77.12, 76.80, 76.66, 75.56, 72.02, 62.25, 56.17, 53.27, 22.44, 13.95 ppm. **IR** (ATR): 3285, 2990, 2934, 2124, 1738, 1279, 1210, 1171 cm<sup>-1</sup>. **MS** (ESI, pos): m/z = 269.2 [M+Na]<sup>+</sup>



**2-(methoxycarbonyl)-2-(prop-2-yn-1-yl)pent-4-ynoic acid (8):** The synthesis of this compound is known and we used a modified procedure.<sup>[1]</sup> A flame-dried 50 mL round bottom flask was charged with bis-propargylated dimethyl

malonate (935 mg, 1.0 equivalents) and potassium hydroxide (245 mg, 1.1 equivalents). Anhydrous ethanol (20 mL, ~0.2M) was added to the flask and the reaction was stirred overnight at 50 °C. After 12-16 hours the solution became heterogeneous and the suspension was concentrated *in vacuo* to dryness. The precipitated crude material was suspended in diethyl ether, filtered, and washed with excess diethyl ether to remove unreacted starting material. The solid was immediately dissolved in 1M HCl and then transferred to a separatory funnel. The aqueous layer was extracted thrice with dichloromethane (DCM), the organic layers were combined, and then dried over magnesium sulfate. Concentration of the organic layers afforded **8** as an off white solid which was pure by <sup>1</sup>H NMR in 55% yield. A <sup>1</sup>H NMR has been included for reference. **<sup>1</sup>H NMR**

(400 MHz, CDCl<sub>3</sub>):  $\delta$  10.14 (bs, 1H), 3.81 (s, 3H), 3.02 (s, 2H), 3.01 (s, 2H), 2.07 (t, J = 2.7 Hz, 2H) ppm. Compound characterization matched similar spectra reported in the literature.



**1-(4-ethynylbenzyl) 3-methyl 2,2-di(prop-2-yn-1-yl)malonate**

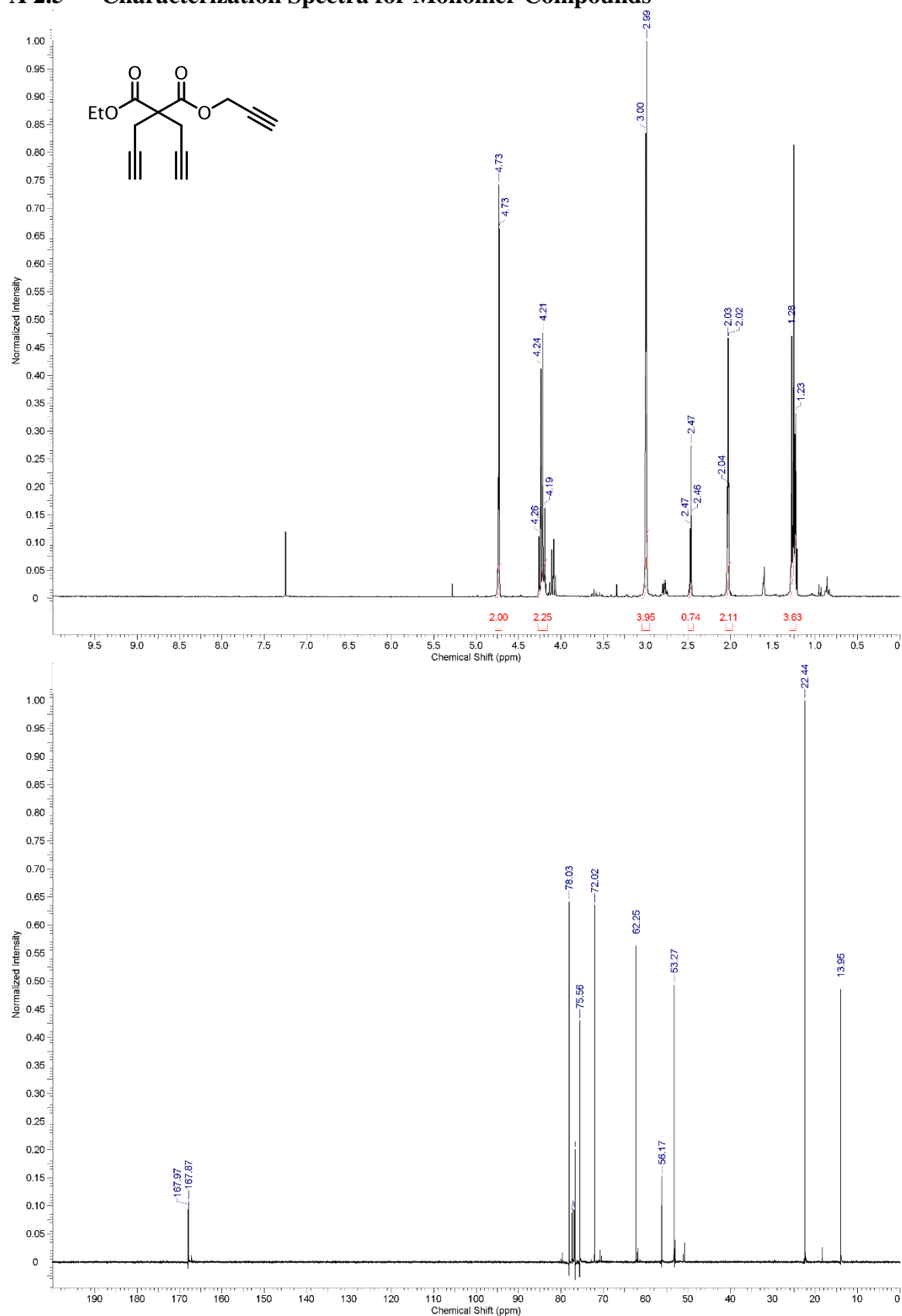
**(10)**: To an oven-dried 250 mL round bottom flask was added mono-acid compound **8** (2.0 g, 10.30 mmol, 1.2 equivalents) and 50 mL of anhydrous dichloromethane (0.2 M). Three drops of dimethylformamide were added followed by dropwise addition of oxalyl chloride (1.03 mL, 12.01 mmol, 1.4 equivalents) and gas evolution was immediately observed. After stirring for 1-2 hours, gas evolution had ceased and the reaction was concentrated *in vacuo*. A separate oven-dried 250 mL flask was charged with 3-ethynyl benzyl alcohol (**9**) (1.13 g, 8.58 mmol, 1.0 equivalents), 4-dimethylaminopyridine (DMAP, 79.0 mg,  $6.49 \times 10^{-3}$  mmol, 0.10 equivalents), trimethylamine (NEt<sub>3</sub>, 2.40 mL, 17.16 mmol, 2.0 equivalents), dichloromethane (DCM, 40 mL, 0.2M) and cooled to -15 °C. The corresponding acid chloride was dissolved in dichloromethane (20 mL), charged to a dropping funnel and added dropwise to the stirred solution at -15 °C over 20 minutes. After three hours at -15 °C (TLC showed consumption of starting material) the reaction was quenched with NH<sub>4</sub>Cl (sat.), extracted three times with dichloromethane (30 mL) and the organic layers were combined. The organic layer was dried over sodium sulfate and dried the crude monomer residue was purified using column chromatography eluting 9:1 hexane:ethyl acetate (Rf: ~0.20) to give a clear oil (**10**) which solidifies to a white solid upon cooling (75%). <sup>1</sup>H NMR (400 MHz, CDCl<sub>3</sub>):  $\delta$  7.45 (d, J = 8.2 Hz, 2H), 7.24 (d, J = 2.3 Hz, 2H), 5.17 (s, 2 H), 3.68 (s, 3H), 3.07 (s, 1H), 2.99 (s, 2H), 2.98 (s, 2H) 2.00 (t, J = .7 Hz, 2H) ppm. <sup>13</sup>C NMR (101 MHz, CDCl<sub>3</sub>)  $\delta$  168.8, 168.2, 135.7, 132.8, 131.6, 128.6, 127.4, 122.23, 83.1,

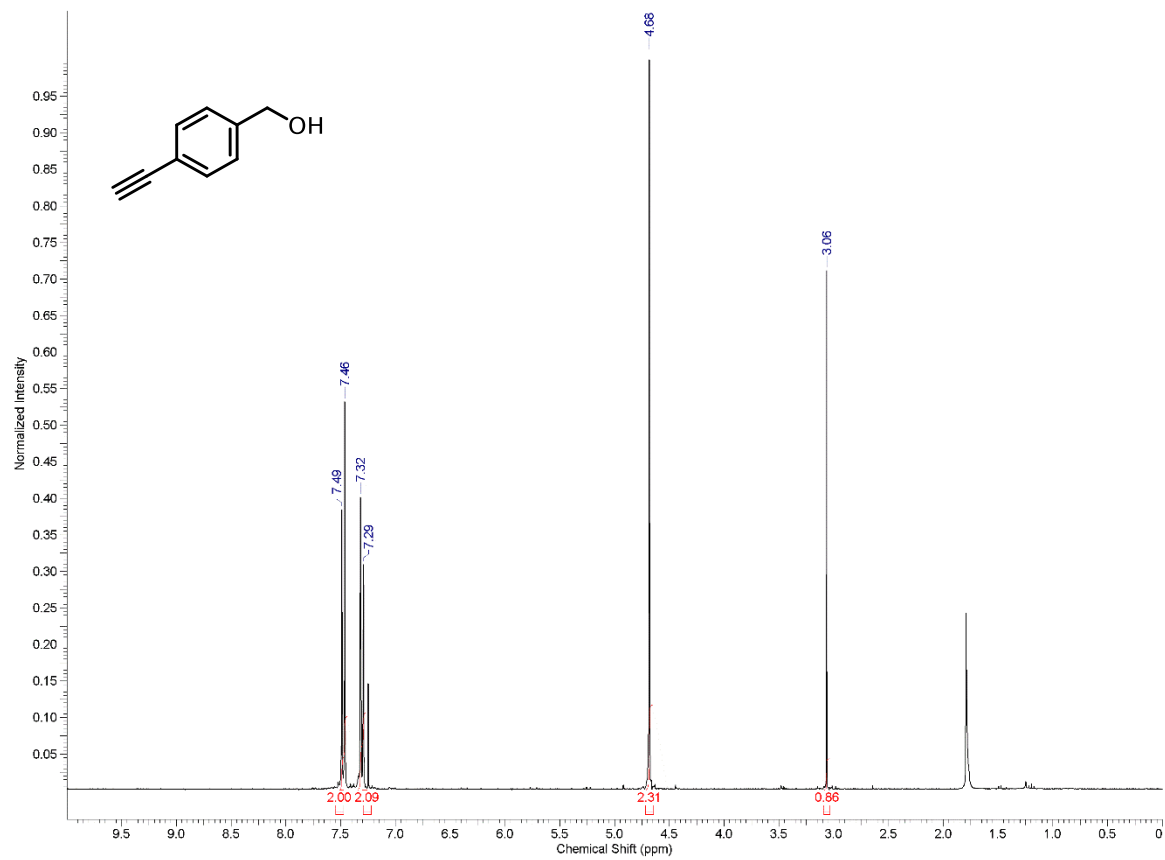
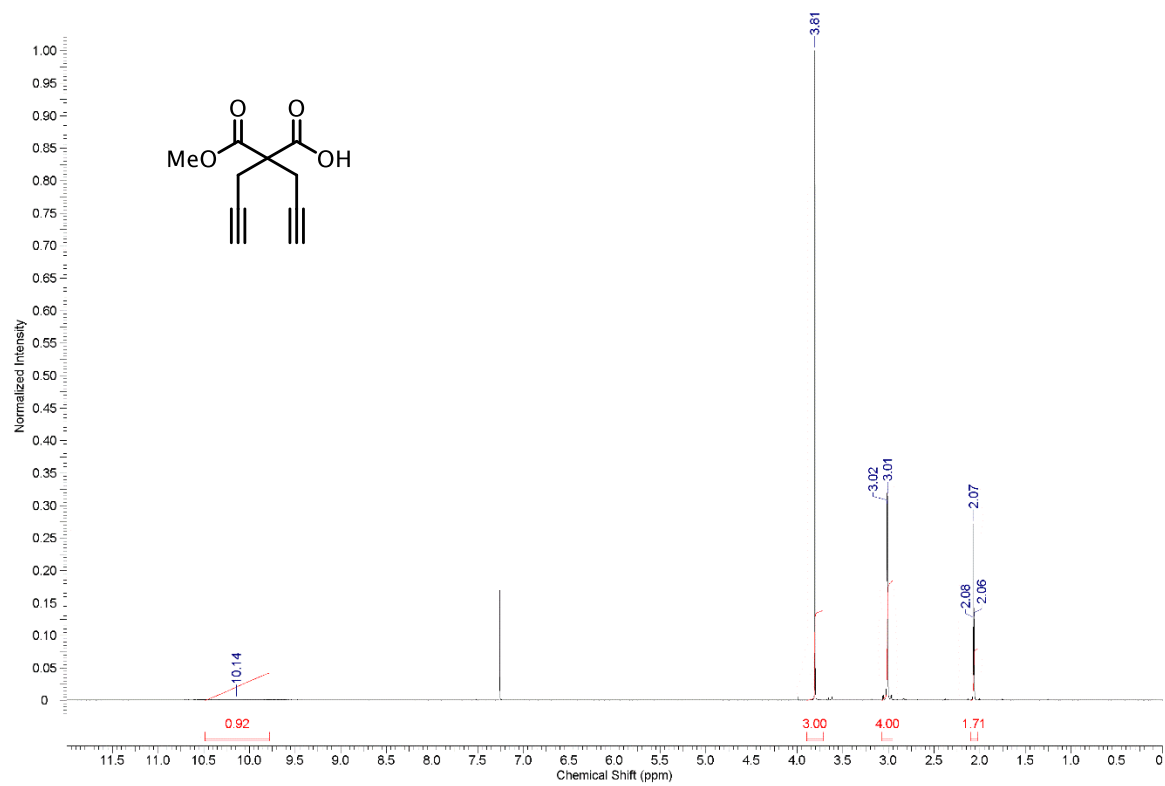
78.1), 72.8, 71.2, 67.0, 56.5, 22.6 ppm. MS (ESI, pos):  $m/z = 309.1 [M+1]^+$ ;  $m/z = 341.2 [M+MeOH]^+$ ; calculated  $C_{19}H_{16}O_4$ , 308.3

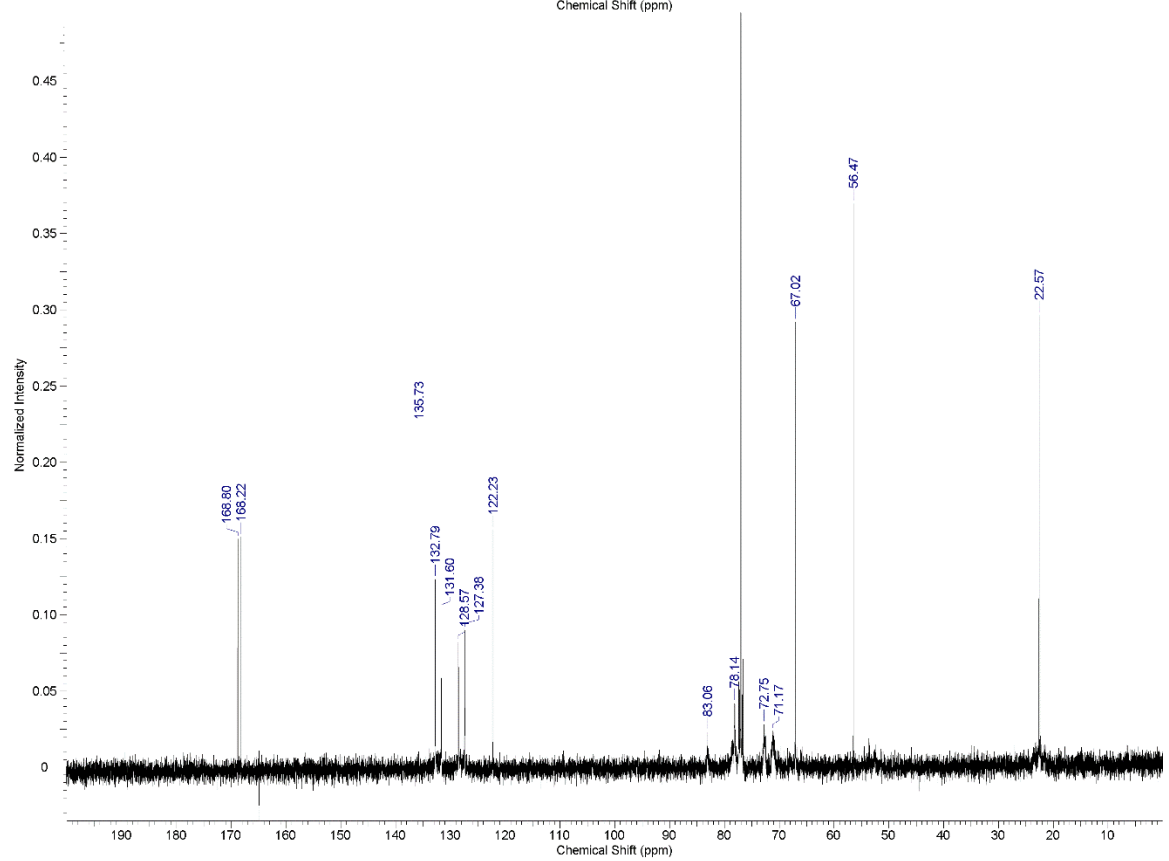
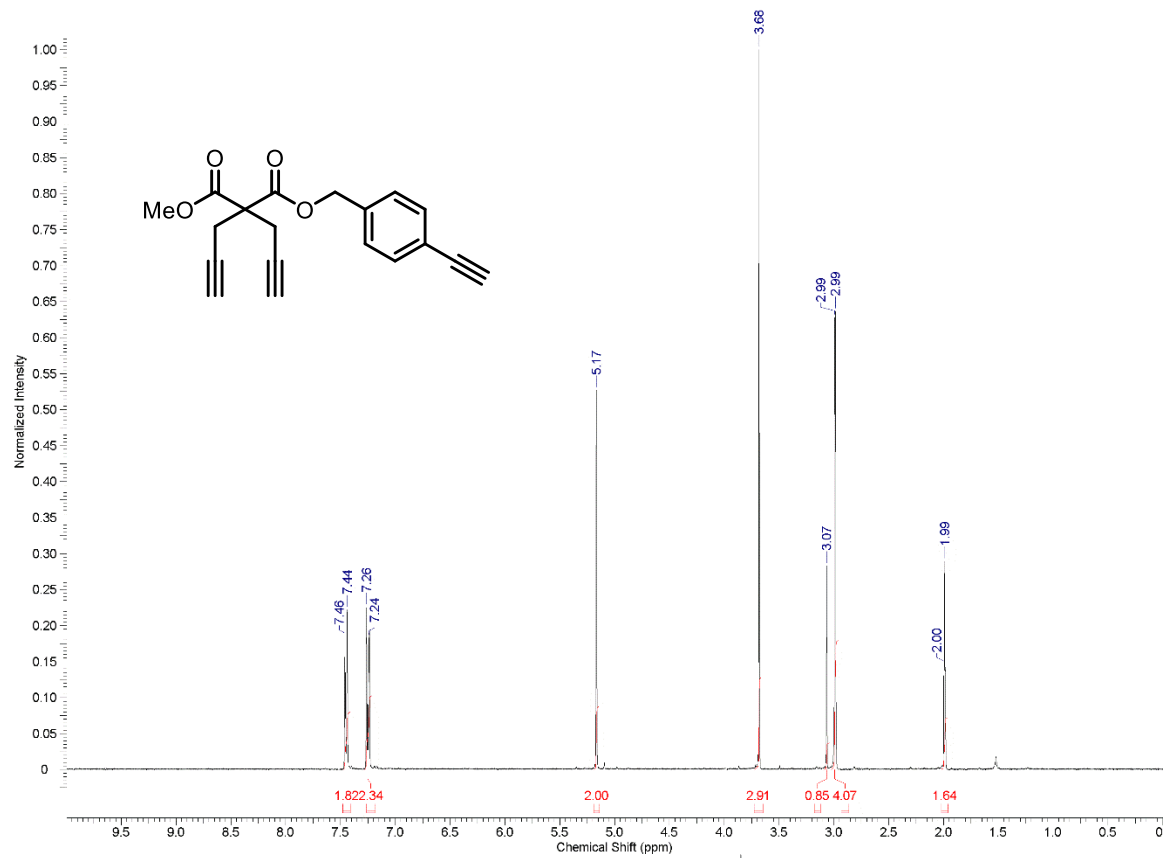
#### A 2.4 --- General Procedure for Polymerization

Under ambient conditions, an oven-dried 1 dram vial is charged with a stir bar.  $CoBr_2(PCy_3)_2$  (5.69 mg, 0.03 equivalents,  $7.30 \times 10^{-3}$  mmol) and  $[Ir(dF-CF_3ppy)_2(dtbbpy)]$  (1.36 mg, 0.005 equivalents,  $1.22 \times 10^{-3}$  mmol) are weighed on a balance under air and directly charged to the vial. The vial is pumped into the glove box. Under an inert atmosphere, anhydrous acetonitrile (MeCN) is added followed by DIPEA (12.7  $\mu$ L, 0.30 equivalents,  $7.30 \times 10^{-2}$  mmol) and a bis alkyne additive (1.72 mg, 0.03 equivalents,  $7.30 \times 10^{-3}$ ). The vessel was then irradiated for 30 minutes. Concurrently, a second vial was charged with triyne monomer (**10**) (75 mg, 1.0 equivalent, 0.24 mmol) and placed under an inert atmosphere. The monomer was fully dissolved in degassed dichloroethane (1.2 mL). The resulting DCE/monomer solution was then quickly transferred to the monomer-containing acetonitrile solution and irradiated for the desired time. Upon monomer consumption the polymerization was concentrated *in vacuo* and the crude material was re-dissolved in dichloromethane. The vial was layered with methanol (open to air) and the dichloromethane was slowly removed *in vacuo* to precipitate the polymer as an off-white solid. The solid was collected on a glass frit, washed with methanol, and dried under high vacuum for 24 hours. GPC samples were prepared by dissolving the polymer in HPLC grade DMF (4-5mg/mL) and filtering through a 0.45  $\mu$ M nylon syringe filter to remove any particulate.

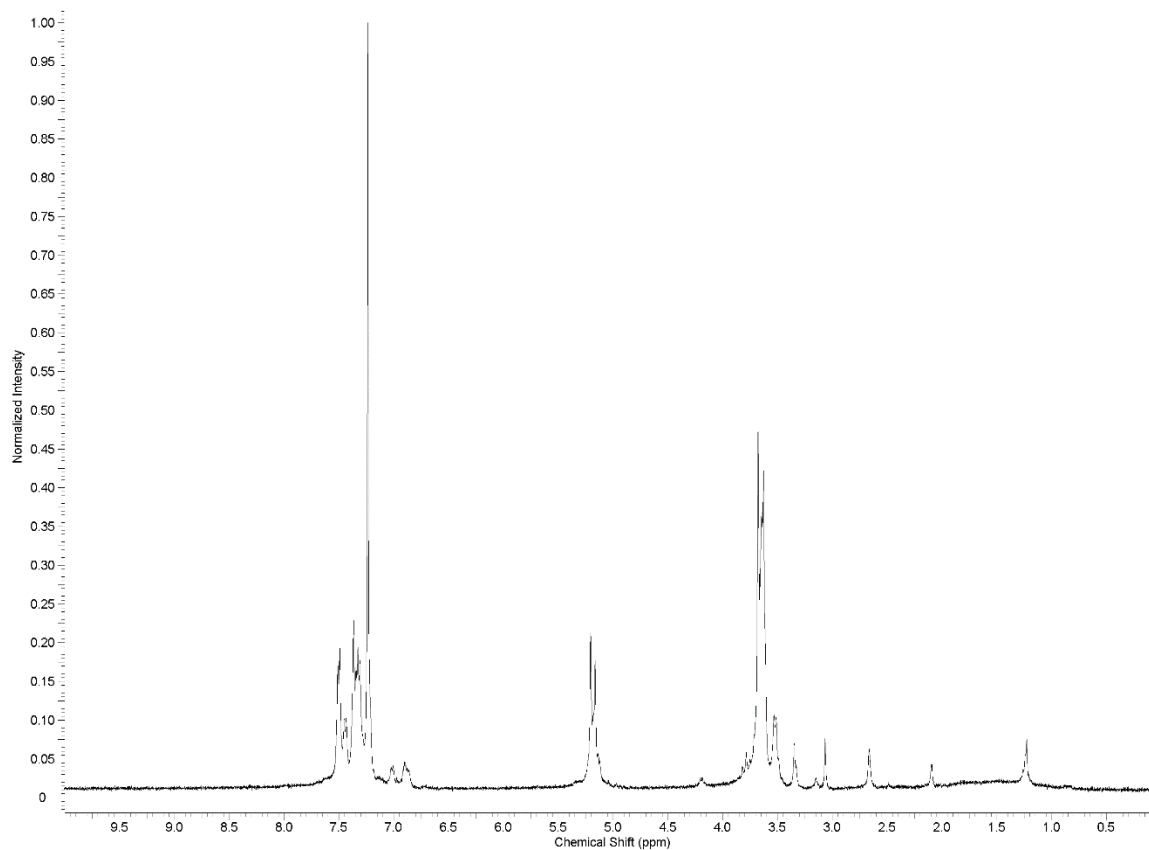
## A 2.5 --- Characterization Spectra for Monomer Compounds







## A 2.6 --- Representative <sup>1</sup>H NMR of Step-Growth Polymer



## A 2.7 --- GPC Traces for Optimization Table and Polymer Growth Experiment

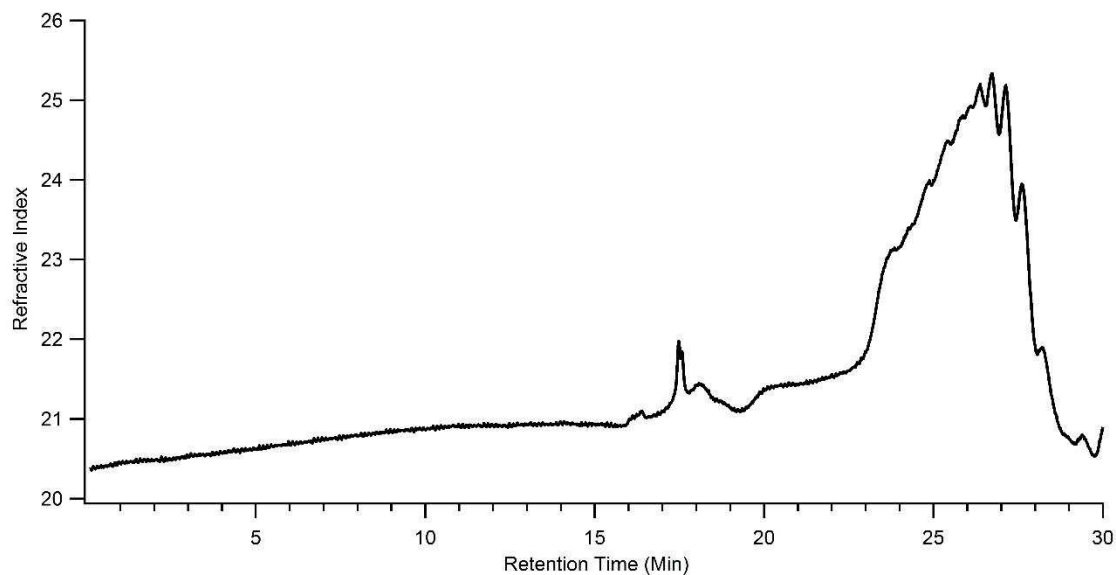


**Figure 2.7.1 – Corresponds to Table 4.1, Entry 2.**

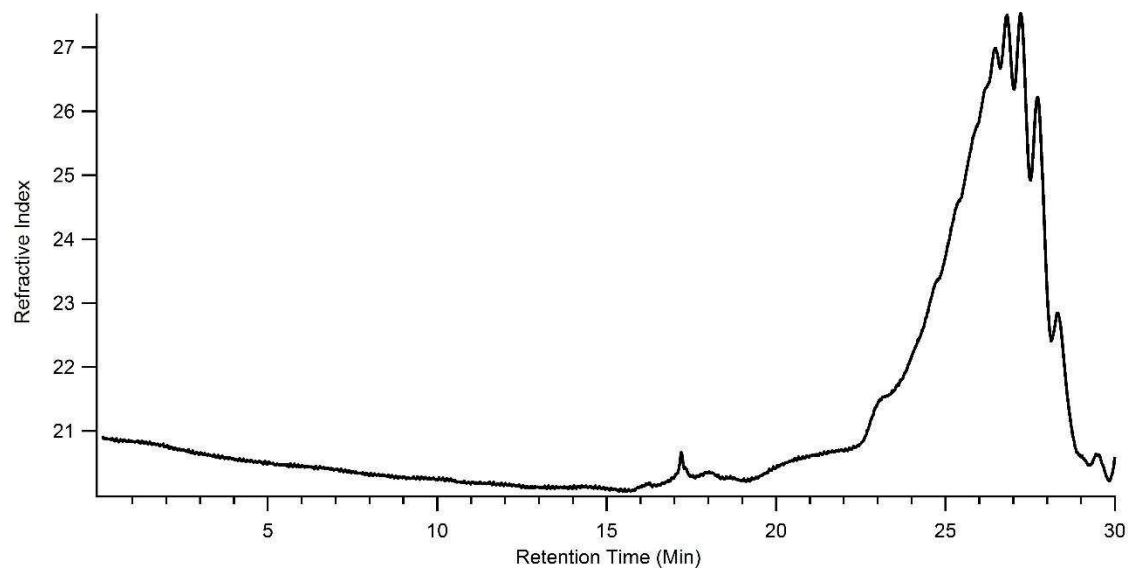


**Figure 2.7.2 – Corresponds to Table 4.1, Entry 3.**



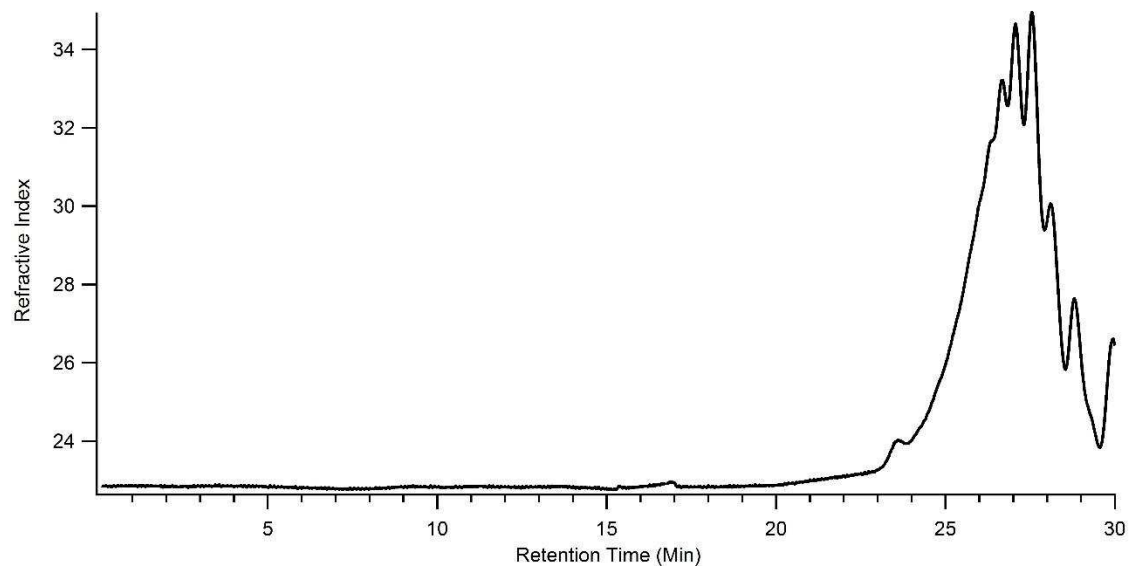


**Figure 2.7.3 – Corresponds to Table 4.1, Entry 4.**

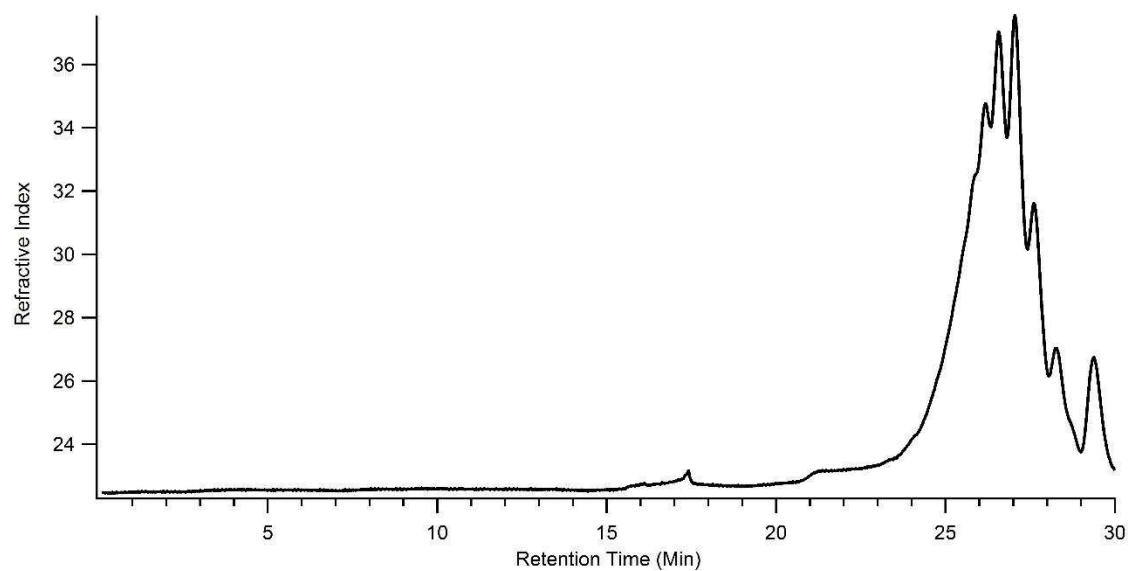


**Figure 2.7.4 – Corresponds to Table 4.1, Entry 5.**

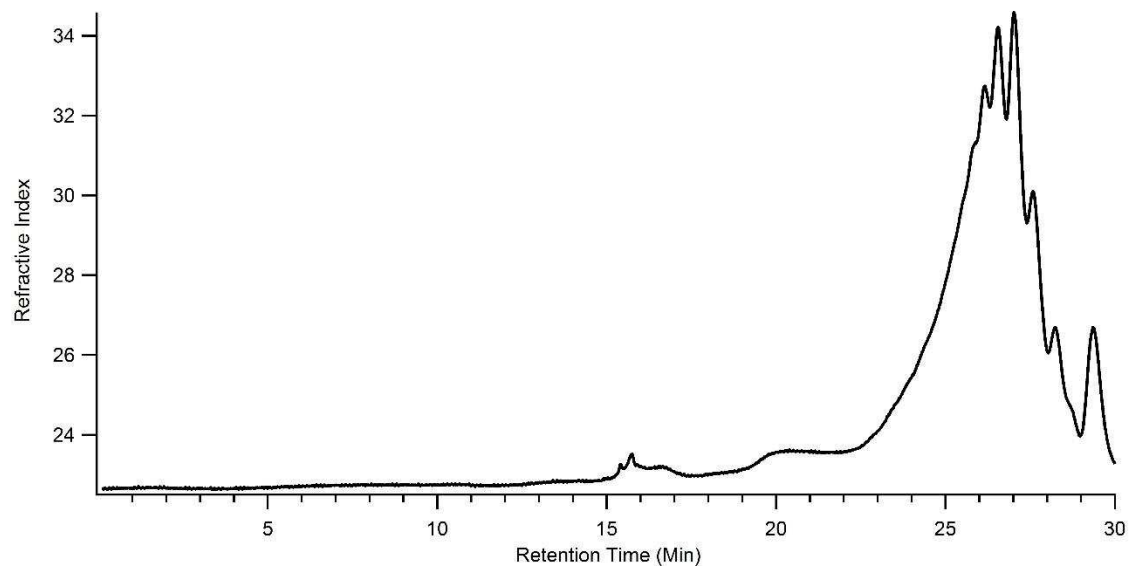


**Figure 2.7.5 – Corresponds to Table 4.1, Entry 6.**

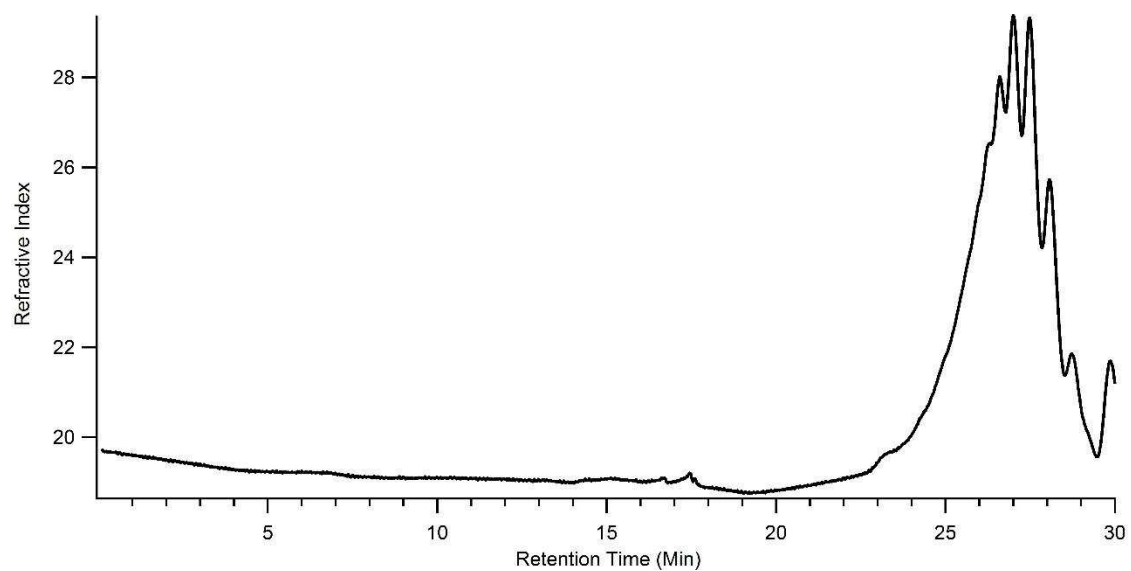


**Figure 2.7.6 – Corresponds to Table 4.1, Entry 7.**

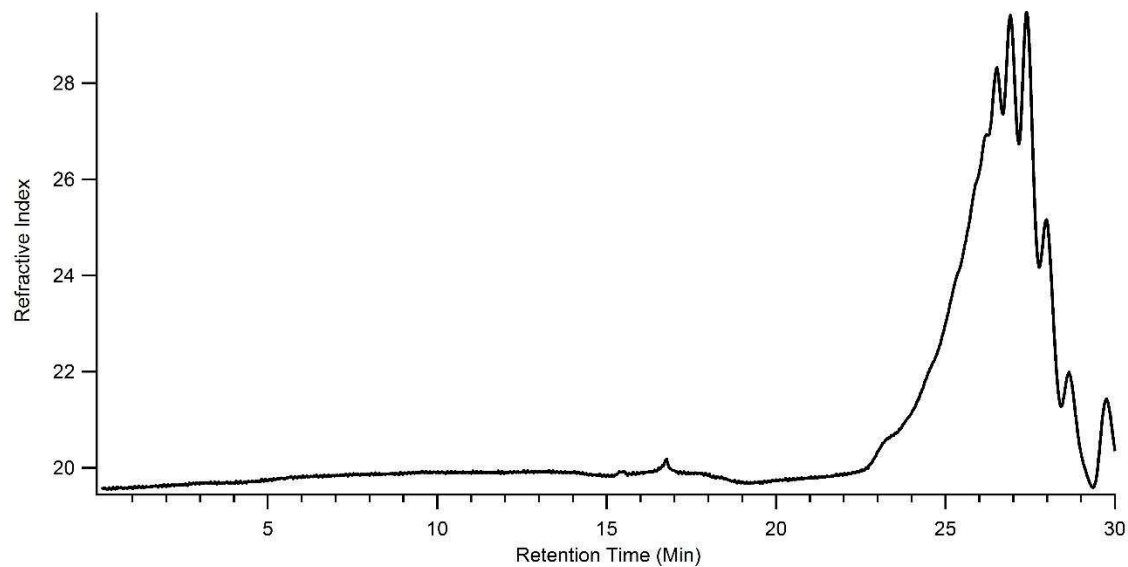


**Figure 2.7.7 – Corresponds to Table 4.1, Entry 8.**

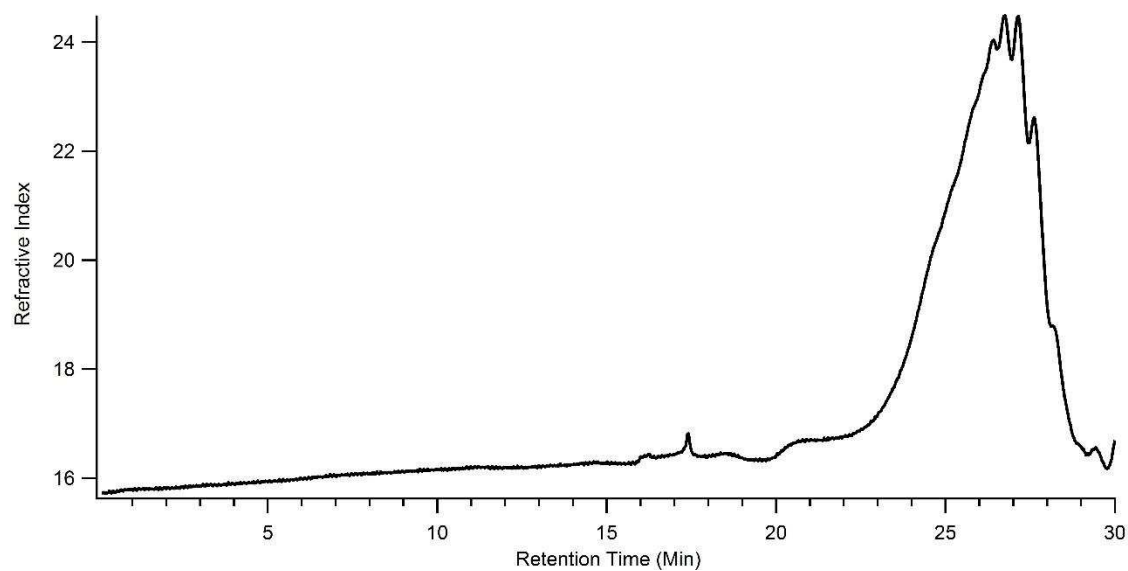


**Figure 2.7.8 – Corresponds to Table 4.1, Entry 9.**

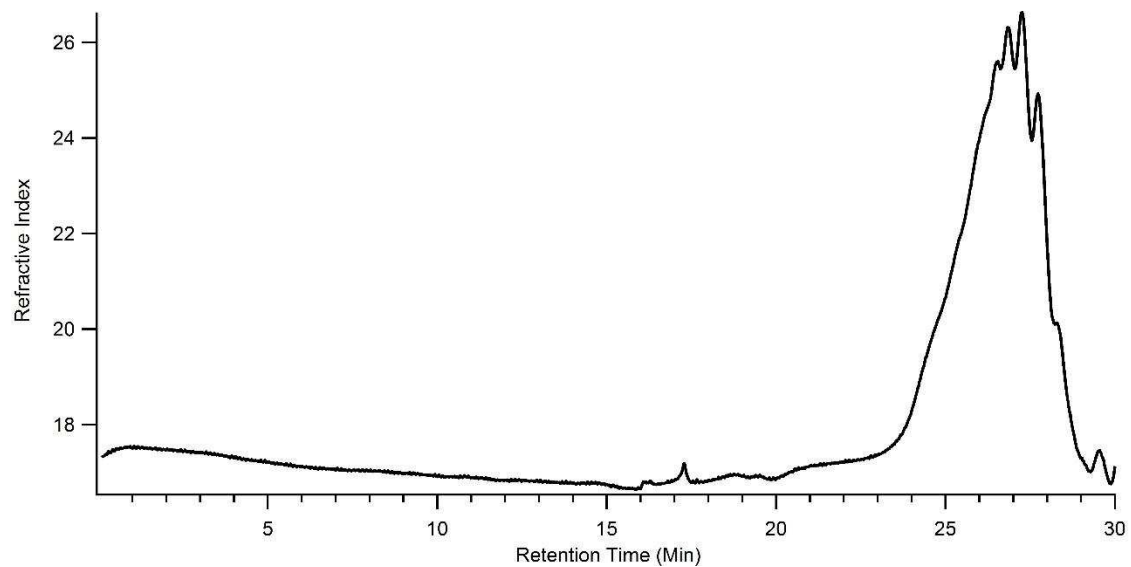


**Figure 2.7.9 – Corresponds to Table 4.1, Entry 10.**

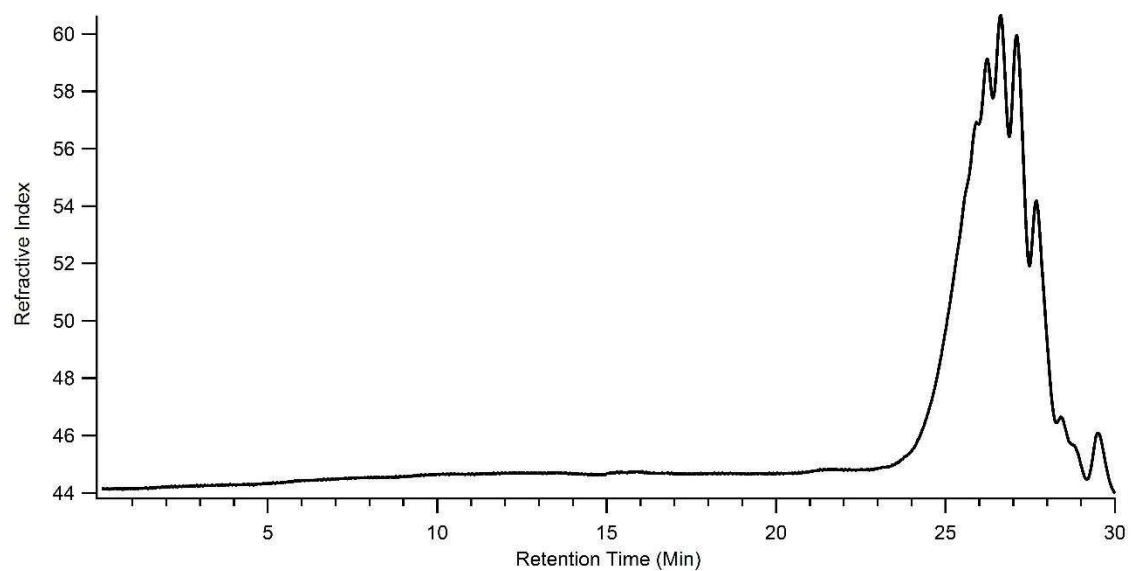


**Figure 2.7.10 – Corresponds to Table 4.1, Entry 11.**

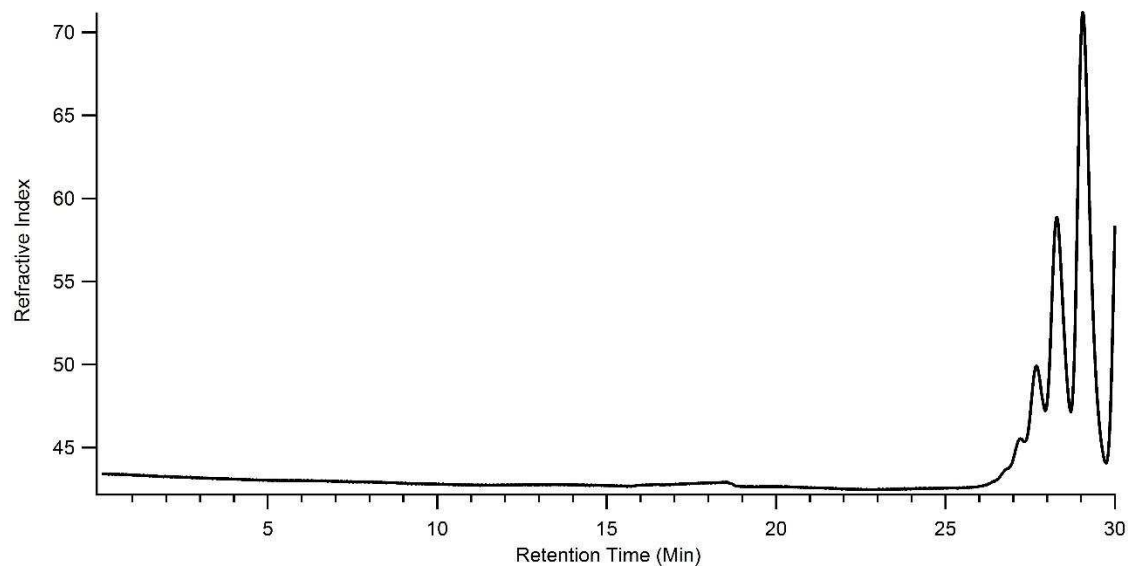


**Figure 2.7.11 – Corresponds to Figure 4.10, 2 Minutes.**

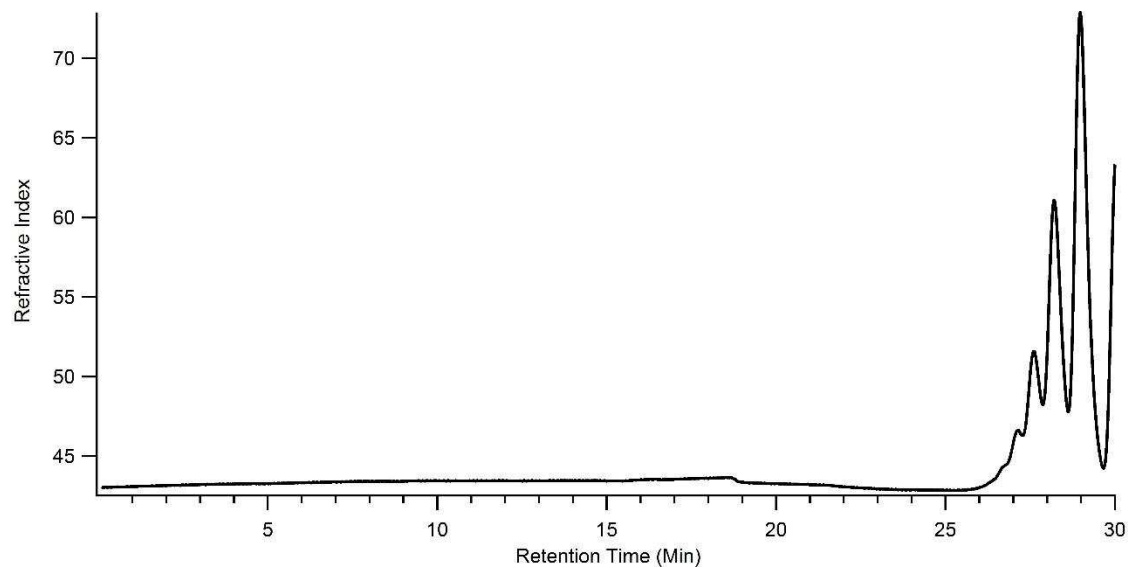


**Figure 2.7.12 – Corresponds to Figure 4.10, 4 Minutes.**

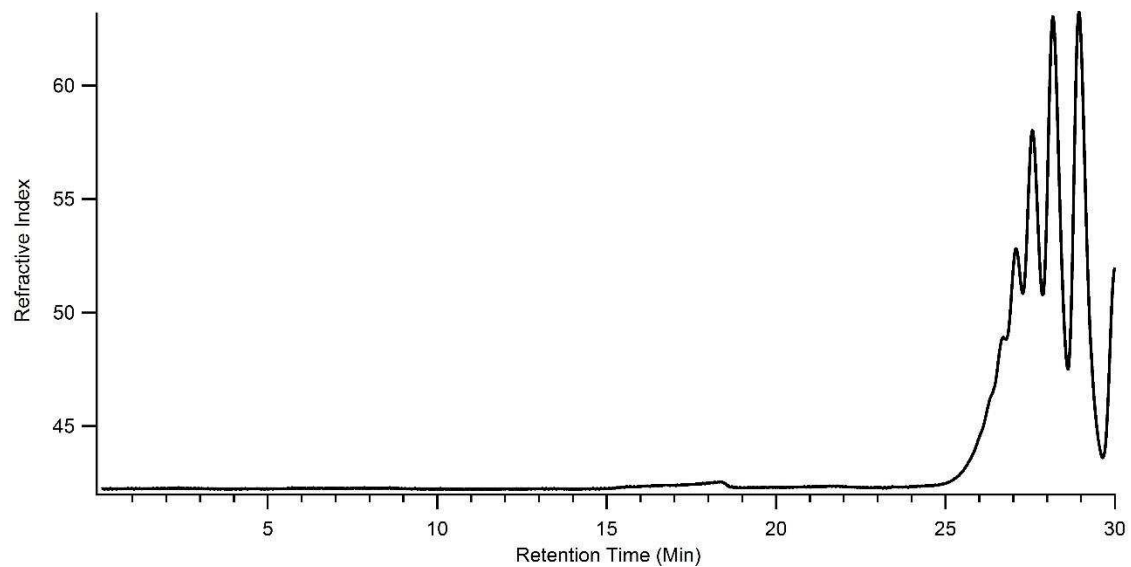


**Figure 2.7.13 – Corresponds to Figure 4.10, 6 Minutes.**

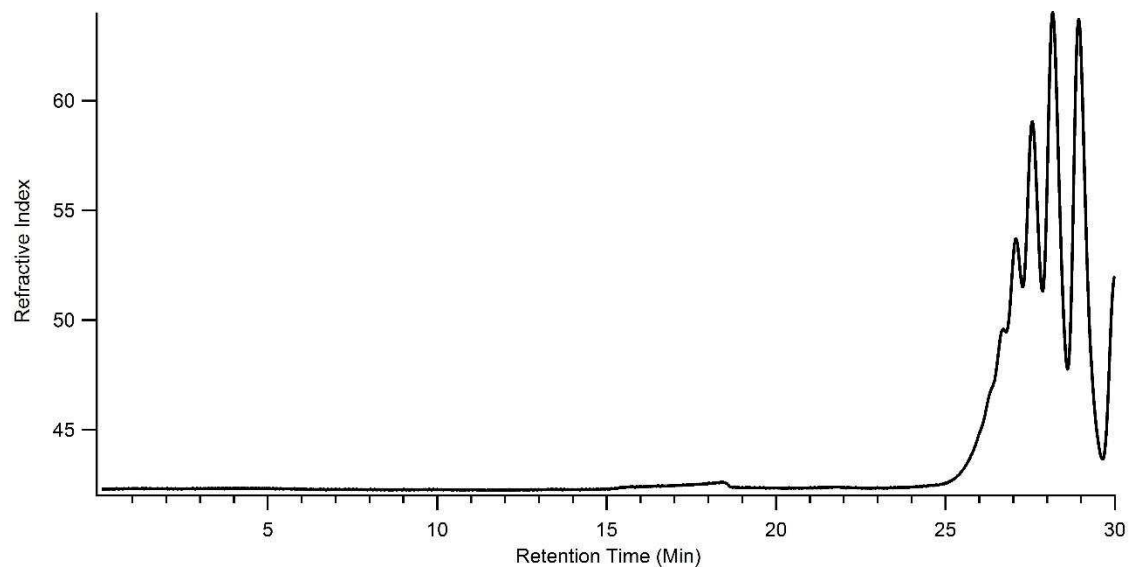


**Figure 2.7.14 – Corresponds to Figure 4.10, 8 Minutes.**

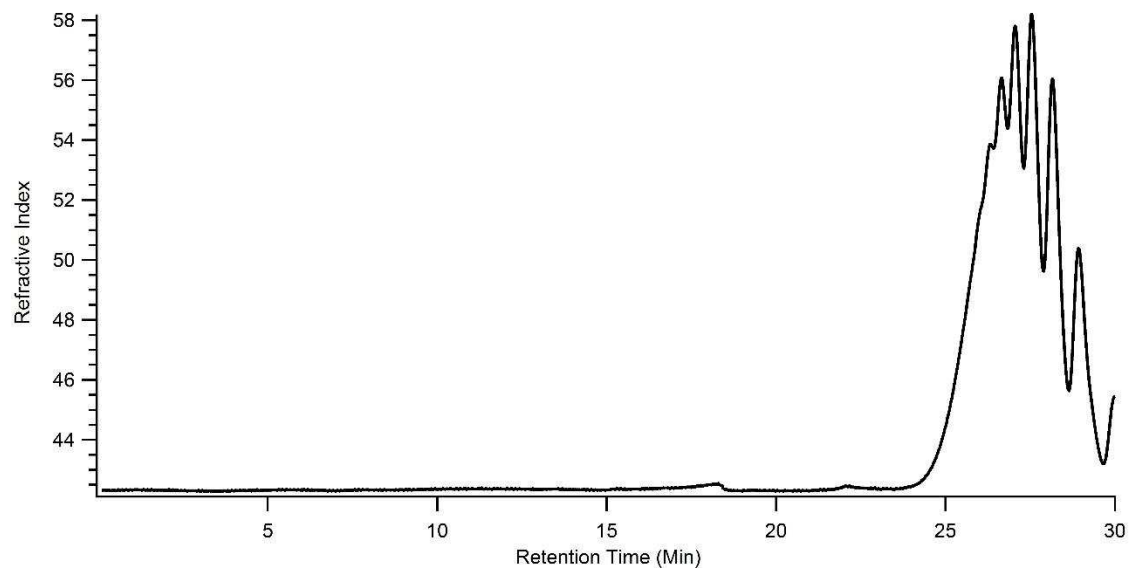


**Figure 2.7.15 – Corresponds to Figure 4.10, 13 Minutes.**

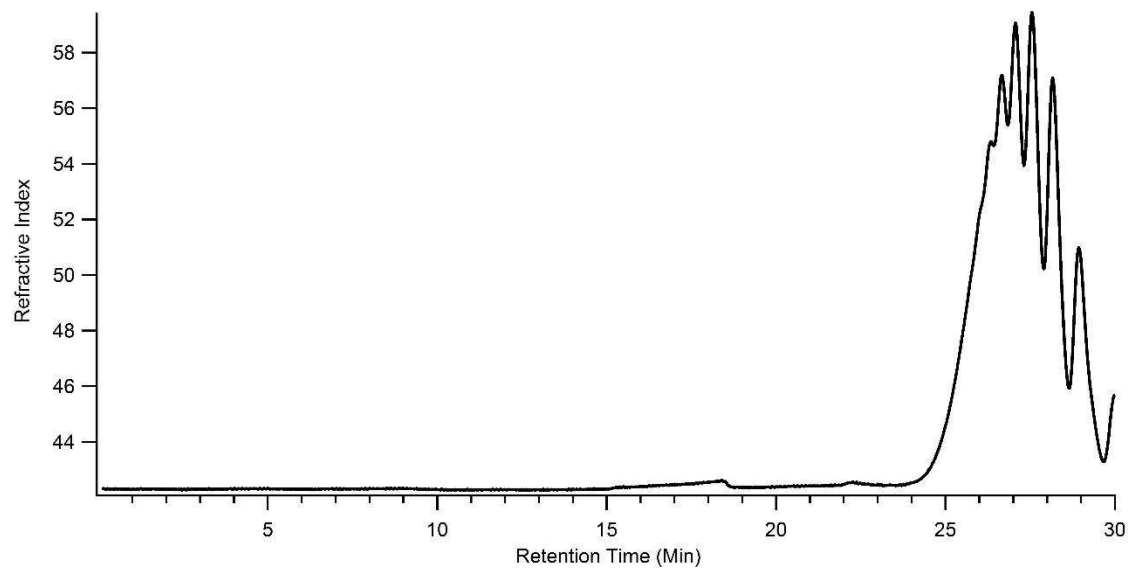


**Figure 2.7.16 – Corresponds to Figure 4.10, 18 Minutes.**

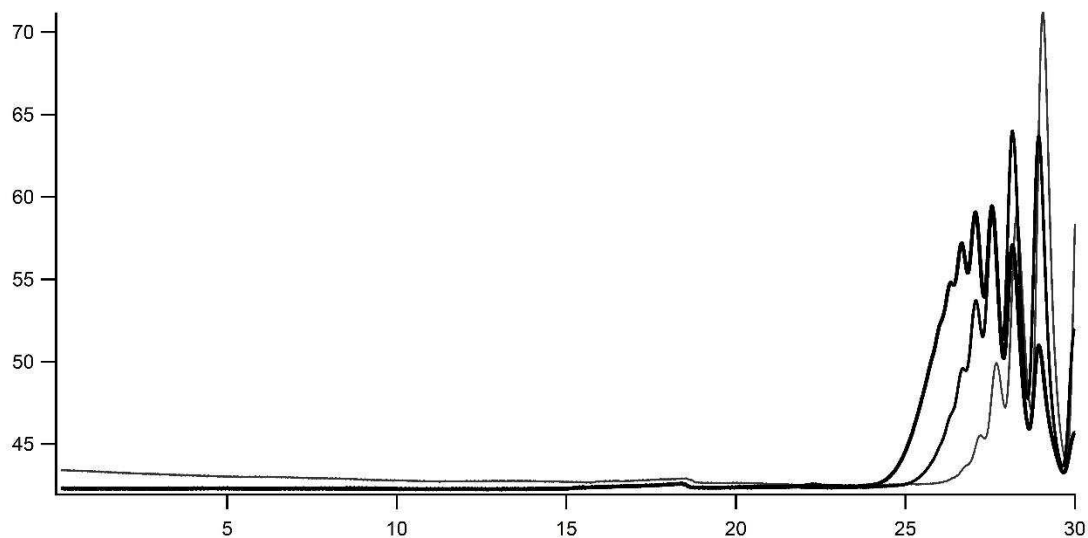


**Figure 2.7.17 – Corresponds to Figure 4.10, Combined.**

**Part B: *Spatially Controlled Arene Formation***

**A 2.8 --- General Methods and Materials**

All reactions or material manipulations were carried out under air free conditions (glove box: MBraun MB 200G) unless otherwise noted. Anhydrous, degassed acetonitrile (MeCN), dichloroethane (DCE) and diisopropylethylamine (DIPEA) were purchased from Sigma Aldrich in Sure-Seal bottles, opened under an inert nitrogen atmosphere and used without further purification. Tetrahydrofuran (THF), dichloromethane (DCM), and diethyl ether (Et<sub>2</sub>O) were degassed with a stream of argon and passed through two columns of neutral alumina before use. Thin layer chromatography was conducted on SiliCycle® 250 μm 60 A (glass-backed) and column chromatography for isolated compounds was performed on SiliCycle® Silica Flash ® 40-63 μm 60A. Anhydrous cobalt halide salts were purchased from Sigma Aldrich or Strem Chemicals and stored under inert conditions. Fluorescein azide (FAM-N<sub>3</sub>) was purchased from Lumiprobe as a 10mM solution in DMSO. Light sources used include: a 410 nm 35W Kessil LED, 450 nm 35W

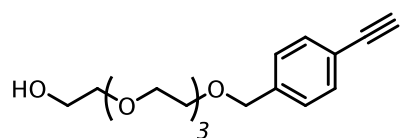


Kessil LED or a standard household 14 W CFL. The photocatalyst  $[\text{Ir}(\text{dF-CF}_3\text{ppy})_2(\text{dtbbpy})]\text{PF}_6$  was synthesized according to literature procedures or purchased from Strem Chemicals. Photomasks were printed by CAD/ART Services, Inc. (Brandon, OR).

## A 2.9 --- Instrumentation

Fluorescence imaging of functionalized PDMS was done using an EVOS FL fluorescence microscope. Any image manipulation was conducted in Fiji software and converted to JPEG format. Proton NMR were collected on a Varian 300 or 400 MHz spectrometer and data is reported as follows: in  $\text{CDCl}_3$  (7.26 ppm); multiplicity (s = singlet, bs = broad singlet, d = doublet, t = triplet, q = quartet, and m = multiplet), coupling constants (Hz). Carbon NMR spectra were collected on a Varian 300 or 400 MHz spectrometer. Chemical shifts are reported in reference to  $\text{CDCl}_3$  (77.2 ppm). Non-polymeric compounds and polymer spectra were conducted in  $\text{CDCl}_3$  at room temperature.

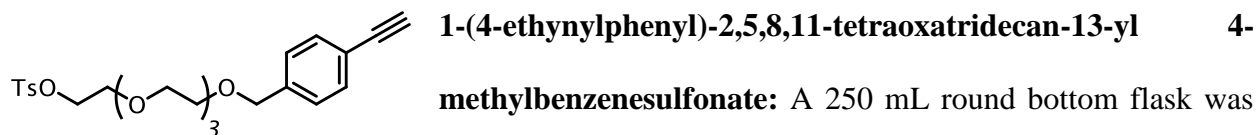
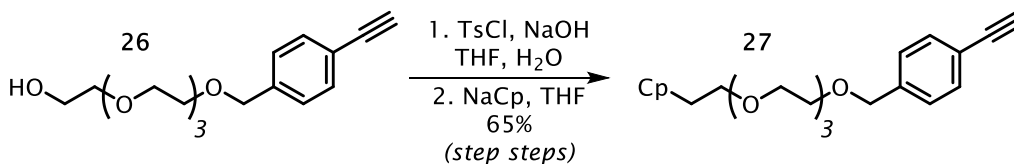
## A 2.10 --- Procedures for Surface Linker Synthesis



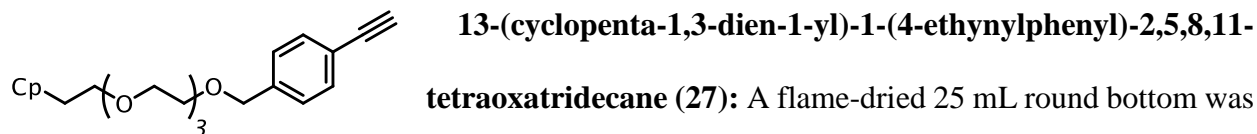
**1-(4-ethynylphenyl)-2,5,8,11-tetraoxatridecan-13-ol (26):** The synthesis of this compound has been reported in the literature.<sup>[2]</sup>

A  $^1\text{H}$  NMR has been included for reference.  $^1\text{H}$  NMR (300 MHz,  $\text{CDCl}_3$ ):  $\delta$  7.45 (d,  $J = 8.2$  Hz, 2H), 7.28 (d,  $J = 8.2$  Hz, 2H), 4.55 (s, 2H), 3.72-3.57 (m, 16H), 3.05n (s, 1H), 2.46 (bs, 1H) ppm. Compound characterization matched spectra reported in the literature.

### A 2.10.1 -- Synthesis of Compound 27:



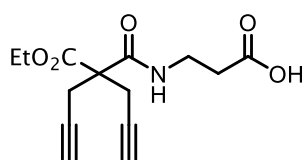
A 250 mL round bottom flask was charged with **26** (470 mg, 1.0 equivalents, 1.52 mmol), sodium hydroxide (106 mg, 1.75 equivalents, 2.66 mmol), a 7:3 mixture of THF and water (10 mL) and a stir bar. The solution was chilled to 0 °C in an ice bath and a THF solution of tosyl chloride (TsCl) was added in three large portions. The ice bath was removed and the reaction was allowed to warm to room temperature over three hours. After three hours, the reaction was quenched with water and transferred to a separatory funnel. The aqueous layer was extracted three times with DCM and the organic layers were combined and dried over magnesium sulfate. After dry, the organic layer was concentrated *in vacuo* to afford the tosylated alcohol as a clear oil and this compound was immediately taken forward without purification. A <sup>1</sup>H NMR has been included for reference. **<sup>1</sup>H NMR** (300 MHz, CDCl<sub>3</sub>): δ 7.78 (d, J = 8.8 Hz, 2H), 7.44 (d, J = 8.8 Hz, 2H), 7.83-7.25 (m, 4H), 4.5 (s, 2 H), 4.15-4.14 (t, J = 4.70 Hz, 2H), 3.68-3.56 (m, 14H), 3.05 (s, 1H), 2.42 (s, 3H) ppm.



A flame-dried 25 mL round bottom was charged with a stir bar and tosylated alcohol (200 mg, 1.0 equivalents, 0.432 mmol). Anhydrous, degassed THF was charged to the flask and the solution was chilled to -78 °C in a dry ice bath. Once the flask had chilled a solution of sodium cyclopentadiene (NaCp – 2M in THF) (324 uL,

1.5 equivalents, 0.649 mmol) was added drop-wise and the dry ice bath was replaced with an ice bath (0 °C). The reaction was allowed to stir for 1.5 hours and then saturated NH<sub>4</sub>Cl solution was added. The aqueous layer was extracted with diethyl ether (3 x 20 mL), the organic extracts were combined and dried over sodium sulfate. Once dry, the diethyl ether was decanted away from the sodium sulfate and concentrated *in vacuo*. The crude, slightly yellow oil was then purified via column chromatography using a 0-20% ethyl acetate:hexane gradient. Compound **27** was isolated as a clear oil in 81% yield (124 mg). Mixture of isomers. <sup>1</sup>H NMR (300 MHz, CDCl<sub>3</sub>) δ 7.45 (d, J = 8.2 Hz, 2H), 7.29 (d, J = 7.63 Hz, 2H), 6.46-6.38 (m, 2H), 6.26-6.20 (m, 1H), 6.06 (s, 1H), 4.55 (s, 2H), 3.68-3.59 (m, 16H), 3.05 (s, 1H), 2.92 (d, J = 7.63 Hz, 2H), 2.72-2.63 (m, 2H), ppm.

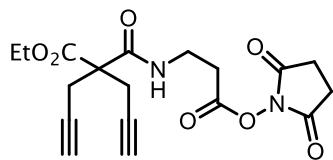
#### A 2.10.2 -- Synthesis of Compound 34:



#### 3-(2-(ethoxycarbonyl)-2-(prop-2-yn-1-yl)pent-4-

**ynamido)propanoic acid (33):** For the synthesis of this compound please see Appendix One, compound **64d**. <sup>1</sup>H NMR (300 MHz, CDCl<sub>3</sub>)

δ 7.21 (m, 1H), 4.24 (q, J = 7.04 Hz, 2H), 3.55 (q, J = 5.87 Hz, 2H), 2.91 (dq, J = 14.67, 9.98, 2.35 Hz, 4H), 2.63 (t, J = 5.87 Hz, 2H), 2.03 (t, J = 2.35 Hz, 2H), 1.28 (t, J = 7.04 Hz, 3H) ppm. MS (ESI, pos): m/z = 280.1 [M+H]<sup>+</sup>; m/z = 302.1 [M+Na]<sup>+</sup>



#### Ethyl

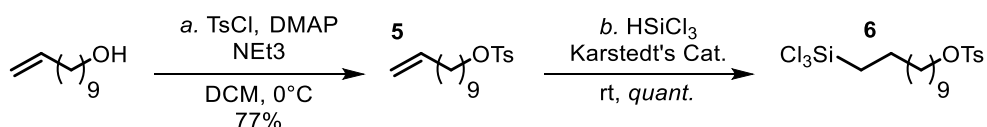
#### 2-((3-((2,5-dioxopyrrolidin-1-yl)oxy)-3-

**oxopropyl)carbamoyl)-2-(prop-2-yn-1-yl)pent-4-ynoate (34):** To a flame-dried 10 mL round bottom flask was added compound **33**

(100mg, 1.0 equivalents, 0.358 mmol), TSTU (129 mg, 1.2 equivalents, 0.429 mmol), and a stir bar. Anhydrous DCM (2 mL, ~0.2M) was then added followed by trimethylamine (NEt<sub>3</sub> – 100 uL, 2.0 equivalents, 0.716 mmol). The reaction was stirred at room temperature for one hour, celite

was added and the volatile solvents were removed *in vacuo*. The crude celite/compound material was loaded directly onto a silica gel column and compound **34** was eluted with a 10-30% ethyl acetate:hexane gradient. Compound **34** was isolated as a white solid in 50% yield (100 mg).  $^1\text{H NMR}$  (300 MHz,  $\text{CDCl}_3$ )  $\delta$  7.23 (bs, 1H), 4.23 (q,  $J = 7.63$  Hz, 2H), 3.67 (q,  $J = 5.87$  Hz, 2H), 2.98-2.78 (m, 11H), 2.09 (t,  $J = 2.35$  Hz, 2H), 1.26 (t,  $J = 7.63$  Hz, 3H) ppm.  $^{13}\text{C NMR}$  (101 MHz,  $\text{CDCl}_3$ )  $\delta$  170.45, 169.15, 168.32, 167.55, 78.86, 78.71, 72.03, 71.81, 62.37, 56.46, 35.26, 31.35, 25.59, 24.04, 13.94 ppm. **IR** (ATR): 3298, 2947, 2986, 1821, 1786, 1730, 1687, 1530, 1205  $\text{cm}^{-1}$ . **MS** (ESI, pos):  $m/z = 377.2$   $[\text{M}+\text{H}]^+$ , 399.1  $[\text{M}+\text{Na}]^+$

### A 2.10.3 -- Synthesis of Compound 6:



**5** **Undec-10-en-1-yl-4-methylbenzenesulfonate (5)**: This compound has been reported.<sup>[3]</sup> A  $^1\text{H NMR}$  has been included for reference.  $^1\text{H NMR}$  (400 MHz,  $\text{CDCl}_3$ ):  $\delta$  7.76 (d,  $J = 8.2$  Hz, 2 H), 7.34 (d,  $J = 8.2$  Hz, 2H), 5.83-5.73 (m, 1H), 4.99-4.89 (m, 2H), 3.99 (t, 7.0 Hz, 2H), 2.42 (s, 3H), 2.00 (q, 7 Hz, 2 H), 1.60 (p, 6.6 Hz, 2H), 1.37-1.20 (m, 12H) ppm.

**6** **11-(trichlorosilyl)undecyl 4-methylbenzenesulfonate (6)**: Preparation was based on a procedure reported in the literature.<sup>[4]</sup> A flame-dried 10mL schlenk flask was charged with a stir bar and compound **5** (1.0 equivalent, 1.54 mmol, 500mg). The flask was evacuated, filled with argon and charged with degassed toluene (~2 mL) followed by neat trichlorosilane (10 equivalents, 15.4 mmol, 1.55 mL). Karstedt's catalyst in xylene (10  $\mu\text{L}$ , 2 wt% Pt in xylene) was added to the flask and stirred at room temperature until the reaction showed

complete consumption of starting material by  $^1\text{H}$  NMR (~1-2 hours). The reaction was concentrated *in vacuo* and stored under argon. Compound was used in subsequent steps without further purification.  $^1\text{H}$  NMR (400 MHz,  $\text{CDCl}_3$ )  $\delta$  7.78 (d, 8.2 Hz, 2H), 7.33 (d, 7.8 Hz, 2H), 4.01 (t, 6.3 Hz, 2H), 2.44 (s, 3H), 1.66-1.53 (m, 4H), 1.42-1.35 (m, 4H), 1.32-1.22 (m, 12H) ppm.  $^{13}\text{C}$  NMR (101 MHz,  $\text{CDCl}_3$ )  $\delta$  144.6 (1C, Aryl), 133.23 (1C, Aryl), 129.8 (2C, Aryl), 127.84 (2C, Aryl), 70.7 (1C), 31.74, (1C), 29.4 (1C), 29.3 (1C), 29.2 (1C), 28.94 (1C), 28.88 (1C), 28.8 (1C), 25.3 (1C), 24.3 (1C), 22.2 (1C), 21.6 (1C) ppm. MS (ESI, pos):  $m/z = 469.2$  [(OMe) $_3$ Si, M+Na] $^+$ ; calculated  $\text{C}_{21}\text{H}_{38}\text{O}_6\text{Ssi}$ , 446.7, calculated  $\text{C}_{18}\text{H}_{29}\text{Cl}_3\text{O}_3\text{Ssi}$ , 459.9.

## A 2.11 --- Preparation of Surface Modification Substrate

### A 2.11.1 -- Preparation of PDMS

Preparation has been reported in the literature using a Sylgard 184 kit from Sigma Aldrich.<sup>[5]</sup> PDMS was formed by mixing ten parts Sylgard 184 elastomer base with one part curing agent in a disposable plastic container. After thoroughly mixing the components, the cup was carefully placed under dynamic vacuum to remove air bubbles. The cup was removed from the vacuum and the contents were slowly poured into petri dishes to the desired thickness. The petri dishes were transferred to an oven at 100 °C and heated for 35 minutes. After curing the petri dishes were removed, checked for solidity, and allowed to cool.

### A 2.11.2 -- Functionalization of PDMS

Large pieces of PDMS polymer (5 cm x 5 cm x 1 mm) were successively washed using 3 x 20 mL portions of HPLC grade tetrahydrofuran (THF)—allowing each wash to age at least 1 hour. A final wash in HPLC grade acetonitrile (MeCN) 20 mL was then used to remove THF and the PDMS was placed in an oven at 100 °C for 15 minutes. After cooling, the clean PDMS was

placed in an O<sub>2</sub> plasma chamber under vacuum (0.30 torr) using a power of 25 watts for 3 minutes. Oxidized PDMS samples were immediately (< 2 min) placed into a glove box under air-free conditions. 125 mg of compound **6** was added to a large flame-dried screw cap jar followed by 20 mL of anhydrous and degassed toluene to fully dissolve compound **6**. The oxidized PDMS was then submerged in the solution and allowed to stand for 15 minutes. After 15 minutes, 150 uL of degassed triethylamine (NEt<sub>3</sub>) was added to the solution, the jar was sealed, and the mixture was allowed to stand for 6 hours. The container was removed from the glove box and the PDMS was washed with toluene and acetonitrile to remove triethylamine salts (observed as white precipitate in toluene). The PDMS was successively washed by 3 x 20 mL portions of THF, 1 x 20 mL MeCN, 1 x 20 mL THF and finally a last 20 mL portion of MeCN then placed in an oven at 100 °C for 10 minutes. Samples were stored in a vacuum desiccator until they were needed.

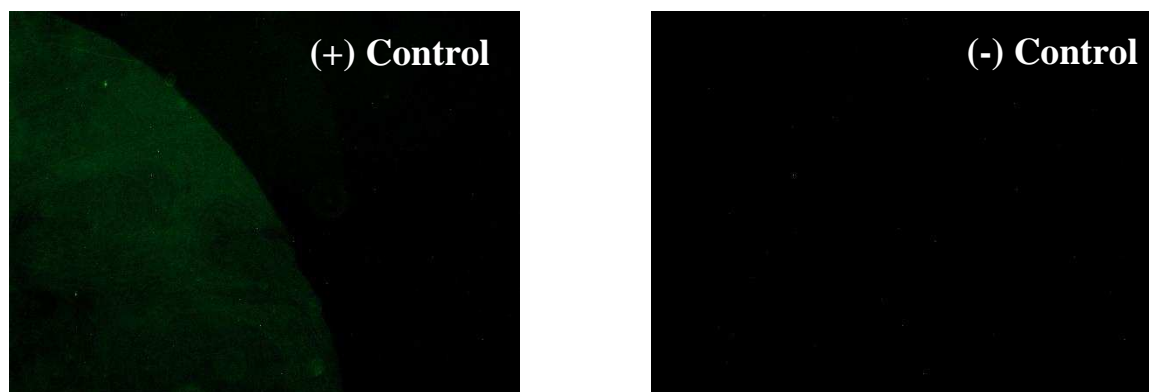
#### **A 2.11.3 -- Functionalization of PDMS – Diyne Installation**

To a large flame-dried large screw cap jar was added 100 mg of compound **1d** followed by ~20 mL of anhydrous dimethylformamide (DMF). The tosyl-functionalized PMDS was added to the mono-acid solution in addition to 150 uL of freshly distilled DBU (1,8-diazabicycloundec-7-ene). The screw cap jar was firmly sealed and briefly stirred. The jar was then placed on a hot-plate to maintain a temperature of 60-70 °C overnight. The PDMS was removed and washed by 3 x 20 mL THF, 1 x 20 mL MeCN, 1 x 20 mL THF and a final 1 x 20 mL MeCN wash. After 10 minutes in an oven at 100 °C the PDMS was stored in a vacuum desiccator. The presence of alkynes on the surface was confirmed by a click reaction using a fluorescent azide.

#### **A 2.11.4 -- Functionalization of PDMS – Click Control**

To confirm the presence of the diyne linker, a small sample of the PDMS (1 cm x 1 cm x 1 mm) was removed from the bulk material using a razor blade. A hole was cut (4mm) into a

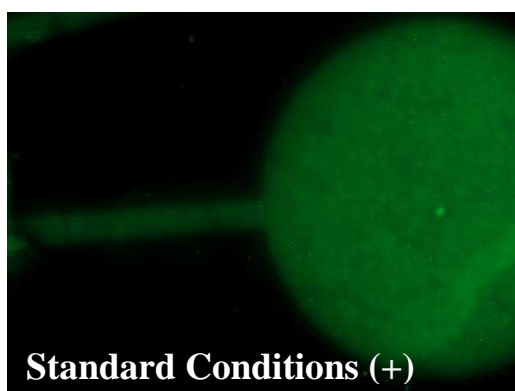
separate piece of unfunctionalized PDMS (1cm x 1cm x 2.5 mm) and the surface was cleaned with scotch tape. This cut PDMS was placed into direct contact with the piece of functionalized material to create a sealed reaction well on the alkyne functionalized surface. Under an argon atmosphere, 5 uL of 2 mM Cu(I)(MeCN)<sub>4</sub> in DMSO, 5 uL of 2mM TBTA in DMSO, 5 uL of 2.6mM sodium ascorbate in water and 1 uL of FAM-Azide in DMSO was added to the well and mixed thoroughly with a pipette. After ~3 hours, the solution was removed and the PDMS washed with copious amount of water, methanol and acetonitrile the dried under an argon stream. Direct imaging on a fluorescence microscope reveals the positive click control shown below.



### A 2.12 --- Patterned Arene Formation Procedure

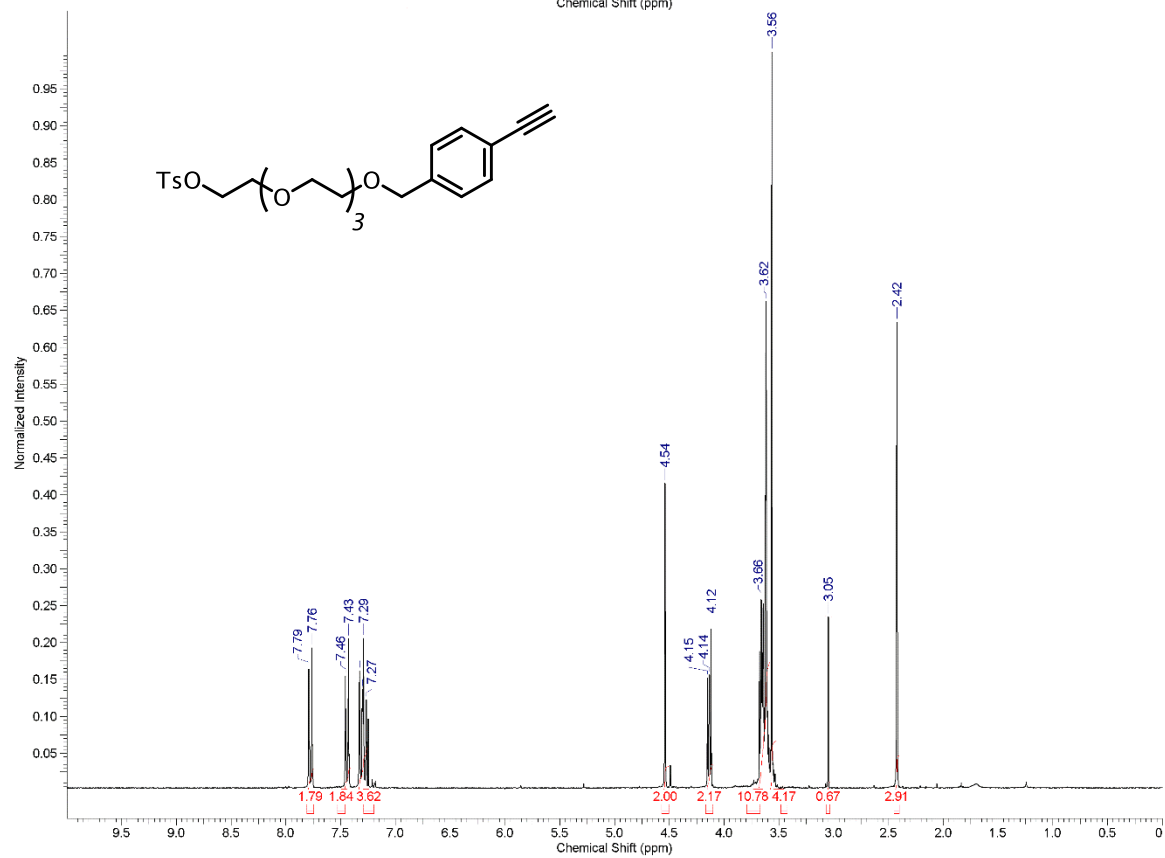
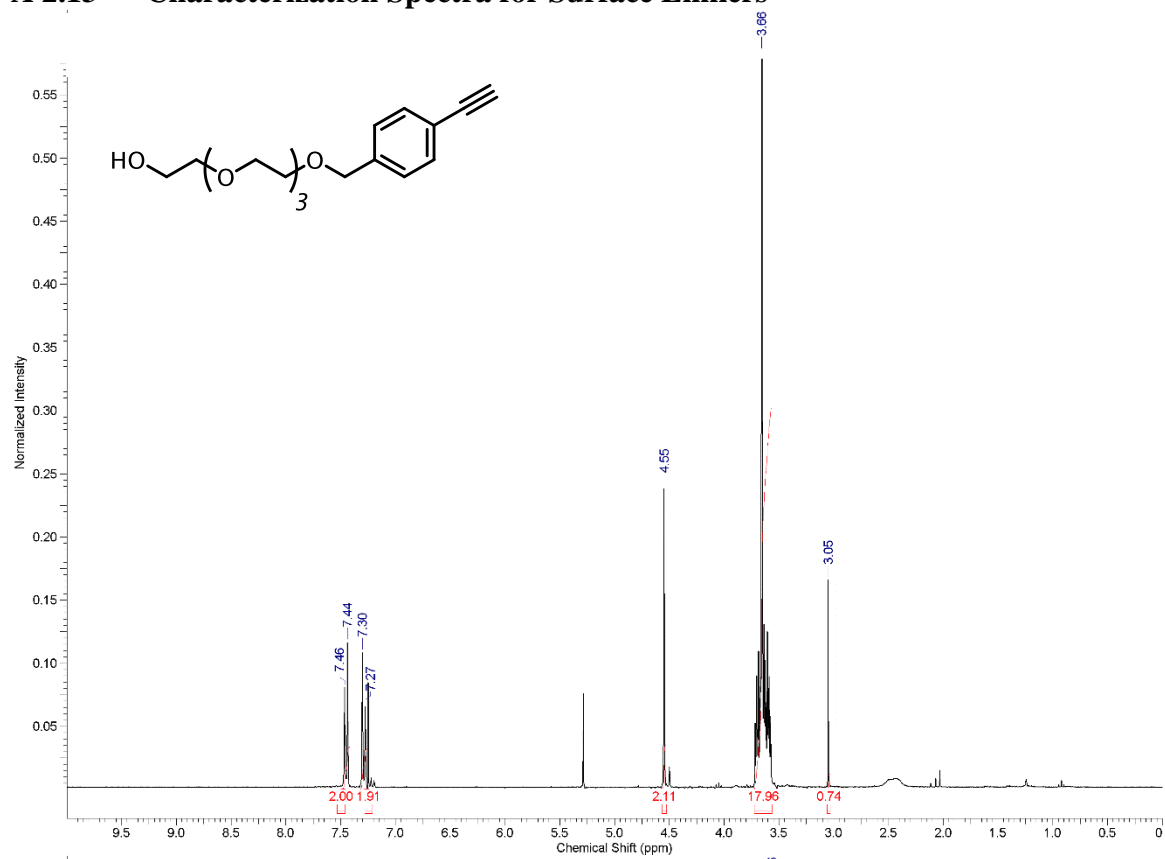
Under atmospheric conditions a 20 mL scintillation vial was charged with CoBr<sub>2</sub>(Pcy<sub>3</sub>)<sub>2</sub> (1mM, 2.34 mg), [Ir(dF-CF<sub>3</sub>ppy)<sub>2</sub>(dtbbpy)] (0.25 mM, 0.84 mg) and 3-ethynyl perylene (1.5 mM, 1.24 mg). Strictly working under red light (red LEDs), the vial was then placed under an argon atmosphere and charged with degassed dichloroethane (1.5 mL), acetonitrile (1.5 mL) and DIPEA (12 mM). The reaction solution was then pipetted onto a 1cm x 1cm piece of functionalized PDMS (~0.75 mm thick) to sufficiently cover the PDMS. Again under red light, the PDMS is placed onto a solid, dark background (un-functionalized silicon wafer) and the desired photomask is placed in direct contact with the reaction solution on top of the PDMS. A 410 nm 35W Kessil was then

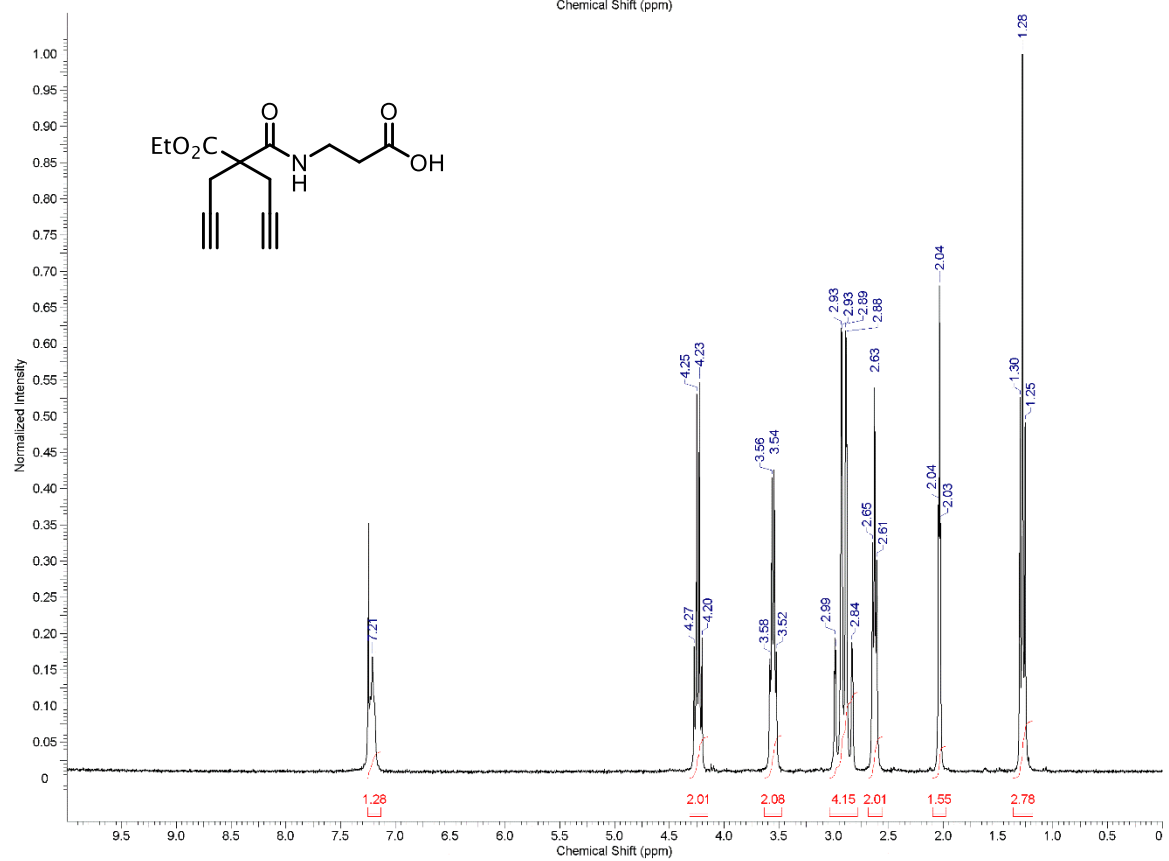
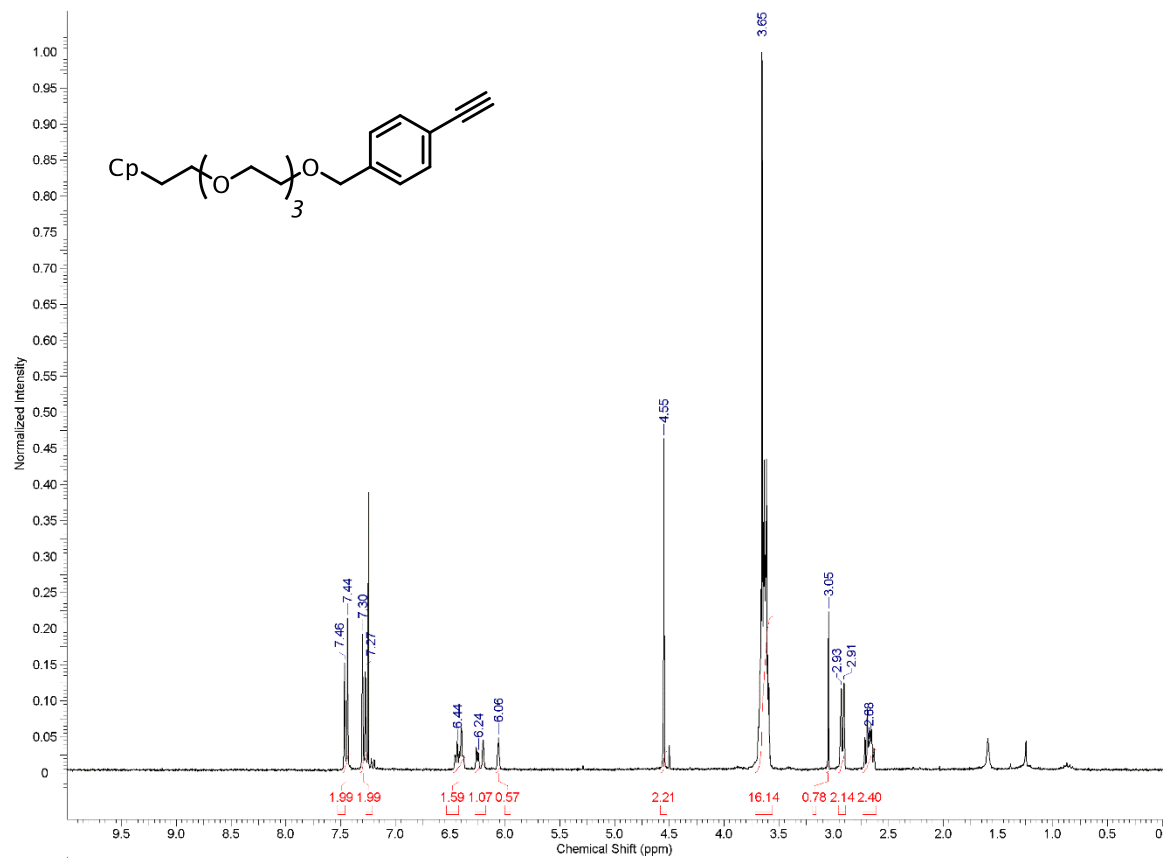
placed ~2-3 feet above the photomask and the PDMS is irradiated for 8-15 minutes. Following irradiation the PDMS was placed into a vial of tetrahydrofuran (~10 mL) and placed on a shaker table for 1 hour (wrapped in foil). After 3 washes with THF, the PDMS is then washed in acetonitrile (10 mL) followed by a second THF wash (10 mL) and final acetonitrile wash (10 mL). The sample is then placed in an oven at 100°C for 15 minutes and after cooling imaged on the fluorescence microscope.

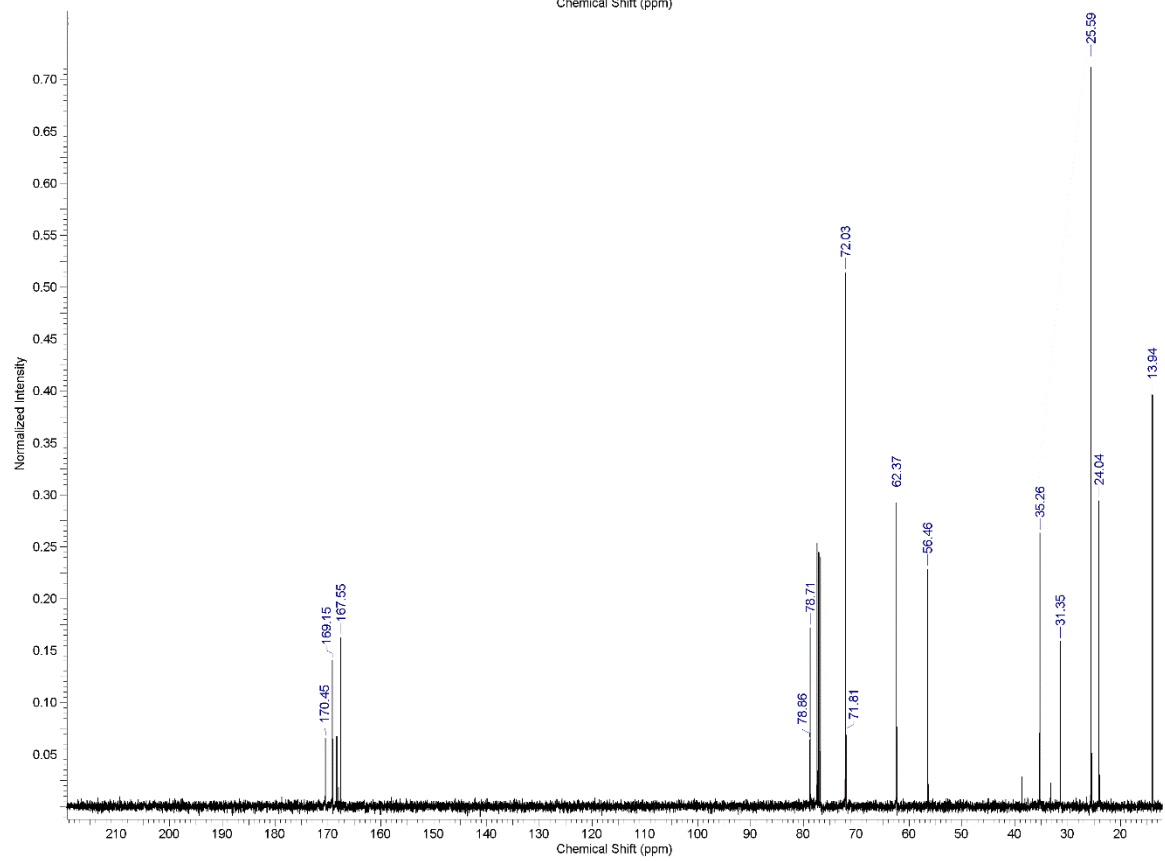
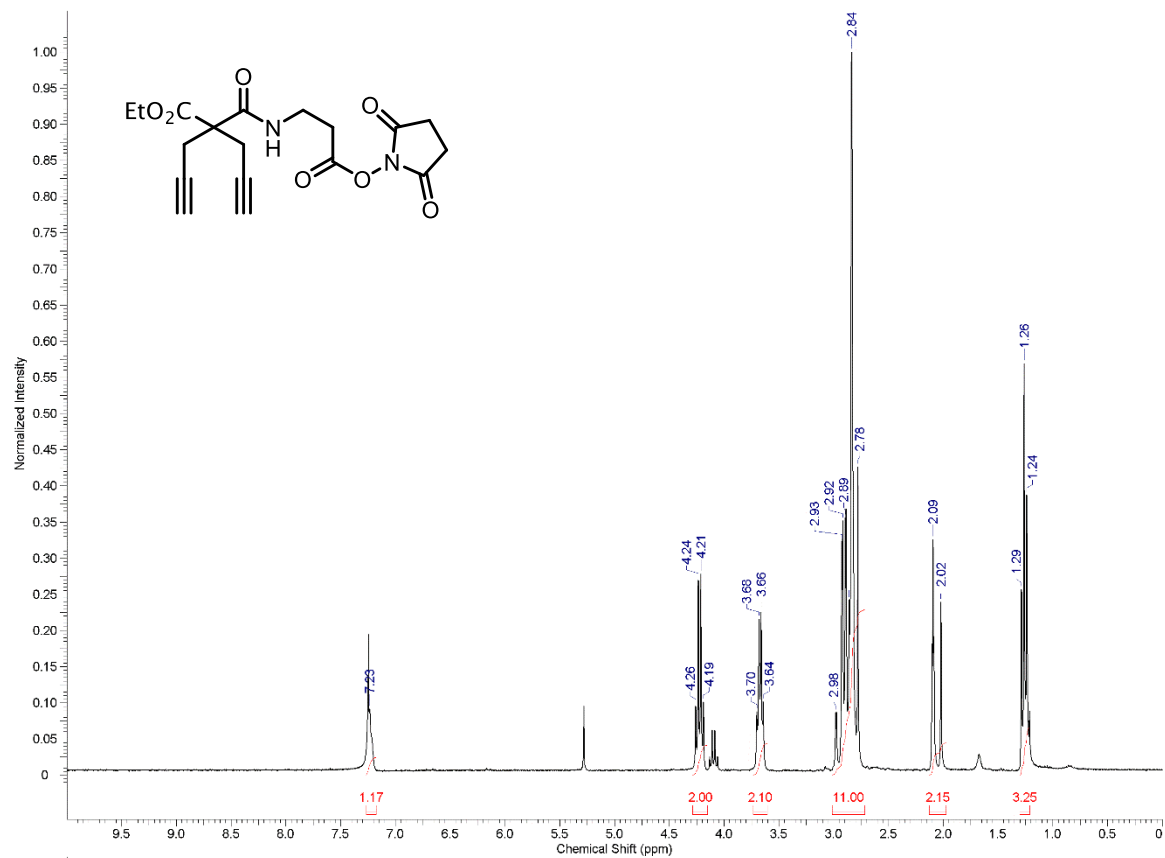


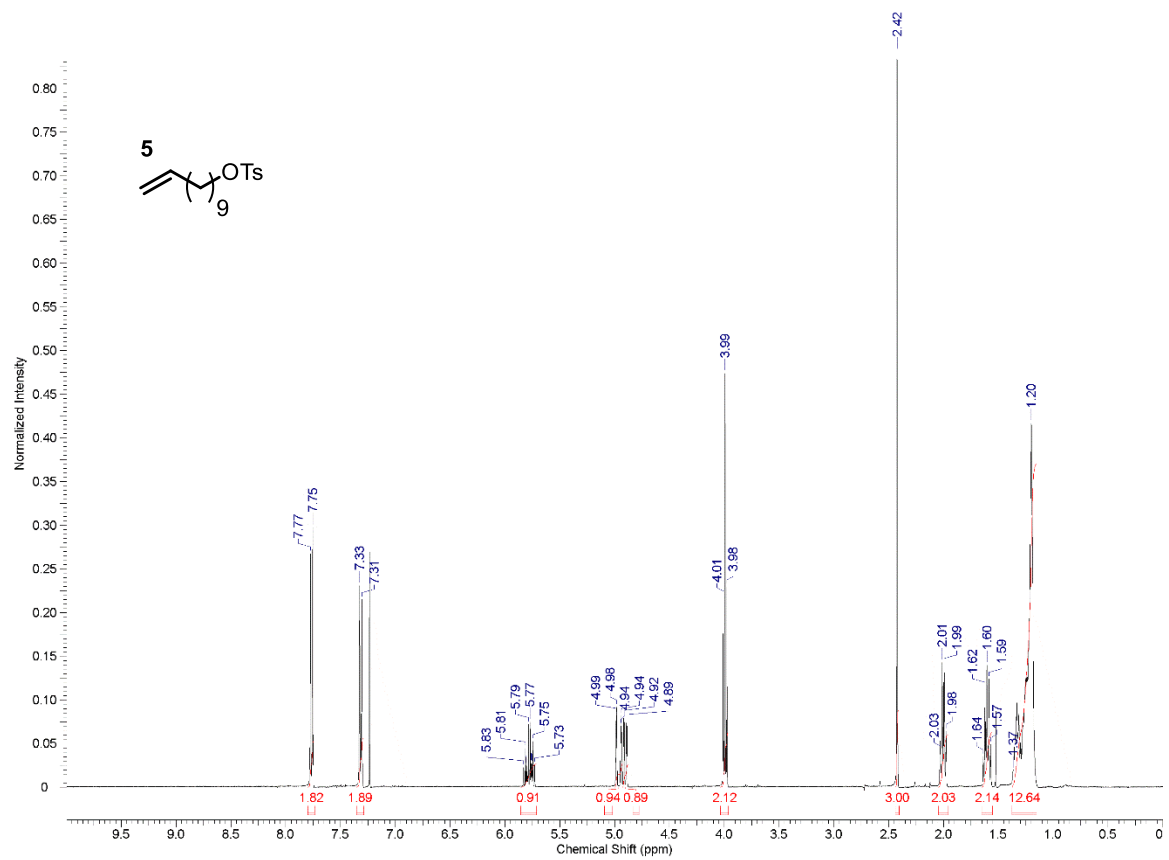


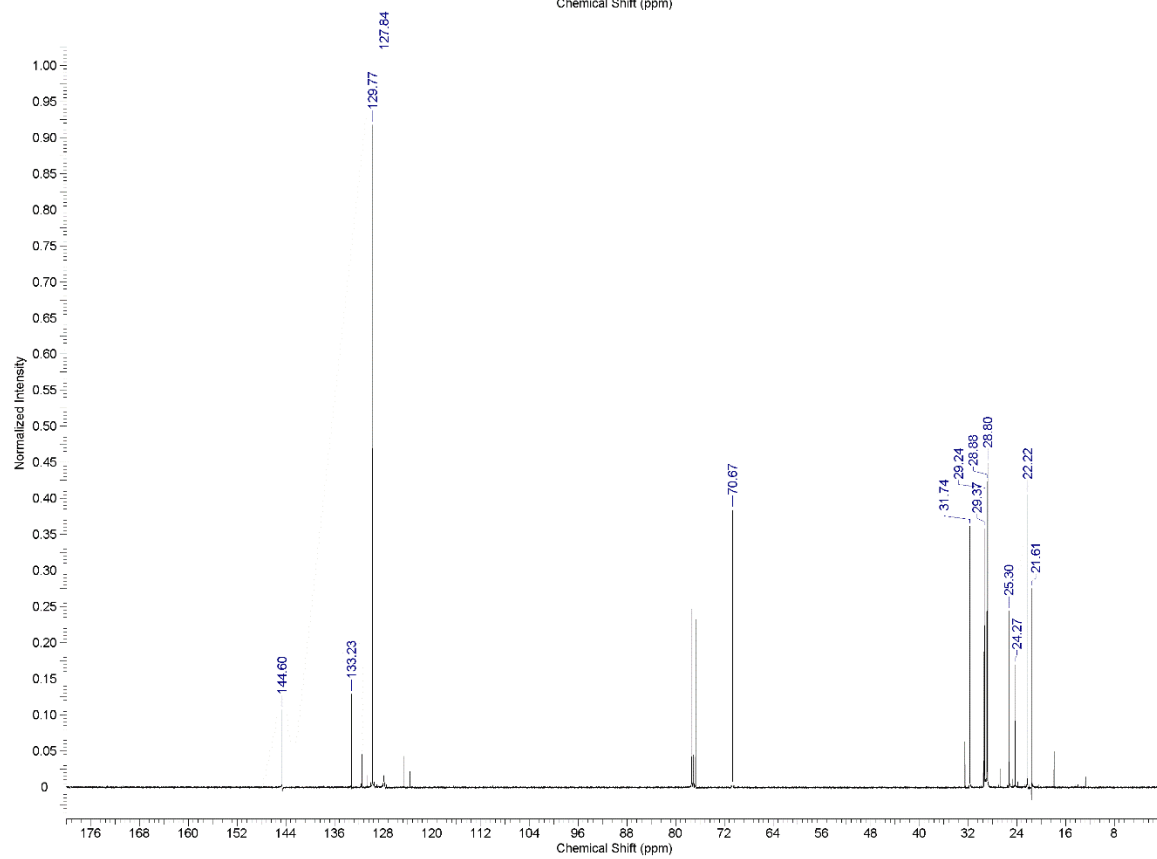
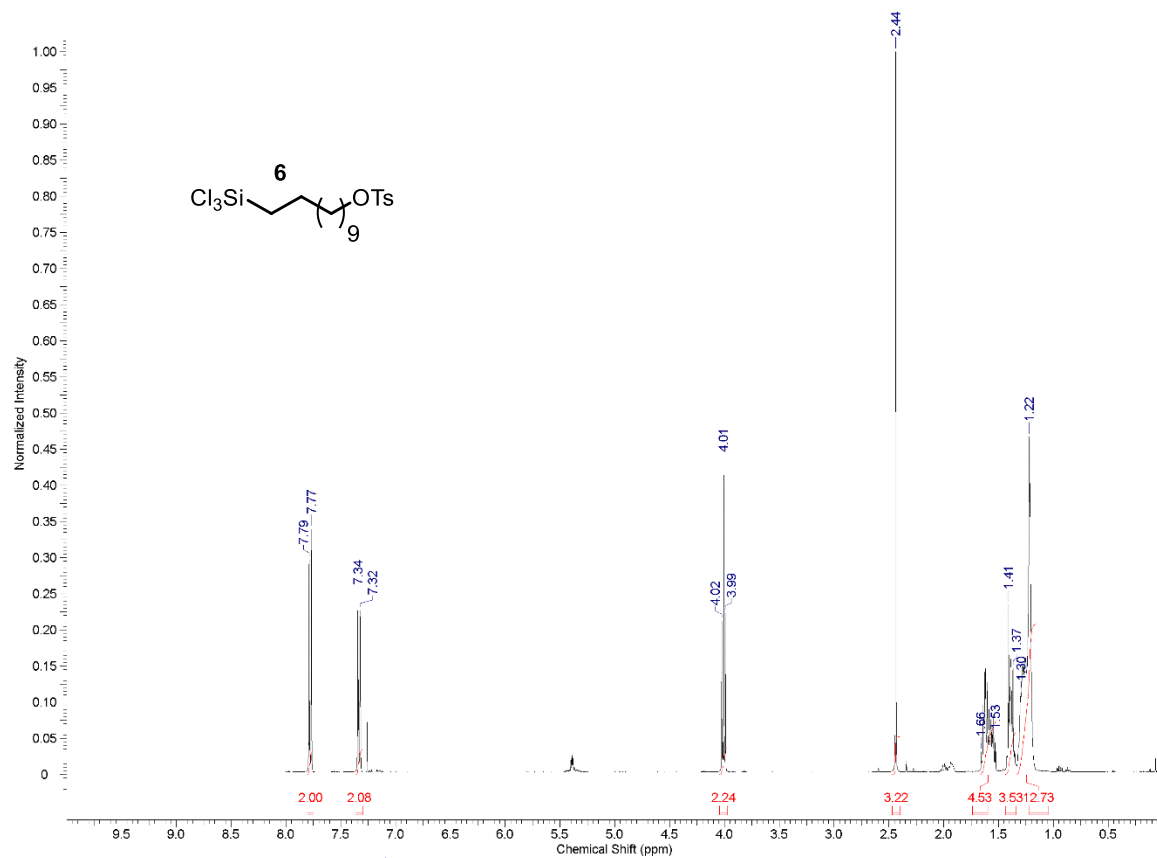
## A 2.13 --- Characterization Spectra for Surface Linkers











## REFERENCES

- [1] Wilking, M.; Mück-Lichtenfeld, C.; Daniliuc, C. G.; Hennecke, U. *J. Am. Chem. Soc.* **2013**, 135, 8133-8136.
- [2] Niikura, K.; Iyo, N.; Higuchi, T.; Nishio, T.; Jinnai, H.; Fujitani, N.; Ijiro, K. *J. Am. Chem. Soc.* **2012**, 134 (18), 7632-7635.
- [3] Molnar, I. G.; Gilmour, R. *J. Am. Chem. Soc.* **2016**, 138, 5004-5007.
- [4] Poelma, J. E.; Fors, B. P.; Meyers, G. F.; Kramer, J. W.; Hawker, C. J. *Angew. Chem. Int. Ed.* **2013**, 52, 6844-6848.
- [5] Guan, Q.; Noblitt, S. D.; Henry, C. S. *Electrophoresis.* **2012**, 379-387.